APPROVAL SHEET

Title of Thesis: Study of a UHF Command Destruct Missile Antenna System

Name of Candidate: Elwood Hatcher Mullins
Master of Science, 1960

Thesis and Abstract Approved: E. A. Schuchard

Dr. E. A. Schuchard
Advisor in Electrical Engineering

Date Approved: 4-14-60

STUDY OF A UHF COMMAND DESTRUCT MISSILE ANTENNA SYSTEM

by

Elwood Hatcher Mullins

Thesis submitted to the Faculty of the Graduate School
of the University of Maryland in partial fulfillment
of the requirements for the degree of
Master of Science
1960

STATEMENT OF CLEARANCE

The thesis "Study of a UHF Command Destruct Missile Antenna System" written by Elwood H. Mullins is cleared by the U. S. Naval Ordnance Laboratory on this 29 day of April 1960.

Released by the Commander,
U. S. Naval Ordnance Laboratory
Silver Spring, Maryland

J Nichter
Technical Information Officer

ACKNOWLEDGMENTS

The assistance, encouragement, and advice of Dr. E. A. Schuchard are gratefully acknowledged. Special thanks are also due to Mr. Lowell Green, Mrs. Eula Paseur, and the Goodyear Aircraft Corporation--to Mr. Green for assistance in the understanding and derivation of the theoretical expressions, to Mrs. Paseur for her great help in editing the manuscript, and to the Goodyear Aircraft Corporation for supplying the photographs and experimental data used in this study.

TABLE OF CONTENTS

LIST OF TABLES

LIST OF FIGURES

Figure Page

Figure Page

Figure Page

Figure Page

Figure Page

Figure Page

INTRODUCTION

The basic problem in recent years of communicating between ground instrumentation and high-speed missiles in flight has stimulated research and development into the theory and application of slot antennas in cylindrical bodies. This study is concerned with a specific application of slot antennas to a ballistic missile for Command Destruct purposes.

A Command Destruct System is one of ground and air-borne instrumentation whereby the Missile Test Range Safety Officer can destruct a missile on command at anytime during the flight of the missile if it becomes necessary to do so to insure the safety of life and property. The launching of missiles, particularly of the ballistic variety, creates a potential hazard which can have drastic effects if no provisions are made for either command- or self-destruction in case the flight becomes erratic. Missiles which are guided in flight, such as the radar-beam-rider, usually incorporate a self-destruct or fail—safe system which automatically destructs the missile if guidance control is lost or if the over-all system malfunctions. This type of destruct system is commonly used in missiles such as the Terrier and the Tarter, whereas the Command Destruct System is commonly used in missiles such as the Atlas, the Thor, and the Snark, which have either inertial or radio-command control guidance systems.

A typical Command Destruct Ground Control System consists of an AN/FRW-2* Transmitter with three or more audio-frequency coders, an appropriate antenna system, a monitoring recorder, and a desensitized receiver and decoder. A second AN/FRW-2 transmitter is used as a standby in case the first one malfunctions. The power radiated is normally between 500 and 1000 watts; however, some installations boost the maximum power output to 10 kilowatts for long-range operations. Also, down-range ground stations are used with the control functions switched from one range safety officer to another as the missile trajectory dictates. Usually, the ground-station radiating antenna system is designed to give circular polarization and to provide omnidirectional coverage, since the ability to communicate with the missile in any orientation or direction relative to the ground station is essential. The carrier output is frequency modulated by subcarriers which may range in frequency from about 7 to 80 kilocycles.

A typical air-borne Command Destruct System consists of a missile antenna system, an ultrahigh frequency receiver decoder and power supply, and one or more explosive destructor assemblies including arming and firing devices.

The various missile test ranges in the United States have recently agreed that Radio Command Destruct Systems will operate in the ultrahigh frequency spectrum between

---

*Radio Remote Control Transmitting Set

406 and 550 megacycles. The specific frequency to be used by a particular test range for a given missile is assigned by the area frequency coordinator. The test ranges have also agreed that the ground control equipment will be so standardized that a given missile may be test fired from any of the test ranges without experiencing problems of incompatibility with the ground control equipment.

Slot-type radiators for the missile antenna system are particularly adaptable to that portion of the ultrahigh frequency spectrum designated for Radio Command Destruct Systems. Also, the slot antenna has the advantage that it can be made flush with the outside surface of the missile, thereby eliminating aerodynamic disturbances associated with protruding designs.

STATEMENT OF PROBLEM

The objective of this study is to develop the theoretical far-field radiating characteristics of a particular Command Destruct Missile Antenna System under certain idealized conditions, and then by use of the reciprocity theorem to compare the calculated results with experimental antenna reception data. Most engineers seem to favor the experimental method for determining radiation-pattern characteristics of antennas other than simple dipoles and where the geometrical configuration of the body on which the antenna is located is complex. This practice challenged the author to investigate the theoretical approach for an idealized model capable of explicit solution by analytical and numerical methods.

The particular missile antenna system under study consists of two circumferential slots of the type illustrated in figure 1. The two slots are mounted diametrically opposed on a cylindrical portion of the missile body at a longitudinal position approximately in the middle of the warhead section. Each slot is dielectric loaded to reduce the physical slot length at the specified operating frequency to a length that is compatible with the available circumferential space on the missile while maintaining the characteristics of a one-half wavelength slot. Figure 2 shows a perspective view of both antennas and the

interconnecting coaxial cabling. The output signal from the tee connector is fed directly to the input of the ultra-high frequency receiver by a 50-ohm coaxial cable. The diameter of the missile is 13 inches at the location of the antenna system.

For background information, the operational requirements for the Command Destruct Antenna System specify that the desired far-field radiation pattern coverage shall be as nearly isotropic as possible, with the maximum null depth not greater than -12 decibels below an isotropic (dipole) pattern. From a practical standpoint, it is generally considered acceptable if at least 95 per cent of the total spherical area surrounding the antenna system meets this requirement. Also, the voltage standing-wave ratio shall not exceed 2.0 with the antenna system terminated in a 50-ohm load. The operating frequency is specified as 445 megacycles, and the bandwidth at the 3-decibel points shall be not less than ±2 megacycles from the center frequency. The aerodynamic requirements prohibit protruding antennas, thus making a flush or near-flush design mandatory. The environmental requirements necessitate that the antenna be capable of operating over a temperature range from -65 to +300 degrees Fahrenheit while being subjected to missile vibration. Also, the system must operate satisfactorily immediately after emergence from salt water.

The space limitations within which the Command Destruct Antenna System is required to fit and the operating frequency

necessitate that dielectric loading be used to reduce the physical size of the equivalent free-space one-half wavelength slots. Even with dielectric loading, the Command Destruct Antenna System can consist of only two antennas without interfering with the other two antenna systems and the instrumentation package. The final Command Destruct antenna design configuration is illustrated in figure 3. It consists of a rectangular box approximately 5 1/2 inches long by 1 inch wide by 2 inches deep at the center of the box where the 2-inch dimension is tangent with the arc formed by the missile surface. The inside of the box forms the slot cavity which is filled with a dielectric loading material composed of 70 per cent titanium dioxide and 30 per cent epoxy base. The slot has a thin metal projection about 1 inch wide by 1/16 inch thick which projects across the slot at the center except for a gap about 1/8 inch wide. This gap serves the function of capacitive loading and provides a means of tuning the slot to the desired resonant frequency by controlling the gap width. Electrical coupling is made by a coaxial fitting positioned near the bottom of the box on the vertical centerline. The center conductor of the coaxial fitting extends across the width of the cavity which terminates in a connection soldered to the opposite wall. The coupling is located to give the best impedance match to a 50-ohm cable.

Two slots of the above type are mounted diametrically opposed about 32 inches from the missile nose. The complete

necessitate that dielectric loading be used to reduce the physical size of the equivalent free-space one-half wavelength slots. Even with dielectric loading, the Command Destruct Antenna System can consist of only two antennas without interfering with the other two antenna systems and the instrumentation package. The final Command Destruct antenna design configuration is illustrated in figure 3. It consists of a rectangular box approximately 5 1/2 inches long by 1 inch wide by 2 inches deep at the center of the box where the 2-inch dimension is tangent with the arc formed by the missile surface. The inside of the box forms the slot cavity which is filled with a dielectric loading material composed of 70 per cent titanium dioxide and 30 per cent epoxy base. The slot has a thin metal projection about 1 inch wide by 1/16 inch thick which projects across the slot at the center except for a gap about 1/8 inch wide. This gap serves the function of capacitive loading and provides a means of tuning the slot to the desired resonant frequency by controlling the gap width. Electrical coupling is made by a coaxial fitting positioned near the bottom of the box on the vertical centerline. The center conductor of the coaxial fitting extends across the width of the cavity which terminates in a connection soldered to the opposite wall. The coupling is located to give the best impedance match to a 50-ohm cable.

Two slots of the above type are mounted diametrically opposed about 32 inches from the missile nose. The complete

missile including propulsion motor is approximately 21 feet in length and has the external contour illustrated in figure 4. The Command Destruct System must be capable of operating during the acceleration phase when the propulsion unit is attached and also after the unit is separated from the primary missile.

THEORETICAL CONSIDERATIONS

Review of Related Work of Others.

A review of the related work of others reveals that many years ago Watson[1] showed how the harmonic series representations for fields in the case of a source near a large sphere—i.e., radio wave propagation over the earth—could be rigorously transformed by a contour integral into a highly convergent form suitable for use in the "shadow" region. Bremmer[2] extended the application of this transformation procedure to obtain what is known as the residue series. He also showed how the integral representations for the field could be evaluated by the saddle-point method and showed that this method led to geometrical-optics representations suitable for the "illuminated" region. Others have applied the same general techniques to the isolated cylinder problem. For instance, Papas[3] derived expressions for calculating radiation patterns from a single transverse slot cut in an infinite-length, perfectly conducting, circular cylinder when the assumed tangential electric field in the slot has

---

[1]G. N. Watson, "The Diffraction of Radio Waves by the Earth", Proc. Roy. Soc. London, vol. A95, pp. 83—99, 1918, vol. A95, pp. 546—563, 1919.

[2]H. Bremmer, Terrestrial Radio Waves, Elsevier Publishing Co., Inc., New York, N. Y., 1949.

[3]C. H. Papas, "Radiation from a Transverse Slot in an Infinite Cylinder", J. Math. Phys., vol. 28, pp. 227—236, January 1950.

only an axial component. At about the same time Pistolkors[4] obtained essentially identical results independently in Russia. Wait and Kahana[5] extended the results obtained by Papas and Pistolkors to include radiation patterns for the cross-polarized component of the radiation field and demonstrated that this component is zero in the equatorial plane. This work is confined to cases in which the diameter of the cylinder is between one-half and two wavelengths. Extensive programed computations were made by Wait and Kates[6] to determine the theoretical radiation patterns produced by thin one-half wavelength circumferential slots cut in circular cylinders of infinite length with diameters of 3 to 21 wavelengths. Also, they considered the case of two diametrically opposed slots when fed both inphase and antiphase. Silver and Saunders[7] derived general expressions for calculating the external field produced by an arbitrarily shaped slot cut in the wall of a perfectly conducting circular cylinder

---

[4]A. A. Pistolkors, "Radiation from a Transverse Slit on the Surface of a Circular Cylinder", J. Tech. Phys. U.S.S.R., vol. 17, pp. 377—388, 1947 (In Russian).

[5]J. R. Wait and S. H. Kahana, "Calculated Patterns of Circumferential Slots on a Circular Conducting Cylinder", Can. J. Tech., vol. 33, pp. 77—97, January 1955.

[6]J. R. Wait and J. Kates, "Radiation Patterns of Circumferential Slots on Moderately Large Conducting Cylinders", Monograph No. 167R, Institution of Electrical Engineers (London), February 1956, republished in Proc. Inst. Elect. Engrs., vol. 103, Pt.C., pp. 289—296, September 1956.

[7]S. Silvers and W. K. Saunders, "The External Field Produced by a Slot in an Infinite Circular Cylinder," J. Appl. Phys., vol. 21, pp. 153—158, February 1950.

of infinite length, where the tangential components of the electric field in the slot are assumed to be prescribed functions. In another paper Silver and Saunders[8] restrict the case to a narrow, transverse, rectangular, one-half wavelength slot in a circular cylinder and compare theoretical patterns with experimental results. Sensipur[9] also derived formulas for accurate numerical evaluation of the radiation patterns from slots on large circular cylinders where the harmonic series converges very slowly; he treats both axial and transverse slots and compares the residue series with the geometrical-optics techniques.

Additional references selected on the basis of pertinence to the specific problem under consideration are listed in the biblography. Even though several authors have treated the general problem of radiation from slots in circular cylinders, an extensive literature search failed to reveal any work by others in which the case of a dielectric-loaded slot has been studied theoretically. The theoretical analysis which follows treats such a case and contributes to the general store of knowledge on the subject of radiation characteristics from slots in cylindrical bodies.

---

[8]S. Silvers and W. K. Saunders, "The Radiation From a Transverse Rectangular Slot in a Circular Cylinder", J. Appl. Phys., vol. 21, pp. 745—749, August 1950.

[9]S. Sensiper, "Cylindrical Radio Waves," Trans. Inst. Radio Engineers, vol. AP-5, pp. 56—70, January, 1957.

Definition of Coordinate Systems Used.

With respect to a cylinder, the cylindrical coordinate system ρ, φ, z is used with the z axis coincident with the cylinder axis and the transverse plane $z = 0$ chosen to pass through the center of the antenna slots. The cylinder radius is designated by $\rho = a$. For the far-field analysis, the spherical coordinate system R, φ, θ is more appropriate, where the polar axis is coincident with the cylinder axis and the plane $\theta = 90^{o}$ passes through the center of the antenna slot. The coordinate systems used in the theoretical analysis are illustrated in figure 5. The orientation of the antenna system, when mounted on the missile, with reference to the spherical coordinate system is illustrated in figure 6.

Assumptions and Approximations.

Before proceeding to calculate the far-field radiation patterns produced by the previously described antenna system, several idealizing assumptions and approximations are made to permit a theoretical analysis. In the first place, the missile body is 13 inches in diameter at the location of the antenna system and does not depart significantly from a circular cylinder for at least a wavelength in either direction. In the theoretical analysis a circular cylinder of infinite length is assumed. Also, the voltage distribution in the φ direction along the slot length is assumed to be cosinusoidal (maximum at center of slot) with only an axial field component, which is directed across the slot width in

the +z direction, i.e., toward the missile nose. This is in agreement with the method of slot excitation and the hypothesis that the tangential component of the electric field must be zero except where the slot opening exists, since the conductivity of the cylinder is assumed to be infinite, and the slot excitation by a cosinusoidal signal is in a manner which produces only an axial field component. Also, the conducting tab which projects part way across the center of the slot, thereby complicating an otherwise simple rectangular slot opening, is ignored in the theoretical analysis, since the effect on the far-field radiation pattern should be negligible, and the added theoretical complexity to account for the tab is considered to be unwarranted. From a practical viewpoint for Command Destruct purposes, the far field is the only one of interest.

Development of Theoretical Expressions.

Several different approaches may be used to calculate the desired radiation fields as discussed by Wait.[10-11] The following approach is based upon the work by Silver and Saunders[12] which assumes a harmonic field distribution in the slot with Fourier series representations for the tangential electric field over the cylinder and for the field in

---

[10] J. R. Wait, "A Survey of the Recent Literature on Slot Radiators", National Bureau of Standards Report No. 5051 of 11 March 1957.

[11] J. R. Wait, Electromagnetic Radiation from Cylindrical Structures, Pergamon Press, New York, N. Y., 1959.

[12] See reference 7.

space. The latter is synthesized by superposition of basic sets of cylindrical waves that satisfy the requisite boundry conditions. By making use of the asymptotic forms of the Hankel functions[13] and subsequently carrying out certain integrations[14] by the saddle-point method, general expressions which represent approximately the far-field radiation from a slot in an infinite-length, perfectly conducting, circular cylinder are obtained. As a preliminary step, some fundamental derivations beginning with Maxwell's field equations and leading to the wave equation expressed in phasor vector form are given in Appendix A (see equation 7). The time dependence of the harmonic fields is represented by the complex exponential factor $e^{j\omega t}$ in the customary manner, where $\omega = 2\pi$ times the exciting frequency and t represents time. In addition, Appendix A gives the derivation of the free-space propagation constant $k = \frac{2\pi}{\lambda}$, and the detailed calculations of the free-space wavelength $\lambda = 26.542$ inches for the specified operating frequency plus the evaluation of the fundamental parameter $ka = 1.53874$. The calculation of the circumferential arc length of the actual antenna slot opening at the outside surface of the missile body is given in Appendix B. This length equals 5.6789 inches and is equivalent to 0.2140λ, where λ is the free-space wavelength,

---

[13] G. N. Watson, A Treatise on the Theory of Bessel Functions, The MacMillan Company, New York, N. Y., 1944, pp. 73-74.

[14] See reference 7, pp. 156-157.

space. The latter is synthesized by superposition of basic sets of cylindrical waves that satisfy the requisite boundry conditions. By making use of the asymptotic forms of the Hankel functions[13] and subsequently carrying out certain integrations[14] by the saddle-point method, general expressions which represent approximately the far-field radiation from a slot in an infinite-length, perfectly conducting, circular cylinder are obtained. As a preliminary step, some fundamental derivations beginning with Maxwell's field equations and leading to the wave equation expressed in phasor vector form are given in Appendix A (see equation 7). The time dependence of the harmonic fields is represented by the complex exponential factor $e^{j\omega t}$ in the customary manner, where $\omega = 2\pi$ times the exciting frequency and $\underline{t}$ represents time. In addition, Appendix A gives the derivation of the free-space propagation constant $k = \frac{2\pi}{\lambda}$, and the detailed calculations of the free-space wavelength $\lambda = 26.542$ inches for the specified operating frequency plus the evaluation of the fundamental parameter $ka = 1.53874$. The calculation of the circumferential arc length of the actual antenna slot opening at the outside surface of the missile body is given in Appendix B. This length equals 5.6789 inches and is equivalent to 0.2140λ, where λ is the free-space wavelength,

---

[13] G. N. Watson, A Treatise on the Theory of Bessel Functions, The MacMillan Company, New York, N. Y., 1944, pp. 73-74.

[14] See reference 7, pp. 156-157.

Appendix C starts with the free-space wave equation of Appendix A and gives step-by-step methods for the solution in cylindrical coordinates in terms of a scalar function for the conventional steady-state time variation. The final solution involves Bessel functions of the third kind, or Hankel functions as they are more commonly called.

The detailed development of general expressions for the far field produced by a slot in the wall of an infinite-length circular cylinder is quite involved. It is started by developing a suitable Fourier expansion for the tangential components of the electric field over the surface of the cylinder. Then the external field is constructed by superposition of basic sets of cylindrical waves as indicated in the general theory by Stratton.[15] Hankel functions of the second kind and order n are involved in the solution of the differential equations to represent outgoing cylindrical waves. Considering only the far field--i.e., a distance greater than approximately 10 wavelengths--the expressions simplify to a large extent. The reduction of the general expressions for this region is effected by making use of the asymptotic forms of the Hankel functions and performing certain integrations by the saddle-point method. For this study the resulting general expressions[16] for the far-field

---

[15] J. A. Stratton, Electromagnetic Theory, McGraw-Hill Book Co., New York, N. Y., 1941, pp. 349—391.

[16] See equation 23 of reference 7, p. 157.

radiation from a slot of arbitrary shape in an infinite-length circular cylinder are restricted to a rectangular circumferential slot as illustrated in figure 5, which is bounded axially by the planes $z_1 = -z_o$ and $z_2 = +z_o$ and in azimuth by the planes $\varphi_1 = \frac{\pi}{2} - \varphi_o$ and $\varphi_2 = \frac{\pi}{2} + \varphi_o$ and is centered at $\varphi = \frac{\pi}{2}$, where it is understood that due to the difference in azimuth reference, φ and β are to be replaced by $\varphi - \frac{\pi}{2}$ and $\beta - \frac{\pi}{2}$, respectively. From the given slot excitation conditions the field components are separable functions of φ and $\underline{z}$; thus

$$E_\varphi(a,\varphi,z) = F_1(\varphi - \tfrac{\pi}{2})\, G_1(z) \qquad (1)$$

$$= 0 \text{ outside the slot,}$$

$$E_z(a,\varphi,z) = F_2(\varphi - \tfrac{\pi}{2})\, G_2(z) \qquad (2)$$

$$= 0 \text{ outside the slot,}$$

where

$$\frac{\pi}{2} - \varphi_o \leq \varphi \leq \frac{\pi}{2} + \varphi_o,$$

$$-z_o \leq z \leq +z_o .$$

Then considering a single mode of E_z and E_φ in the slot, the far-field radiation components[17] expressed in phasor[18] form reduce to equations (3) through (5) on taking $\frac{\ell}{2} = z_o$,

---

[17] See equation 4 of reference 8, p. 746.

[18] B. J. Ley, S. G. Lutz, and C. F. Rehberg, Linear Circuit Analysis, McGraw-Hill Book Co., New York, N. Y., 1959, pp. 134—136.

$$\overset{v}{E}_\theta \cong \frac{-e^{-jkR}}{R} \frac{1}{2\pi^2 \sin\theta} \sum_{n=-\infty}^{-\infty} \left\{ \frac{j^{n+1} e^{-jn(\varphi - \frac{\pi}{2})}}{H_n^{(2)}(ka \sin\theta)} \right.$$

$$\left. \times \int_{-z_o}^{z_o} \overset{v}{G}_2(\xi) e^{jk\xi \cos\theta} d\xi \int_{\frac{\pi}{2}-\varphi_o}^{\frac{\pi}{2}+\varphi_o} \overset{v}{F}_2(\beta - \tfrac{\pi}{2}) e^{jn(\beta - \frac{\pi}{2})} d\beta \right\}, \tag{3}$$

$$\overset{v}{E}_\varphi \cong \frac{e^{-jkR}}{R} \frac{1}{2\pi^2} \sum_{n=-\infty}^{+\infty} \frac{j^n e^{-jn(\varphi - \frac{\pi}{2})}}{H_n^{(2)'}(ka \sin\theta)} \left\{ \int_{-z_o}^{z_o} \overset{v}{G}_1(\xi) e^{jk\xi\cos\theta} d\xi \right.$$

$$\times \int_{\frac{\pi}{2}-\varphi_o}^{\frac{\pi}{2}+\varphi_o} \overset{v}{F}_1(\beta - \tfrac{\pi}{2}) e^{jn(\beta - \frac{\pi}{2})} d\beta + \frac{n \cot\theta}{ka \sin\theta}$$

$$\left. \times \int_{-z_o}^{z_o} \overset{v}{G}_2(\xi) e^{jk\xi\cos\theta} d\xi \int_{\frac{\pi}{2}-\varphi_o}^{\frac{\pi}{2}+\varphi_o} \overset{v}{F}_2(\beta - \tfrac{\pi}{2}) e^{jn(\beta - \frac{\pi}{2})} d\beta \right\}, \tag{4}$$

$$\overset{v}{E}_R \cong 0 \text{ being of the order of } \frac{1}{R^2} \tag{5}$$

where

$$\overset{v}{\vec{E}} = (\overset{v}{\vec{E}}_R, \overset{v}{\vec{E}}_\theta, \overset{v}{\vec{E}}_\varphi) = \vec{1}_R \overset{v}{E}_R + \vec{1}_\theta \overset{v}{E}_\theta + \vec{1}_\varphi \overset{v}{E}_\varphi, \tag{6}$$

with

$$\overset{v}{E}_R = \overset{v}{E}_R(R,\theta,\varphi), \tag{7}$$

$$\overset{v}{E}_\theta = \overset{v}{E}_\theta(R,\theta,\varphi), \tag{8}$$

$$\overset{v}{E}_\varphi = \overset{v}{E}_\varphi(R,\theta,\varphi), \tag{9}$$

and

$$\overset{v}{\vec{E}}(t) = \overset{v}{\vec{E}} e^{j\omega t} = \vec{1}_R \overset{v}{E}_R e^{j\omega t} + \vec{1}_\theta \overset{v}{E}_\theta e^{j\omega t} + \vec{1}_\varphi \overset{v}{E}_\varphi e^{j\omega t}. \tag{10}$$

In equations (3) through (5) the time dependence factor is suppressed and the unit directional vectors are omitted. The symbols $\overset{v}{\rightarrow}$ in, for example, equation (10) designate a phasor vector where it is understood that the real part of $\vec{E}(t)$ is used to obtain the time function, i.e.,

$$\vec{E}(t) = \mathrm{Re}[\vec{E}(t)] = \mathrm{Re}[\vec{E}e^{j\omega t}] \ . \tag{11}$$

Since the slot excitation is assumed to be a cosinusoidal function of φ (midpoint $\varphi = \frac{\pi}{2}$ has a maximum) and exhibits a constant field in the z direction, then

$$\vec{F}_1 = \vec{G}_1 = 0 \tag{12}$$

$$\vec{F}_2(\varphi - \tfrac{\pi}{2}) = \cos \frac{\pi}{2\varphi_o}(\beta - \tfrac{\pi}{2}) \tag{13}$$

$$\tfrac{\pi}{2} - \varphi_o \leq \beta \leq \tfrac{\pi}{2} + \varphi_o \ ;$$

$$\vec{G}_2(z) = \frac{V}{2z_o} \tag{14}$$

$$-z_o \leq z \leq +z_o \ ,$$

where V is the voltage across the center of the slot and $2z_o$ is small ($2z_o$ = 1 inch by figure 3) in comparison to R and the wavelength. For these conditions the integral over the slot width in equations (3) and (4) reduces to

$$I_z = \int_{-z_o}^{z_o} \vec{G}_2(\xi) e^{jk\xi\cos\theta} d\xi = \frac{V}{2z_o} \int_{-z_o}^{z_o} e^{jk\xi\cos\theta} d\xi \ ;$$

or

$$I_z = \frac{V}{2z_o jk\cos\theta} e^{jk\xi\cos\theta}\Big]_{-z_o}^{z_o}$$

$$I_z = \frac{V}{2z_o jk \cos\theta}\left[e^{jkz_o\cos\theta} - e^{-jkz_o\cos\theta}\right]$$

$$= \frac{V}{2jz_o k \cos\theta}\, 2j \sin(kz_o\cos\theta)$$

$$= V\,\frac{\sin(kz_o\cos\theta)}{kz_o\cos\theta} \cong V\ , \qquad (15)$$

where by the small angle sine function approximation

$$\sin(kz_o\cos\theta) = \sin\left[\frac{2\pi(0.5\text{ inch})\cos\theta}{26.54\text{ inches}}\right]$$

$$= \sin(0.118\cos\theta)$$

$$\cong 0.118\cos\theta\ .$$

Likewise, in equations (3) and (4) the integral over the slot length angle for a free-space $\frac{\lambda}{2}$ length slot, reduces to

$$\int_{\frac{\pi}{2}-\varphi_o}^{\frac{\pi}{2}+\varphi_o} V F_2(\beta-\tfrac{\pi}{2}) e^{jn(\beta-\frac{\pi}{2})} d\beta = \int_{-\varphi_o}^{\varphi_o} V F_2(\beta) e^{jn\beta} d\beta$$

$$= \frac{2ka\cos\frac{n\pi}{2ka}}{(ka)^2 - n^2}\ ; \qquad (16)$$

and for the dielectric-loaded slot with a physical arc length of 0.2140λ where λ is the free-space wavelength

$$\int_{\frac{\pi}{2}-\varphi_o'}^{\frac{\pi}{2}+\varphi_o'} V F_2(\beta-\tfrac{\pi}{2}) e^{jn(\beta-\frac{\pi}{2})} d\beta = \int_{-\varphi_o'}^{\varphi_o'} V F_2(\beta) e^{jn\beta} d\beta$$

$$= \frac{\frac{ka}{0.2140}\cos n\,\frac{0.2140\pi}{ka}}{2} \equiv F(n,ka). \qquad (17)$$

$$\left(\frac{ka}{0.4280}\right) - n^2$$

Details of the integral evaluations [equations (16) and (17)] are given in Appendix D.

Also, from equation (3) the summation

$$S_1 = \sum_{n=-\infty}^{+\infty} \frac{-j^{n+1} e^{-jn(\varphi - \frac{\pi}{2})}}{H_n^{(2)}(ka \sin\theta)} F(n,ka) \qquad (18)$$

can be reduced to

$$S_1 = \sum_{n=0}^{+\infty} \frac{\varepsilon_n e^{j(n-1)\frac{\pi}{2}}}{H_n^{(2)}(ka \sin\theta)} \cos n(\varphi - \tfrac{\pi}{2}) F(n,ka), \qquad (19)$$

where

$$\varepsilon_n = \begin{cases} 1 \text{ for } n = 0 \\ 2 \text{ for } n > 0 \end{cases} . \qquad (20)$$

This can be shown as follows (since F(n,ka) is an even function of $\underline{n}$):

$$-j^{n+1} \equiv -j\, j^n \equiv e^{-j\frac{\pi}{2}} e^{jn\frac{\pi}{2}} \equiv e^{j(n-1)\frac{\pi}{2}} \; ; \qquad (21)$$

and

$$H_{-n}^{(2)}(ka \sin\theta) = (-1)^n H_n^{(2)}(ka \sin\theta); \qquad (22)$$

therefore,

$$S_1 = \frac{-j[F(0,ka)]}{H_o^{(2)}(ka \sin\theta)} + \sum_{n=1}^{+\infty} \frac{-j\, j^n e^{-jn(\varphi - \frac{\pi}{2})}}{H_n^{(2)}(ka \sin\theta)}$$

$$+ \frac{-j\, j^{-n} e^{jn(\varphi - \frac{\pi}{2})}}{(-1)^n H_n^{(2)}(ka \sin\theta)} F(n,ka); \qquad (23)$$

but

$$j^{-n} = \frac{j^{-n}\, j^{-n}}{j^{-n}} = \frac{j^{-2n}}{j^{-n}} = \frac{(j^{-2})^n}{j^{-n}} = \frac{(-1)^n}{j^{-n}} = (-1)^n j^n; \qquad (24)$$

hence,

$$S_1 = \frac{-j[F(0,ka)]}{H_o^{(2)}(ka \sin\theta)} + \sum_{n=1}^{+\infty} \left\{ -j\, j^n \right.$$

$$\left. \times \frac{e^{jn(\varphi - \frac{\pi}{2})} + e^{-jn(\varphi - \frac{\pi}{2})}}{H_n^{(2)}(ka \sin\theta)} F(n,ka); \right. \tag{25}$$

however,

$$e^{jn(\varphi - \frac{\pi}{2})} + e^{-jn(\varphi - \frac{\pi}{2})} = \varepsilon_n \cos n(\varphi - \tfrac{\pi}{2}) \ , \tag{26}$$

where ε_n is defined by equation (20). Therefore, using equations (21) and (26) in equation (25)

$$S_1 = \sum_{n=0}^{+\infty} \frac{\varepsilon_n\, e^{j(n-1)\frac{\pi}{2}}}{H_n^{(2)}(ka \sin\theta)} \cos n(\varphi - \tfrac{\pi}{2})\, F(n,ka) \ . \tag{27}$$

Likewise, from equation (4) the term

$$S_2 = \frac{n \cot\theta}{ka \sin\theta} \sum_{n=-\infty}^{+\infty} \frac{j^n\, e^{-jn(\varphi - \frac{\pi}{2})}}{H_n^{(2)'}(ka \sin\theta)} F(n,ka) \tag{28}$$

can be reduced to

$$S_2 = \frac{\cos\theta}{ka \sin^2\theta} \sum_{n=1}^{+\infty} \frac{-2n\, e^{j(n-1)\frac{\pi}{2}}}{H_n^{(2)'}(ka \sin\theta)} \sin n(\varphi - \tfrac{\pi}{2})\, F(n,ka) \ . \tag{29}$$

This can be shown as follows: From equations (22) and (24), equation (28) reduces to

$$S_2 = \frac{\cot\theta}{ka \sin\theta} \sum_{n=1}^{+\infty} \left[\frac{n j^n\, e^{-jn(\varphi - \frac{\pi}{2})}}{H_n^{(2)'}(ka \sin\theta)} \right.$$

$$\left. + \frac{-n(-1)^n j^n\, e^{jn(\varphi - \frac{\pi}{2})}}{(-1)^n H_n^{(2)'}(ka \sin\theta)} \right] F(n,ka) \ , \tag{30}$$

since

$$H_n^{(2)'}(ka \sin\theta) = \frac{d\, H_n^{(2)}(ka \sin\theta)}{d(ka \sin\theta)}$$

$$= \frac{H_{n-1}^{(2)}(ka \sin\theta) - H_{n+1}^{(2)}(ka \sin\theta)}{2}, \tag{31}$$

giving

$$H_{-n}^{(2)'}(ka \sin\theta) = (-1)^n H_n^{(2)'}(ka \sin\theta) \tag{32}$$

by use of equations (22) and (31). Then by the substitution of

$$\cot\theta = \frac{\cos\theta}{\sin\theta} \tag{33}$$

and by equation (30),

$$S_2 = \frac{\cos\theta}{ka \sin^2\theta} \sum_{n=1}^{+\infty} nj^n \left[\frac{e^{-jn(\varphi - \frac{\pi}{2})} - e^{jn(\varphi - \frac{\pi}{2})}}{H_n^{(2)'}(ka \sin\theta)}\right] F(n,ka) ; \tag{34}$$

but

$$e^{jn(\varphi - \frac{\pi}{2})} - e^{-jn(\varphi - \frac{\pi}{2})} = 2j \sin n(\varphi - \tfrac{\pi}{2}) ; \tag{35}$$

therefore,

$$S_2 = \frac{\cos\theta}{ka \sin^2\theta} \sum_{n=1}^{+\infty} \frac{-2nj\, j^n \sin n(\varphi - \frac{\pi}{2})}{H_n^{(2)'}(ka \sin\theta)} F(n,ka) . \tag{36}$$

Substituting for $-j\, j^n$ from equation (21), then

$$S_2 = \frac{\cos\theta}{ka \sin^2\theta} \sum_{n=1}^{+\infty} \frac{2n\, e^{j(n-1)\frac{\pi}{2}}}{H_n^{(2)'}(ka \sin\theta)} \sin n(\varphi - \tfrac{\pi}{2})\, F(n,ka) . \tag{37}$$

Therefore, for a narrow circumferential one-half wavelength slot in free space, equations (3) through (5) reduce to

$$\overset{v}{E}_\theta \cong \frac{e^{-jkR}}{R} V \overset{v}{P}_\theta(\theta,\varphi), \tag{38}$$

$$\overset{v}{E}_\varphi \cong \frac{e^{-jkR}}{R} V \overset{v}{P}_\varphi(\theta,\varphi), \tag{39}$$

and

$$\overset{v}{E}_R \cong 0, \tag{40}$$

where

$$\overset{v}{P}_\theta = \frac{ka}{\pi^2 \sin\theta} \sum_{n=0}^{\infty} \frac{\varepsilon_n e^{j(n-1)\frac{\pi}{2}}}{H_n^{(2)}(ka \sin\theta}$$

$$x \frac{\cos \frac{n\pi}{2ka}}{(ka)^2 - n^2} \cos n(\varphi - \tfrac{\pi}{2}) \tag{41}$$

with

$$\varepsilon_n = \begin{cases} 1 \text{ for } n = 0 \\ 2 \text{ for } n > 0 \text{ ;} \end{cases}$$

and

$$\overset{v}{P}_\varphi = \frac{ka \cos\theta}{\pi^2 ka \sin^2\theta} \sum_{n=1}^{\infty} \frac{2n\, e^{j(n-1)\frac{\pi}{2}}}{H_n^{(2)'}(ka \sin\theta)}$$

$$x \frac{\cos \frac{n\pi}{2ka}}{(ka)^2 - n^2} \sin n(\varphi - \tfrac{\pi}{2}) \text{ .} \tag{42}$$

And for the narrow dielectric-loaded slot with a physical arc length of 0.2140λ where λ is the free-space wavelength, equations (3) through (5) reduce to

$$\overset{v}{E}_\theta \cong \frac{e^{-jkR}}{R} V \overset{v}{P}_\theta(\theta,\varphi), \tag{43}$$

$$\overset{v}{E}_\varphi \cong \frac{e^{-jkR}}{R} V \overset{v}{P}_\varphi(\theta,\varphi), \tag{44}$$

$$\overset{v}{E}_R \cong 0, \tag{45}$$

where the pattern functions $\overset{v}{P}_\theta$ and $\overset{v}{P}_\varphi$ are

$$\overset{v}{P}_\theta = \frac{1}{2\pi^2 \sin\theta} \sum_{n=0}^{\infty} \frac{\varepsilon_n e^{j(n-1)\frac{\pi}{2}}}{H_n^{(2)}(ka \sin\theta)} \times \frac{\frac{ka}{0.2140} \cos n\frac{0.2140\pi}{ka}}{(\frac{ka}{0.4280})^2 - n^2} \cos n(\varphi - \tfrac{\pi}{2}) \tag{46}$$

with

$$\varepsilon_n = \begin{cases} 1 \text{ for } n = 0 \\ 2 \text{ for } n > 0 \end{cases};$$

and

$$\overset{v}{P}_\varphi = \frac{\cos\theta}{2\pi^2 ka \sin^2\theta} \sum_{n=1}^{\infty} \frac{2n\, e^{j(n-1)\frac{\pi}{2}}}{H_n^{(2)'}(ka \sin\theta)} \times \frac{\frac{ka}{0.2140} \cos n\frac{0.2140\pi}{ka}}{(\frac{ka}{0.4280})^2 - n^2} \sin n(\varphi - \tfrac{\pi}{2}) \; . \tag{47}$$

Calculation of Radiation Patterns from Two Diametrically Opposed Slots Considered Separately.

Since the theoretical radiation patterns are to be compared with the experimental results on a relative basis, it is necessary to calculate only the pattern functions [equations (46) and (47)], omitting the amplitude multiplier and the time and space exponential factors. To determine the radiation patterns first from the two diametrically opposed slots, assuming that each slot is operating independently,

and then from both slots operating simultaneously with controlled electrical phasing between the slots, a large number of calculations are involved. Also, both pattern functions contain series summations of complex quantities which make the calculations difficult and very time consuming to do by hand methods, even with the aid of a desk calculator. For these reasons, arrangements were made to program the desired calculations for an IBM 704 Computer. Considerable difficulty was experienced at first in getting the functions programed correctly; however, once this was accomplished, the results were obtained quickly and accurately.

Table 1 gives the amplitude and phase (in degrees) of $\overset{v}{P}_{\theta_1}(\theta,\varphi)$, $\overset{v}{P}_{\theta_2}(\theta,\varphi+\pi)$, $\overset{v}{P}_{\varphi_1}(\theta,\varphi)$ and $\overset{v}{P}_{\varphi_2}(\theta,\varphi+\pi)$ where the subscripts 1 and 2 designate the first slot centered at $\varphi = \frac{\pi}{2}$ and the second slot centered at $\varphi = -\frac{\pi}{2}$, respectively. The computations were made for φ varied in 10-degree increments from -90 to +90 degrees for each 5-degree increment of θ from 5 to 90 degrees. By trial and error it was found that eight terms are necessary to obtain three-significant-figure accuracy over the full spherical range; therefore, all data presented in tables 1 through 3 involve eight terms in the summations. Figures 7 through 15 give polar plots of the amplitudes of $\overset{v}{P}_{\theta_1}$ and $\overset{v}{P}_{\varphi_1}$ from the data given in table 1. Only the pattern function amplitudes are plotted since no phase measurements were obtained experimentally; therefore,

the comparisons between theoretical and experimental results are confined to amplitudes.

From the symmetry of the $\overset{v}{P}_{\theta}$ function, the full spherical pattern can be developed from the results for only one quadrant of θ values and two quadrants of φ values. This is obvious since the sine θ terms give symmetry for the first and second quadrants about $\theta = 90^{o}$ and the cosine $n(\varphi - \frac{\pi}{2})$ term gives symmetry about the $\varphi = 90^{o}$ plane. Therefore, the required two quadrants of θ values and all four quadrants of φ values can be developed from the data given in table 1. Since the function $\overset{v}{P}_{\theta_2}$ is identical to $\overset{v}{P}_{\theta_1}$ with a 180-degree phase shift, then $\overset{v}{P}_{\theta_2}$ for $\varphi = +90^{o}$ to -90^{o} is identical to $\overset{v}{P}_{\theta_1}$ for $\varphi = -90^{o}$ to $+90^{o}$. It is of interest to note that the $\overset{v}{P}_{\theta}$ functions become infinite for $\theta = 0^{o}$ or 180^{o} and multiples thereof, due to the sine θ term in the denominator.

Similarly, the full spherical pattern for the $\overset{v}{P}_{\varphi}$ function can be developed from the results for only one quadrant of θ values and two quadrants of φ values, provided a 180-degree phase shift is introduced for the second quadrant of θ and for the second and third quadrants of φ values to account for the antisymmetrical characteristics. This is obvious from the fact that the $\frac{\cos \theta}{\sin \theta}$ term introduces antisymmetry about the $\theta = 90^{o}$ plane and the sin $n(\varphi - \frac{\pi}{2})$ term introduces antisymmetry about the $\varphi = 90^{o}$ plane. It is of interest to note that the $\overset{v}{P}_{\varphi}$ function is zero for $\theta = 90^{o}$

the comparisons between theoretical and experimental results are confined to amplitudes.

From the symmetry of the $\overset{v}{P}_{\theta}$ function, the full spherical pattern can be developed from the results for only one quadrant of θ values and two quadrants of φ values. This is obvious since the sine θ terms give symmetry for the first and second quadrants about $\theta = 90^{o}$ and the cosine $n(\varphi - \frac{\pi}{2})$ term gives symmetry about the $\varphi = 90^{o}$ plane. Therefore, the required two quadrants of θ values and all four quadrants of φ values can be developed from the data given in table 1. Since the function $\overset{v}{P}_{\theta_2}$ is identical to $\overset{v}{P}_{\theta_1}$ with a 180-degree phase shift, then $\overset{v}{P}_{\theta_2}$ for $\varphi = +90^{o}$ to -90^{o} is identical to $\overset{v}{P}_{\theta_1}$ for $\varphi = -90^{o}$ to $+90^{o}$. It is of interest to note that the $\overset{v}{P}_{\theta}$ functions become infinite for $\theta = 0^{o}$ or 180^{o} and multiples thereof, due to the sine θ term in the denominator.

Similarly, the full spherical pattern for the $\overset{v}{P}_{\varphi}$ function can be developed from the results for only one quadrant of θ values and two quadrants of φ values, provided a 180-degree phase shift is introduced for the second quadrant of θ and for the second and third quadrants of φ values to account for the antisymmetrical characteristics. This is obvious from the fact that the $\frac{\cos \theta}{\sin \theta}$ term introduces antisymmetry about the $\theta = 90^{o}$ plane and the sin $n(\varphi - \frac{\pi}{2})$ term introduces antisymmetry about the $\varphi = 90^{o}$ plane. It is of interest to note that the $\overset{v}{P}_{\varphi}$ function is zero for $\theta = 90^{o}$

and for all odd multiples of 90 degrees. Also, the same situation exists for $\varphi = \pm 90^{o}$ and for all even multiples of 90 degrees. Since the $\overset{v}{P}_{\varphi_2}$ function is identical to $\overset{v}{P}_{\varphi_1}$ with a 180-degree phase shift, then $\overset{v}{P}_{\varphi_2}$ for $\varphi = +90^{o}$ to -90^{o} is identical to $\overset{v}{P}_{\varphi_1}$ for $\varphi = -90^{o}$ to $+90^{o}$, provided a 180-degree phase shift is introduced to account for the antisymmetry of the $\overset{v}{P}_{\varphi}$ function.

Calculation of Radiation Patterns from Two Diametrically Opposed Slots Operating Simultaneously with Selected Electrical Phasing.

To obtain the radiation patterns produced when both of the diametrically opposed slots are operating simultaneously, the patterns from both slots were added vectorially to give

$$\overset{v}{P}_{\theta}' = |\overset{v}{P}_{\theta_1}(\theta,\varphi)|\underline{/\alpha_1} + |\overset{v}{P}_{\theta_2}(\theta,\varphi+\pi)|\underline{/\alpha_2+\beta} \qquad (48)$$

and

$$\overset{v}{P}_{\varphi}' = |\overset{v}{P}_{\varphi_1}(\theta,\varphi)|\underline{/\alpha_1} + |\overset{v}{P}_{\varphi_2}(\theta,\varphi+\pi)|\underline{/\alpha_2+\beta} \qquad (49)$$

where $|\overset{v}{P}(\theta,\varphi)|$ and $\underline{/\alpha}$ designate the amplitude and phase angle, respectively, and β designates a selected phase angle which is included in order to study the effect of deliberately introducing a controlled phase shift between the two antennas. In practice the controlled phase shift would normally be accomplished by introducing an appropriate difference in the cable lengths between the antennas and the tee connector. The summation functions $\overset{v}{P}_{\theta}'$ and $\overset{v}{P}_{\varphi}'$ were

each computed for the conditions where θ is varied in 10-degree increments from 10 to 90 degrees; φ is varied in 10-degree increments from -90 to +90 degrees; and β is varied in 60-degree increments from 0 to 180 degrees. The results of these computations are given in table 2 and the corresponding radiation pattern plots are given in figures 16 through 51. The $\overset{v}{P}_{\varphi}'$ function is plotted only for the cases where $\beta = 0^{o}$ and 180^{o}, since this function is of secondary interest and there are no experimental data for comparison. In addition, the data for two longitudinal patterns are given in table 3 for the conditions where the phase angle $\beta = 0^{o}$ and θ is varied in 5-degree increments from 5 to 175 degrees and $\varphi = 90^{o}$ and 180^{o}, respectively. Figures 52 and 53 give polar pattern plots of the $\overset{v}{P}_{\theta}'$ amplitudes from the data given in table 3.

EXPERIMENTAL MEASUREMENTS

Model Configuration.

For the experimental measurements, a full scale mock-up of the warhead section was fabricated from aluminum sheet stock. The mock-up warhead contained provisions for mounting two Command Destruct antennas, three beacon antennas, and two telemetry antennas. The two Command Destruct antennas were mounted diametrically opposed at the desired longitudinal location. The three beacon antennas and the two telemetry antennas were also installed during certain tests to reveal the extent, if any, of interference between the three antenna systems when all were operating simultaneously. Since a full scale mock-up of the entire weapon was too large for the antenna range-measuring equipment, only the warhead section and a short portion of the cylindrical body immediately aft of the warhead were used.

Coordinate System and Description of Radiation Pattern Measurements.

The spherical coordinate system used for pattern measurements is illustrated in figure 5. Pattern measurements were made for the E_θ component only and at 10-degree increments of θ from $\theta = 0^\circ$ to 180°. These were made by rotating the mock-up about the missile axis for a complete revolution for each value of θ. Figure 54 illustrates the technique used to obtain the pattern measurements. The missile mock-up was mounted on a standoff pedestal in a

horizontal position. Rotation of the mock-up about its own horizontal axis and rotation in the horizontal plane about a vertical axis which passes through the center point between the two antennas were made by remote control. By making use of the reciprocity theorem, the radiation patterns were obtained using the missile antennas as receiving antennas. The latter was illuminated by a directional, fixed-position, horizontally polarized, transmitting antenna, mounted on a nearby tower about 30 feet from the missile mock-up in the same horizontal plane as the missile. When the missile nose points directly toward the radiating antenna, i.e., the projected missile axis passes through the center of the radiating antenna, the angle $\theta = 0^{o}$. With the missile in this position, a pattern is taken by rotating the missile for one full revolution about its own axis; this corresponds to a rotation in the φ direction from $\varphi = 0^{o}$ to 360^{o}. The same technique was repeated for each 10-degree increment of θ from $\theta = 0^{o}$ to 180^{o}. The 19 patterns obtained in this manner are given in figures 55 through 73. In addition, two longitudinal patterns were made for the E_{θ} component by rotating the missile from $\theta = 0^{o}$ to 360^{o} for a constant value of φ. Figure 74 gives the longitudinal pattern for $\varphi = 90^{o}$ which passes through the center of the slots, and figure 75 gives the longitudinal pattern for $\varphi = 180^{o}$ which is a plane bisecting the angle between the two slots.

Interference Tests

Since it is vitally important to communicate a Command Destruct signal from the ground station to an erratic missile, interference tests were made to determine whether simultaneous operation of the telemetry and tracking beacon systems adversely affect the Command Destruct System. Figures 76 through 87 give the results of these tests for $\theta = 90^{o}$, 135^{o}, and 165^{o}. Four patterns were made for each θ value for the following conditions, respectively:

a. Command Destruct System only.

b. Command Destruct System with beacon operating.

c. Command Destruct System with telemetry radiating full power at the most adverse frequency assignment.

d. Command Destruct System with both beacon and telemetry radiating.

ANALYSIS OF EXPERIMENTAL DATA

Description of Graphical Integration Techniques.

Using the Poynting vector method,[19] the set of experimentally obtained conical radiation patterns can be analyzed by graphical integration techniques to give, on a relative basis, the total energy received (or radiated) and the average effective field strength of the Command Destruct Antenna System. The antenna system is assumed to be at the center of a very large sphere; and by an averaging process, the set of conical radiation patterns are related to the spherical surface which is then integrated by graphical summation techniques.

Since the family of conical patterns was made with a polar recorder with response set for a square-root function to compensate for the square-law detector used, the resulting patterns are voltage or field-strength plots. Therefore, the relative effective field strength is directly proportional to the average radius of the respective patterns, and the average radius squared is directly proportional to the effective radiation intensity. For a given θ angle, the relative effective field strength is defined as the field strength which, if constant for a full revolution of φ, represents the

---

[19] F. E. Terman, Radio Engineer's Handbook, McGraw Hill Book Co., New York, N. Y., 1943, pp. 782—784.

same total energy as the actual field pattern. In other words, an average radius is found which, when revolved a full revolution of φ, describes a circle which has the same inscribed area as the inscribed area of the pattern. The average radius squared for each conical pattern is found by measuring the inscribed pattern area with a planimeter and dividing the area by π.

Relative Field Strength Calculations.

Referring to the spherical diagram of figure 88, an elemental surface area dA is generated if a segment of arc $Rd\theta$ is revolved through an angle $d\varphi$ giving a surface area of

$$R \sin \theta d\varphi \cdot Rd\theta = R^2 \sin \theta d\theta d\varphi \qquad (50)$$

and the total surface area of the sphere is

$$\int_{\varphi=0}^{2\pi} \int_{\theta=0}^{\pi} R^2 \sin \theta d\theta d\varphi = 4\pi R^2 \text{ for a constant R.} \qquad (51)$$

If we let E = the instantaneous field-strength pattern measurements which are a $f(\theta,\varphi)$, then by definition

$$E^2_{avg} = \frac{1}{4\pi R^2} \int_{\varphi=0}^{2\pi} \int_{\theta=0}^{\pi} E^2(\theta,\varphi) R^2 \sin \theta d\theta d\varphi \ . \qquad (52)$$

Since E was measured as a continuous function of φ from $\varphi = 0$ to 2π, for finite increments of $\theta = \frac{\pi}{18}$ or 10^o, then by the trapezoidal rule

$$E^2_{avg} \cong \frac{1}{4\pi R^2} \sum_{i=1}^{18} \frac{\pi}{18} \int_{\varphi=0}^{2\pi} E^2(\theta_i,\varphi) R^2 \sin \theta_i d\varphi \qquad (53)$$

where i refers to $\theta = 10^o, 20^o \ldots\ldots 180^o$. Since R is taken as constant, then

$$E^2_{avg} = \frac{1}{4\pi} \frac{\pi}{18} \sum_{i=1}^{18} \sin \theta_i \int_{\varphi=0}^{2\pi} E^2(\theta_i, \varphi) d\varphi$$

$$= \frac{1}{2\pi} \frac{\pi}{36} \sum_{i=1}^{18} \sin \theta_i \int_{\varphi=0}^{2\pi} E^2_i(\varphi) d\varphi \qquad (54)$$

where by definition

$$E^2_i(\varphi) = E^2(\theta_i, \varphi) \qquad (55)$$

then

$$E^2_{i\,avg} = \frac{1}{2\pi} \int_{\varphi=0}^{2\pi} E^2_i \, d\varphi \qquad (56)$$

therefore

$$E^2_{avg} = \frac{\pi}{36} \sum_{i=1}^{18} E^2_{i\,avg} \sin \theta_i$$

$$= \frac{1}{36} \sum_{i=1}^{18} \pi E^2_{i\,avg} \sin \theta_i \, . \qquad (57)$$

But $E^2_{i\,avg}$ equals the average relative field strength squared of the respective conical patterns, and the respective pattern areas are equal to the average field strength squared multiplied by π. Therefore, the process of graphical integration reduces to a process of measuring the individual conical pattern areas and multiplying each area by the sine of the corresponding θ angle, and then forming a summation of the results.

For the patterns given in figures 55 through 73, the total summation of the pattern areas, after each is multiplied by the corresponding sine of θ, is 156.645 square inches. The individually tabulated area values are given in table 4. Therefore, the average relative field strength expressed in inches of pattern radius is

$$E_{avg} = \sqrt{\frac{156.645}{36}} = \sqrt{4.35125} = 2.086 \qquad (58)$$

Since the polar pattern charts are divided radially into 10 major scale units of 0.375 inches per unit, then

$$1 \text{ inch} = \frac{8}{3} \text{ scale units}$$

and the relative field strength is equivalent to 5.5626 scale units since

$$2.086 \text{ inches } \frac{8}{3} \frac{\text{scale units}}{\text{inch}} = 5.5626 \text{ scale units.}$$

The power radiated by the actual antenna system is unknown; however, it is known that the radiation pattern of an equivalent isotropic radiator (in radiated energy) can be represented by a spherical pattern with a radius of 5.5626 scale units. If it is now assumed that 1 watt is being radiated and that the field measurements are made at a distance of 1 mile, then each scale unit of the pattern radius is equivalent to

$$\frac{3.404 \text{ millivolts/meter}}{5.5626 \text{ scale units}}$$

= 0.6119 millivolts/meter/scale unit(1 watt, 1 statue mile). Since the power density P_d at a point in space due to the power transmitted P_t from an isotropic radiator[20] is

$$P_d = \frac{P_t}{4\pi R^2}$$

---

[20]International Telephone and Telegraph Corp., Reference Data for Radio Engineers (4th ed.), American Book-Stratford Press, Inc., New York, N. Y., 1956.

where P_t is in watts and R is in meters, and

$$E^2 = P_d(120\pi)$$

where E is in volts per meter, then

$$E^2 = \frac{P_t}{4\pi R^2}(120\pi) = \frac{30P_t}{R^2}$$

or

$$E = \frac{\sqrt{30\ P_t}}{R} = \frac{\sqrt{30}}{1609} = 3.404 \text{ millivolts/meter.} \quad (59)$$

Therefore for the assumed conditions of 1 watt at 1 mile, the field strength in millivolts per meter in any of the measured (θ,φ) defined directions is simply the number of pattern radius scale units times 0.6119. For example, the maximum field strength occurs at approximately $\theta = 140^o$ with a pattern radius of about 9 scale units which is equivalent to 5.5 millivolts per meter. The pattern shape at this conical angle is almost circular, indicating nearly uniform field strength for the full revolution of φ.

Directivity, Gain, and Bandwidth Characteristics.

The antenna system directivity D is defined as the ratio of the maximum radiation intensity of the test antenna to the maximum radiation intensity of the reference antenna, with the same input to both. Since in this case the only reference antenna is an equivalent isotropic source, the directivity is

$$D = \frac{\text{maximum radiation intensity}}{\text{average radiation intensity}} . \quad (60)$$

If both numerator and denominator are multiplied by 4π, the directivity is

$$D = \frac{4\pi \text{ (maximum radiation intensity)}}{\text{total power radiated}}$$

$$= \frac{4\pi \, f(\theta,\varphi)_{max}}{\iint f(\theta,\varphi) \, d\Omega} \tag{61}$$

where $f(\theta,\varphi)$ = relative radiation intensity as a function of the space angles (θ,φ) and $d\Omega = \sin\theta d\theta d\varphi$ = element of solid angle.

Since the radiation intensity is proportional to the square of the field strength, the directivity can be expressed as

$$D = \frac{4\pi \, [F^2(\theta,\varphi)_{max}]}{\iint F^2(\theta,\varphi) \, d\Omega}$$

$$\frac{4\pi \, [F^2(\theta,\varphi)_{max}]}{\int_{\varphi=0}^{2\pi} \int_{\theta=0}^{\pi} F^2(\theta,\varphi) \sin\theta d\theta d\varphi} \tag{62}$$

where $F(\theta,\varphi)$ = relative field pattern, i.e., the total field intensity as a function of θ and φ.

For the conical patterns given in figures 55 through 73, the maximum relative field strength occurs at a conical angle of approximately $\theta = 140^{\circ}$ with a pattern radius of about 9.0 scale units; therefore the directivity is

$$D = \frac{4\pi \, (9.0)^2}{4\pi \, (5.563)^2} = \frac{81}{30.95} = 2.62 \, . \tag{63}$$

The gain of an antenna is always measured with respect to a reference antenna. Since an isotropic source is a hypothetical reference, it is common practice to make actual gain measurements with respect to a one-half wavelength dipole. If the dipole antenna is assumed to be lossless,

then the gain of the dipole over a lossless isotropic source is 1.64 on a power basis or $\sqrt{1.64} = 1.28$ on a voltage basis[21]. For the system being analyzed, no actual gain measurements were made; therefore, if the system is assumed to be lossless, the gain equals the directivity.

Figure 89 gives a plot of the measured voltage standing-wave ratio as a function of the input frequency, when the Command Destruct Antenna is terminated in a 50-ohm resistive load. The voltage standing-wave ratio is about 1.15 at the center frequency of 445 megacycles, indicating a good impedance match to the 50-ohm load. The bandpass characteristics on each side of the center frequency are indicated by a voltage standing-wave ratio of about 1.4 at ±2 megacycles and about 5.0 at ±10 megacycles.

Results of Interference Tests.

The results of the interference tests to determine if the simultaneous operation of the telemetry and radar tracking beacon adversely affects the Command Destruct System were negative. This is determined by comparing the radiation patterns of the Command Destruct System when operated alone against the pattern obtained when one or both of the other radiating antenna systems are operating. For example, if figure 76 is superimposed on either figures 77, 78 or 79,

---

[21] H. R. Reed and C. M. Russell, Ultra High Frequency Propagation, John Wiley and Sons, Inc., New York, N. Y., 1953, p. 78.

no significant pattern distortion is noted. Likewise, for the other conical angles of $\theta = 135^{o}$ and 165^{o}, the Command Destruct radiation pattern is not disturbed significantly by the presence of the radiation fields from either the telemetry or the beacon or from both the telemetry and beacon systems operating simultaneously with the Command Destruct System.

Since the second harmonic of the telemetry system when operating at 227.2 megacycles is close to the Command Destruct frequency, cross coupling could be a problem. To check for this effect, a tuned radio receiver having a minimum input sensitivity of 11 microvolts across a 50-ohm load was connected to the Command Destruct Antenna System output and tuned to 445 megacycles. With the telemetry system operating at full-power output, no coupling was detectable.

DISCUSSION OF RESULTS

In practice, the geometrical configuration of a typical missile body presents a formidable task to take into account the full effect of the complex geometry on the radiation patterns produced by a flush-mounted slot-antenna system. This soon becomes apparent when an attempt is made to develop an accurate mathematical model to describe the radiation characteristics of a practical application of a missile antenna system such as the one considered in this study.

In order to make the theoretical analysis feasible in this case, it was necessary to idealize the geometrical shape of the missile body so that the general mathematical expressions which have been derived for describing the radiation from slots in circular cylinders could be applied. The applicable theoretical expressions for describing the far-field radiation from a narrow circumferential slot in a circular cylinder involves several significant assumptions and approximations. In the first place, the missile is assumed to be a perfectly conducting, constant-diameter, circular cylinder of infinite length in both directions from the antenna slots, and the slot field distribution is assumed to vary cosinusoidally along the slot length and to be constant across the slot width. Also, the theoretical expressions are not valid for conical elevation angles at or near the missile axis. The lack of validity of, for example, the

E_θ expression when the elevation angle coincides with the missile axis can be readily seen by observing that the sine θ term in the denominator causes the expression to become infinite when $\theta = 0^o$ or 180^o. Also, the Hankel function cannot be used to express physically finite fields in the neighborhood of the origin due to the singularity of the Newman function at the origin--*i.e.*, $Y_n(x)$ becomes infinite in the negative direction for $x = 0$. Furthermore, the asymptotic form of the Hankel function which has been used in deriving the general far-field cylinder expressions is valid only when the argument ($kR \sin \theta$) is large in comparison to unity.[22] Therefore, to maintain validity of the far-field expressions, the fields near the origin and the two solid angles of $\theta \leq 30^o$ on both ends of the missile axis must be disregarded.

By inspection of figures 7 through 15 which give the calculated radiation patterns for a single slot positioned at $\varphi = 90^o$, for each 10-degree angle of θ from 10 to 90 degrees, it can be observed that the pattern starts increasing rapidly as θ becomes less than 30 degrees. This is even more apparent when it is noted that the patterns for $\theta = 10^o$ (figure 7) are plotted to a scale which is one-half of that used for the patterns given in figures 8 through 15. A slight increase in the pattern function amplitude is to be expected as θ approaches the missile axis due to the effect of the finite curvature of the slot. The slot curvature introduces a phase

---

[22]See reference 16, p. 359.

difference into the radiation from different portions of the slot which has a maximum effect towards reducing the pattern amplitude when $\theta = 90^{\circ}$. As the angle θ becomes small, the pattern amplitude should tend to increase slightly since the phase difference effect tends to become negligible as θ approaches the missile axis. Before leaving the subject of validity of the theoretical results, a quick inspection of figures 52 and 53, which represent calculated longitudinal patterns for both diametrically opposed slots operating simultaneously and in phase, reveals how the amplitude tends to become infinite for small θ angles. Figure 52 is a longitudinal cut in the φ plane through the center of the two slots and figure 53 is a similar longitudinal cut in the φ plane which bisects the angle between the two slots. To compensate for the inadequacy of the theoretical expressions for conical angles of less than 30 degrees from the missile axis, the estimated pattern shape is indicated by dashed lines on both figures 52 and 53. The estimated patterns are based on the assumption that the field must reduce to zero on the missile axis due to the finite diameter and length of the missile body, and the fact that only zero electric fields can exist on the surface of the missile (assumed infinitely conducting) except in the antenna slots. The fact that the missile is not a constant-diameter circular cylinder without discontinuities is ignored in estimating the patterns. It is of interest to note in figures 7 through 15 that the radiation field from a single slot is elliptically polarized

except in the equatorial plane. The amplitude of the E_φ component is small in comparison to the E_θ component for elevation angles near the equatorial plane, but becomes relatively quite significant as θ approaches the missile axis. Also, the direction of the E_φ component is at right angles to the E_θ component and the shape of the E_φ pattern tends to be asymmetrical except near the missile axis. Since at a given point in space the two components are not in time phase, a complete description of the field must include both amplitude and phase of both components as given by the calculated data in tables 1 and 2. In addition to the results plotted in figures 7 through 15, the calculated data given in table 1 includes each intermediate 5-degree increment of θ starting with $\theta = 5^\circ$.

Progressing to the results obtained by vectorial summation of the radiation patterns from two diametrically opposed slots operating simultaneously, figures 16 through 51 give the resultant patterns for each 10-degree elevation angle from 10 to 90 degrees and for selected phase angles of $\beta = 0^\circ$, 60°, 120° and 180°, where 0 and 180 degrees corresponds to inphase and antiphase, respectively. Starting with the equatorial plane patterns ($\theta = 90^\circ$), it is obvious that the two slots should be inphase for the best pattern coverage throughout the full φ plane. When $\beta = 180^\circ$, the resultant pattern gives two symmetrical lobes on the $\varphi = 90^\circ$ plane, but also gives two deep nulls on the $\varphi = 0^\circ$ plane. Likewise, but to a lesser degree, undesirable nulls are caused by both the

60- and 120-degree phase angles. By comparing the inphase theoretical pattern with the corresponding experimental pattern--i.e., figure 48 with figure 64--it is apparent that the experimental pattern has four lobes of nearly equal amplitude, one on or near each of the 90-degree axes, and likewise has four rather deep nulls. Some additional explanations for the rather significant difference between the theoretical and experimental patterns will be discussed later.

It is interesting to observe that the experimental pattern for $\theta = 80^{\circ}$(figure 63) has approximately the same shape as the $\theta = 90^{\circ}$ theoretical E_{θ} pattern (figure 48). As the elevation angle moves away from the equatorial plane, the cross-polarized component E_{φ} enters the picture. For θ angles near 90 degrees the amplitude of the E_{φ} component is small in comparison to the E_{θ} component. But when θ is reduced to 30 degrees or less from the missile axis, the E_{φ} component becomes relatively very significant, particularly for the antiphase case. It is also interesting to note that for the antiphase case ($\beta = 180^{\circ}$) the E_{φ} lobes tend to compensate for the E_{θ} nulls, thereby giving a possibility for full spherical coverage to circular polarization except in the equatorial plane (see for example figure 31). However, it is also apparent from the various inphase patterns that the E_{φ} lobes in general tend to compensate for the nulls in the E_{θ} patterns (see for example figure 28).

Based upon the calculated pattern results, it appears that the best over-all spherical coverage can be obtained

with the two slots operating inphase. By observing patterns such as figures 21 and 22, it seems obvious that a phase angle between either the inphase or antiphase cases produces undesirable pattern distortion. It must be recognized, however, that even though patterns such as figures 16, 52, and 53 indicate strong E_θ coverage over the sphere poles--i.e., along the missile axis--the theoretical results are not valid in these zones for reasons which were previously discussed. On the other hand, if the estimated pattern shapes as indicated by the dashed lines on figures 52 and 53 are considered valid for the practical missile of idealized uniform shape, then nulls exist for small solid conical angles on both ends of the missile axis.

Referring now to the experimental patterns given by figures 55 through 75, it is apparent that considerable pattern distortion exists in the experimental results. The two slots were electrically inphase for all of the experimental measurements and no data for the cross-polarized component E_φ were obtained. From observation of figures 55 and 73, some coverage apparently exists along the missile axis. This can probably be explained as the result of some radiation by the body of the missile mock-up and refraction over the ends. The lack of symmetry between the corresponding θ angles on each side of the equatorial plane can be explained by the fact that the shape of the missile mock-up was made to approximate a portion of the actual missile which is not symmetrical with respect to the antenna slot position and,

therefore, could be expected to produce patterns that are quite different for the two θ angle quadrants. Also, the rather short finite length of the mock-up body and the difference in length, as measured from the position of the slots to each end, can be expected to produce standing-wave characteristics which are not symmetrical for both sections. Figures 74 and 75, which are longitudinal cuts through the center of the slots and in a plane which bisects the angle between the two slots, respectively, reveal the lack of symmetry and lack of uniformity of radiation over the two θ quadrants. By observing how the maximums and nulls from figures 74 and 75 add vectorially for a given θ angle, the apparent pattern rotation, for example, between θ = 80° and 100° (figures 63 and 65) can readily be explained.

The experimental patterns are not considered to be as valid as they should be for the final missile application. In the first place, a scaled-down model of, for example, one-fourth size would have been a better choice, since the antenna range equipment would then be able to accommodate a complete mock-up of the entire missile. Also, the difference, if any, in the radiation patterns could then be observed for both conditions of missile assembly--i.e., both with the propulsion unit attached and after separation from the primary missile. In addition, the scaled-down test would aid in avoiding undesirable reflections from nearby structures, since the operating frequency is multiplied by the scaling factor and the higher frequency is more readily confined to the desired direction.

In connection with the problem of radiation reflected from nearby objects, it should be noted that the pedestal used to support the missile mock-up was mounted on top of a one-story building. The building roof was flat and the pedestal was positioned about four feet from the edge of the roof, facing the transmitting tower, the latter being about 30 feet from the missile mock-up. The test setup was such that unwanted reflections probably existed which contributed to the pattern distortion. The unknown effects of reflections and shielding make interpretation of the experimental data difficult. Figures 76 through 87 represent interference test patterns to determine if simultaneous operation of either the beacon and/or the telemetry antenna systems would produce adverse effects on the Command Destruct System. No significant interference was observed, as has already been discussed in the section on Analysis of Experimental Data. However, comparing the pattern given in figure 76 with the pattern given in figure 64, it is apparent that there is virtually no similarity between the two patterns, although they both supposedly represent the same experimental antenna measurement setup and the same conical angle--i.e., $\theta = 90^{\circ}$. One possible explanation for this very significant disagreement is that the set of interference pattern measurements (figures 76 through 87) was made on a date different from that on which the family of conical patterns was made (figures 55 through 75), thereby introducing the possibility that the exact test conditions were not duplicated. For example,

there is no assurance that the undesired reflection characteristics did not change due to changes in the arrangement of nearby objects such as automobiles parked temporarily near the test tower.

At this point a few statements should be made concerning the probable influence on the radiation pattern, due to the presence of the propulsion motor during the acceleration phase. Since the pattern-measuring equipment would not support the full 21-foot-missile-length mock-up, only a portion of the total length was used; this did not include any of the propulsion section. The radiation pattern of a well-designed slot antenna with cavity resonator in an infinite ground plane is a semicircle if taken in a plane normal to the slot major axis. Whenever the ground plane normal to the slot major axis is shortened to only a few wavelengths, standing waves are set up along the ground plane in such a manner as to give pattern distortion. In general, a shortened ground plane reduces the radiation intensity in the plane normal to the slot major axis, and sets up perturbations in the pattern away from the ground plane. Therefore, the expected effect of adding the additional body length would be to enhance the radiation pattern intensity and to improve the pattern contour characteristics, particularly in the aft conical direction. A slight shadowing effect in the aft direction near the missile axis is to be expected due to the larger diameter of the propulsion section.

CONCLUSIONS

Although there is a significant lack of agreement between the theoretical and experimental results presented in this study, the theoretical investigation is justified in that it gives evidence of the complexity and limitations of a theoretical approach to the practical application of slot antennas to missiles. To make the theoretical approach feasible for a complex problem of the type considered in this study, it is necessary to idealize the geometrical shape of the body of the missile and to make certain approximations and assumptions. For example, when the missile shape is idealized to a perfectly conducting, constant-diameter, infinite-length, circular cylinder, the far-field theoretical expressions are obtainable in approximate form but are still so complex that an automatic computer is almost mandatory to obtain a significant number of data points. Also, the extent and effect of the many assumptions and approximations which are still necessary to carry out the theoretical study produce inaccuracies and lack of validity for certain zones, thereby making the theoretical approach rather incomplete. It is therefore concluded that for most practical applications of slot antennas to missiles, the radiation-pattern characteristics are determined more accurately and economically by experimental methods unless costs of the experimental setup are prohibitive.

Assuming that the experimental method is selected, considerable caution and effort must still be exercised to minimize undesirable effects such as those which can easily result from reflections or from not using a sufficiently accurate model to represent the missile body. For all missiles except the very small types such as the Sidewinder, a scaled-down model should be used. It is not essential to duplicate all of the minor details of the external missile shape, but this does not mean that great liberty can be taken in omitting significant portions of the missile body or in representing the missile shape correctly.

In this study the Command Destruct Antenna System had already been designed and the experimental pattern measurements made when the theoretical study was initiated. Since the experimental results were obtained on a model mock-up which did not accurately represent the external contour of the missile body, they are not considered to be as valid as they should be; therefore, both the intrinsic difficulties in the theoretical approach and the lack of reliable experimental data are reflected in the agreement obtained between the theoretical and experimental results.

TABLE 1

PATTERN FUNCTIONS FOR TWO DIAMETRICALLY OPPOSED SLOTS CONSIDERED SEPARATELY

θ°	φ°	$\lvert P_{\theta_1} \rvert$	Phase$^\circ$	$\lvert P_{\theta_2} \rvert$	Phase$^\circ$	$\lvert P_{\varphi_1} \rvert$	Phase$^\circ$	$\lvert P_{\varphi_2} \rvert$	Phase$^\circ$
5	-90	.1495	174.1	.2852	-120.6	.0000	----	.0000	----
5	-80	.1498	174.9	.2838	-120.9	.0236	-97.86	.0235	96.25
5	-70	.1508	177.1	.2796	-121.8	.0464	-97.54	.0463	95.92
5	-60	.1527	-179.3	.2729	-123.2	.0678	-97.01	.0676	95.39
5	-50	.1560	-174.5	.2639	-125.3	.0872	-96.30	.0870	94.68
5	-40	.1610	-168.9	.2529	-128.0	.1039	-95.42	.1037	93.79
5	-30	.1679	-162.9	.2405	-131.3	.1174	-94.39	.1172	92.77
5	-20	.1770	-156.6	.2271	-135.2	.1274	-93.26	.1272	91.64
5	-10	.1878	-150.6	.2135	-139.8	.1335	-92.06	.1334	90.43
5	0	.2002	-144.9	.2002	-144.9	.1355	-90.81	.1355	89.19
5	10	.2135	-139.8	.1878	-150.6	.1334	-89.57	.1335	87.94
5	20	.2271	-135.2	.1770	-156.6	.1272	-88.36	.1274	86.74
5	30	.2405	-131.3	.1679	-162.9	.1172	-87.23	.1174	85.61
5	40	.2529	-128.0	.1610	-168.9	.1037	-86.21	.1039	84.58
5	50	.2639	-125.3	.1560	-174.5	.0870	-85.32	.0872	83.70
5	60	.2729	-123.2	.1527	-179.3	.0676	-84.61	.0678	82.99
5	70	.2796	-121.8	.1508	177.1	.0463	-84.08	.0464	82.46
5	80	.2838	-120.9	.1498	174.9	.0235	-83.75	.0236	82.14
5	90	.2852	-120.6	.1495	174.1	.0000	----	.0000	----
10	-90	.0792	155.5	.2229	-105.4	.0000	----	.0000	----
10	-80	.0793	156.9	.2215	-105.8	.0241	-106.9	.0234	100.7
10	-70	.0799	161.1	.2174	-106.9	.0474	-106.3	.0462	100.1
10	-60	.0813	167.9	.2106	-108.9	.0692	-105.3	.0676	99.01
10	-50	.0844	176.5	.2014	-111.6	.0888	-103.9	.0870	97.59
10	-40	.0898	-173.7	.1903	-115.1	.1057	-102.2	.1039	95.85
10	-30	.0977	-163.6	.1775	-119.4	.1193	-100.2	.1177	93.83
10	-20	.1081	-154.0	.1635	-124.5	.1291	-97.98	.1280	91.60
10	-10	.1206	-145.2	.1489	-130.5	.1350	-95.63	.1344	89.24
10	0	.1344	-137.3	.1344	-137.3	.1368	-93.20	.1368	86.80
10	10	.1489	-130.5	.1206	-145.2	.1344	-90.76	.1350	84.37
10	20	.1635	-124.5	.1081	-154.0	.1280	-88.40	.1291	82.02
10	30	.1775	-119.4	.0977	-163.6	.1177	-86.17	.1193	79.82
10	40	.1903	-115.1	.0898	-173.7	.1039	-84.15	.1057	77.83
10	50	.2014	-111.6	.0844	176.5	.0870	-82.41	.0888	76.12
10	60	.2106	-108.9	.0813	167.9	.0676	-80.99	.0692	74.73
10	70	.2174	-106.9	.0799	161.1	.0462	-79.95	.0474	73.71
10	80	.2215	-105.8	.0793	156.9	.0234	-79.31	.0241	73.09
10	90	.2229	-105.4	.0792	155.5	.0000	----	.0000	----

TABLE 1 (continued)

θ°	φ°	$\lvert P_{\theta_1} \rvert$	Phase$^\circ$	$\lvert P_{\theta_2} \rvert$	Phase$^\circ$	$\lvert P_{\varphi_1} \rvert$	Phase$^\circ$	$\lvert P_{\varphi_2} \rvert$	Phase$^\circ$
15	-90	.0534	138.7	.1973	-94.15	.0000	----	.0000	----
15	-80	.0533	140.8	.1959	-94.66	.0244	-116.9	.0225	104.1
15	-70	.0535	147.0	.1919	-96.17	.0480	-116.0	.0444	103.2
15	-60	.0547	156.8	.1853	-98.66	.0699	-114.5	.0651	101.6
15	-50	.0578	169.2	.1764	-102.1	.0896	-112.5	.0840	99.40
15	-40	.0637	-177.4	.1656	-106.5	.1062	-110.0	.1006	96.76
15	-30	.0724	-164.4	.1532	-111.8	.1193	-107.1	.1144	93.71
15	-20	.0836	-152.6	.1395	-117.9	.1286	-103.9	.1250	90.36
15	-10	.0966	-142.2	.1252	-125.0	.1338	-100.4	.1319	86.82
15	0	.1107	-133.1	.1107	-133.1	.1349	-96.80	.1349	83.20
15	10	.1252	-125.0	.0966	-142.2	.1319	-93.18	.1338	79.60
15	20	.1395	-117.9	.0836	-152.6	.1250	-89.64	.1286	76.13
15	30	.1532	-111.8	.0724	-164.4	.1144	-86.29	.1193	72.90
15	40	.1656	-106.5	.0637	-177.4	.1006	-83.24	.1062	70.00
15	50	.1764	-102.1	.0578	-169.2	.0840	-80.60	.1896	67.50
15	60	.1853	-98.66	.0547	-156.8	.0651	-78.44	.0699	65.49
15	70	.1919	-96.17	.0535	-147.0	.0444	-76.85	.0480	64.01
15	80	.1959	-94.66	.0533	-140.8	.0225	-75.87	.0244	63.10
15	90	.1973	-94.15	.0534	-138.7	.0000	----	.0000	----
20	-90	.0398	123.2	.1824	-84.24	.0000	----	.0000	----
20	-80	.0397	125.9	.1810	-84.86	.0244	-127.4	.0205	108.1
20	-70	.0397	134.1	.1770	-86.73	.0478	-126.2	.0406	106.7
20	-60	.0407	147.0	.1705	-89.80	.0694	-124.3	.0596	104.5
20	-50	.0441	163.0	.1618	-94.03	.0885	-121.6	.0773	101.4
20	-40	.0504	179.4	.1512	-99.37	.1043	-118.4	.0930	97.73
20	-30	.0597	-165.5	.1391	-105.7	.1164	-114.6	.1065	93.50
20	-20	.0712	-152.3	.1259	-113.1	.1246	-110.3	.1171	88.89
20	-10	.0842	-140.8	.1121	-121.3	.1286	-105.7	.1246	84.05
20	0	.0980	-130.5	.0980	-130.5	.1285	-100.9	.1285	79.13
20	10	.1121	-121.3	.0842	-140.8	.1246	-95.95	.1286	74.30
20	20	.1259	-113.1	.0712	-152.3	.1171	-91.11	.1246	69.68
20	30	.1391	-105.7	.0597	-165.5	.1065	-86.50	.1164	65.40
20	40	.1512	-99.37	.0504	179.4	.0930	-82.27	.1043	61.59
20	50	.1618	-94.03	.0441	163.0	.0773	-78.58	.0885	58.33
20	60	.1705	-89.80	.0407	147.0	.0596	-75.55	.0694	55.71
20	70	.1770	-86.73	.0397	134.1	.0406	-73.30	.0478	53.79
20	80	.1810	-84.86	.0397	125.9	.0205	-71.92	.0244	52.62
20	90	.1824	-84.24	.0398	123.2	.0000	----	.0000	----

TABLE 1 (continued)

θ°	φ°	$\lvert P_{\theta_1} \rvert$	Phase°	$\lvert P_{\theta_2} \rvert$	Phase°	$\lvert P_{\varphi_1} \rvert$	Phase°	$\lvert P_{\varphi_2} \rvert$	Phase°
25	-90	.0316	108.7	.1728	-75.09	.0000	----	.0000	----
25	-80	.0314	112.1	.1714	-75.83	.0238	-137.8	.0180	114.3
25	-70	.0312	122.3	.1673	-78.04	.0466	-136.4	.0356	112.4
25	-60	.0322	138.3	.1607	-81.68	.0674	-134.0	.0525	109.3
25	-50	.0358	157.5	.1519	-86.69	.0854	-130.8	.0683	105.2
25	-40	.0426	176.3	.1413	-92.98	.0999	-126.8	.0826	100.2
25	-30	.0521	-167.3	.1294	-100.5	.1105	-122.0	.0951	94.50
25	-20	.0636	-153.0	.1165	-109.0	.1170	-116.6	.1055	88.34
25	-10	.0763	-140.4	.1032	-118.5	.1195	-110.7	.1133	81.95
25	0	.0896	-129.0	.0896	-129.0	.1181	-104.5	.1181	75.54
25	10	.1032	-118.5	.0763	-140.4	.1133	-98.05	.1195	69.30
25	20	.1165	-109.0	.0636	-153.0	.1055	-91.66	.1170	63.40
25	30	.1294	-100.5	.0521	-167.3	.0951	-85.50	.1105	58.01
25	40	.1413	-92.98	.0426	176.3	.0826	-79.82	.0999	53.25
25	50	.1519	-86.69	.0358	157.5	.0683	-74.81	.0854	49.21
25	60	.1607	-81.68	.0322	138.3	.0525	-70.69	.0674	45.98
25	70	.1673	-78.04	.0312	122.3	.0356	-67.63	.0466	43.63
25	80	.1714	-75.83	.0314	112.1	.0180	-65.73	.0238	42.20
25	90	.1728	-75.09	.0316	108.7	.0000	----	.0000	----
30	-90	.0261	95.17	.1664	-66.61	.0000	----	.0000	----
30	-80	.0258	99.21	.1649	-67.46	.0229	-147.7	.0158	123.5
30	-70	.0254	111.4	.1607	-69.98	.0447	-146.0	.0312	121.0
30	-60	.0265	130.5	.1539	-74.15	.0643	-143.2	.0458	117.0
30	-50	.0304	152.6	.1449	-79.89	.0809	-139.4	.0595	111.6
30	-40	.0374	173.1	.1342	-87.10	.0937	-134.5	.0719	105.1
30	-30	.0471	-169.5	.1222	-95.66	.1025	-128.8	.0830	97.60
30	-20	.0583	-154.3	.1095	-105.4	.1073	-122.1	.0925	89.57
30	-10	.0706	-140.6	.0964	-116.2	.1081	-114.8	.1002	81.30
30	0	.0834	-128.0	.0834	-128.0	.1056	-106.9	.1056	73.08
30	10	.0964	-116.2	.0706	-140.6	.1002	-98.70	.1081	65.20
30	20	.1095	-105.4	.0583	-154.3	.0925	-90.43	.1073	57.86
30	30	.1222	-95.66	.0471	-169.5	.0830	-82.40	.1025	51.24
30	40	.1342	-87.10	.0374	173.1	.0719	-74.93	.0937	45.45
30	50	.1449	-79.89	.0304	152.6	.0595	-68.36	.0809	40.60
30	60	.1539	-74.15	.0265	130.5	.0458	-62.96	.0643	36.76
30	70	.1607	-69.98	.0254	111.4	.0312	-58.95	.0447	33.98
30	80	.1649	-67.46	.0258	99.21	.0158	-56.48	.0227	32.30
30	90	.1664	-66.61	.0261	95.17	.0000	----	,0000	----

TABLE 1 (continued)

θ°	φ°	$\lvert P_{\theta_1} \rvert$	Phase°	$\lvert P_{\theta_2} \rvert$	Phase°	$\lvert P_{\varphi_1} \rvert$	Phase°	$\lvert P_{\varphi_2} \rvert$	Phase°
35	-90	.0221	82.58	.1619	-58.81	.0000	----	.0000	----
35	-80	.0218	87.25	.1604	-59.75	.0218	-156.9	.0144	134.7
35	-70	.0214	101.4	.1560	-62.56	.0424	-155.0	.0282	131.8
35	-60	.0225	123.6	.1489	-67.20	.0606	-151.8	.0411	126.9
35	-50	.0266	148.0	.1397	-73.59	.0755	-147.3	.0528	120.3
35	-40	.0339	169.7	.1288	-81.64	.0866	-141.6	.0632	112.2
35	-30	.0434	-172.0	.1167	-91.21	.0936	-134.7	.0725	102.9
35	-20	.0543	-155.9	.1040	-102.1	.0966	-126.8	.0806	92.75
35	-10	.0661	-141.2	.0911	-114.2	.0961	-117.8	.0875	82.30
35	0	.0784	-127.3	.0784	-127.3	.0929	-108.0	.0929	71.99
35	10	.0911	-114.2	.0661	-141.2	.0875	-97.70	.0961	62.21
35	20	.1040	-102.1	.0543	-155.9	.0806	-87.25	.0966	53.24
35	30	.1167	-91.21	.0434	-172.0	.0725	-77.12	.0936	45.25
35	40	.1288	-81.64	.0339	169.7	.0632	-67.78	.0866	38.38
35	50	.1397	-73.59	.0266	148.0	.0528	-59.66	.0755	32.69
35	60	.1489	-67.20	.0225	123.6	.0411	-53.07	.0606	28.22
35	70	.1560	-62.56	.0214	101.4	.0282	-48.24	.0424	25.00
35	80	.1604	-59.75	.0218	87.25	.0144	-45.30	.0218	23.07
35	90	.1619	-58.81	.0221	82.58	.0000	----	.0000	----
40	-90	.0192	70.95	.1586	-51.67	.0000	----	.0000	----
40	-80	.0189	76.22	.1570	-52.69	.0205	-165.5	.0136	145.3
40	-70	.0184	92.33	.1525	-55.76	.0397	-163.3	.0266	142.1
40	-60	.0196	117.3	.1453	-60.82	.0564	-159.7	.0384	136.9
40	-50	.0240	143.8	.1358	-67.81	.0696	-154.6	.0486	129.6
40	-40	.0313	166.3	.1246	-76.61	.0790	-148.0	.0573	120.3
40	-30	.0406	-174.7	.1123	-87.10	.0843	-140.0	.0645	109.4
40	-20	.0511	-157.7	.0995	-99.09	.0859	-130.6	.0708	97.35
40	-10	.0624	-141.8	.0868	-112.4	.0845	-119.8	.0763	84.68
40	0	.0743	-126.7	.0743	-126.7	.0811	-107.9	.0811	72.10
40	10	.0868	-112.4	.0624	-141.8	.0763	-95.32	.0845	60.22
40	20	.0995	-99.09	.0511	-157.7	.0708	-82.65	.0859	49.44
40	30	.1123	-87.10	.0406	-174.7	.0645	-70.56	.0843	39.99
40	40	.1246	-76.61	.0313	166.3	.0573	-59.67	.0790	31.97
40	50	.1358	-67.81	.0240	143.8	.0486	-50.44	.0696	25.41
40	60	.1453	-60.82	.0196	117.3	.0384	-43.13	.0564	20.32
40	70	.1525	-55.76	.0184	92.33	.0266	-37.87	.0397	16.68
40	80	.1570	-52.69	.0189	76.22	.0136	-34.70	.0205	14.51
40	90	.1586	-51.67	.0192	70.95	.0000	----	.0000	----

TABLE 1 (continued)

θ°	φ°	$\lvert P_{\theta_1} \rvert$	Phase$^\circ$	$\lvert P_{\theta_2} \rvert$	Phase$^\circ$	$\lvert P_{\varphi_1} \rvert$	Phase$^\circ$	$\lvert P_{\varphi_2} \rvert$	Phase$^\circ$
45	-90	.0171	60.29	.1561	-45.17	.0000	----	.0000	----
45	-80	.0166	66.13	.1545	-46.28	.0190	-173.5	.0132	153.6
45	-70	.0161	84.13	.1499	-49.58	.0367	-171.0	.0257	150.4
45	-60	.0174	111.7	.1424	-55.02	.0518	-167.0	.0368	145.0
45	-50	.0220	139.8	.1327	-62.54	.0635	-161.3	.0460	137.5
45	-40	.0294	163.0	.1213	-72.02	.0712	-153.9	.0532	127.8
45	-30	.0384	-177.4	.1089	-83.32	.0750	-144.7	.0587	116.0
45	-20	.0485	-159.6	.0960	-96.28	.0756	-133.7	.0631	102.5
45	-10	.0593	-142.5	.0832	-110.6	.0737	-121.0	.0670	87.86
45	0	.0709	-126.2	.0709	-126.2	.0706	-106.9	.0706	73.07
45	10	.0832	-110.6	.0593	-142.5	.0670	-92.14	.0737	59.01
45	20	.0960	-96.28	.0485	-159.6	.0631	-77.54	.0756	46.31
45	30	.1089	-83.32	.0384	-177.4	.0587	-64.02	.0750	35.32
45	40	.1213	-72.02	.0294	163.0	.0532	-52.23	.0712	26.12
45	50	.1327	-62.54	.0220	139.8	.0460	-42.51	.0635	18.70
45	60	.1424	-55.02	.0174	111.7	.0368	-34.97	.0518	12.99
45	70	.1499	-49.58	.0161	84.13	.0257	-29.62	.0367	8.96
45	80	.1545	-46.28	.0166	66.13	.0132	-26.42	.0190	6.55
45	90	.1561	-45.17	.0171	60.29	.0000	----	.0000	----
50	-90	.0154	50.64	.1541	-39.32	.0000	----	.0000	----
50	-80	.0149	57.02	.1525	-40.50	.0174	179.2	.0127	159.4
50	-70	.0144	76.80	.1478	-44.01	.0335	-178.2	.0246	156.2
50	-60	.0158	106.8	.1402	-49.80	.0470	-173.8	.0351	150.9
50	-50	.0205	136.0	.1304	-57.80	.0570	-167.5	.0436	143.4
50	-40	.0278	159.7	.1187	-67.88	.0632	-159.2	.0498	133.6
50	-30	.0366	179.9	.1061	-79.91	.0659	-148.8	.0540	121.5
50	-20	.0463	-161.3	.0930	-93.71	.0656	-136.3	.0568	107.2
50	-10	.0567	-143.1	.0802	-109.1	.0638	-121.6	.0590	91.23
50	0	.0681	-125.7	.0681	-125.7	.0613	-105.5	.0613	74.54
50	10	.0802	-109.1	.0567	-143.1	.0590	-88.77	.0638	58.36
50	20	.0930	-93.71	.0463	-161.3	.0568	-72.77	.0656	43.72
50	30	.1061	-79.91	.0366	179.9	.0540	-58.47	.0659	31.15
50	40	.1187	-67.88	.0278	159.7	.0498	-46.36	.0632	20.77
50	50	.1304	-57.80	.0205	136.0	.0436	-36.57	.0570	12.50
50	60	.1402	-49.80	.0158	106.8	.0351	-29.07	.0470	6.21
50	70	.1478	-44.01	.0144	76.80	.0246	-23.76	.0335	1.80
50	80	.1525	-40.50	.0149	57.02	.0127	-20.61	.0174	-0.82
50	90	.1541	-39.32	.0154	50.64	.0000	----	.0000	----

TABLE 1 (continued)

θ°	φ°	$\lvert P_{\theta_1} \rvert$	Phase$^\circ$	$\lvert P_{\theta_2} \rvert$	Phase$^\circ$	$\lvert P_{\varphi_1} \rvert$	Phase$^\circ$	$\lvert P_{\varphi_2} \rvert$	Phase$^\circ$
55	-90	.0141	42.03	.1526	-34.11	.0000	----	.0000	----
55	-80	.0136	48.90	.1510	-35.35	.0157	172.4	.0119	163.4
55	-70	.0130	70.35	.1462	-39.05	.0300	175.2	.0230	160.2
55	-60	.0146	102.4	.1385	-45.16	.0418	-180.0	.0327	155.0
55	-50	.0194	132.5	.1284	-53.59	.0503	-173.2	.0405	147.6
55	-40	.0266	156.6	.1167	-64.20	.0552	-164.1	.0460	137.9
55	-30	.0351	177.5	.1039	-76.87	.0568	-152.5	.0494	125.7
55	-20	.0444	-162.9	.0907	-91.42	.0562	-138.4	.0510	111.2
55	-10	.0546	-143.7	.0778	-107.6	.0545	-121.9	.0519	94.35
55	0	.0657	-125.2	.0657	-125.2	.0529	-103.8	.0529	76.18
55	10	.0778	-107.6	.0546	-143.7	.0519	-85.65	.0545	58.12
55	20	.0907	-91.42	.0444	-162.9	.0510	-68.84	.0562	41.60
55	30	.1039	-76.87	.0351	177.5	.0494	-54.25	.0568	27.47
55	40	.1167	-64.20	.0266	156.6	.0460	-42.14	.0552	15.93
55	50	.1284	-53.59	.0194	132.5	.0405	-32.44	.0503	6.84
55	60	.1385	-45.16	.0146	102.4	.0327	-25.02	.0418	-0.01
55	70	.1462	-39.05	.0130	70.35	.0230	-19.78	.0300	-4.75
55	80	.1510	-35.35	.0136	48.90	.0119	-16.65	.0157	-7.56
55	90	.1526	-34.11	.0141	42.03	.0000	----	.0000	----
60	-90	.0130	34.50	.1514	-29.55	.0000	----	.0000	----
60	-80	.0125	41.81	.1497	-30.85	.0137	166.4	.0106	166.1
60	-70	.0120	64.76	.1448	-34.72	.0262	169.4	.0206	163.0
60	-60	.0136	98.61	.1371	-41.11	.0363	174.5	.0294	157.7
60	-50	.0185	129.4	.1269	-49.91	.0433	-178.2	.0364	150.4
60	-40	.0256	153.8	.1150	-61.00	.0471	-168.4	.0414	140.8
60	-30	.0338	175.3	.1021	-74.22	.0480	-155.7	.0441	128.8
60	-20	.0428	-164.2	.0888	-89.41	.0472	-140.1	.0451	114.2
60	-10	.0528	-144.2	.0759	-106.3	.0458	-121.8	.0450	96.96
60	0	.0638	-124.7	.0638	-124.7	.0451	-102.2	.0451	77.79
60	10	.0759	-106.3	.0528	-144.2	.0450	-83.04	.0458	58.15
60	20	.0888	-89.41	.0428	-164.2	.0451	-65.85	.0472	39.91
60	30	.1021	-74.22	.0338	175.3	.0441	-51.24	.0480	24.29
60	40	.1150	-61.00	.0256	153.8	.0414	-39.23	.0471	11.64
60	50	.1269	-49.91	.0185	129.4	.0364	-29.63	.0433	1.79
60	60	.1371	-41.11	.0136	98.61	.0294	-22.25	.0363	-5.54
60	70	.1448	-34.72	.0120	64.76	.0206	-17.02	.0262	-10.62
60	80	.1497	-30.85	.0125	41.81	.0106	-13.88	.0137	-13.60
60	90	.1514	-29.55	.0130	34.50	.0000	----	.0000	----

TABLE 1 (continued)

θ°	φ°	$\lvert P_{\theta_1}\rvert$	Phase°	$\lvert P_{\theta_2}\rvert$	Phase°	$\lvert P_{\varphi_1}\rvert$	Phase°	$\lvert P_{\varphi_2}\rvert$	Phase°
65	-90	.0122	28.08	.1505	-25.67	.0000	----	.0000	----
65	-80	.0117	35.76	.1488	-27.01	.0117	161.1	.0091	168.2
65	-70	.0112	60.04	.1438	-31.03	.0222	164.3	.0178	165.0
65	-60	.0129	95.38	.1360	-37.66	.0305	169.6	.0254	159.7
65	-50	.0178	126.6	.1257	-46.78	.0362	177.4	.0315	152.3
65	-40	.0248	151.4	.1137	-58.28	.0390	-172.0	.0358	142.8
65	-30	.0328	173.3	.1007	-71.97	.0394	-158.4	.0381	130.8
65	-20	.0416	-165.4	.0873	-87.70	.0386	-141.4	.0387	116.3
65	-10	.0513	-144.6	.0743	-105.3	.0376	-121.6	.0382	99.00
65	0	.0622	-124.3	.0622	-124.3	.0375	-100.8	.0375	79.21
65	10	.0743	-105.3	.0513	-144.6	.0382	-81.00	.0376	58.36
65	20	.0873	-87.70	.0416	-165.4	.0387	-63.68	.0386	38.61
65	30	.1007	-71.97	.0328	173.3	.0381	-49.15	.0394	21.62
65	40	.1137	-58.28	.0248	151.4	.0358	-37.24	.0390	7.96
65	50	.1257	-46.78	.0178	126.6	.0315	-27.67	.0362	-2.58
65	60	.1360	-37.66	.0129	95.38	.0254	-20.28	.0305	-10.37
65	70	.1438	-31.03	.0112	60.04	.0178	-15.00	.0222	-15.72
65	80	.1488	-27.01	.0117	35.76	.0091	-11.83	.0117	-18.85
65	90	.1505	-25.67	.0122	28.08	.0000	----	.0000	----
70	-90	.0116	22.78	.1497	-22.46	.0000	----	.0000	----
70	-80	.0111	30.78	.1480	-23.84	.0095	156.8	.0074	169.8
70	-70	.0105	56.18	.1430	-27.98	.0179	160.0	.0145	166.5
70	-60	.0123	92.73	.1351	-34.81	.0246	165.6	.0207	161.2
70	-50	.0173	124.3	.1247	-42.41	.0290	173.8	.0258	153.7
70	-40	.0242	149.3	.1127	-56.04	.0310	-175.1	.0294	144.2
70	-30	.0320	171.7	.0996	-70.12	.0311	-160.5	.0313	132.3
70	-20	.0406	-166.4	.0861	-86.30	.0303	-142.3	.0317	117.8
70	-10	.0502	-144.9	.0731	-104.4	.0298	-121.3	.0310	100.5
70	0	.0610	-124.0	.0610	-124.0	.0301	-99.60	.0301	80.40
70	10	.0731	-104.4	.0502	-144.9	.0310	-79.47	.0298	58.66
70	20	.0861	-86.30	.0406	-166.4	.0317	-62.15	.0303	37.65
70	30	.0996	-70.12	.0320	171.7	.0313	-47.71	.0311	19.48
70	40	.1127	-56.04	.0242	149.3	.0294	-35.85	.0310	4.92
70	50	.1247	-42.41	.0173	124.3	.0258	-26.27	.0290	-6.22
70	60	.1351	-34.81	.0123	92.73	.0207	-18.82	.0246	-14.39
70	70	.1430	-27.98	.0105	56.18	.0145	-13.46	.0179	-19.98
70	80	.1480	-23.84	.0111	30.78	.0074	-10.23	.0095	-23.23
70	90	.1497	-22.46	.0116	22.78	.0000	----	.0000	----

TABLE 1 (continued)

θ°	φ°	$\lvert P_{\theta_1} \rvert$	Phase$^\circ$	$\lvert P_{\theta_2} \rvert$	Phase$^\circ$	$\lvert P_{\varphi_1} \rvert$	Phase$^\circ$	$\lvert P_{\varphi_2} \rvert$	Phase$^\circ$
75	-90	.0112	18.64	.1492	-19.95	.0000	----	.0000	----
75	-80	.0107	26.89	.1475	-21.37	.0072	153.3	.0056	171.0
75	-70	.0101	53.18	.1424	-25.60	.0136	156.7	.0110	167.7
75	-60	.0119	90.64	.1344	-32.58	.0185	162.4	.0158	162.3
75	-50	.0169	122.5	.1240	-42.20	.0217	170.9	.0197	154.8
75	-40	.0237	147.6	.1119	-54.29	.0231	-177.5	.0225	145.1
75	-30	.0313	170.5	.0987	-68.68	.0230	-162.1	.0240	133.3
75	-20	.0398	-167.2	.0852	-85.20	.0224	-143.0	.0242	118.9
75	-10	.0493	-145.1	.0722	-103.6	.0222	-121.0	.0236	101.6
75	0	.0601	-123.7	.0601	-123.7	.0227	-98.69	.0227	81.31
75	10	.0722	-103.6	.0493	-145.1	.0236	-78.39	.0222	58.96
75	20	.0852	-85.20	.0398	-167.2	.0242	-61.11	.0224	36.99
75	30	.0987	-68.68	.0313	170.5	.0240	-46.74	.0230	17.85
75	40	.1119	-54.29	.0237	147.6	.0225	-34.88	.0231	2.55
75	50	.1240	-42.20	.0169	122.5	.0197	-25.25	.0217	-9.09
75	60	.1344	-32.58	.0119	90.64	.0158	-17.71	.0185	-17.56
75	70	.1424	-25.60	.0101	53.18	.0110	-12.27	.0136	-23.33
75	80	.1475	-21.37	.0107	26.89	.0056	-8.96	.0072	-26.69
75	90	.1492	-19.95	.0112	18.64	.0000	----	.0000	----
80	-90	.0109	15.67	.1488	-18.14	.0000	----	.0000	----
80	-80	.0104	24.10	.1471	-19.59	.0048	150.8	.0038	172.0
80	-70	.0098	51.04	.1420	-23.89	.0091	154.2	.0074	168.6
80	-60	.0117	89.15	.1340	-30.99	.0124	160.1	.0106	163.1
80	-50	.0166	121.1	.1235	-40.75	.0145	168.9	.0132	155.5
80	-40	.0233	146.4	.1113	-53.03	.0153	-179.1	.0152	145.8
80	-30	.0309	169.5	.0981	-67.65	.0152	-163.3	.0162	133.9
80	-20	.0392	-167.7	.0846	-84.41	.0148	-143.4	.0164	119.6
80	-10	.0487	-145.3	.0716	-103.1	.0147	-120.8	.0159	102.3
80	0	.0595	-123.5	.0595	-123.5	.0152	-98.06	.0152	81.94
80	10	.0716	-103.1	.0487	-145.3	.0159	-77.68	.0147	59.22
80	20	.0846	-84.41	.0392	-167.7	.0164	-60.44	.0148	36.57
80	30	.0981	-67.65	.0309	169.5	.0162	-46.11	.0152	16.71
80	40	.1113	-53.03	.0233	146.4	.0152	-34.23	.0153	-0.86
80	50	.1235	-40.75	.0166	121.1	.0132	-24.54	.0145	-11.14
80	60	.1340	-30.99	.0117	89.15	.0106	-16.92	.0124	-19.85
80	70	.1420	-23.89	.0098	51.04	.0074	-11.39	.0091	-25.76
80	80	.1471	-19.59	.0104	24.10	.0038	-8.02	.0048	-29.18
80	90	.1488	-18.14	.0109	15.67	.0000	----	.0000	----

TABLE 1 (continued)

θ°	φ°	$\lvert P_{\theta_1} \rvert$	Phase$^\circ$	$\lvert P_{\theta_2} \rvert$	Phase$^\circ$	$\lvert P_{\varphi_1} \rvert$	Phase$^\circ$	$\lvert P_{\varphi_2} \rvert$	Phase$^\circ$
85	-90	.0107	13.88	.1486	-17.06	.0000	----	.0000	----
85	-80	.0102	22.43	.1469	-18.51	.0024	149.3	.0019	172.6
85	-70	.0096	49.76	.1418	-22.86	.0046	152.8	.0037	169.2
85	-60	.0115	88.25	.1337	-30.02	.0062	158.8	.0053	163.6
85	-50	.0165	120.3	.1232	-39.88	.0072	167.6	.0066	155.9
85	-40	.0231	145.7	.1110	-52.28	.0076	179.8	.0076	146.1
85	-30	.0306	169.0	.0978	-67.03	.0076	-164.0	.0082	134.3
85	-20	.0389	-168.1	.0843	-83.94	.0074	-143.7	.0082	119.9
85	-10	.0483	-145.4	.0712	-102.8	.0073	-120.6	.0080	102.7
85	0	.0591	-123.4	.0591	-123.4	.0076	-97.68	.0076	82.32
85	10	.0712	-102.8	.0483	-145.4	.0080	-77.27	.0073	59.39
85	20	.0843	-83.94	.0389	-168.1	.0082	-60.07	.0074	36.34
85	30	.0978	-67.03	.0306	169.0	.0082	-45.75	.0076	16.04
85	40	.1110	-52.28	.0231	145.7	.0076	-33.86	.0076	-0.16
85	50	.1232	-39.88	.0165	120.3	.0066	-24.11	.0072	-12.38
85	60	.1337	-30.02	.0115	88.25	.0053	-16.43	.0062	-21.23
85	70	.1418	-22.86	.0096	49.76	.0037	-10.84	.0046	-27.22
85	80	.1469	-18.51	.0102	22.43	.0019	-7.44	.0024	-30.69
85	90	.1486	-17.06	.0107	13.88	.0000	----	.0000	----
90	-90	.0106	13.29	.1485	-16.70	.0000	----	.0000	----
90	-80	.0101	21.87	.1468	-18.16	.0000	----	.0000	----
90	-70	.0095	49.33	.1417	-22.52	.0000	----	.0000	----
90	-60	.0115	87.95	.1336	-29.70	.0000	----	.0000	----
90	-50	.0164	120.0	.1231	-39.59	.0000	----	.0000	----
90	-40	.0231	145.5	.1109	-52.03	.0000	----	.0000	----
90	-30	.0305	168.8	.0977	-66.82	.0000	----	.0000	----
90	-20	.0388	-168.2	.0842	-83.79	.0000	----	.0000	----
90	-10	.0482	-145.4	.0711	-102.7	.0000	----	.0000	----
90	0	.0590	-123.4	.0590	-123.4	.0000	----	.0000	----
90	10	.0711	-102.7	.0482	-145.4	.0000	----	.0000	----
90	20	.0842	-83.79	.0388	-168.2	.0000	----	.0000	----
90	30	.0977	-66.82	.0305	168.8	.0000	----	.0000	----
90	40	.1109	-52.03	.0231	145.5	.0000	----	.0000	----
90	50	.1231	-39.59	.0164	120.0	.0000	----	.0000	----
90	60	.1336	-29.70	.0115	87.95	.0000	----	.0000	----
90	70	.1417	-22.52	.0095	49.33	.0000	----	.0000	----
90	80	.1468	-18.16	.0101	21.87	.0000	----	.0000	----
90	90	.1485	-16.70	.0106	13.29	.0000	----	.0000	----

TABLE 2

PATTERN SUMMATION FUNCTIONS FOR TWO DIAMETRICALLY OPPOSED SLOTS OPERATING SIMULTANEOUSLY WITH SELECTED PHASING

θ°	φ°	β°	$\lvert P_\theta' \rvert$	Phase$^\circ$	$\lvert P_\varphi' \rvert$	Phase$^\circ$
10	-90	0	.2245	-125.8	.0000	----
10	-80	0	.2256	-126.2	.0114	180.0
10	-70	0	.2291	-127.3	.0214	180.0
10	-60	0	.2345	-129.0	.0288	180.0
10	-50	0	.2414	-131.0	.0328	180.0
10	-40	0	.2492	-133.0	.0329	180.0
10	-30	0	.2467	-134.8	.0289	180.0
10	-20	0	.2631	-136.2	.0215	180.0
10	-10	0	.2673	-137.0	.0114	180.0
10	0	0	.2688	-137.3	.0000	-8.62
10	10	0	.2673	-137.0	.0114	-0.03
10	20	0	.2631	-136.2	.0215	-0.03
10	30	0	.2567	-134.8	.0289	-0.03
10	40	0	.2492	-133.0	.0329	-0.03
10	50	0	.2414	-131.0	.0328	-0.03
10	60	0	.2345	-129.0	.0288	-0.03
10	70	0	.2291	-127.3	.0214	-0.03
10	80	0	.2256	-126.2	.0114	-0.03
10	90	0	.2245	-125.8	.0000	----
10	-90	60	.1516	-56.12	.0000	----
10	-80	60	.1515	-57.44	.0329	-152.3
10	-70	60	.1516	-61.31	.0640	-152.3
10	-60	60	.1534	-67.40	.0918	-152.4
10	-50	60	.1582	-75.06	.1148	-152.5
10	-40	60	.1672	-83.29	.1319	-152.5
10	-30	60	.1804	-91.11	.1426	-152.7
10	-20	60	.1969	-97.84	.1467	-152.8
10	-10	60	.2150	-103.2	.1445	-153.0
10	0	60	.2328	-107.3	.1368	-153.2
10	10	60	.2489	-110.3	.1247	-153.5
10	20	60	.2624	-112.4	.1095	-153.8
10	30	60	.2727	-113.8	.0926	-154.1
10	40	60	.2800	-114.7	.0751	-154.5
10	50	60	.2846	-115.1	.0581	-154.8
10	60	60	.2871	-115.3	.0420	-155.2
10	70	60	.2883	-115.4	.0271	-155.5
10	80	60	.2887	-115.4	.0133	-155.7
10	90	60	.2888	-115.3	.0000	----

TABLE 2 (continued)

θ°	φ°	β°	$\lvert P_\theta' \rvert$	Phase$^\circ$	$\lvert P_\varphi' \rvert$	Phase$^\circ$
10	-90	120	.1690	31.82	.0000	----
10	-80	120	.1655	31.11	.0456	-122.9
10	-70	120	.1554	28.81	.0896	-122.9
10	-60	120	.1396	24.38	.1320	-122.9
10	-50	120	.1201	16.66	.1660	-122.9
10	-40	120	.1006	3.57	.1957	-123.0
10	-30	120	.0876	-17.16	.2181	-123.0
10	-20	120	.0894	-42.53	.2326	-123.1
10	-10	120	.1071	-63.67	.2388	-123.1
10	0	120	.1344	-77.34	.2369	-123.2
10	10	120	.1650	-85.68	.2274	-123.3
10	20	120	.1951	-90.89	.2111	-123.4
10	30	120	.2225	-94.24	.1892	-123.5
10	40	120	.2461	-96.46	.1629	-123.6
10	50	120	.2653	-97.93	.1333	-123.7
10	60	120	.2800	-98.90	.1015	-123.7
10	70	120	.2902	-99.50	.0683	-123.8
10	80	120	.2963	-99.84	.0343	-123.8
10	90	120	.2983	-99.94	.0000	----
10	-90	180	.2481	93.00	.0000	----
10	-80	180	.2446	93.00	.0461	-93.29
10	-70	180	.2340	92.99	.0911	-93.29
10	-60	180	.2166	92.98	.1338	-93.27
10	-50	180	.1926	92.96	.1728	-93.26
10	-40	180	.1626	92.95	.2070	-93.24
10	-30	180	.1271	92.93	.2352	-93.22
10	-20	180	.0873	92.92	.2562	-93.21
10	-10	180	.0445	92.91	.2692	-93.20
10	0	180	.0000	63.43	.2736	-93.20
10	10	180	.0445	-87.09	.2692	-93.20
10	20	180	.0873	-87.08	.2562	-93.21
10	30	180	.1271	-87.07	.2352	-93.22
10	40	180	.1626	-87.05	.2070	-93.24
10	50	180	.1926	-87.04	.1728	-93.26
10	60	180	.2166	-87.02	.1338	-93.27
10	70	180	.2340	-87.01	.0911	-93.29
10	80	180	.2446	-87.00	.0462	-93.29
10	90	180	.2481	-87.00	.0000	----

TABLE 2 (continued)

θ°	φ°	β°	$\lvert P_\theta' \rvert$	Phase$^\circ$	$\lvert P_\varphi' \rvert$	Phase$^\circ$
20	-90	0	.1482	-91.35	.0000	----
20	-80	0	.1483	-92.74	.0212	179.6
20	-70	0	.1493	-96.73	.0399	179.6
20	-60	0	.1521	-102.7	.0540	179.6
20	-50	0	.1578	-109.8	.0618	179.6
20	-40	0	.1665	-116.8	.0621	179.6
20	-30	0	.1768	-122.7	.0550	179.6
20	-20	0	.1865	-127.0	.0410	179.6
20	-10	0	.1935	-129.7	.0219	179.6
20	0	0	.1960	-130.5	.0000	-9.86
20	10	0	.1935	-129.7	.0219	-40.67
20	20	0	.1865	-127.0	.0410	-40.80
20	30	0	.1768	-122.7	.0550	-41.00
20	40	0	.1665	-116.8	.0621	-41.24
20	50	0	.1578	-109.8	.0618	-41.50
20	60	0	.1521	-102.7	.0540	-41.74
20	70	0	.1493	-96.73	.0399	-41.95
20	80	0	.1483	-92.74	.0211	-42.08
20	90	0	.1482	-91.35	.0000	----
20	-90	60	.1504	-16.03	.0000	----
20	-80	60	.1476	-17.32	.0380	-156.6
20	-70	60	.1401	-21.39	.0737	-156.7
20	-60	60	.1299	-28.80	.1050	-156.8
20	-50	60	.1203	-40.18	.1300	-157.1
20	-40	60	.1162	-55.12	.1470	-157.4
20	-30	60	.1210	-71.05	.1551	-157.9
20	-20	60	.1343	-84.61	.1542	-158.6
20	-10	60	.1520	-94.32	.1448	-159.5
20	0	60	.1697	-100.5	.1285	-160.9
20	10	60	.1843	-104.1	.1075	-162.7
20	20	60	.1941	-105.6	.0845	-165.5
20	30	60	.1987	-105.7	.0620	-169.4
20	40	60	.1990	-104.6	.0422	-175.5
20	50	60	.1963	-102.8	.0268	175.4
20	60	60	.1923	-100.7	.0160	162.5
20	70	60	.1885	-98.66	.0090	147.4
20	80	60	.1859	-97.20	.0042	135.2
20	90	60	.1849	-96.67	.0000	----

TABLE 2 (continued)

θ°	φ°	β°	$\lvert P_\theta' \rvert$	Phase$^\circ$	$\lvert P_\varphi' \rvert$	Phase$^\circ$
20	-90	120	.1884	47.96	.0000	----
20	-80	120	.1848	47.55	.0448	-129.5
20	-70	120	.1740	46.22	.0882	-129.5
20	-60	120	.1564	43.64	.1284	-129.5
20	-50	120	.1330	39.02	.1639	-129.5
20	-40	120	.1058	30.57	.1931	-129.7
20	-30	120	.0794	14.13	.2143	-129.8
20	-20	120	.0644	-16.05	.2265	-130.1
20	-10	120	.0728	-50.00	.2292	-130.4
20	0	120	.0980	-70.53	.2226	-130.9
20	10	120	.1273	-80.76	.2077	-131.5
20	20	120	.1543	-85.98	.1863	-132.2
20	30	120	.1765	-88.68	.1603	-133.0
20	40	120	.1931	-89.96	.1321	-134.0
20	50	120	.2043	-90.42	.1034	-135.0
20	60	120	.2112	-90.41	.0756	-136.0
20	70	120	.2149	-90.20	.0492	-136.8
20	80	120	.2166	-89.99	.0242	-137.4
20	90	120	.2170	-89.91	.0000	----
20	-90	180	.2185	100.6	.0000	----
20	-80	180	.2161	100.5	.0398	-102.2
20	-70	180	.2087	100.4	.0791	-102.1
20	-60	180	.1958	100.2	.1176	-101.9
20	-50	180	.1770	100.0	.1542	-101.7
20	-40	180	.1519	99.78	.1876	-101.4
20	-30	180	.1207	99.57	.2162	-101.2
20	-20	180	.0839	99.41	.2383	-101.0
20	-10	180	.0431	99.31	.2523	-100.9
20	0	180	.0000	-180.0	.2570	-100.9
20	10	180	.0431	-80.69	.2523	-100.9
20	20	180	.0839	-80.59	.2383	-101.0
20	30	180	.1207	-80.43	.2162	-101.2
20	40	180	.1519	-80.22	.1876	-101.4
20	50	180	.1770	-79.99	.1542	-101.7
20	60	180	.1958	-79.77	.1176	-101.9
20	70	180	.2087	-79.59	.0791	-102.1
20	80	180	.2161	-79.46	.0398	-102.2
20	90	180	.2185	-79.42	.0000	----

TABLE 2 (continued)

θ°	φ°	β°	$\lvert P_\theta' \rvert$	Phase$^\circ$	$\lvert P_\varphi' \rvert$	Phase$^\circ$
30	-90	0	.1418	-63.32	.0000	----
30	-80	0	.1400	-65.03	.0281	178.1
30	-70	0	.1352	-70.24	.0532	178.1
30	-60	0	.1303	-79.02	.0724	178.2
30	-50	0	.1287	-90.67	.0834	178.2
30	-40	0	.1330	-103.2	.0845	178.2
30	-30	0	.1427	-114.1	.0752	178.2
30	-20	0	.1542	-122.0	.0564	178.3
30	-10	0	.1633	-126.5	.0302	178.3
30	0	0	.1667	-128.0	.0000	-16.31
30	10	0	.1633	-126.5	.0302	-1.74
30	20	0	.1542	-122.0	.0564	-1.75
30	30	0	.1427	-114.1	.0752	-1.77
30	40	0	.1330	-103.2	.0845	-1.79
30	50	0	.1287	-90.67	.0834	-1.81
30	60	0	.1303	-79.02	.0724	-1.84
30	70	0	.1352	-70.24	.0532	-1.85
30	80	0	.1400	-65.03	.0281	-1.87
30	90	0	.1418	-63.32	.0000	----
30	-90	60	.1630	2.39	.0000	----
30	-80	60	.1594	1.45	.0376	-159.4
30	-70	60	.1490	-1.60	.0729	-159.5
30	-60	60	.1331	-7.55	.1038	-159.6
30	-50	60	.1148	-17.90	.1280	-159.9
30	-40	60	.0998	-34.52	.1436	-160.4
30	-30	60	.0959	-56.41	.1490	-161.1
30	-20	60	.1061	-76.75	.1437	-162.2
30	-10	60	.1249	-90.44	.1286	-164.0
30	0	60	.1444	-98.00	.1056	-166.9
30	10	60	.1592	-101.3	.0782	-172.1
30	20	60	.1671	-101.6	.0509	177.4
30	30	60	.1683	-99.49	.0294	153.1
30	40	60	.1647	-95.48	.0218	106.7
30	50	60	.1590	-90.05	.0252	73.79
30	60	60	.1537	-84.02	.0266	60.11
30	70	60	.1501	-78.53	.0221	54.05
30	80	60	.1484	-74.71	.0125	51.32
30	90	60	.1479	-73.35	.0000	----

TABLE 2 (continued)

θ°	φ°	β°	$\lvert P_\theta' \rvert$	Phase$^\circ$	$\lvert P_\varphi' \rvert$	Phase$^\circ$
30	-90	120	.1866	58.73	.0000	----
30	-80	120	.1836	58.40	.0374	-135.0
30	-70	120	.1743	57.37	.0739	-134.9
30	-60	120	.1585	55.42	.1085	-134.8
30	-50	120	.1362	52.00	.1397	-134.7
30	-40	120	.1081	45.73	.1657	-134.7
30	-30	120	.0774	32.69	.1842	-134.9
30	-20	120	.0535	2.44	.1938	-135.2
30	-10	120	.0567	-42.67	.1933	-135.9
30	0	120	.0834	-68.00	.1829	-136.9
30	10	120	.1138	-78.15	.1641	-138.5
30	20	120	.1397	-82.17	.1396	-140.6
30	30	120	.1585	-83.29	.1123	-143.6
30	40	120	.1698	-82.74	.0854	-147.5
30	50	120	.1750	-81.18	.0614	-152.4
30	60	120	.1761	-79.13	.0413	-158.0
30	70	120	.1753	-77.10	.0251	-163.6
30	80	120	.1741	-75.61	.0118	-167.8
30	90	120	.1736	-75.06	.0000	----
30	-90	180	.1913	110.9	.0000	----
30	-80	180	.1901	110.8	.0276	-112.8
30	-70	180	.1861	110.2	.0558	-112.1
30	-60	180	.1783	109.4	.0851	-111.2
30	-50	180	.1651	108.5	.1149	-110.1
30	-40	180	.1453	107.6	.1441	-109.1
30	-30	180	.1181	106.8	.1707	-108.2
30	-20	180	.0836	106.3	.1922	-107.5
30	-10	180	.0434	105.9	.2063	-107.1
30	0	180	.0000	-63.43	.2112	-106.9
30	10	180	.0434	-74.11	.2063	-107.1
30	20	180	.0836	-73.75	.1922	-107.5
30	30	180	.1181	-73.16	.1707	-108.2
30	40	180	.1453	-72.39	.1441	-109.1
30	50	180	.1651	-71.50	.1149	-110.1
30	60	180	.1783	-70.59	.0851	-111.2
30	70	180	.1861	-69.80	.0558	-112.1
30	80	180	.1901	-69.25	.0276	-112.8
30	90	180	.1913	-69.09	.0000	----

TABLE 2 (continued)

θ°	φ°	β°	$\lvert P_\theta' \rvert$	Phase$^\circ$	$\lvert P_\varphi' \rvert$	Phase$^\circ$
40	-90	0	.1491	-45.42	.0000	----
40	-80	0	.1459	-46.92	.0312	175.1
40	-70	0	.1372	-51.70	.0592	175.2
40	-60	0	.1257	-60.53	.0812	175.3
40	-50	0	.1160	-74.02	.0942	175.4
40	-40	0	.1138	-90.81	.0962	175.5
40	-30	0	.1210	-106.7	.0863	175.6
40	-20	0	.1335	-118.2	.0651	175.6
40	-10	0	.1444	-124.6	.0350	175.7
40	0	0	.1486	-126.7	.0000	-24.78
40	10	0	.1444	-124.6	.0350	-4.33
40	20	0	.1335	-118.2	.0651	-4.38
40	30	0	.1210	-106.7	.0863	-4.45
40	40	0	.1138	-90.81	.0962	-4.54
40	50	0	.1160	-74.02	.0942	-4.64
40	60	0	.1257	-60.53	.0812	-4.73
40	70	0	.1372	-51.70	.0592	-4.81
40	80	0	.1459	-46.92	.0312	-4.86
40	90	0	.1491	-45.42	.0000	----
40	-90	60	.1683	14.16	.0000	----
40	-80	60	.1648	13.44	.0340	-161.2
40	-70	60	.1542	11.08	.0662	-161.1
40	-60	60	.1371	6.48	.0947	-161.1
40	-50	60	.1153	-2.13	.1172	-161.1
40	-40	60	.0933	-17.60	.1312	-161.3
40	-30	60	.0810	-42.69	.1348	-161.7
40	-20	60	.0874	-69.97	.1270	-162.6
40	-10	60	.1073	-87.91	.1083	-164.3
40	0	60	.1287	-96.69	.0811	-167.9
40	10	60	.1440	-99.66	.0497	-176.6
40	20	60	.1506	-98.63	.0223	151.1
40	30	60	.1495	-94.33	.0232	72.80
40	40	60	.1441	-87.13	.0395	48.40
40	50	60	.1385	-77.77	.0485	41.14
40	60	60	.1359	-67.85	.0476	37.99
40	70	60	.1366	-59.39	.0375	36.40
40	80	60	.1384	-53.90	.0205	35.63
40	90	60	.1393	-52.03	.0000	----

TABLE 2 (continued)

θ°	φ°	β°	$\lvert P_\theta' \rvert$	Phase$^\circ$	$\lvert P_\varphi' \rvert$	Phase$^\circ$
40	-90	120	.1778	68.62	.0000	----
40	-80	120	.1757	68.26	.0281	-138.2
40	-70	120	.1689	67.18	.0562	-137.8
40	-60	120	.1565	65.28	.0839	-137.2
40	-50	120	.1372	62.25	.1099	-136.6
40	-40	120	.1107	57.13	.1322	-136.2
40	-30	120	.0786	46.77	.1486	-135.9
40	-20	120	.0484	19.49	.1558	-136.0
40	-10	120	.0458	-36.21	.1532	-136.6
40	0	120	.0743	-66.69	.1404	-137.9
40	10	120	.1064	-76.46	.1193	-140.2
40	20	120	.1319	-79.21	.0930	-144.1
40	30	120	.1482	-78.65	.0660	-151.0
40	40	120	.1559	-76.02	.0426	-163.2
40	50	120	.1573	-71.97	.0264	175.6
40	60	120	.1555	-67.20	.0182	147.6
40	70	120	.1530	-62.65	.0134	125.8
40	80	120	.1513	-59.37	.0075	114.6
40	90	120	.1507	-58.18	.0000	----
40	-90	180	.1697	122.9	.0000	----
40	-80	180	.1695	122.3	.0155	-123.7
40	-70	180	.1684	120.9	.0325	-121.4
40	-60	180	.1648	119.0	.0521	-118.4
40	-50	180	.1567	116.8	.0746	-115.4
40	-40	180	.1416	114.8	.0989	-112.7
40	-30	180	.1178	113.1	.1228	-110.5
40	-20	180	.0850	111.8	.1433	-109.1
40	-10	180	.0446	111.1	.1572	-108.2
40	0	180	.0000	----	.1622	-107.9
40	10	180	.0446	-68.95	.1572	-108.2
40	20	180	.0850	-68.19	.1433	-109.1
40	30	180	.1178	-66.94	.1228	-110.5
40	40	180	.1416	-65.25	.0989	-112.7
40	50	180	.1567	-63.21	.0746	-115.4
40	60	180	.1648	-61.04	.0521	-118.4
40	70	180	.1684	-59.07	.0325	-121.4
40	80	180	.1695	-57.66	.0155	-123.7
40	90	180	.1697	-57.15	.0000	----

TABLE 2 (continued)

θ°	φ°	β°	$\lvert P_\theta' \rvert$	Phase$^\circ$	$\lvert P_\varphi' \rvert$	Phase$^\circ$
50	-90	0	.1549	-33.63	.0000	----
50	-80	0	.1513	-34.89	.0297	170.8
50	-70	0	.1410	-38.99	.0567	171.0
50	-60	0	.1259	-46.94	.0783	171.2
50	-50	0	.1105	-60.34	.0916	171.5
50	-40	0	.1021	-79.49	.0945	171.7
50	-30	0	.1059	-99.78	.0854	171.9
50	-20	0	.1187	-114.8	.0649	172.1
50	-10	0	.1311	-123.1	.0350	172.2
50	0	0	.1361	-125.7	.0000	-18.43
50	10	0	.1311	-123.1	.0350	-7.76
50	20	0	.1187	-114.8	.0649	-7.87
50	30	0	.1059	-99.78	.0854	-8.05
50	40	0	.1021	-79.49	.0945	-8.28
50	50	0	.1105	-60.34	.0916	-8.54
50	60	0	.1259	-46.94	.0783	-8.79
50	70	0	.1410	-38.99	.0567	-9.01
50	80	0	.1513	-34.89	.0297	-9.15
50	90	0	.1549	-33.63	.0000	----
50	-90	60	.1676	23.30	.0000	----
50	-80	60	.1646	22.67	.0284	-164.0
50	-70	60	.1553	20.62	.0556	-163.7
50	-60	60	.1393	16.66	.0802	-163.2
50	-50	60	.1171	9.47	.1001	-162.8
50	-40	60	.0918	-4.14	.1128	-162.4
50	-30	60	.0727	-29.74	.1159	-162.2
50	-20	60	.0745	-63.20	.1080	-162.3
50	-10	60	.0949	-85.67	.0890	-163.1
50	0	60	.1179	-95.65	.0613	-165.5
50	10	60	.1336	-98.36	.0292	-174.3
50	20	60	.1390	-96.22	.0096	82.52
50	30	60	.1361	-89.89	.0334	36.34
50	40	60	.1299	-79.66	.0517	30.66
50	50	60	.1262	-66.79	.0594	28.60
50	60	60	.1279	-54.02	.0560	27.59
50	70	60	.1334	-44.10	.0431	27.02
50	80	60	.1389	-38.14	.0233	26.73
50	90	60	.1411	-36.19	.0000	----

TABLE 2 (continued)

θ°	φ°	β°	$\lvert P_\theta' \rvert$	Phase$^\circ$	$\lvert P_\varphi' \rvert$	Phase$^\circ$
50	-90	120	.1676	78.05	.0000	----
50	-80	120	.1664	77.54	.0197	-141.3
50	-70	120	.1622	76.06	.0400	-140.3
50	-60	120	.1532	73.72	.0612	-138.9
50	-50	120	.1375	70.44	.0823	-137.5
50	-40	120	.1135	65.63	.1014	-136.2
50	-30	120	.0816	56.89	.1157	-135.2
50	-20	120	.0476	33.64	.1224	-134.7
50	-10	120	.0383	-29.39	.1193	-134.7
50	0	120	.0681	-65.65	.1062	-135.5
50	10	120	.1015	-75.18	.0847	-137.5
50	20	120	.1267	-76.89	.0585	-142.2
50	30	120	.1410	-74.86	.0347	-154.2
50	40	120	.1460	-70.23	.0152	164.9
50	50	120	.1453	-63.65	.0165	102.4
50	60	120	.1429	-56.11	.0210	82.00
50	70	120	.1413	-49.10	.0192	75.15
50	80	120	.1410	-44.19	.0113	72.41
50	90	120	.1410	-42.44	.0000	----
50	-90	180	.1549	135.0	.0000	----
50	-80	180	.1552	134.0	.0070	-142.6
50	-70	180	.1556	131.4	.0155	-134.8
50	-60	180	.1549	127.9	.0273	-125.9
50	-50	180	.1504	124.1	.0435	-118.4
50	-40	180	.1390	120.6	.0635	-113.0
50	-30	180	.1182	117.8	.0849	-109.3
50	-20	180	.0867	115.8	.1042	-107.1
50	-10	180	.0460	114.7	.1178	-105.9
50	0	180	.0000	-45.00	.1226	-105.5
50	10	180	.0460	-65.33	.1178	-105.9
50	20	180	.0867	-64.15	.1042	-107.1
50	30	180	.1182	-62.17	.0849	-109.3
50	40	180	.1390	-59.39	.0635	-113.0
50	50	180	.1504	-55.93	.0435	-118.4
50	60	180	.1549	-52.13	.0273	-125.9
50	70	180	.1556	-48.55	.0155	-134.8
50	80	180	.1552	-45.97	.0070	-142.6
50	90	180	.1549	-45.02	.0000	----

TABLE 2 (continued)

θ°	φ°	β°	$\lvert P_\theta' \rvert$	Phase$^\circ$	$\lvert P_\varphi' \rvert$	Phase$^\circ$
60	-90	0	.1576	-25.29	.0000	----
60	-80	0	.1539	-26.39	.0244	166.3
60	-70	0	.1434	-30.00	.0468	166.6
60	-60	0	.1270	-37.14	.0650	167.0
60	-50	0	.1084	-49.79	.0768	167.5
60	-40	0	.0952	-69.83	.0799	168.0
60	-30	0	.0956	-93.56	.0729	168.4
60	-20	0	.1082	-111.9	.0557	168.7
60	-10	0	.1219	-121.7	.0302	168.9
60	0	0	.1276	-124.7	.0000	-10.30
60	10	0	.1219	-121.7	.0302	-11.05
60	20	0	.1082	-111.9	.0557	-11.26
60	30	0	.0956	-93.56	.0729	-11.60
60	40	0	.0952	-69.83	.0799	-12.04
60	50	0	.1084	-49.79	.0768	-12.53
60	60	0	.1270	-37.14	.0650	-13.02
60	70	0	.1434	-30.00	.0468	-13.44
60	80	0	.1539	-26.39	.0244	-13.72
60	90	0	.1576	-25.29	.0000	----
60	-90	60	.1644	30.77	.0000	----
60	-80	60	.1620	30.12	.0212	-167.9
60	-70	60	.1543	28.10	.0419	-167.2
60	-60	60	.1401	24.37	.0611	-166.3
60	-50	60	.1190	17.89	.0773	-165.2
60	-40	60	.0925	5.76	.0881	-164.1
60	-30	60	.0690	-18.86	.0913	-163.1
60	-20	60	.0660	-56.81	.0850	-162.4
60	-10	60	.0863	-83.63	.0690	-162.0
60	0	60	.1105	-94.74	.0451	-162.2
60	10	60	.1263	-97.28	.0167	-165.1
60	20	60	.1307	-94.23	.0116	27.26
60	30	60	.1263	-86.15	.0350	22.42
60	40	60	.1199	-73.27	.0504	21.55
60	50	60	.1185	-57.63	.0559	21.12
60	60	60	.1243	-43.23	.0517	20.82
60	70	60	.1337	-32.93	.0393	20.61
60	80	60	.1415	-27.12	.0211	20.47
60	90	60	.1445	-25.27	.0000	----

TABLE 2 (continued)

θ°	φ°	β°	$\lvert P_\theta' \rvert$	Phase$^\circ$	$\lvert P_\varphi' \rvert$	Phase$^\circ$
60	-90	120	.1591	86.55	.0000	----
60	-80	120	.1585	85.81	.0125	-146.1
60	-70	120	.1561	83.74	.0261	-144.1
60	-60	120	.1499	80.64	.0411	-141.4
60	-50	120	.1373	76.74	.0573	-138.7
60	-40	120	.1157	71.73	.0729	-136.3
60	-30	120	.0847	63.72	.0853	-134.5
60	-20	120	.0486	43.62	.0915	-133.1
60	-10	120	.0336	-22.76	.0893	-132.4
60	0	120	.0638	-64.74	.0781	-132.2
60	10	120	.0982	-74.16	.0592	-133.0
60	20	120	.1228	-75.09	.0359	-136.0
60	30	120	.1355	-71.87	.0130	-150.7
60	40	120	.1386	-65.50	.0090	85.14
60	50	120	.1369	-56.68	.0208	64.74
60	60	120	.1353	-46.79	.0251	60.84
60	70	120	.1358	-37.94	.0217	59.36
60	80	120	.1375	-32.00	.0124	58.72
60	90	120	.1384	-29.94	.0000	----
60	-90	180	.1462	145.8	.0000	----
60	-80	180	.1465	144.5	.0031	167.3
60	-70	180	.1473	140.7	.0062	-168.5
60	-60	180	.1477	135.5	.0117	-139.3
60	-50	180	.1454	130.0	.0226	-120.9
60	-40	180	.1368	125.1	.0383	-111.5
60	-30	180	.1182	121.3	.0565	-106.6
60	-20	180	.0879	118.6	.0736	-103.9
60	-10	180	.0471	117.1	.0857	-102.6
60	0	180	.0000	-21.80	.0901	-102.2
60	10	180	.0471	-62.92	.0857	-102.6
60	20	180	.0879	-61.36	.0736	-103.9
60	30	180	.1182	-58.69	.0565	-106.6
60	40	180	.1368	-54.87	.0383	-111.5
60	50	180	.1454	-50.00	.0226	-120.9
60	60	180	.1477	-44.52	.0117	-139.3
60	70	180	.1473	-39.32	.0062	-168.5
60	80	180	.1465	-35.54	.0031	-167.3
60	90	180	.1462	-34.16	.0000	----

TABLE 2 (continued)

θ°	φ°	β°	$\lvert P_\theta' \rvert$	Phase$^\circ$	$\lvert P_\varphi' \rvert$	Phase$^\circ$
70	-90	0	.1581	-19.46	.0000	----
70	-80	0	.1547	-20.49	.0168	162.5
70	-70	0	.1445	-23.82	.0324	162.9
70	-60	0	.1279	-30.42	.0453	163.6
70	-50	0	.1078	-42.38	.0539	164.3
70	-40	0	.0914	-62.52	.0566	165.1
70	-30	0	.0890	-88.57	.0520	165.7
70	-20	0	.1013	-109.5	.0400	166.2
70	-10	0	.1159	-120.7	.0218	166.6
70	0	0	.1220	-124.0	.0000	-8.43
70	10	0	.1159	-120.7	.0218	-13.45
70	20	0	.1013	-109.5	.0400	-13.76
70	30	0	.0890	-88.57	.0520	-14.27
70	40	0	.0914	-62.52	.0566	-14.92
70	50	0	.1078	-42.38	.0539	-15.66
70	60	0	.1279	-30.42	.0453	-16.42
70	70	0	.1445	-23.82	.0324	-17.07
70	80	0	.1547	-20.49	.0168	-17.51
70	90	0	.1581	-19.46	.0000	----
70	-90	60	.1610	36.49	.0000	----
70	-80	60	.1591	35.78	.0136	-171.8
70	-70	60	.1527	33.64	.0272	-170.7
70	-60	60	.1403	29.85	.0401	-169.2
70	-50	60	.1204	23.62	.0515	-167.4
70	-40	60	.0938	12.39	.0595	-165.7
70	-30	60	.0676	-11.00	.0623	-164.1
70	-20	60	.0608	-51.59	.0584	-162.7
70	-10	60	.0808	-81.99	.0472	-161.4
70	0	60	.1057	-94.01	.0301	-159.6
70	10	60	.1215	-96.44	.0097	-153.1
70	20	60	.1250	-92.70	.0110	10.62
70	30	60	.1195	-83.25	.0278	15.43
70	40	60	.1133	-68.30	.0385	16.31
70	50	60	.1140	-50.74	.0420	16.51
70	60	60	.1229	-35.56	.0384	16.47
70	70	60	.1346	-25.36	.0290	16.36
70	80	60	.1437	-19.81	.0155	16.25
70	90	60	.1471	-18.08	.0000	----

TABLE 2 (continued)

θ°	φ°	β°	$\lvert P_\theta' \rvert$	Phase$^\circ$	$\lvert P_\varphi' \rvert$	Phase$^\circ$
70	-90	120	.1532	93.34	.0000	----
70	-80	120	.1530	92.37	.0070	-152.1
70	-70	120	.1517	89.68	.0149	-148.7
70	-60	120	.1473	85.82	.0244	-144.3
70	-50	120	.1368	81.23	.0353	-140.2
70	-40	120	.1171	75.82	.0465	-136.7
70	-30	120	.0870	68.05	.0559	-134.0
70	-20	120	.0500	49.89	.0611	-132.0
70	-10	120	.0308	-17.29	.0601	-130.6
70	0	120	.0610	-64.01	.0522	-129.6
70	10	120	.0959	-73.41	.0383	-129.0
70	20	120	.1201	-73.79	.0212	-128.7
70	30	120	.1315	-69.67	.0039	-130.6
70	40	120	.1332	-61.96	.0102	53.15
70	50	120	.1313	-51.39	.0189	52.72
70	60	120	.1309	-39.81	.0214	52.59
70	70	120	.1335	-29.84	.0180	52.52
70	80	120	.1370	-23.41	.0102	52.47
70	90	120	.1385	-21.23	.0000	----
70	-90	180	.1418	154.2	.0000	----
70	-80	180	.1419	152.5	.0028	119.7
70	-70	180	.1423	147.8	.0039	135.2
70	-60	180	.1429	141.3	.0042	-172.2
70	-50	180	.1417	134.4	.0100	-124.2
70	-40	180	.1349	128.4	.0211	-109.4
70	-30	180	.1180	123.7	.0345	-103.8
70	-20	180	.0887	120.5	.0475	-101.2
70	-10	180	.0478	118.6	.0568	-99.96
70	0	180	.0000	-14.04	.0602	-99.60
70	10	180	.0478	-61.37	.0568	-99.96
70	20	180	.0887	-59.52	.0475	-101.2
70	30	180	.1180	-53.31	.0345	-103.8
70	40	180	.1349	-51.64	.0211	-109.4
70	50	180	.1417	-45.60	.0100	-124.2
70	60	180	.1429	-38.73	.0042	-172.2
70	70	180	.1423	-32.21	.0039	135.2
70	80	180	.1419	-27.51	.0028	119.7
70	90	180	.1418	-25.80	.0000	----

TABLE 2 (continued)

θ°	φ°	β°	$\lvert P_\theta' \rvert$	Phase$^\circ$	$\lvert P_\varphi' \rvert$	Phase$^\circ$
80	-90	0	.1580	-15.95	.0000	----
80	-80	0	.1547	-16.94	.0085	160.1
80	-70	0	.1449	-20.15	.0163	160.7
80	-60	0	.1285	-26.48	.0230	161.5
80	-50	0	.1078	-38.00	.0275	162.5
80	-40	0	.0897	-58.01	.0290	163.4
80	-30	0	.0854	-85.34	.0268	164.2
80	-20	0	.0973	-108.0	.0207	164.8
80	-10	0	.1125	-120.0	.0113	165.2
80	0	0	.1189	-123.5	.0000	-3.95
80	10	0	.1125	-120.0	.0113	-14.78
80	20	0	.0973	-108.0	.0207	-15.16
80	30	0	.0854	-85.34	.0268	-15.79
80	40	0	.0897	-58.01	.0290	-16.60
80	50	0	.1078	-38.00	.0275	-17.54
80	60	0	.1285	-26.48	.0230	-18.50
80	70	0	.1449	-20.15	.0163	-19.34
80	80	0	.1547	-16.94	.0085	-19.91
80	90	0	.1580	-15.95	.0000	----
80	-90	60	.1587	40.12	.0000	----
80	-80	60	.1570	39.35	.0066	-174.6
80	-70	60	.1515	37.06	.0132	-173.2
80	-60	60	.1401	33.16	.0196	-171.2
80	-50	60	.1212	26.97	.0254	-168.9
80	-40	60	.0948	16.17	.0297	-166.7
80	-30	60	.0673	-6.36	.0314	-164.7
80	-20	60	.0581	-48.20	.0296	-162.9
80	-10	60	.0776	-80.94	.0240	-161.0
80	0	60	.1030	-93.55	.0152	-158.1
80	10	60	.1188	-95.91	.0046	-144.7
80	20	60	.1217	-91.75	.0064	4.28
80	30	60	.1156	-81.40	.0151	12.03
80	40	60	.1095	-65.13	.0206	13.60
80	50	60	.1117	-46.47	.0222	14.04
80	60	60	.1223	-31.00	.0202	14.08
80	70	60	.1353	-20.95	.0152	13.98
80	80	60	.1450	-15.61	.0081	13.87
80	90	60	.1485	-13.95	.0000	----

TABLE 2 (continued)

θ°	φ°	β°	$\lvert P_\theta' \rvert$	Phase$^\circ$	$\lvert P_\varphi' \rvert$	Phase$^\circ$
80	-90	120	.1499	97.70	.0000	----
80	-80	120	.1499	96.57	.0030	-157.7
80	-70	120	.1491	93.45	.0066	-152.7
80	-60	120	.1456	89.03	.0111	-146.7
80	-50	120	.1364	83.92	.0166	-141.2
80	-40	120	.1179	78.19	.0225	-136.9
80	-30	120	.0884	70.46	.0276	-133.7
80	-20	120	.0510	53.30	.0306	-131.4
80	-10	120	.0293	-13.77	.0303	-129.6
80	0	120	.0595	-63.55	.0263	-128.1
80	10	120	.0946	-72.94	.0191	-126.5
80	20	120	.1184	-73.00	.0100	-123.5
80	30	120	.1290	-63.32	.0012	-83.00
80	40	120	.1300	-59.74	.0066	44.51
80	50	120	.1280	-48.07	.0110	48.01
80	60	120	.1286	-35.50	.0121	48.99
80	70	120	.1326	-24.98	.0100	49.37
80	80	120	.1372	-18.37	.0056	49.52
80	90	120	.1391	-16.16	.0000	----
80	-90	180	.1399	159.4	.0000	----
80	-80	180	.1398	157.5	.0019	104.6
80	-70	180	.1398	152.2	.0027	111.5
80	-60	180	.1402	144.9	.0019	143.7
80	-50	180	.1394	137.1	.0035	-128.4
80	-40	180	.1336	130.3	.0092	-107.5
80	-30	180	.1178	125.1	.0164	-101.8
80	-20	180	.0890	121.5	.0234	-99.41
80	-10	180	.0482	119.5	.0285	-98.36
80	0	180	.0000	-33.69	.0303	-98.06
80	10	180	.0482	-60.50	.0285	-98.36
80	20	180	.0890	-58.47	.0234	-99.41
80	30	180	.1178	-54.91	.0164	-101.8
80	40	180	.1336	-49.69	.0092	-107.5
80	50	180	.1394	-42.88	.0034	-128.4
80	60	180	.1402	-35.11	.0019	143.7
80	70	180	.1398	-27.76	.0027	111.5
80	80	180	.1398	-22.52	.0019	104.6
80	90	180	.1399	-20.63	.0000	----

TABLE 2 (continued)

θ°	φ°	β°	$\lvert P_\theta' \rvert$	Phase$^\circ$	$\lvert P_\varphi' \rvert$	Phase$^\circ$
90	-90	0	.1578	-14.76	.0000	----
90	-80	0	.1547	-15.75	.0000	159.3
90	-70	0	.1449	-18.93	.0000	159.9
90	-60	0	.1287	-25.18	.0000	160.8
90	-50	0	.1079	-36.55	.0000	161.8
90	-40	0	.0892	-56.49	.0000	162.9
90	-30	0	.0843	-84.22	.0000	163.7
90	-20	0	.0961	-107.5	.0000	164.4
90	-10	0	.1114	-119.8	.0000	164.8
90	0	0	.1179	-123.4	.0000	0.00
90	10	0	.1114	-119.8	.0000	-15.19
90	20	0	.0961	-107.5	.0000	-15.60
90	30	0	.0843	-84.22	.0000	-16.27
90	40	0	.0892	-56.49	.0000	-17.14
90	50	0	.1079	-36.55	.0000	-18.16
90	60	0	.1287	-25.18	.0000	-19.19
90	70	0	.1449	-18.93	.0000	-20.10
90	80	0	.1547	-15.75	.0000	-20.72
90	90	0	.1578	-14.76	.0000	----
90	-90	60	.1578	41.37	.0000	----
90	-80	60	.1563	40.58	.0000	-175.6
90	-70	60	.1510	38.23	.0000	-174.0
90	-60	60	.1401	34.26	.0000	-171.9
90	-50	60	.1215	28.08	.0000	-169.4
90	-40	60	.0952	17.40	.0000	-167.1
90	-30	60	.0673	-4.84	.0000	-164.9
90	-20	60	.0573	-47.03	.0000	-162.9
90	-10	60	.0766	-80.58	.0000	-160.8
90	0	60	.1021	-93.39	.0000	-157.6
90	10	60	.1179	-95.73	.0000	-142.0
90	20	60	.1206	-91.42	.0000	2.53
90	30	60	.1142	-80.76	.0000	11.01
90	40	60	.1083	-64.04	.0000	12.77
90	50	60	.1110	-45.02	.0000	13.28
90	60	60	.1222	-29.48	.0000	13.33
90	70	60	.1355	-19.51	.0000	13.22
90	80	60	.1454	-14.23	.0000	13.10
90	90	60	.1489	-12.59	.0000	----

TABLE 2 (continued)

θ°	φ°	β°	$\lvert P_\theta' \rvert$	Phase$^\circ$	$\lvert P_\varphi' \rvert$	Phase$^\circ$
90	-90	120	.1489	99.20	.0000	----
90	-80	120	.1489	98.01	.0000	-160.1
90	-70	120	.1482	94.73	.0000	-154.3
90	-60	120	.1451	90.11	.0000	-147.6
90	-50	120	.1362	84.82	.0000	-141.6
90	-40	120	.1181	78.97	.0000	-137.0
90	-30	120	.0888	71.23	.0000	-133.6
90	-20	120	.0514	54.38	.0000	-131.1
90	-10	120	.0289	-12.56	.0000	-129.2
90	0	120	.0590	-63.39	.0000	-127.6
90	10	120	.0942	-72.78	.0000	-125.6
90	20	120	.1179	-72.73	.0000	-121.6
90	30	120	.1281	-67.86	.0000	-62.50
90	40	120	.1289	-58.98	.0000	42.44
90	50	120	.1269	-46.94	.0000	46.71
90	60	120	.1278	-34.05	.0000	47.95
90	70	120	.1324	-23.36	.0000	48.45
90	80	120	.1373	-16.71	.0000	48.64
90	90	120	.1394	-14.51	.0000	----
90	-90	180	.1394	161.1	.0000	----
90	-80	180	.1392	159.2	.0000	101.1
90	-70	180	.1390	153.7	.0000	106.2
90	-60	180	.1393	146.1	.0000	129.8
90	-50	180	.1387	138.0	.0000	-130.9
90	-40	180	.1331	131.0	.0000	-106.8
90	-30	180	.1176	125.6	.0000	-101.1
90	-20	180	.0892	121.9	.0000	-98.81
90	-10	180	.0483	119.8	.0000	-97.84
90	0	180	.0000	14.04	.0000	-97.56
90	10	180	.0483	-60.21	.0000	-97.84
90	20	180	.0892	-58.12	.0000	-98.81
90	30	180	.1176	-54.45	.0000	-101.1
90	40	180	.1331	-49.04	.0000	-106.8
90	50	180	.1387	-41.96	.0000	-130.9
90	60	180	.1393	-33.88	.0000	129.8
90	70	180	.1390	-26.26	.0000	106.2
90	80	180	.1392	-20.83	.0000	101.1
90	90	180	.1394	-18.88	.0000	----

TABLE 3

PATTERN SUMMATION FUNCTIONS FOR TWO DIAMETRICALLY OPPOSED SLOTS OPERATING SIMULTANEOUSLY INPHASE (LONGITUDINAL CUTS)

θ°	φ°	β°	$\lvert P_\theta' \rvert$	Phase$^\circ$	φ°	β°	$\lvert P_\theta' \rvert$	Phase$^\circ$
5	90	0	.3732	-141.9	180	0	.4004	-144.9
10	90	0	.2245	-125.8	180	0	.2685	-137.3
15	90	0	.1705	-108.6	180	0	.2214	-133.1
20	90	0	.1482	-91.35	180	0	.1960	-130.5
25	90	0	.1413	-75.93	180	0	.1792	-129.0
30	90	0	.1418	-63.32	180	0	.1667	-128.0
35	90	0	.1452	-53.35	180	0	.1568	-127.3
40	90	0	.1491	-45.42	180	0	.1486	-126.7
45	90	0	.1524	-38.98	180	0	.1418	-126.2
50	90	0	.1549	-33.63	180	0	.1361	-125.7
55	90	0	.1566	-29.11	180	0	.1314	-125.2
60	90	0	.1576	-25.29	180	0	.1276	-124.7
65	90	0	.1580	-22.08	180	0	.1245	-124.3
70	90	0	.1581	-19.46	180	0	.1220	-124.0
75	90	0	.1581	-17.42	180	0	.1202	-123.7
80	90	0	.1580	-15.95	180	0	.1189	-123.5
85	90	0	.1579	-15.06	180	0	.1182	-123.4
90	90	0	.1578	-14.76	180	0	.1179	-123.4
95	90	0	.1579	-15.06	180	0	.1182	-123.4
100	90	0	.1580	-15.95	180	0	.1189	-123.5
105	90	0	.1581	-17.42	180	0	.1202	-123.7
110	90	0	.1581	-19.46	180	0	.1220	-124.0
115	90	0	.1580	-22.08	180	0	.1245	-124.3
120	90	0	.1576	-25.29	180	0	.1276	-124.7
125	90	0	.1566	-29.11	180	0	.1314	-125.2
130	90	0	.1549	-33.63	180	0	.1361	-125.7
135	90	0	.1524	-38.98	180	0	.1418	-126.2
140	90	0	.1491	-45.42	180	0	.1486	-126.7
145	90	0	.1452	-53.35	180	0	.1568	-127.3
150	90	0	.1418	-63.32	180	0	.1667	-128.0
155	90	0	.1413	-75.93	180	0	.1792	-129.0
160	90	0	.1482	-91.35	180	0	.1960	-130.5
165	90	0	.1705	-108.6	180	0	.2214	-133.1
170	90	0	.2245	-125.8	180	0	.2688	-137.3
175	90	0	.3732	-141.9	180	0	.4004	-144.9

TABLE 4

EXPERIMENTAL PATTERN AREAS AND SUMMATION

θ°	$A_\theta (in^2)$	Sin θ	A_θ(Sin θ)
0	0.20	0.000	0.000
10	3.25	0.174	0.566
20	9.72	0.342	3.324
30	16.23	0.500	8.115
40	21.50	0.643	13.825
50	18.35	0.766	14.056
60	11.20	0.866	9.699
70	13.37	0.940	12.568
80	10.04	0.985	9.889
90	6.12	1.000	6.120
100	7.42	0.985	7.309
110	9.07	0.940	8.526
120	13.42	0.866	11.622
130	20.24	0.766	15.504
140	27.37	0.643	17.599
150	25.17	0.500	12.585
160	13.80	0.342	4.720
170	3.55	0.174	0.618
180	0.07	0.000	0.000
		TOTAL	156.645

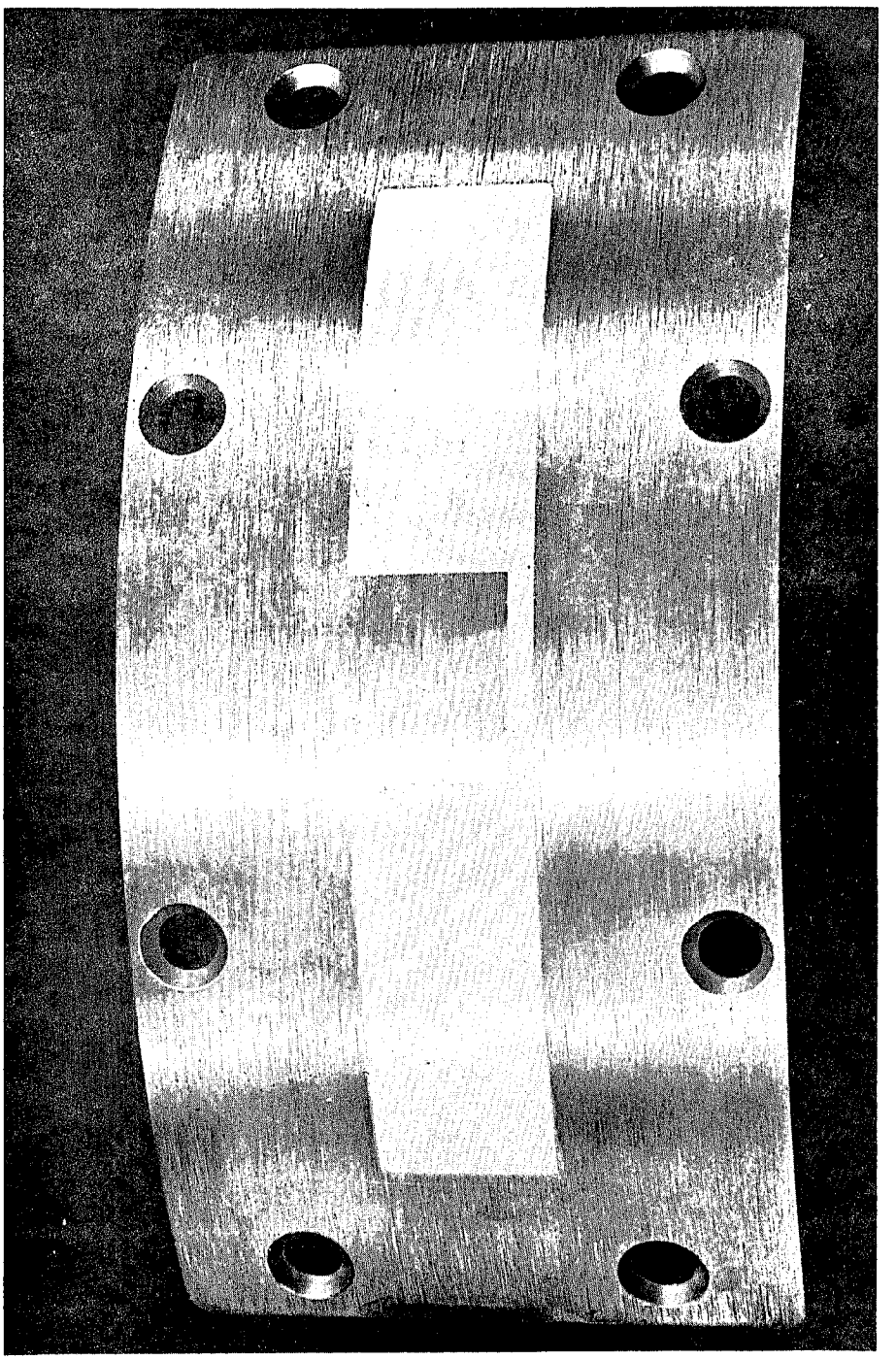

FIGURE 1

COMMAND DESTRUCT ANTENNA

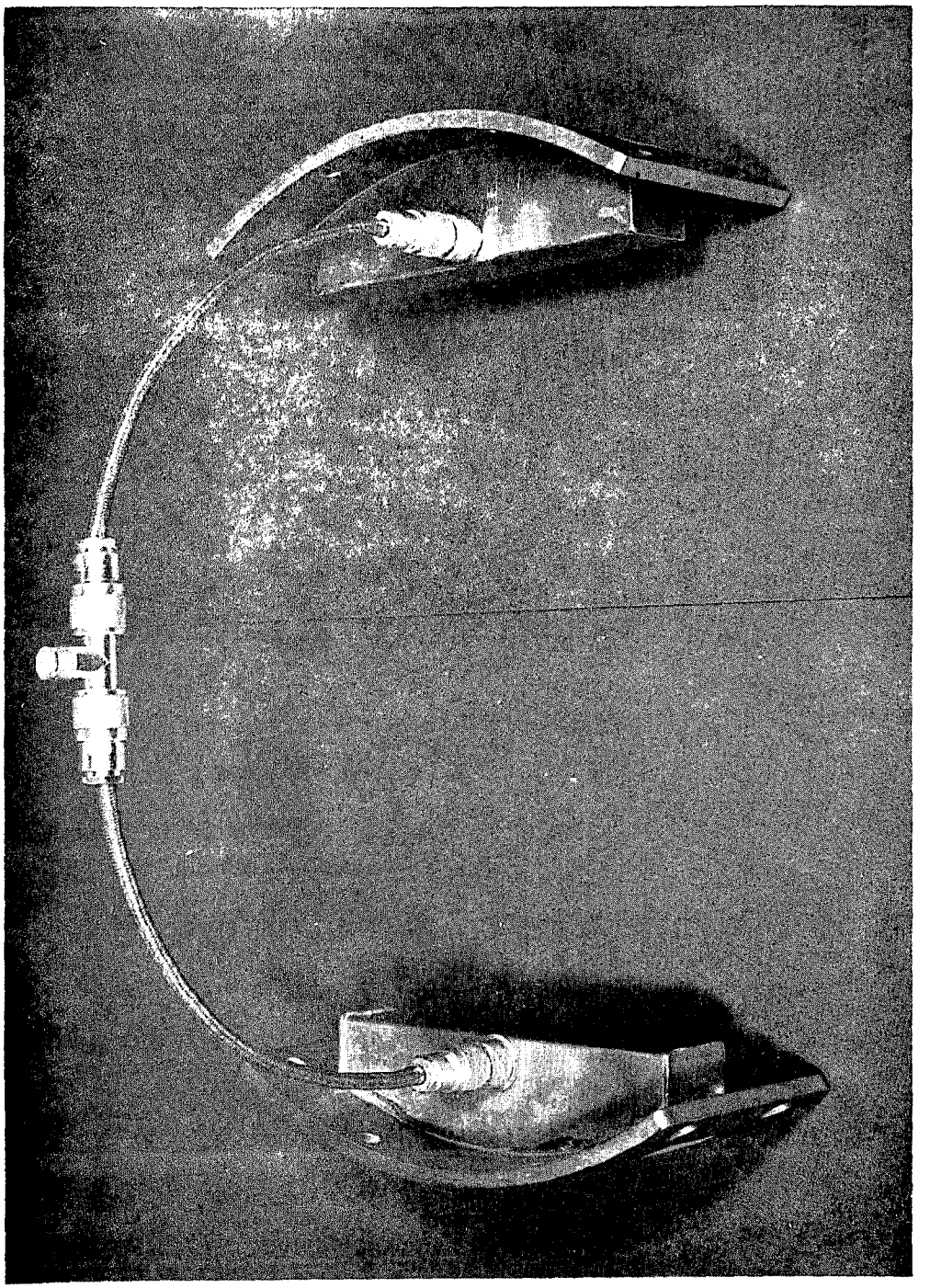

FIGURE 2

BOTH COMMAND DESTRUCT ANTENNAS WITH

INTERCONNECTING COAXIAL CABLE

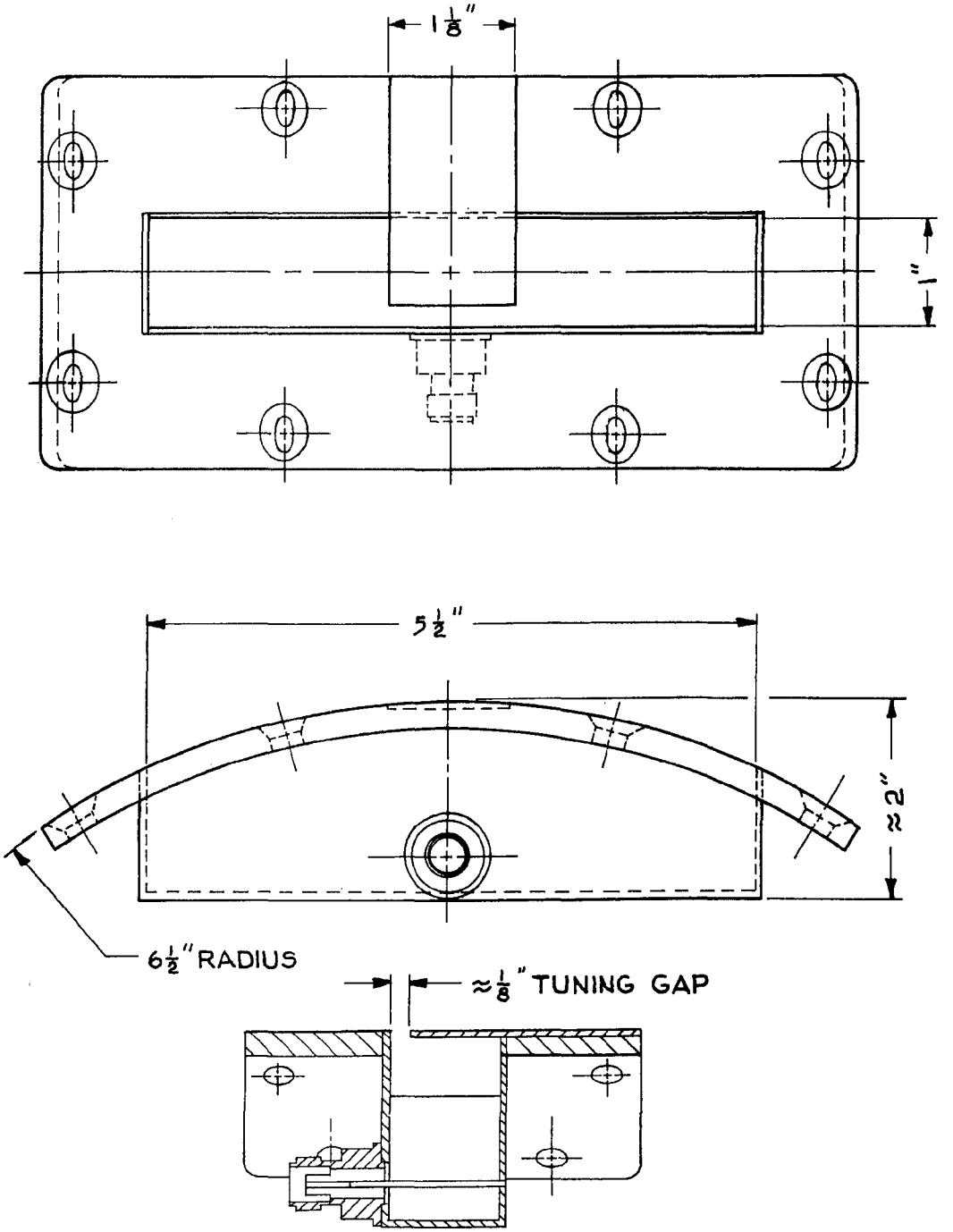

FIGURE 3

COMMAND DESTRUCT ANTENNA DESIGN

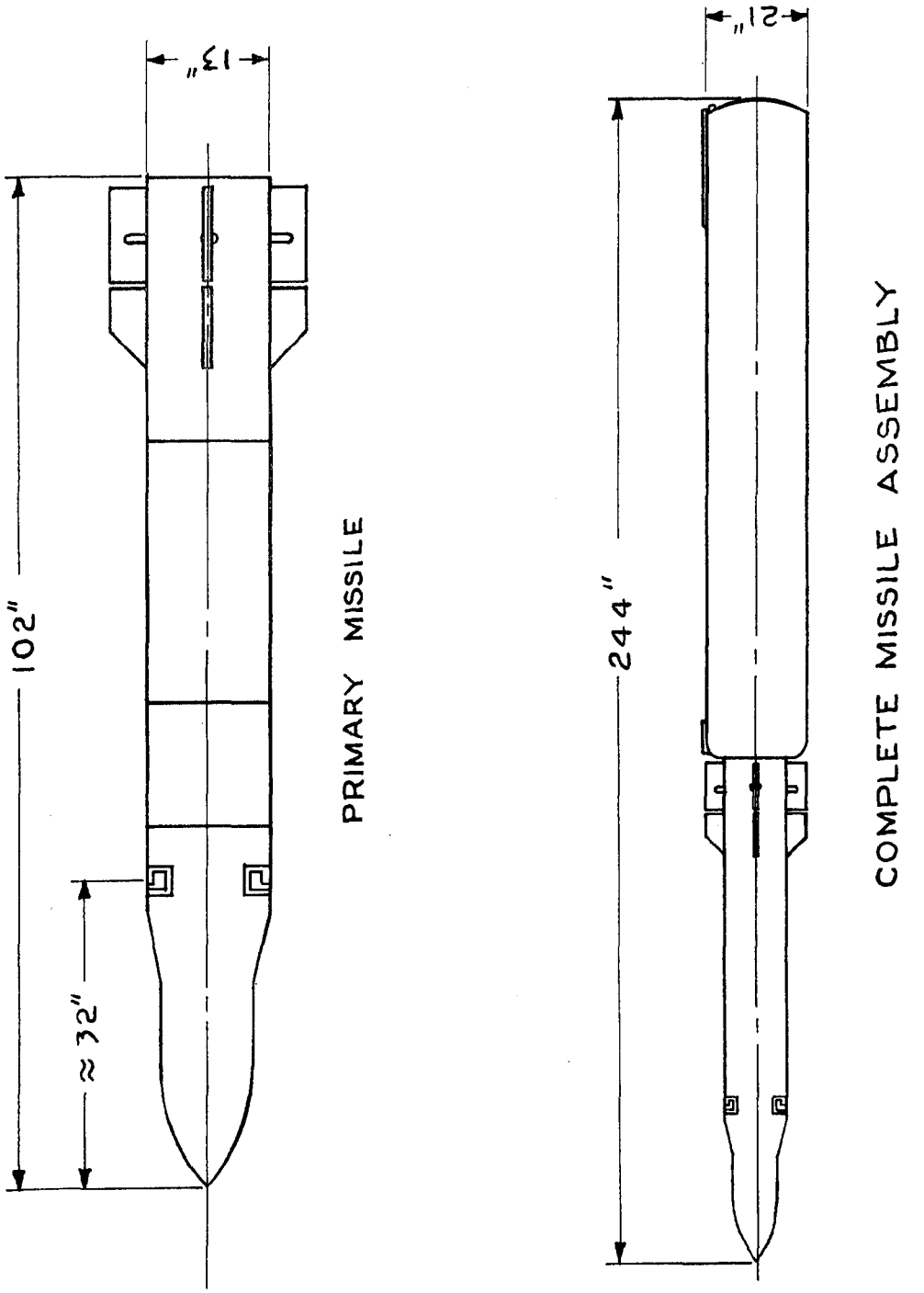

FIGURE 4

MISSILE CONFIGURATIONS

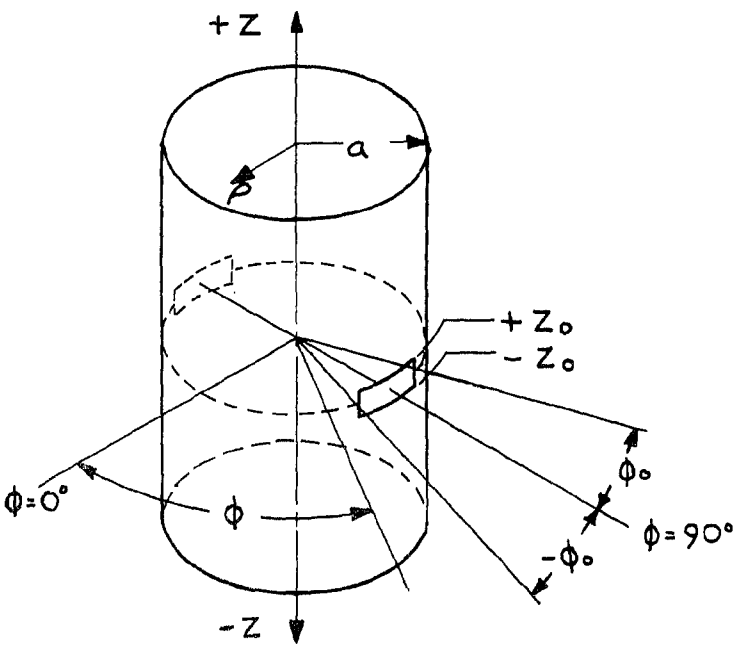

CYLINDERICAL COORDINATE SYSTEM

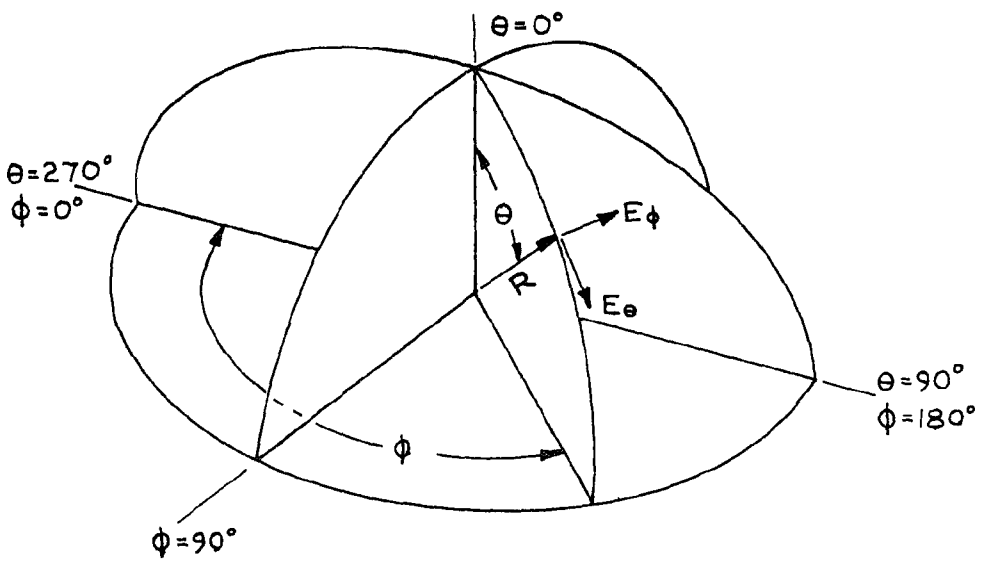

SPHERICAL COORDINATE SYSTEM

FIGURE 5

COORDINATE SYSTEMS

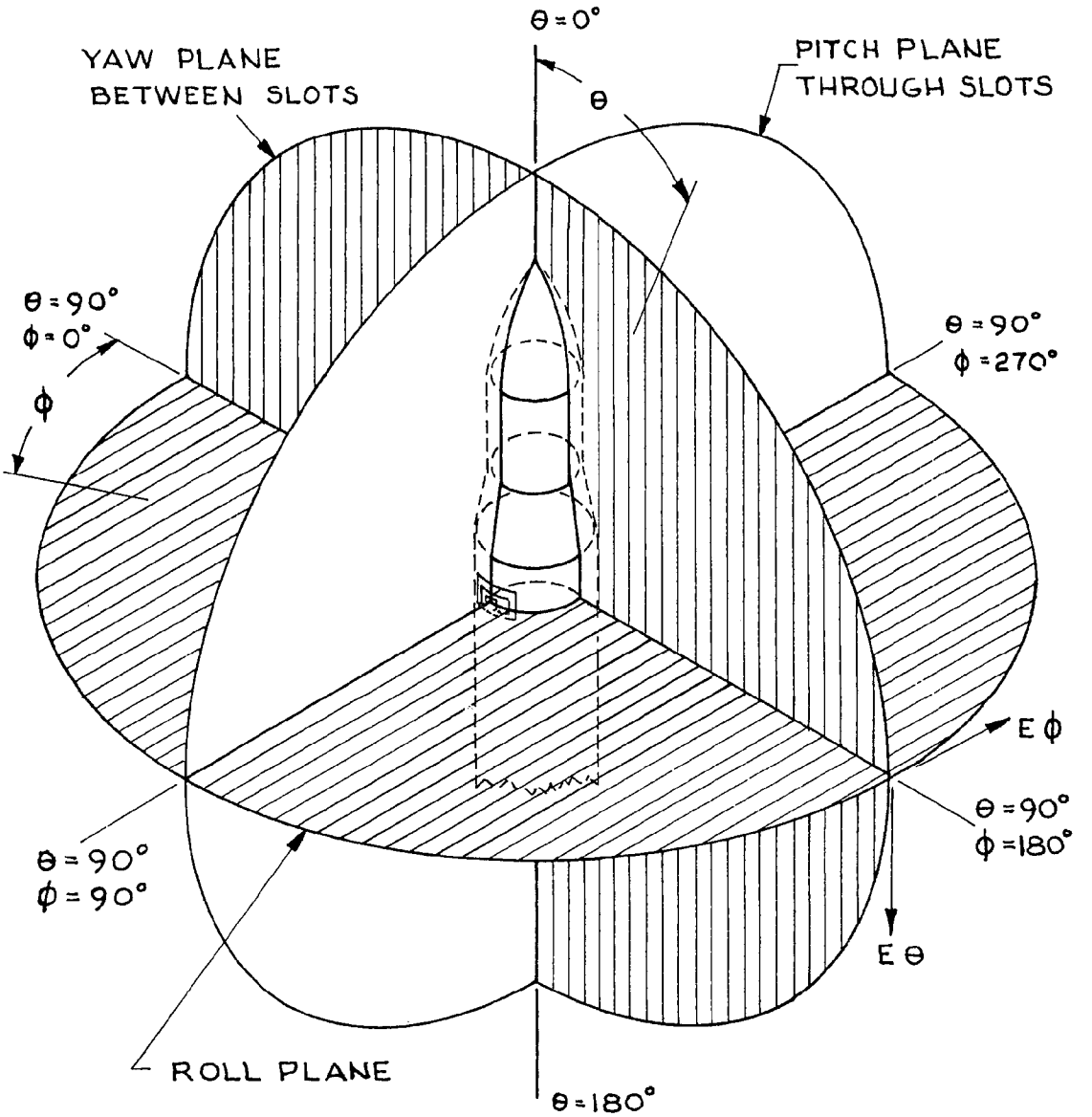

FIGURE 6

MISSILE ORIENTATION WITH REFERENCE TO

THE SPHERICAL COORDINATE SYSTEM

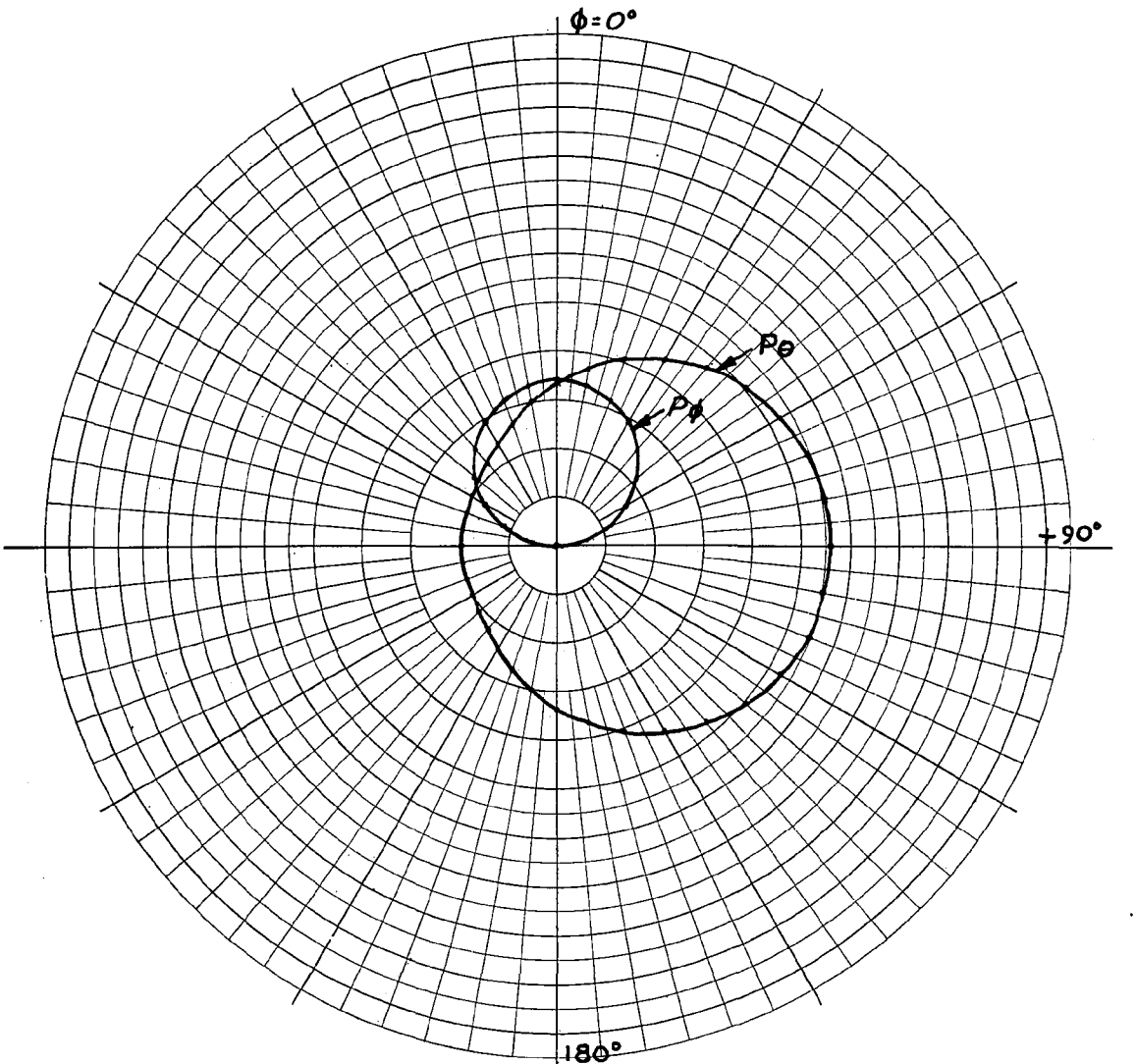

ANTENNA TYPE C.D.	LOCATION	USE	
TEST MODEL:		FREQUENCY: 445 MCS	
MODEL SCALE: 1:1		SCALE FREQUENCY: 1:1 MCS	
CONDITIONS:		POLARIZATION:	
CURVES PLOTTED IN:		Eθ: X	
VOLTAGE: X		Eϕ: X	θ=10°
POWER:		PATTERN AREA:	
ENGINEER	OPERATOR	FILE NO.	DATE

Pattern scale: Each major radial increment = 0.04 units

FIGURE 7

PATTERN FUNCTION PLOTS FOR A SINGLE SLOT

CENTERED AT $\varphi = 90^{\circ}$ FOR $\theta = 10^{\circ}$

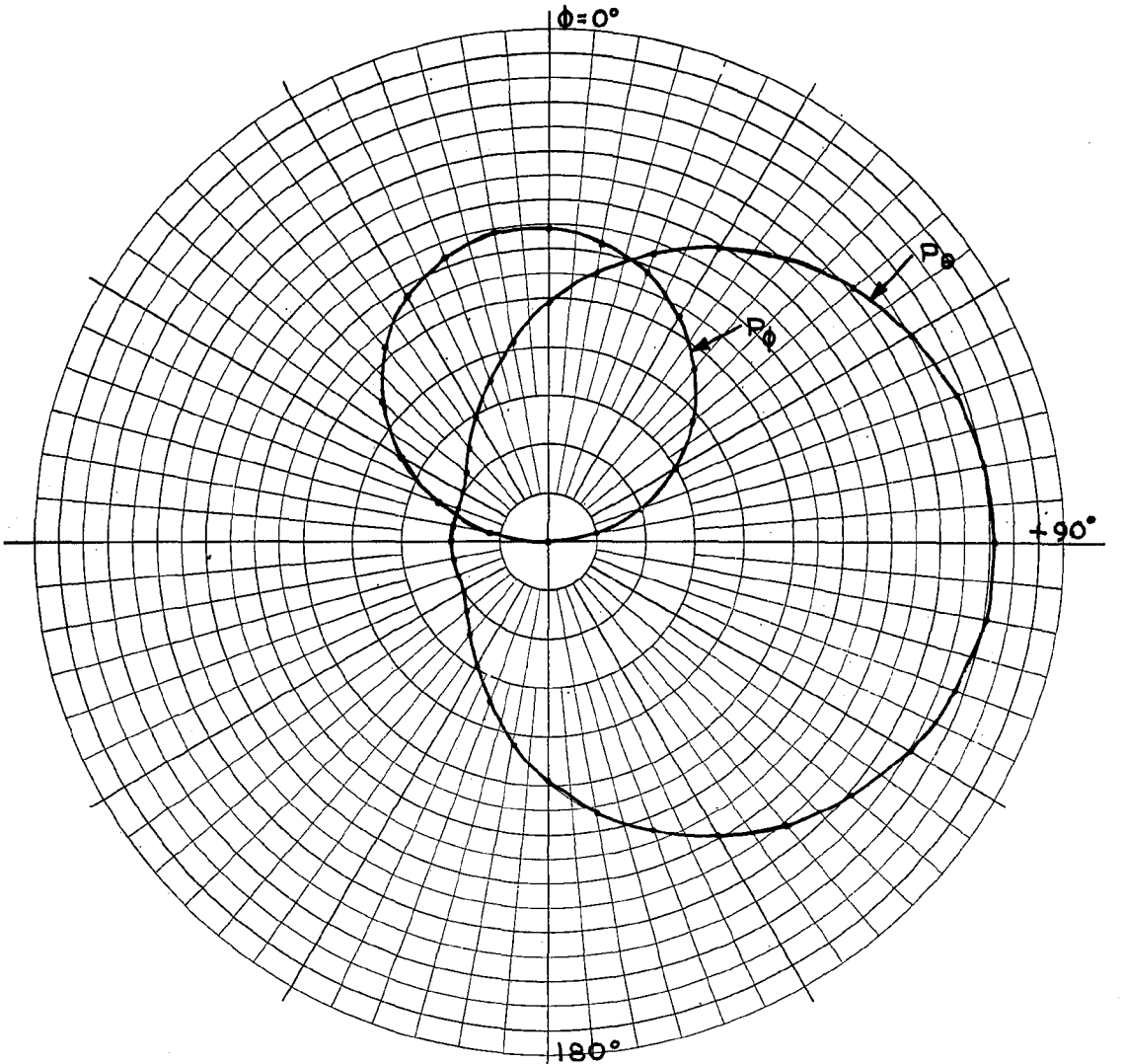

ANTENNA TYPE C.D.	LOCATION	USE	
TEST MODEL:		FREQUENCY: 445 MCS	
MODEL SCALE: 1:1		SCALE FREQUENCY: 1:1 MCS	
CONDITIONS:		POLARIZATION:	
CURVES PLOTTED IN:		E θ: X	
VOLTAGE: X		E φ: X	θ= 20°
POWER:		PATTERN AREA:	
ENGINEER	OPERATOR	FILE NO.	DATE

Pattern scale: Each major radial increment = 0.02 units

FIGURE 8

PATTERN FUNCTION PLOTS FOR A SINGLE SLOT

CENTERED AT $\varphi = 90^{\circ}$ FOR $\theta = 20^{\circ}$

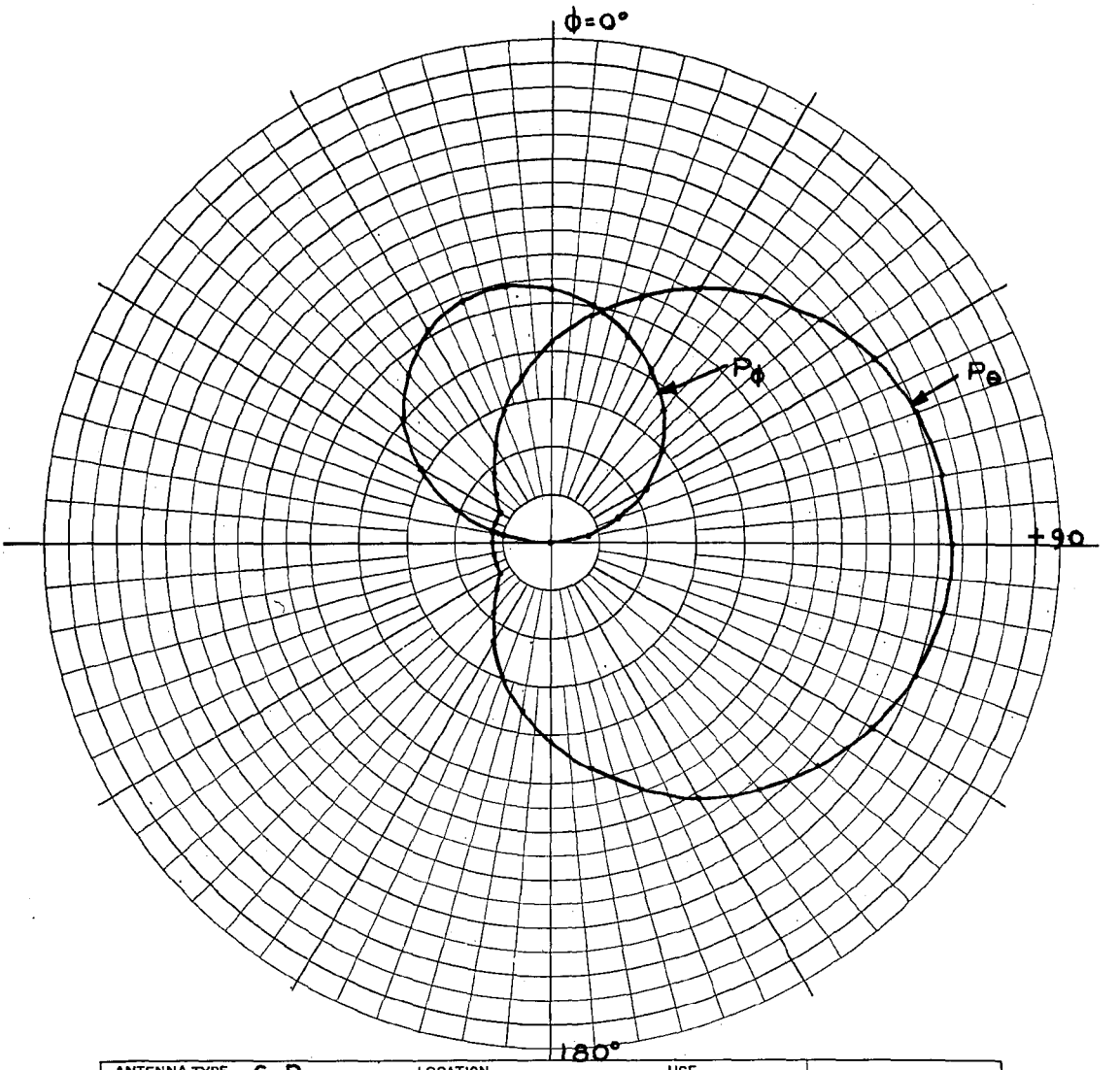

ANTENNA TYPE C. D.	LOCATION	USE	
TEST MODEL:		FREQUENCY: 445 MCS	
MODEL SCALE: 1:1		SCALE FREQUENCY: 1:1 MCS	
CONDITIONS:		POLARIZATION:	
CURVES PLOTTED IN:		E θ: X	
VOLTAGE: X		E ϕ: X	θ=30°
POWER:		PATTERN AREA:	
ENGINEER	OPERATOR	FILE NO.	DATE

Pattern scale: Each major radial increment = 0.02 units

FIGURE 9

PATTERN FUNCTION PLOTS FOR A SINGLE SLOT

CENTERED AT $\varphi = 90^\circ$ FOR $\theta = 30^\circ$

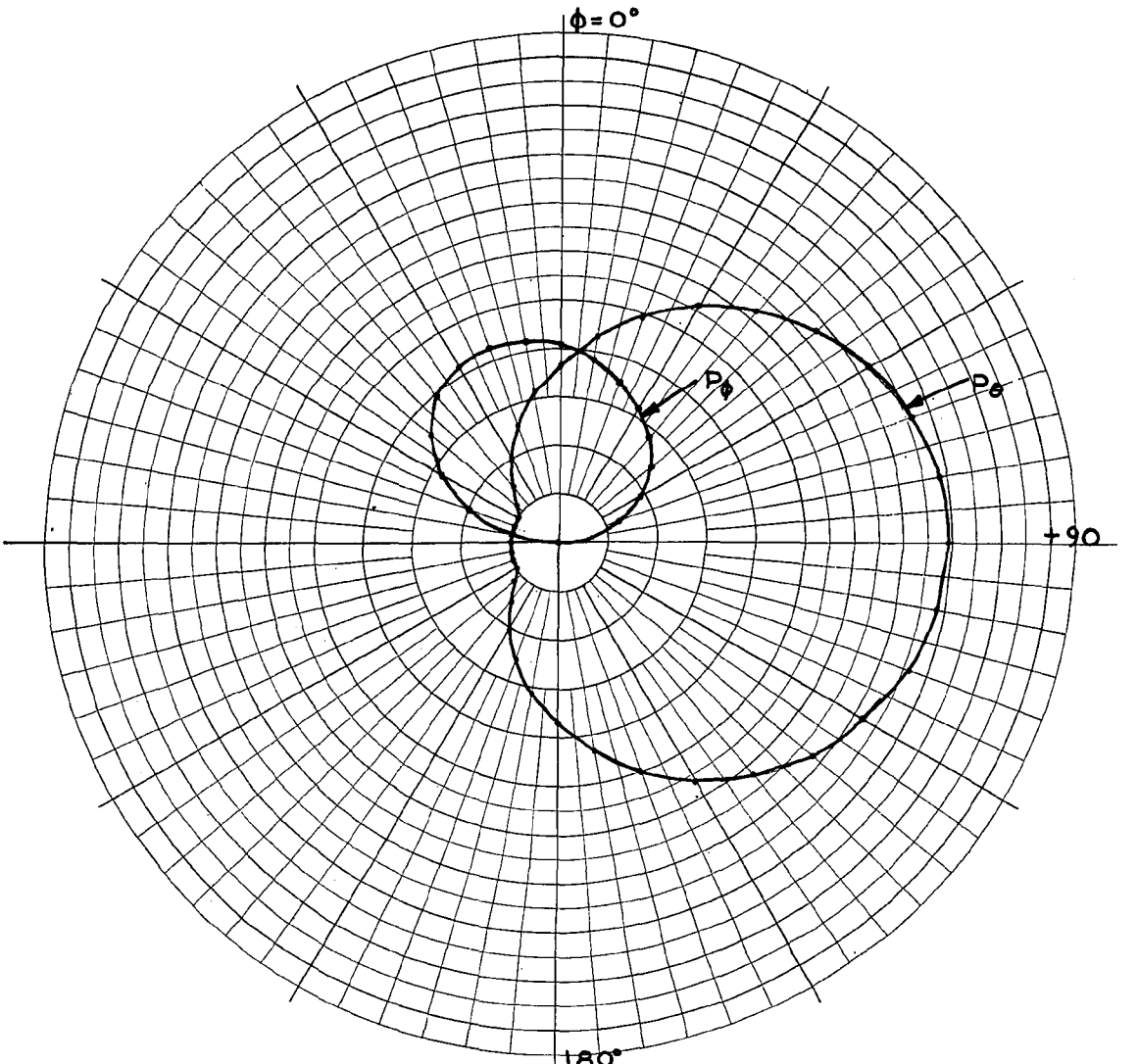

ANTENNA TYPE C. D.	LOCATION	USE	
TEST MODEL:		FREQUENCY: 445 MCS	
MODEL SCALE: 1:1		SCALE FREQUENCY: 1:1 MCS	
CONDITIONS:		POLARIZATION:	
CURVES PLOTTED IN:		Eθ: X	
VOLTAGE: X		Eϕ: X	θ=40°
POWER:		PATTERN AREA:	
ENGINEER	OPERATOR	FILE NO.	DATE

Pattern scale: Each major radial increment = 0.02 units

FIGURE 10

PATTERN FUNCTION PLOTS FOR A SINGLE SLOT

CENTERED AT $\varphi = 90^{\circ}$ FOR $\theta = 40^{\circ}$

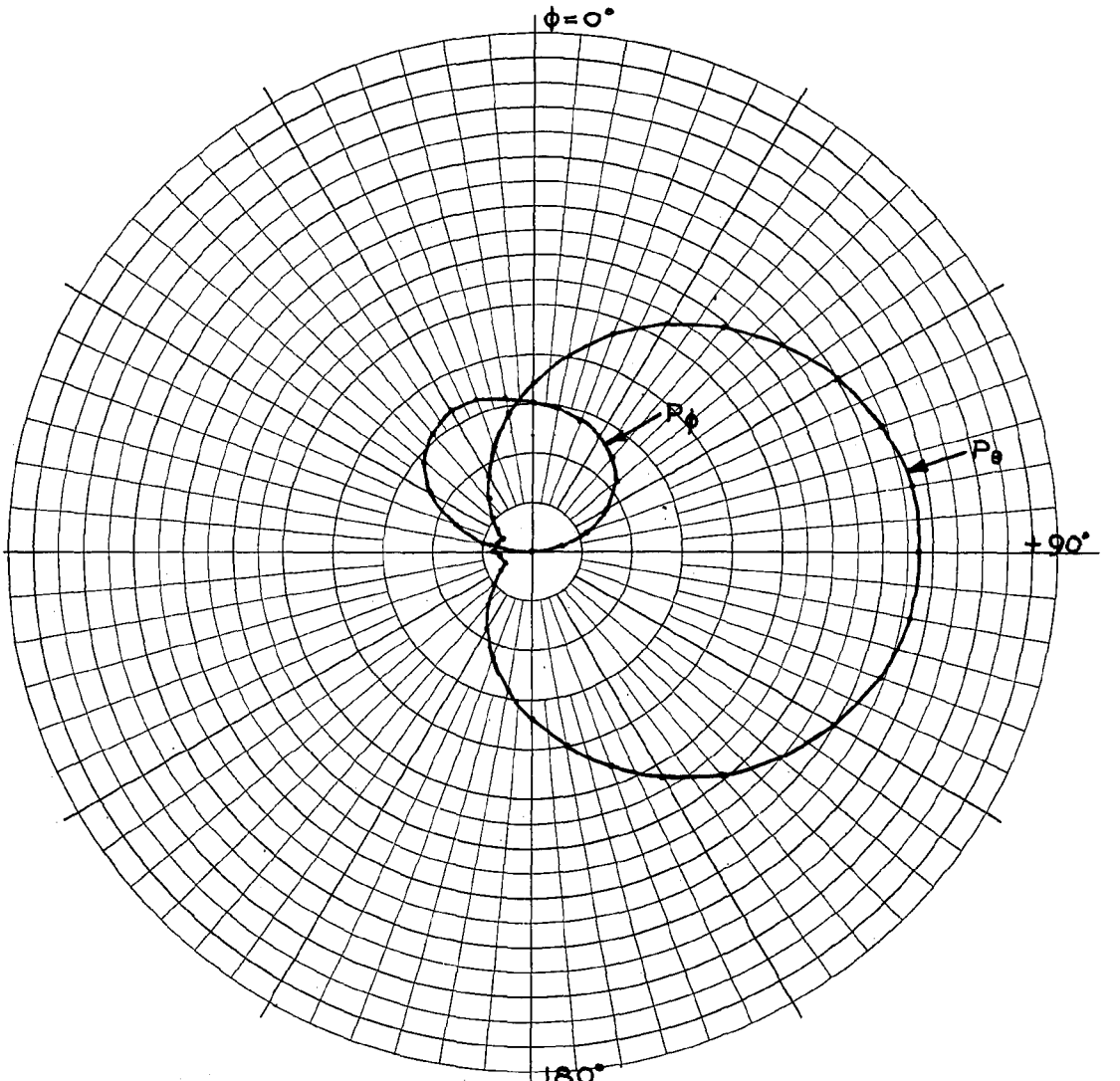

ANTENNA TYPE C.D.	LOCATION	USE	
TEST MODEL:		FREQUENCY: 445 MCS	
MODEL SCALE: 1:1		SCALE FREQUENCY: 1:1 MCS	
CONDITIONS:		POLARIZATION:	
CURVES PLOTTED IN:		Eφ: X	
VOLTAGE: X		Eϕ: X	θ=50°
POWER:		PATTERN AREA:	
ENGINEER	OPERATOR	FILE NO.	DATE

Pattern scale: Each major radial increment = 0.02 units

FIGURE 11

PATTERN FUNCTION PLOTS FOR A SINGLE SLOT

CENTERED AT $\varphi = 90^{\circ}$ FOR $\theta = 50^{\circ}$

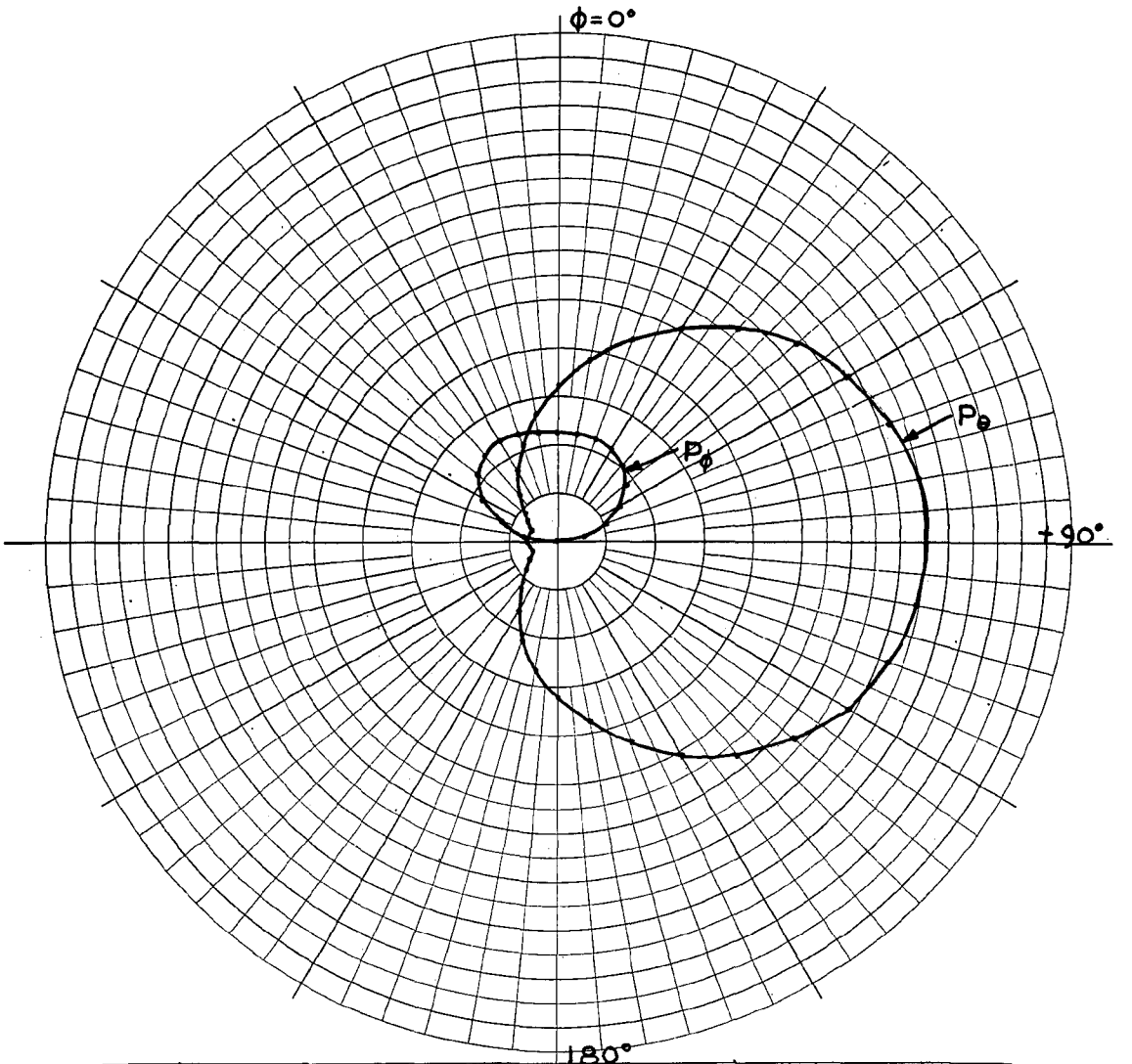

ANTENNA TYPE C. D.	LOCATION	USE	
TEST MODEL:		FREQUENCY: 445 MCS	
MODEL SCALE: 1:1		SCALE FREQUENCY: 1:1 MCS	
CONDITIONS:		POLARIZATION:	
CURVES PLOTTED IN:		E θ: X	
VOLTAGE: X		E ϕ: X	θ=60°
POWER:		PATTERN AREA:	
ENGINEER	OPERATOR	FILE NO.	DATE

Pattern scale: Each major radial increment = 0.02 units

FIGURE 12

PATTERN FUNCTION PLOTS FOR A SINGLE SLOT

CENTERED AT $\varphi = 90^{\circ}$ FOR $\theta = 60^{\circ}$

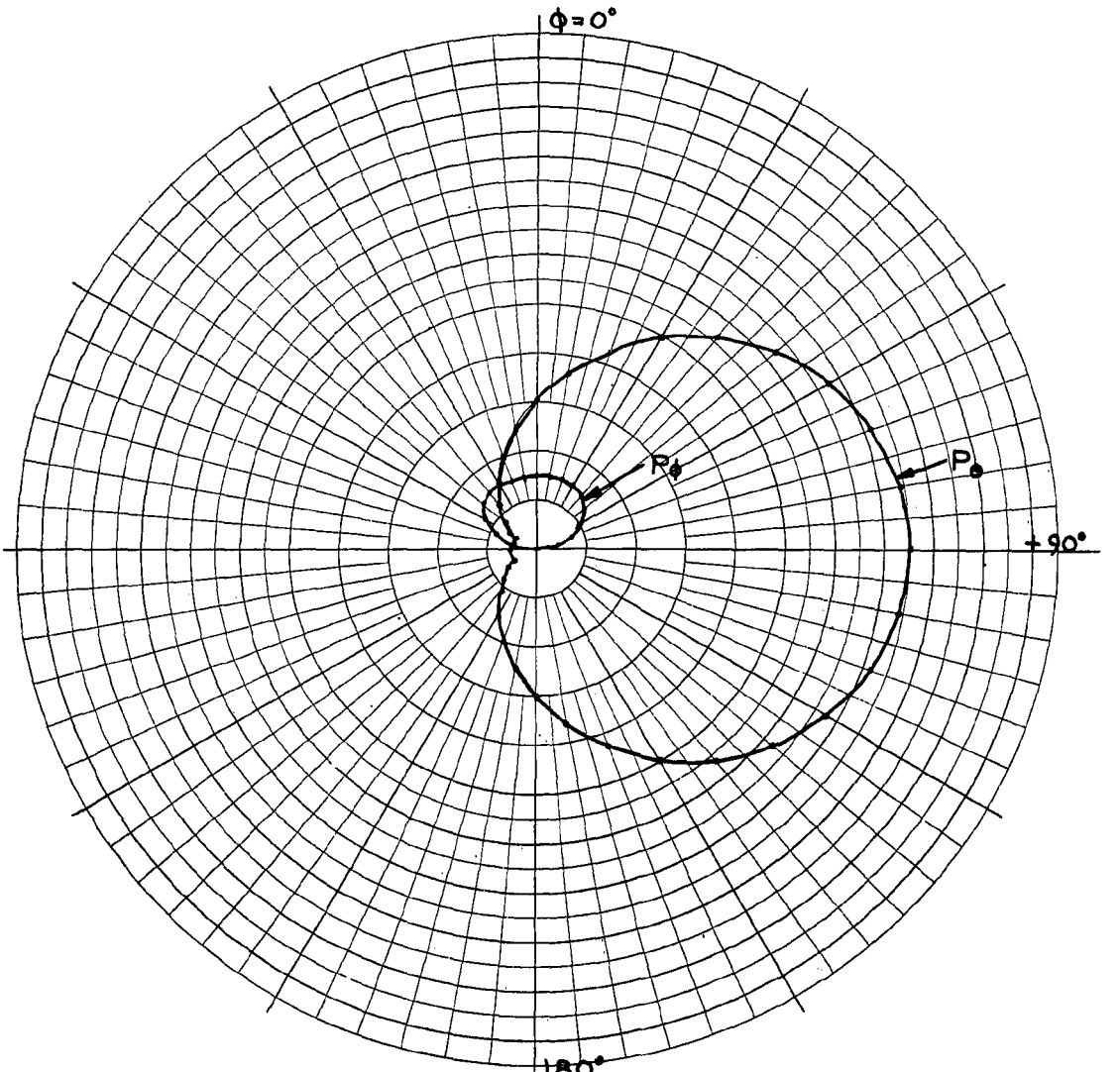

ANTENNA TYPE C.D.	LOCATION	USE	
TEST MODEL:		FREQUENCY: 445 MCS	
MODEL SCALE: 1:1		SCALE FREQUENCY: 1:1 MCS	
CONDITIONS:		POLARIZATION:	
CURVES PLOTTED IN:		E θ: X	
VOLTAGE: X		E ϕ: X	θ=70°
POWER:		PATTERN AREA:	
ENGINEER	OPERATOR	FILE NO.	DATE

Pattern scale: Each major radial increment = 0.02 units

FIGURE 13

PATTERN FUNCTION PLOTS FOR A SINGLE SLOT

CENTERED AT $\varphi = 90^{\circ}$ FOR $\theta = 70^{\circ}$

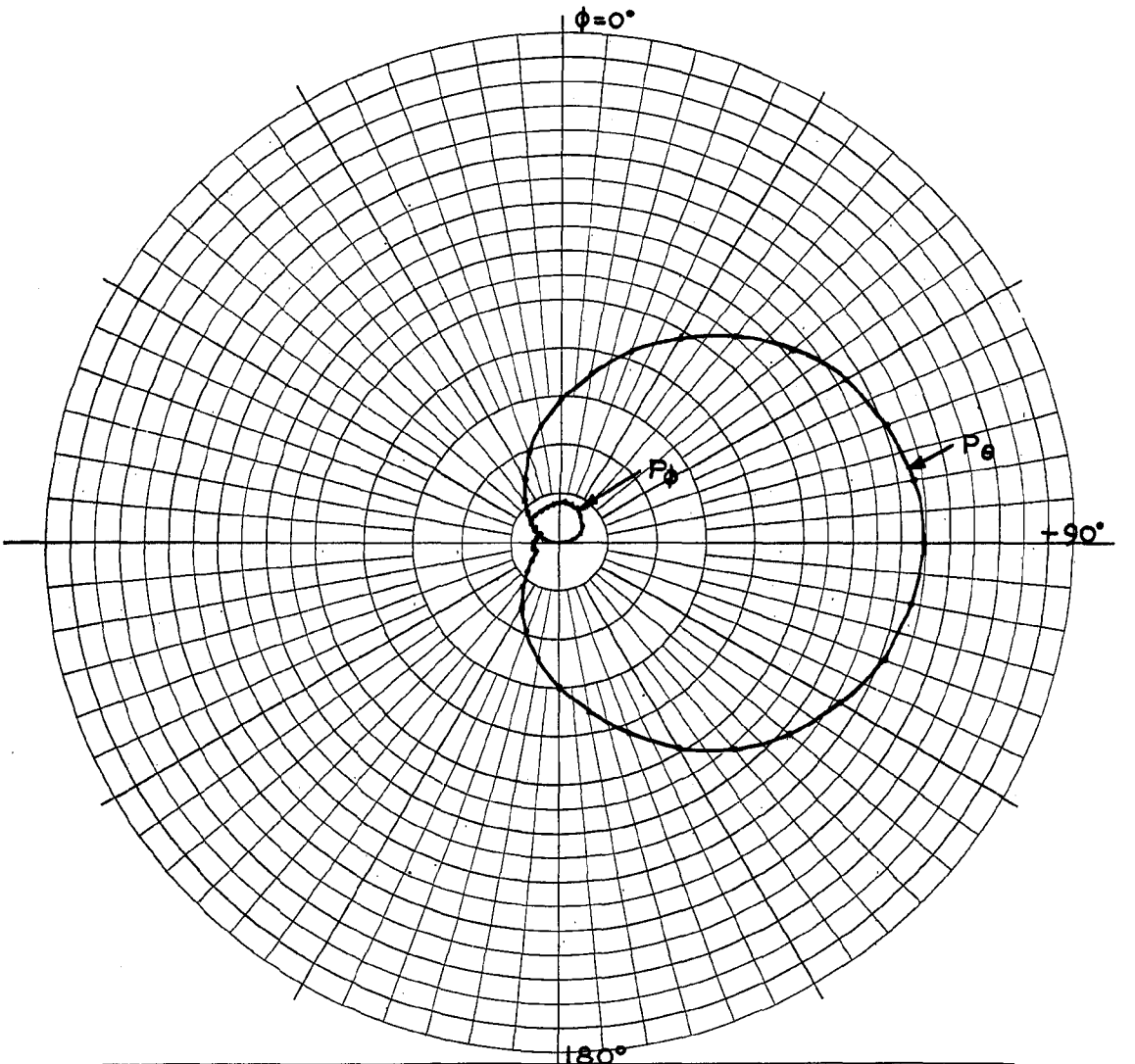

ANTENNA TYPE C.D.	LOCATION	USE	
TEST MODEL:		FREQUENCY: 445 MCS	
MODEL SCALE: 1:1		SCALE FREQUENCY: 1:1 MCS	
CONDITIONS:		POLARIZATION:	
CURVES PLOTTED IN:		E θ: X	
VOLTAGE: X		E ϕ: X	θ=80°
POWER:		PATTERN AREA:	
ENGINEER	OPERATOR	FILE NO.	DATE

Pattern scale: Each major radial increment = 0.02 units

FIGURE 14

PATTERN FUNCTION PLOTS FOR A SINGLE SLOT

CENTERED AT $\varphi = 90^{\circ}$ FOR $\theta = 80^{\circ}$

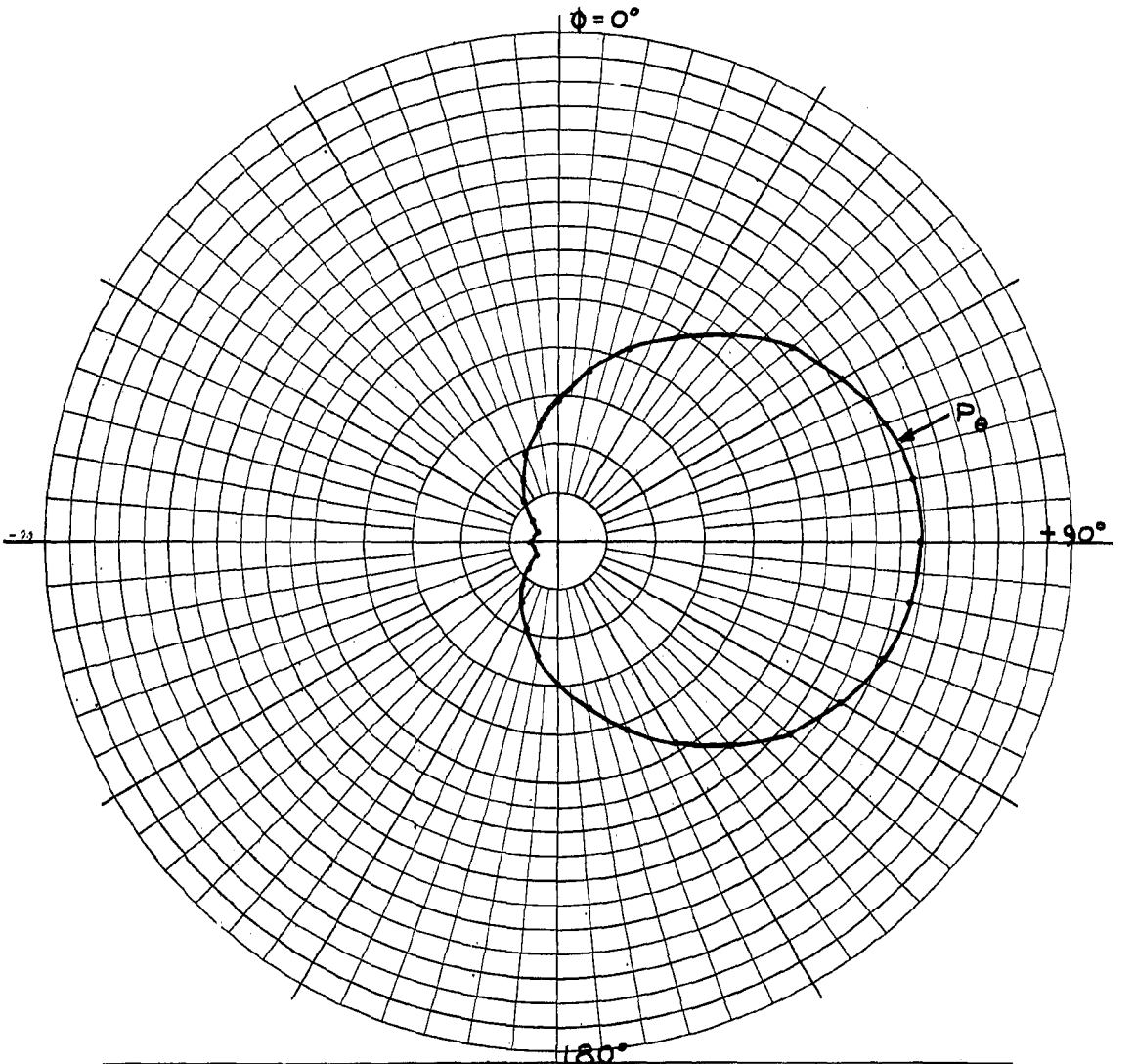

ANTENNA TYPE C. D.	LOCATION	USE
TEST MODEL:	FREQUENCY: 445 MCS	
MODEL SCALE: 1:1	SCALE FREQUENCY: 1:1 MCS	
CONDITIONS:	POLARIZATION:	
CURVES PLOTTED IN:	E θ: X	
VOLTAGE: X	E ϕ:	θ=90°
POWER:	PATTERN AREA:	
ENGINEER	OPERATOR	FILE NO. / DATE

Pattern scale: Each major radial increment = 0.02 units

FIGURE 15

PATTERN FUNCTION PLOT FOR A SINGLE SLOT

CENTERED AT $\varphi = 90^{\circ}$ FOR $\theta = 90^{\circ}$

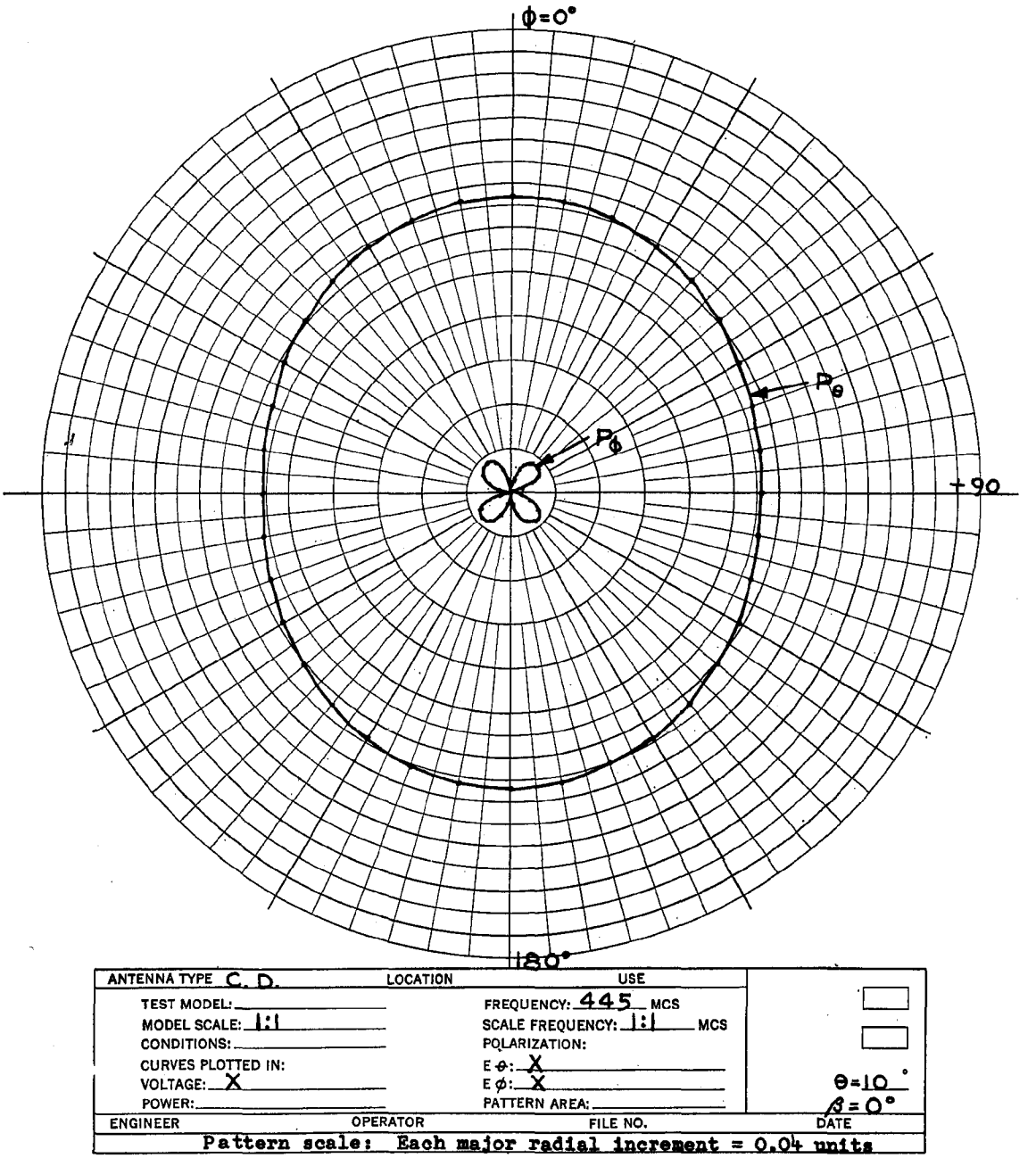

FIGURE 16

PATTERN SUMMATION PLOTS FOR TWO DIAMETRICALLY OPPOSED SLOTS OPERATING SIMULTANEOUSLY FOR $\theta = 10^{\circ}$ AND $\beta = 0^{\circ}$

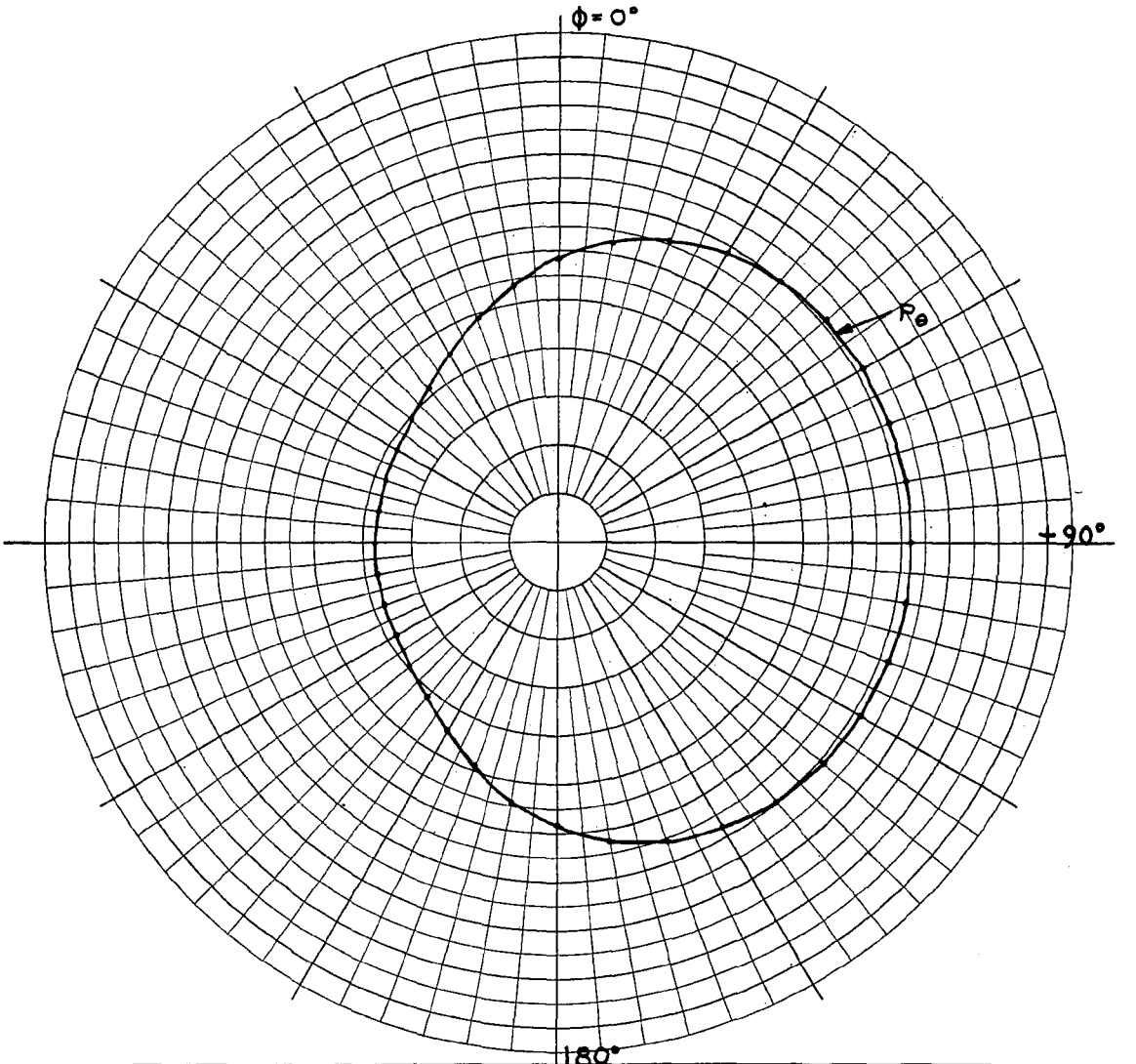

ANTENNA TYPE C.D.	LOCATION	USE	
TEST MODEL:		FREQUENCY: 445 MCS	
MODEL SCALE: 1:1		SCALE FREQUENCY: 1:1 MCS	
CONDITIONS:		POLARIZATION:	
CURVES PLOTTED IN:		Eθ: X	
VOLTAGE: X		Eϕ:	θ=10°
POWER:		PATTERN AREA:	β=60°
ENGINEER	OPERATOR	FILE NO.	DATE
Pattern scale: Each major radial increment = 0.04 units			

FIGURE 17

PATTERN SUMMATION PLOT FOR TWO DIAMETRICALLY OPPOSED SLOTS OPERATING SIMULTANEOUSLY FOR $\theta = 10^{\circ}$ AND $\beta = 60^{\circ}$

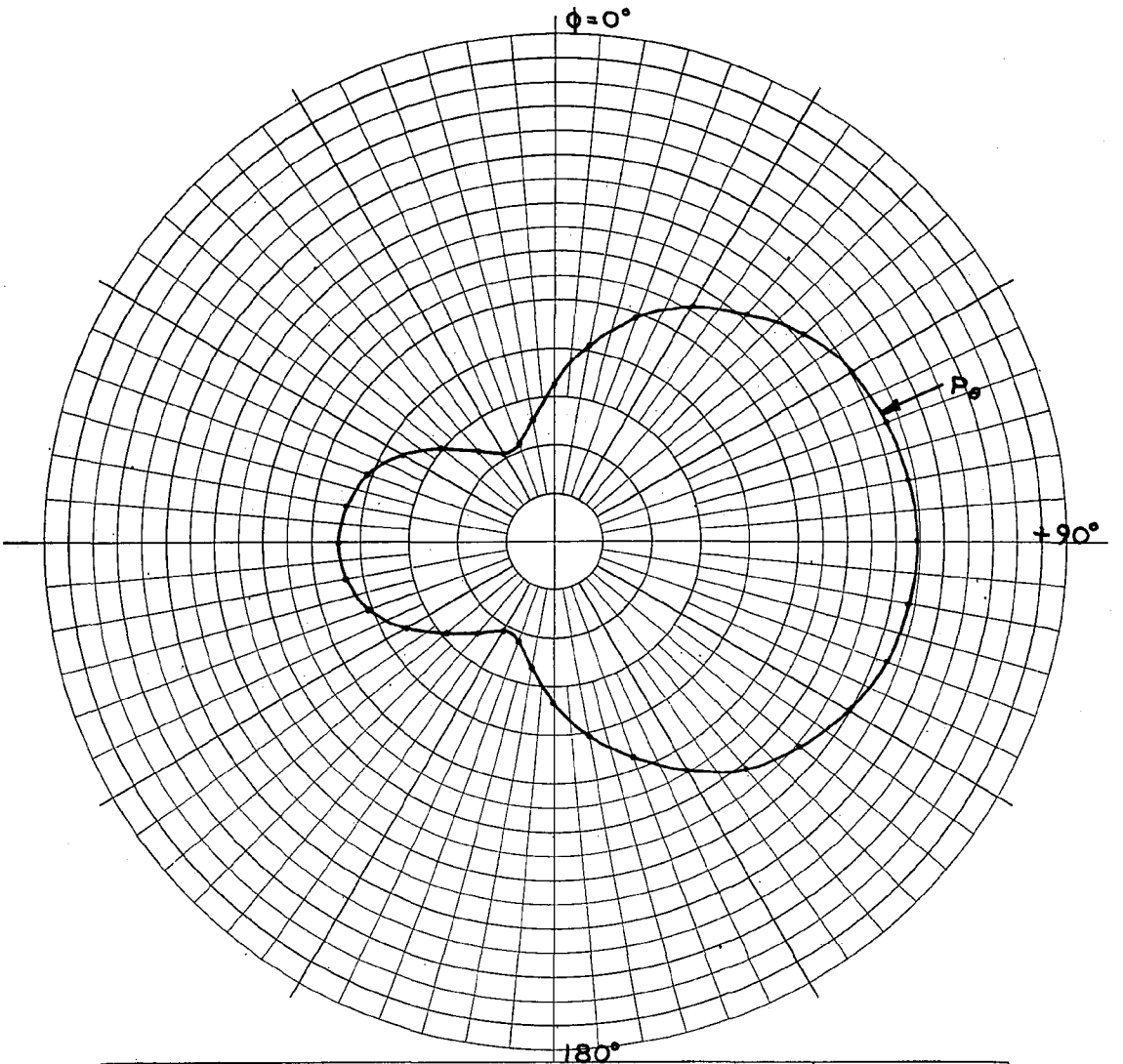

ANTENNA TYPE C. D.	LOCATION	USE
TEST MODEL:	FREQUENCY: 445 MCS	
MODEL SCALE: 1:1	SCALE FREQUENCY: 1:1 MCS	
CONDITIONS:	POLARIZATION:	
CURVES PLOTTED IN:	E θ: X	
VOLTAGE: X	E ϕ:	θ=10°
POWER:	PATTERN AREA:	β=120°
ENGINEER	OPERATOR	FILE NO. DATE

Pattern scale: Each major radial increment = 0.04 units

FIGURE 18

PATTERN SUMMATION PLOT FOR TWO DIAMETRICALLY OPPOSED SLOTS OPERATING SIMULTANEOUSLY FOR $\theta = 10^\circ$ AND $\beta = 120^\circ$

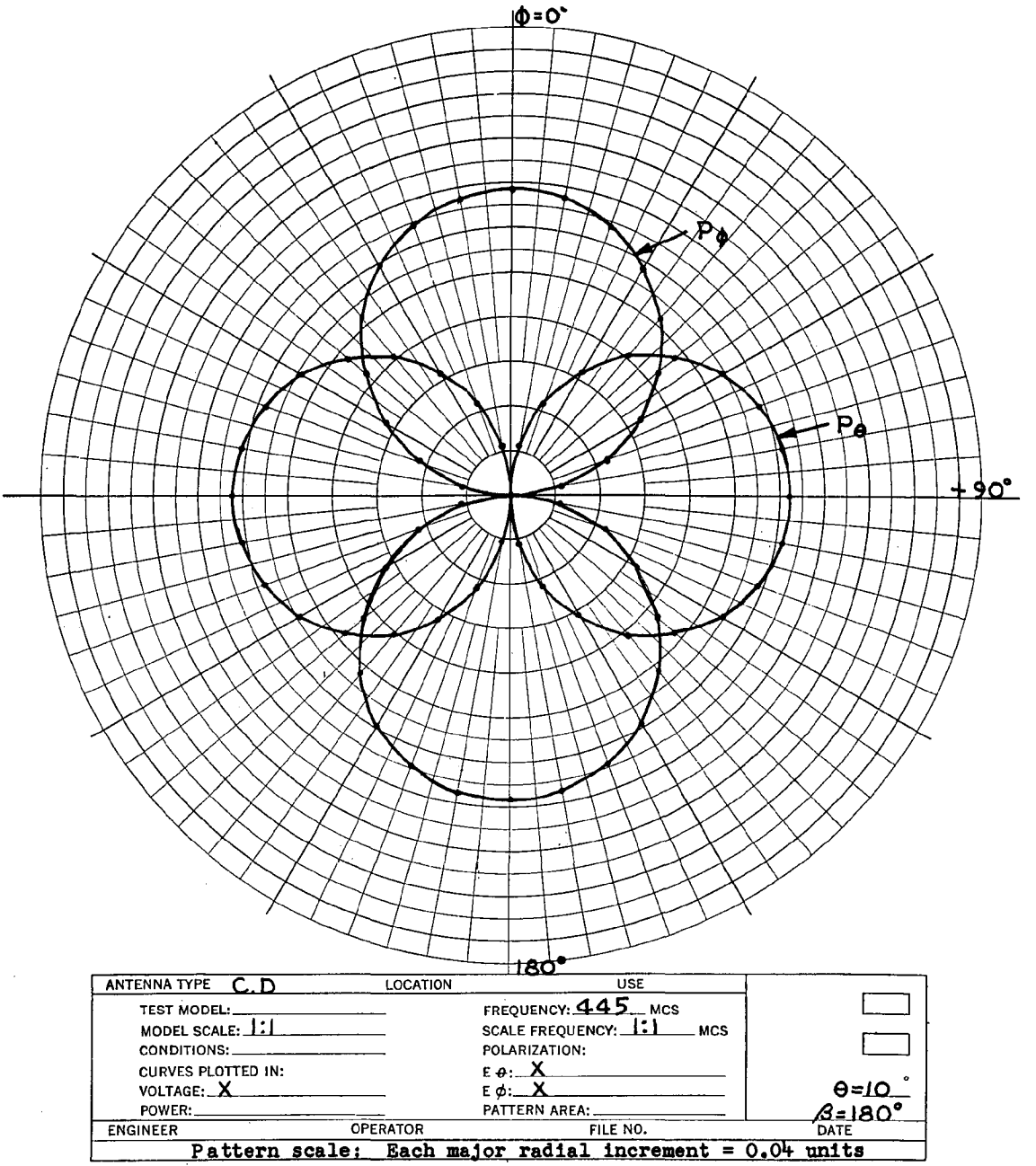

FIGURE 19

PATTERN SUMMATION PLOTS FOR TWO DIAMETRICALLY OPPOSED SLOTS OPERATING SIMULTANEOUSLY FOR $\theta = 10^{\circ}$ AND $\beta = 180^{\circ}$

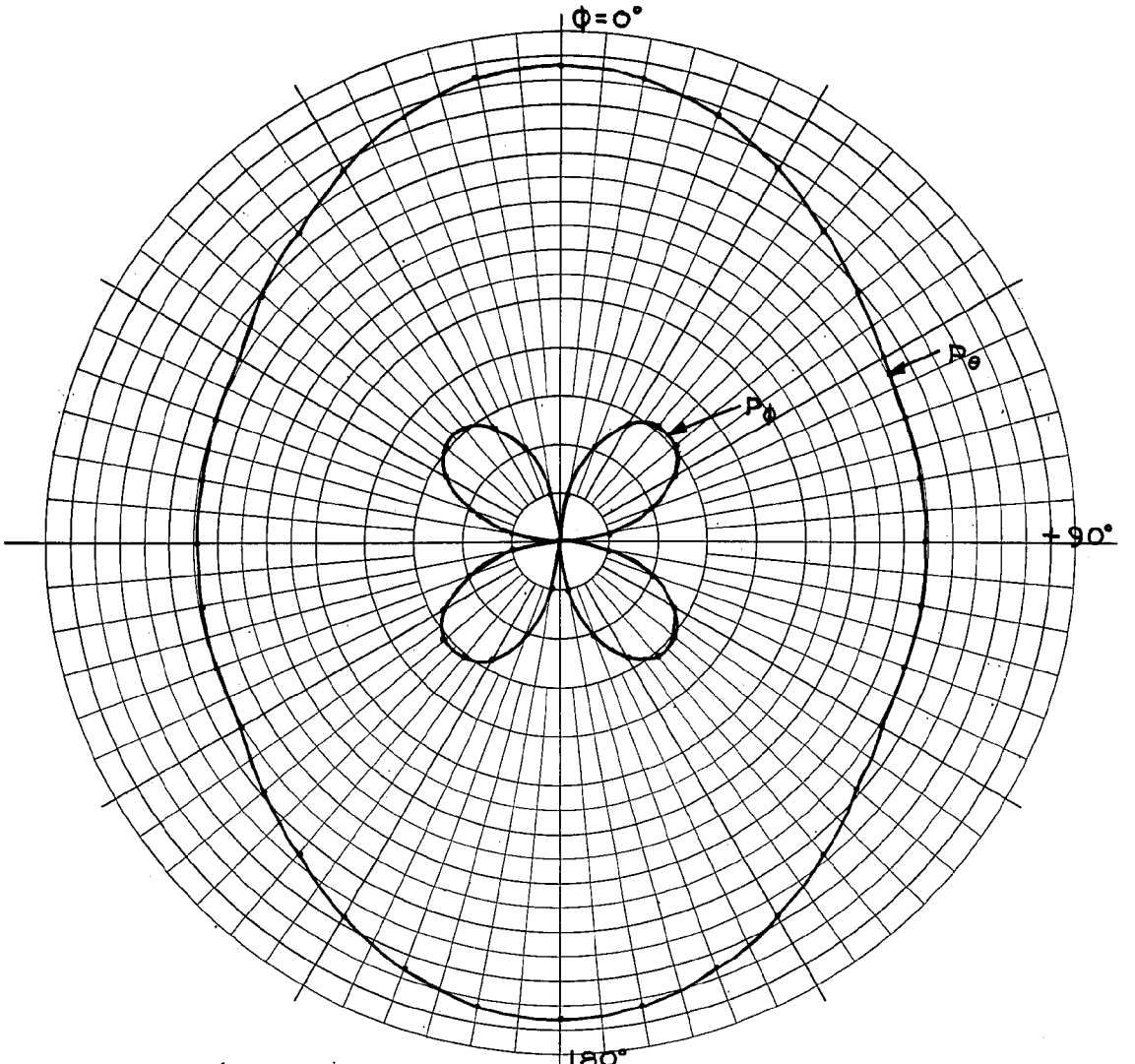

ANTENNA TYPE C. D.	LOCATION	USE	
TEST MODEL:		FREQUENCY: 445 MCS	
MODEL SCALE: 1:1		SCALE FREQUENCY: 1:1 MCS	
CONDITIONS:		POLARIZATION:	
CURVES PLOTTED IN:		E_θ: X	
VOLTAGE: X		E_ϕ: X	θ = 20°
POWER:		PATTERN AREA:	β = 0°
ENGINEER	OPERATOR	FILE NO.	DATE

Pattern scale: Each major radial increment = 0.02 units

FIGURE 20

PATTERN SUMMATION PLOTS FOR TWO DIAMETRICALLY OPPOSED SLOTS OPERATING SIMULTANEOUSLY FOR $\theta = 20^\circ$ AND $\beta = 0^\circ$

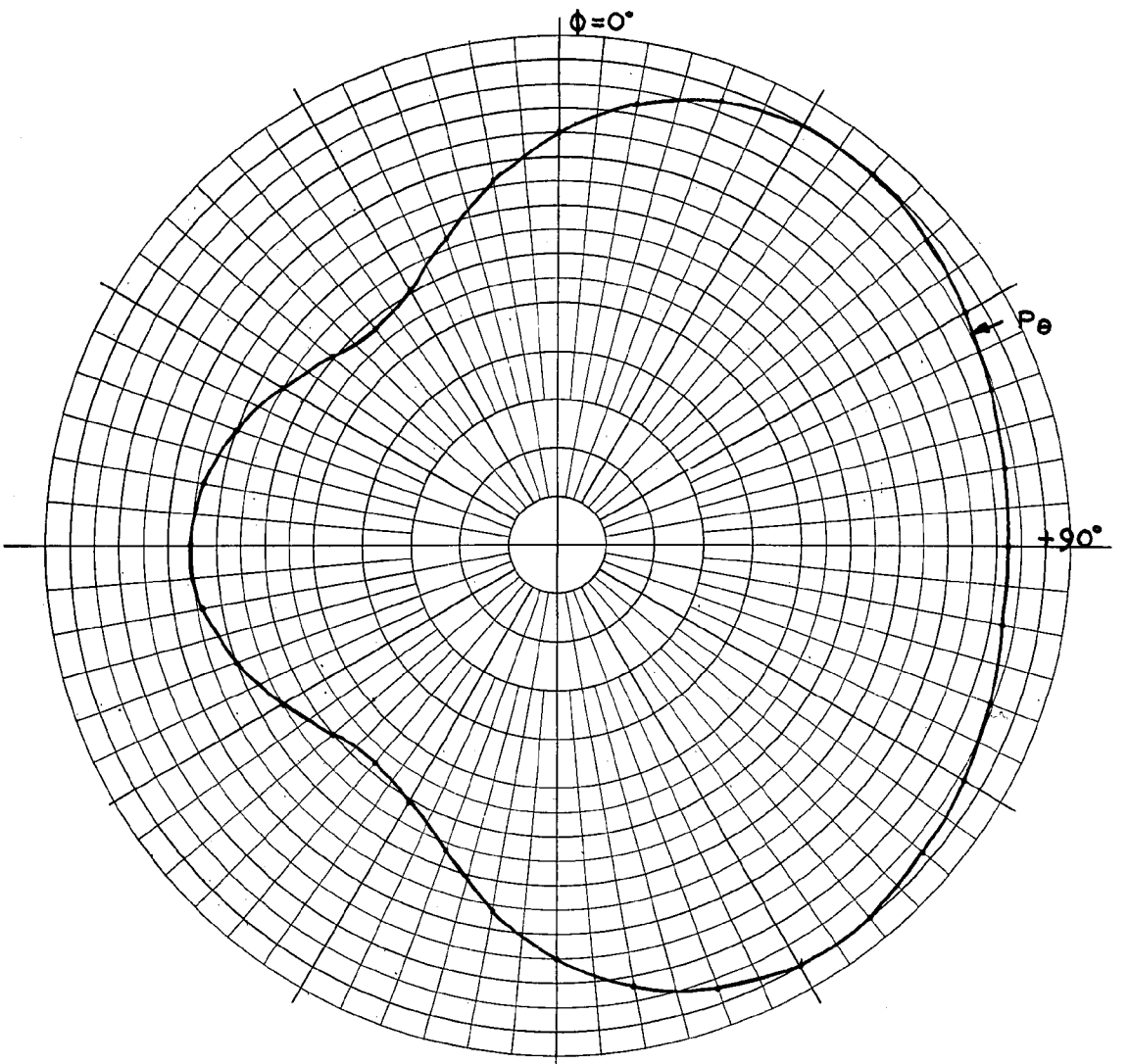

ANTENNA TYPE C.D.	LOCATION	USE
TEST MODEL:	FREQUENCY: 445 MCS	
MODEL SCALE: 1:1	SCALE FREQUENCY: 1:1 MCS	
CONDITIONS:	POLARIZATION:	
CURVES PLOTTED IN:	Eθ: X	
VOLTAGE: X	Eϕ:	θ=20°
POWER:	PATTERN AREA:	β=60°
ENGINEER	OPERATOR	FILE NO. / DATE

Pattern scale: Each major radial increment = 0.02 units

FIGURE 21

PATTERN SUMMATION PLOT FOR TWO DIAMETRICALLY OPPOSED SLOTS OPERATING SIMULTANEOUSLY FOR $\theta = 20^{\circ}$ AND $\beta = 60^{\circ}$

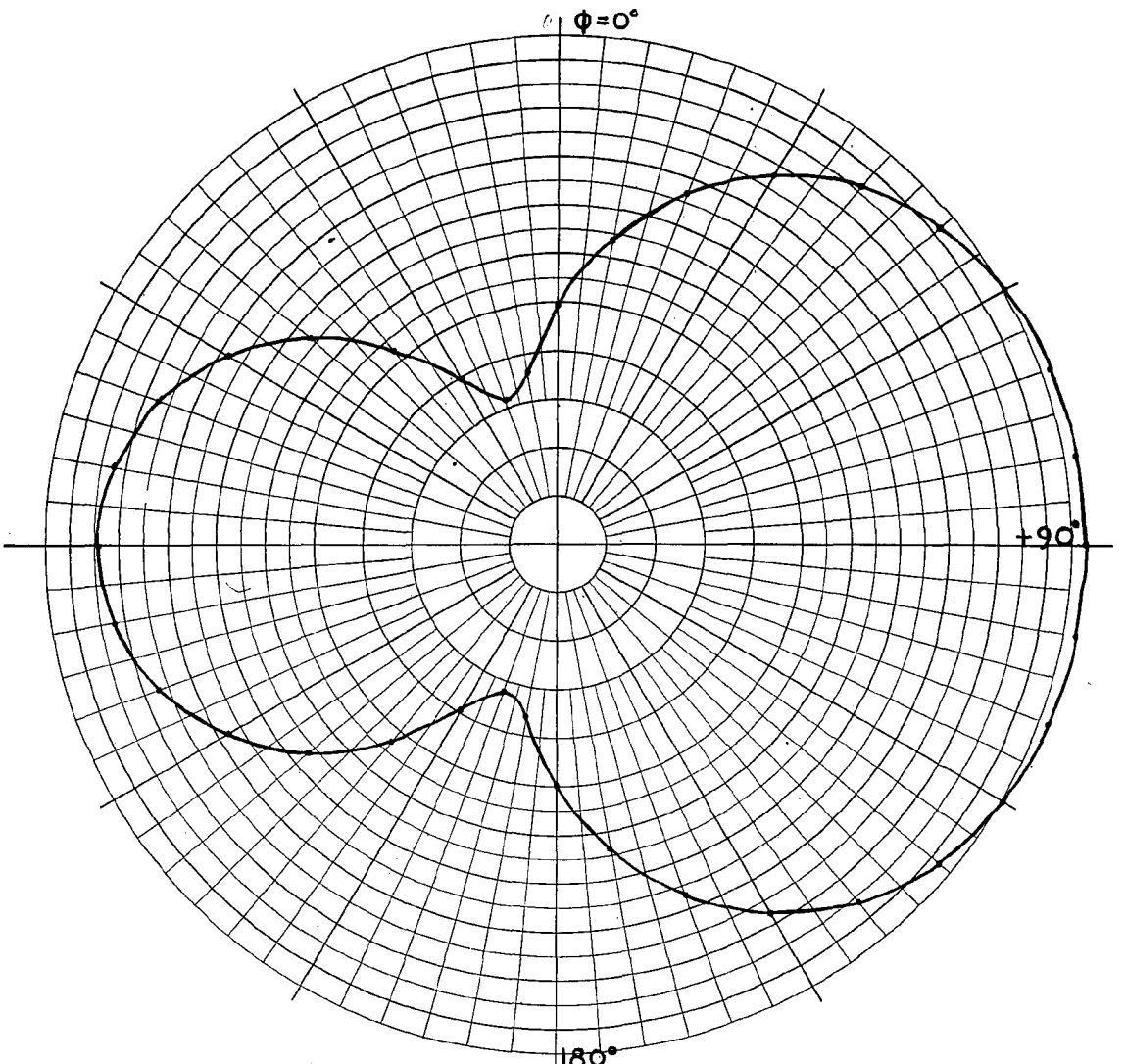

ANTENNA TYPE C. D.	LOCATION	USE	
TEST MODEL:		FREQUENCY: 445 MCS	
MODEL SCALE: 1:1		SCALE FREQUENCY: 1:1 MCS	
CONDITIONS:		POLARIZATION:	
CURVES PLOTTED IN:		E θ: X	
VOLTAGE: X		E φ:	θ=20°
POWER:		PATTERN AREA:	β=120°
ENGINEER	OPERATOR	FILE NO.	DATE

Pattern scale: Each major radial increment = 0.02 units

FIGURE 22

PATTERN SUMMATION PLOT FOR TWO DIAMETRICALLY OPPOSED SLOTS OPERATING SIMULTANEOUSLY FOR $\theta = 20^{\circ}$ AND $\beta = 120^{\circ}$

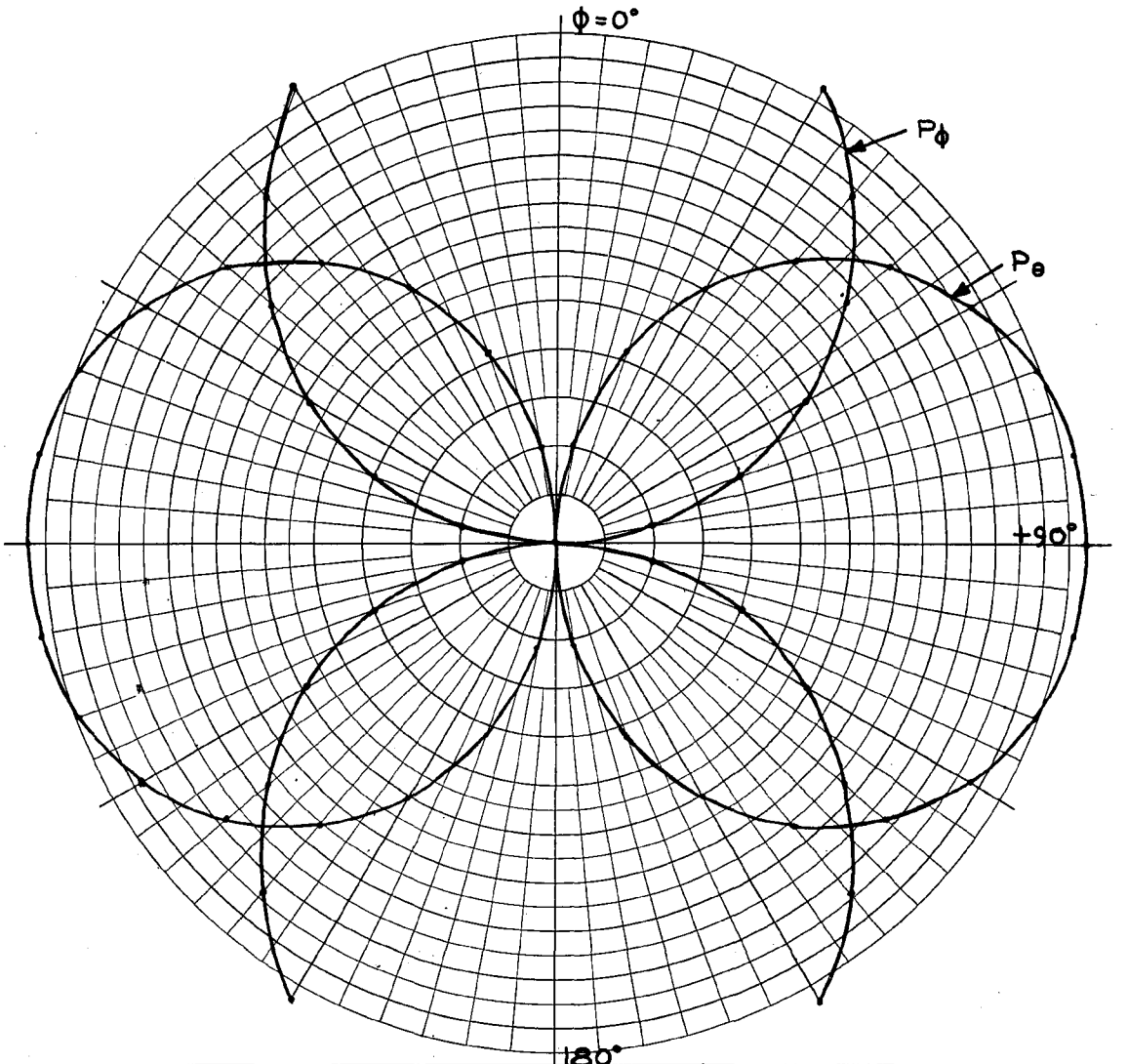

ANTENNA TYPE C.D.	LOCATION	USE	
TEST MODEL:		FREQUENCY: 445 MCS	
MODEL SCALE: 1:1		SCALE FREQUENCY: 1:1 MCS	
CONDITIONS:		POLARIZATION:	
CURVES PLOTTED IN:		E θ: X	
VOLTAGE: X		E ϕ: X	θ=20°
POWER:		PATTERN AREA:	β=180°
ENGINEER	OPERATOR	FILE NO.	DATE

Pattern scale: Each major radial increment = 0.02 units

FIGURE 23

PATTERN SUMMATION PLOTS FOR TWO DIAMETRICALLY OPPOSED SLOTS OPERATING SIMULTANEOUSLY FOR $\theta = 20^{\circ}$ AND $\beta = 180^{\circ}$

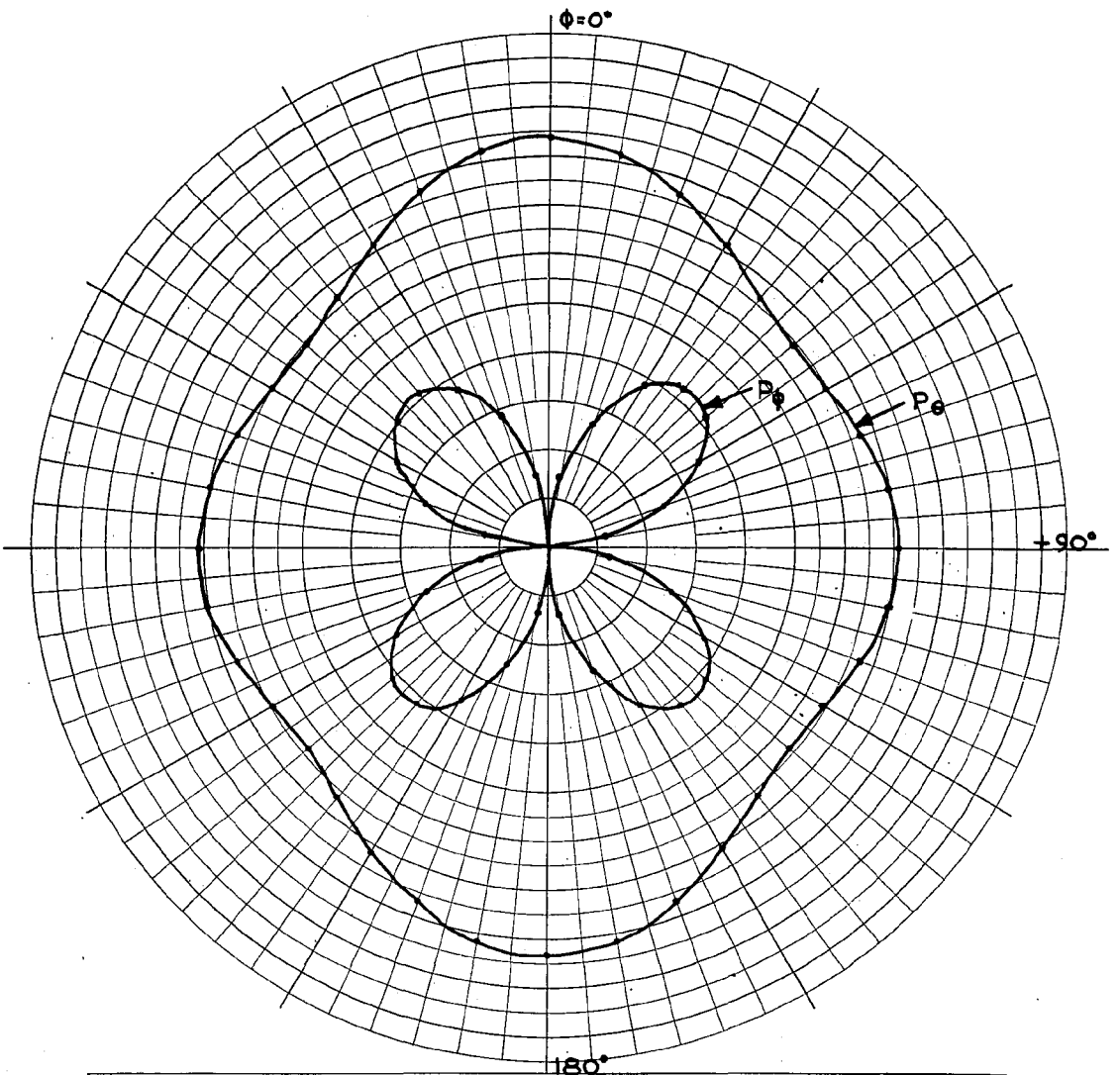

ANTENNA TYPE C.D.	LOCATION	USE	
TEST MODEL:		FREQUENCY: 445 MCS	
MODEL SCALE: 1:1		SCALE FREQUENCY: 1:1 MCS	
CONDITIONS:		POLARIZATION:	
CURVES PLOTTED IN:		Eθ: X	
VOLTAGE: X		Eφ: X	θ=30°
POWER:		PATTERN AREA:	β=0°
ENGINEER	OPERATOR	FILE NO.	DATE

Pattern scale: Each major radial increment = 0.02 units

FIGURE 24

PATTERN SUMMATION PLOTS FOR TWO DIAMETRICALLY OPPOSED SLOTS OPERATING SIMULTANEOUSLY FOR $\theta = 30^{\circ}$ AND $\beta = 0^{\circ}$

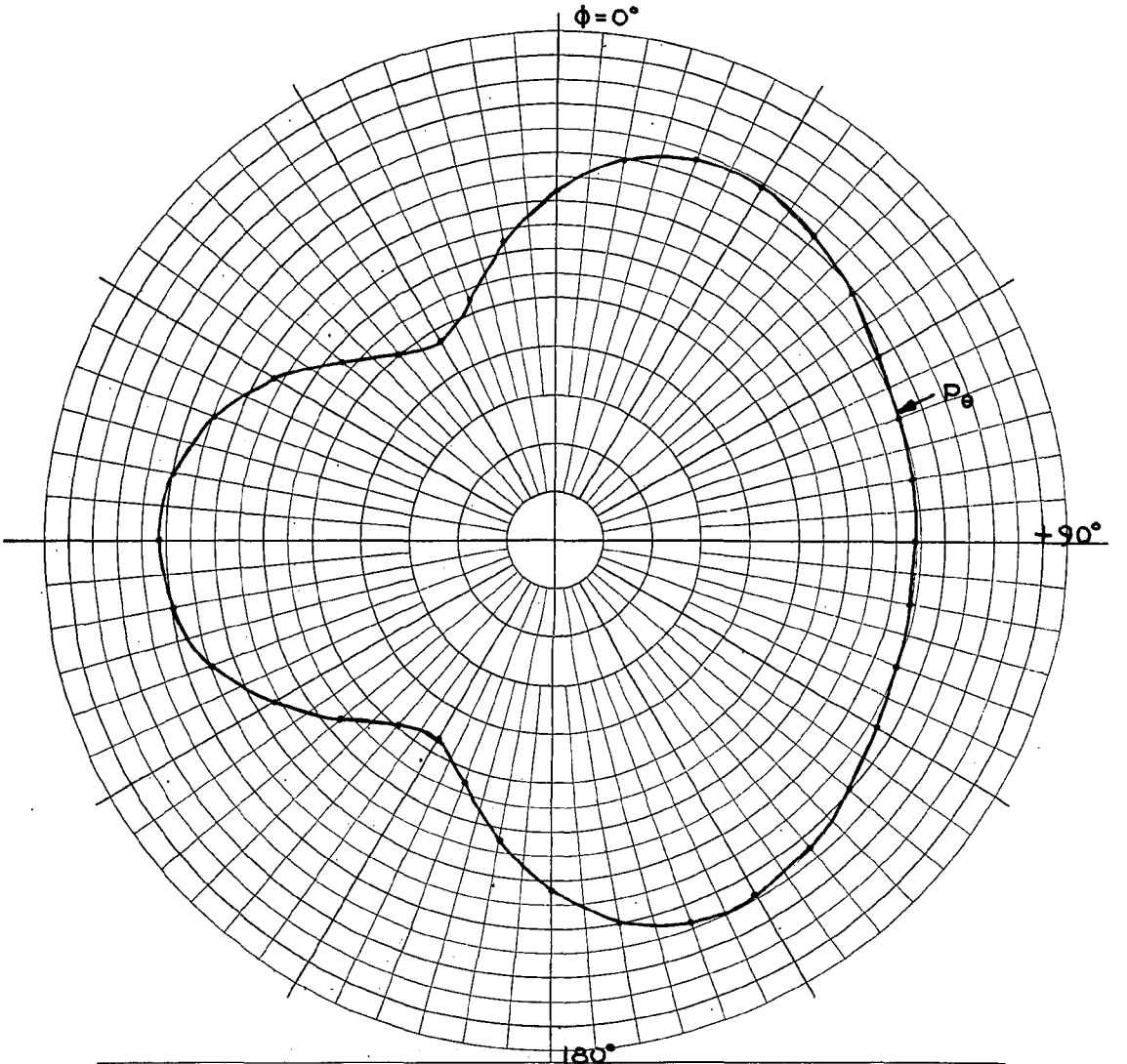

ANTENNA TYPE C.D	LOCATION	USE	
TEST MODEL: 1:1	FREQUENCY: 445 MCS		
MODEL SCALE:	SCALE FREQUENCY: 1:1 MCS		
CONDITIONS:	POLARIZATION:		
CURVES PLOTTED IN:	E θ: X		
VOLTAGE: X	E ϕ:		θ=30°
POWER:	PATTERN AREA:		β=60°
ENGINEER	OPERATOR	FILE NO.	DATE

Pattern scale: Each major radial increment = 0.02 units

FIGURE 25

PATTERN SUMMATION PLOT FOR TWO DIAMETRICALLY OPPOSED SLOTS OPERATING SIMULTANEOUSLY FOR $\theta = 30^\circ$ AND $\beta = 60^\circ$

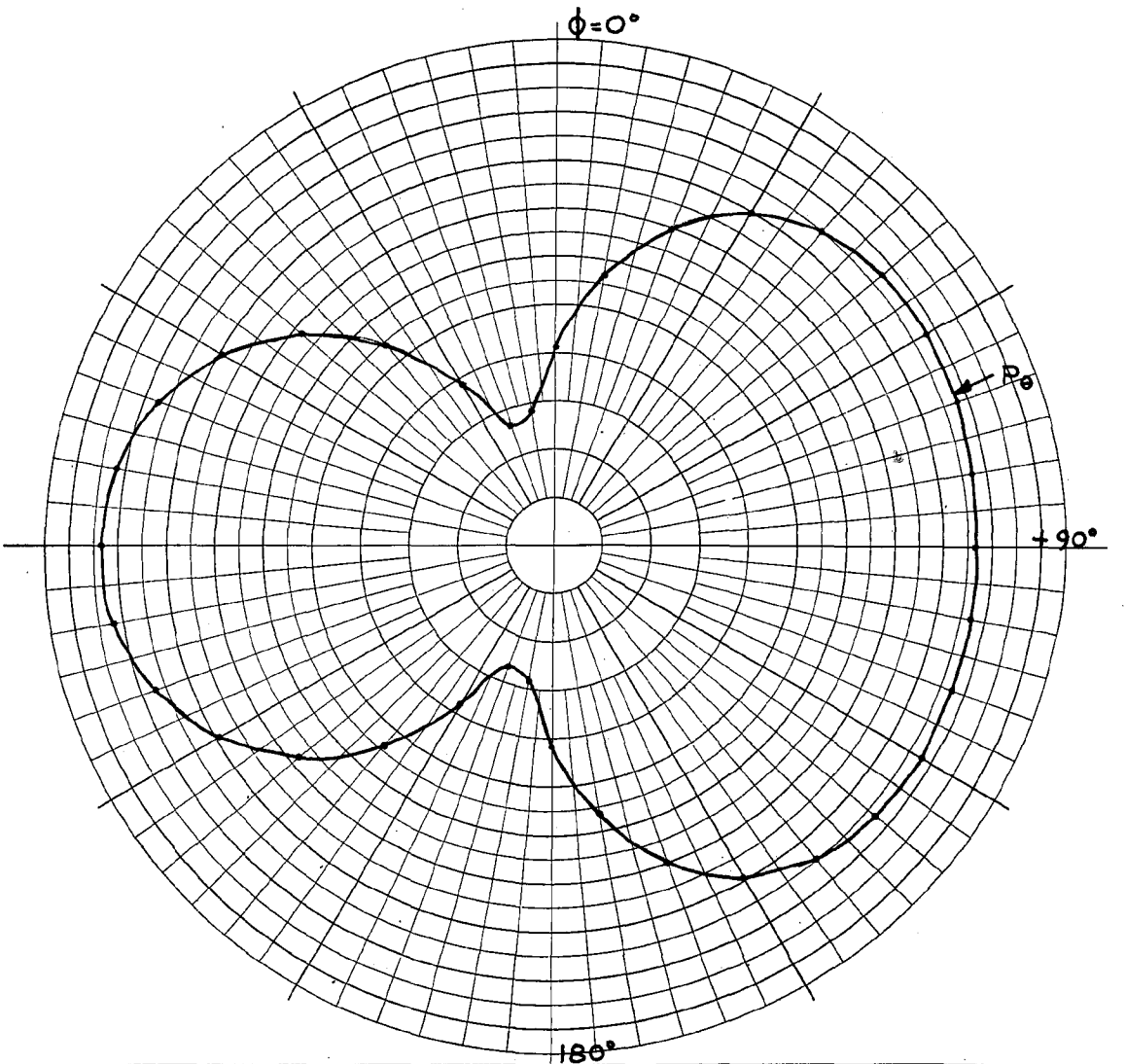

FIGURE 26

PATTERN SUMMATION PLOT FOR TWO DIAMETRICALLY OPPOSED SLOTS OPERATING SIMULTANEOUSLY FOR $\theta = 30^\circ$ AND $\beta = 120^\circ$

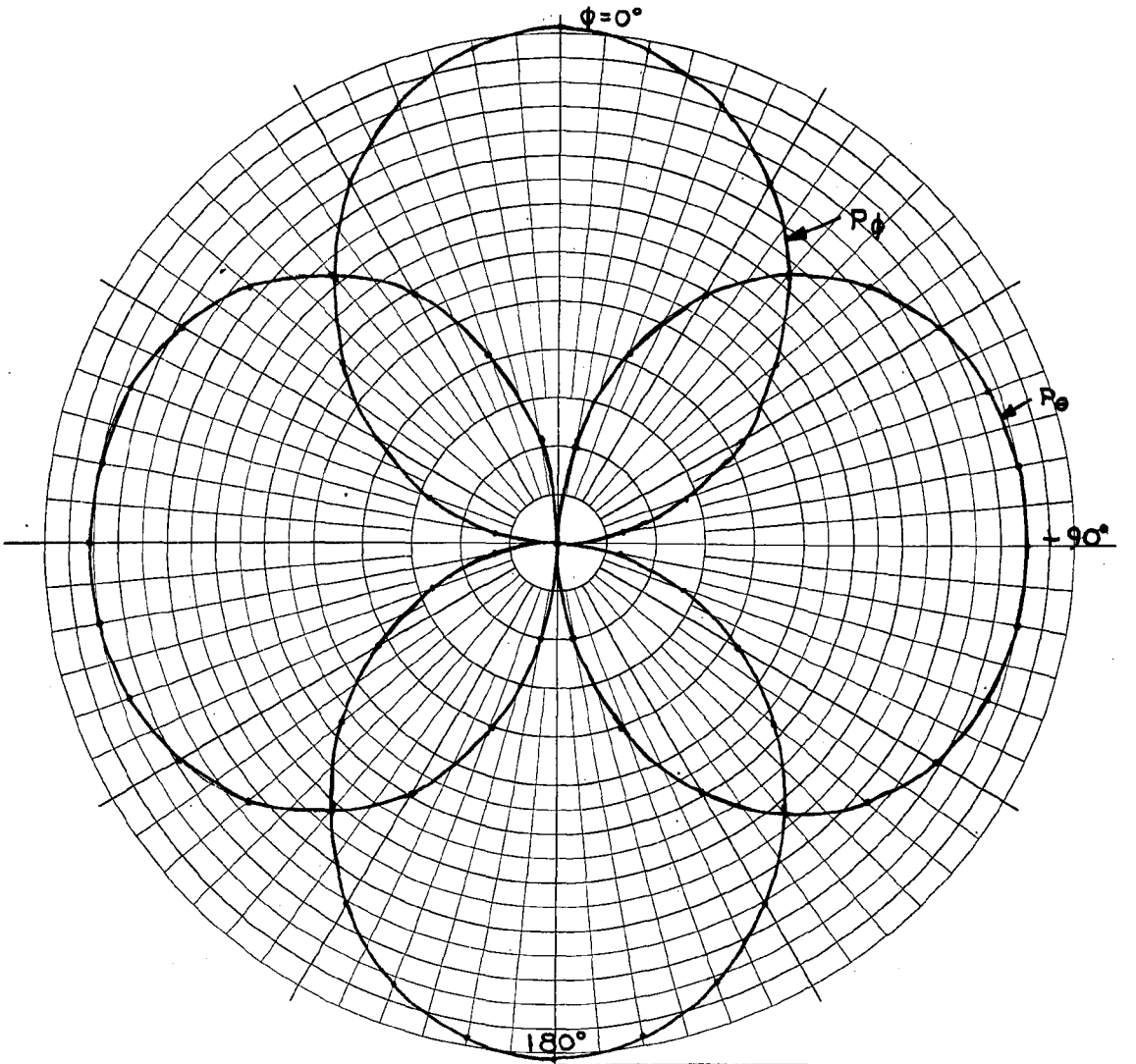

ANTENNA TYPE C. D.	LOCATION	USE	
TEST MODEL:		FREQUENCY: 445 MCS	
MODEL SCALE: 1:1		SCALE FREQUENCY: 1:1 MCS	
CONDITIONS:		POLARIZATION:	
CURVES PLOTTED IN:		Eθ: X	
VOLTAGE: X		Eφ: X	θ=30°
POWER:		PATTERN AREA:	β=180°
ENGINEER	OPERATOR	FILE NO.	DATE

Pattern scale: Each major radial increment = 0.02 units

FIGURE 27

PATTERN SUMMATION PLOTS FOR TWO DIAMETRICALLY OPPOSED SLOTS OPERATING SIMULTANEOUSLY FOR $\theta = 30^{\circ}$ AND $\beta = 180^{\circ}$

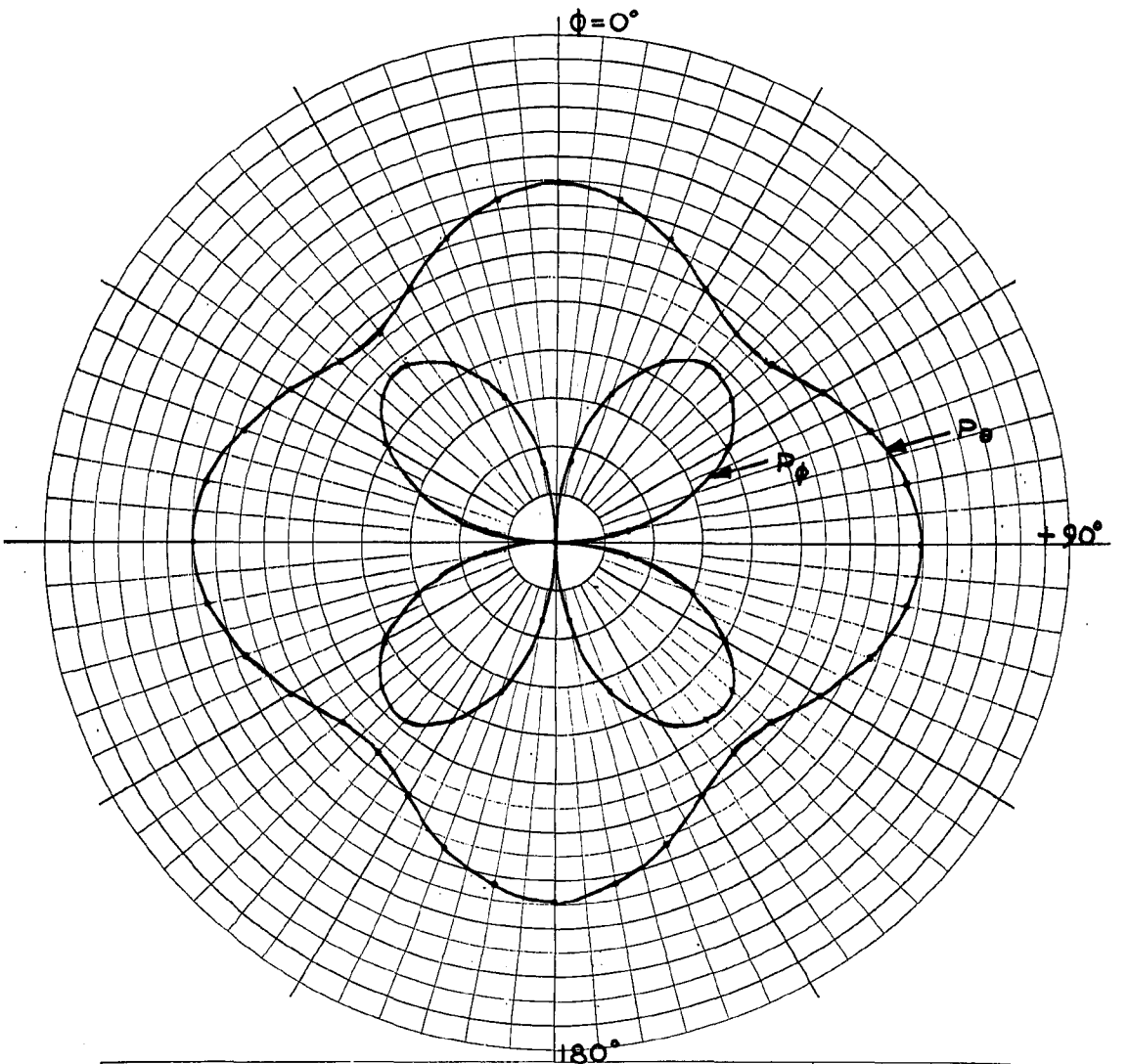

FIGURE 28

PATTERN SUMMATION PLOTS FOR TWO DIAMETRICALLY OPPOSED SLOTS OPERATING SIMULTANEOUSLY FOR $\theta = 40^\circ$ AND $\beta = 0^\circ$

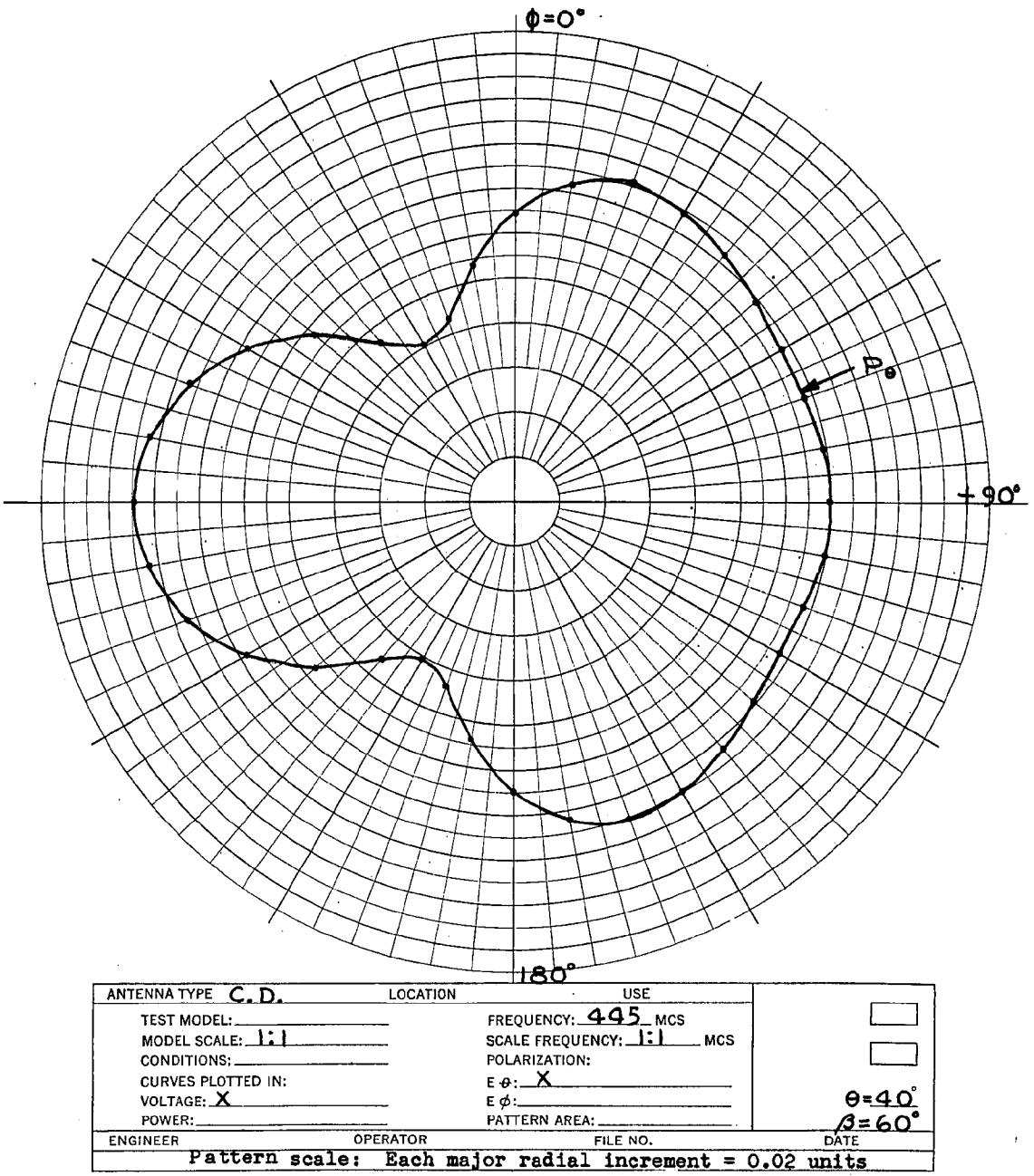

FIGURE 29

PATTERN SUMMATION PLOT FOR TWO DIAMETRICALLY OPPOSED SLOTS OPERATING SIMULTANEOUSLY FOR $\theta = 40^{\circ}$ AND $\beta = 60^{\circ}$

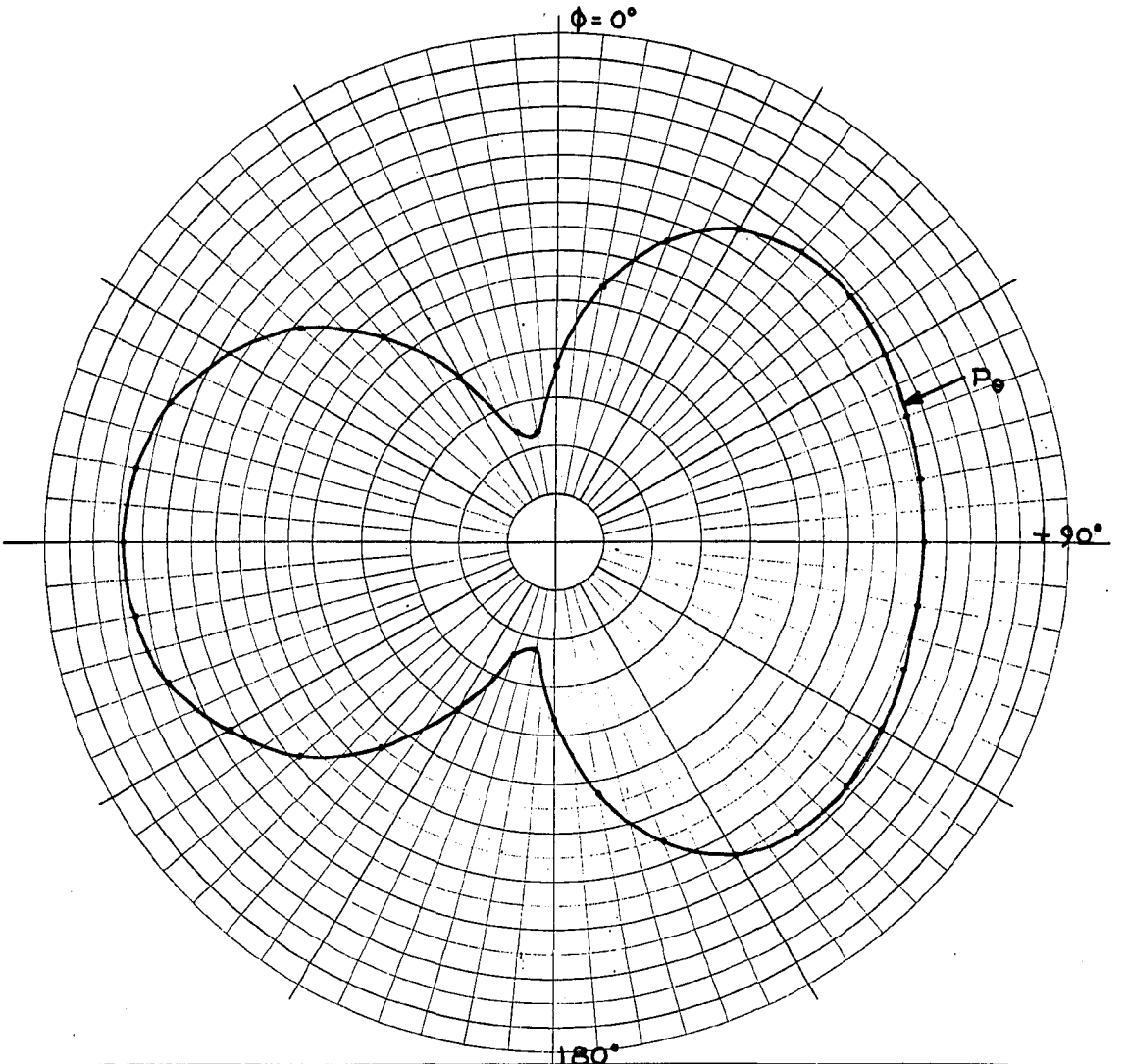

ANTENNA TYPE C.D.	LOCATION	USE	
TEST MODEL:		FREQUENCY: 445 MCS	
MODEL SCALE: 1:1		SCALE FREQUENCY: 1:1 MCS	
CONDITIONS:		POLARIZATION:	
CURVES PLOTTED IN:		E θ: X	
VOLTAGE: X		E ϕ:	θ = 40°
POWER:		PATTERN AREA:	β = 120°
ENGINEER	OPERATOR	FILE NO.	DATE

Pattern scale: Each major radial increment = 0.02 units

FIGURE 30

PATTERN SUMMATION PLOT FOR TWO DIAMETRICALLY OPPOSED SLOTS OPERATING SIMULTANEOUSLY FOR $\theta = 40^\circ$ AND $\beta = 120^\circ$

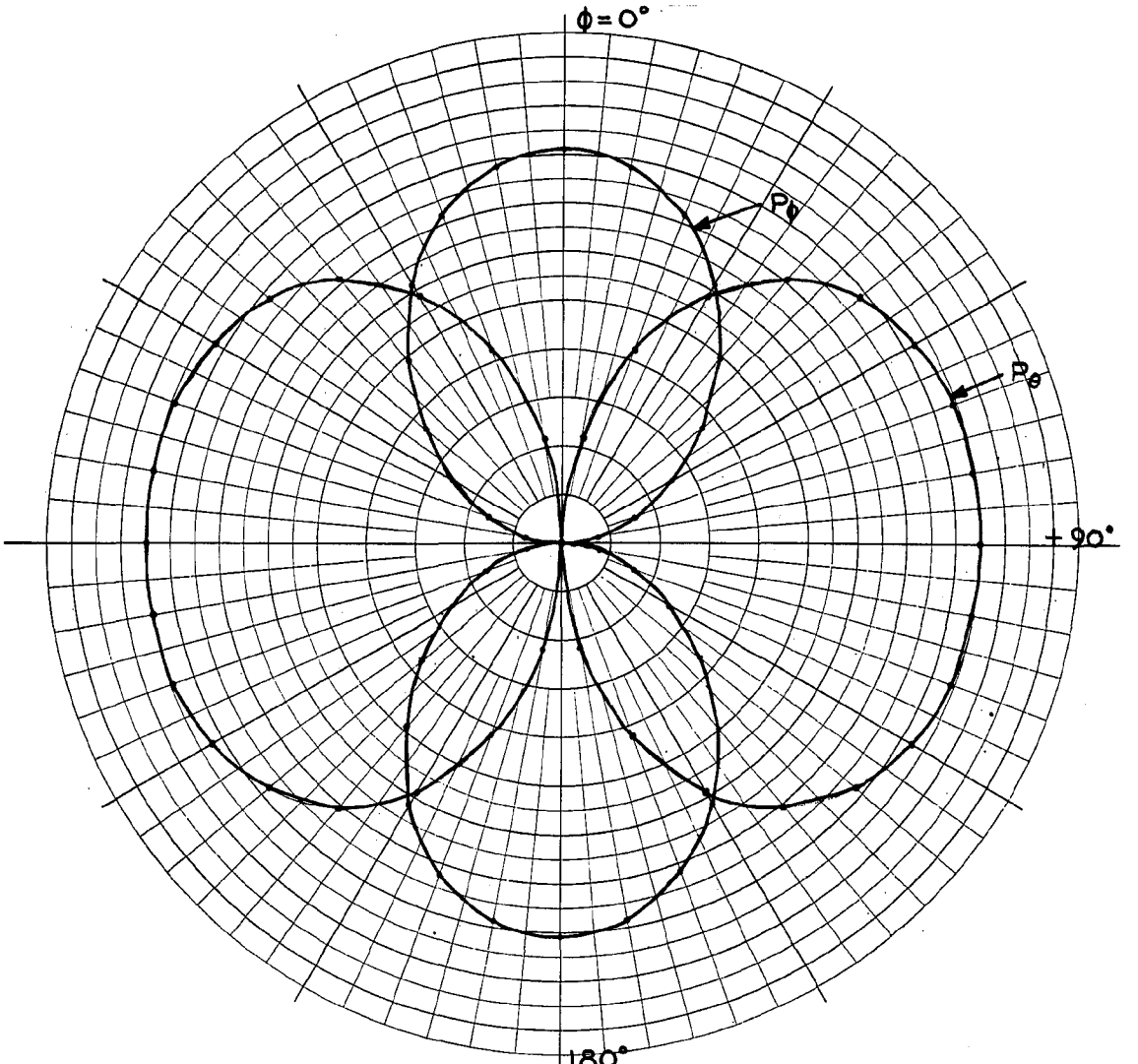

ANTENNA TYPE C.D.	LOCATION	USE	
TEST MODEL:		FREQUENCY: 445 MCS	
MODEL SCALE: 1:1		SCALE FREQUENCY: 1:1 MCS	
CONDITIONS:		POLARIZATION:	
CURVES PLOTTED IN:		Eθ: X	
VOLTAGE: X		Eϕ: X	θ=40°
POWER:		PATTERN AREA:	β=180°
ENGINEER	OPERATOR	FILE NO.	DATE

Pattern scale: Each major radial increment = 0.02 units

FIGURE 31

PATTERN SUMMATION PLOTS FOR TWO DIAMETRICALLY OPPOSED SLOTS OPERATING SIMULTANEOUSLY FOR $\theta = 40^{\circ}$ AND $\beta = 180^{\circ}$

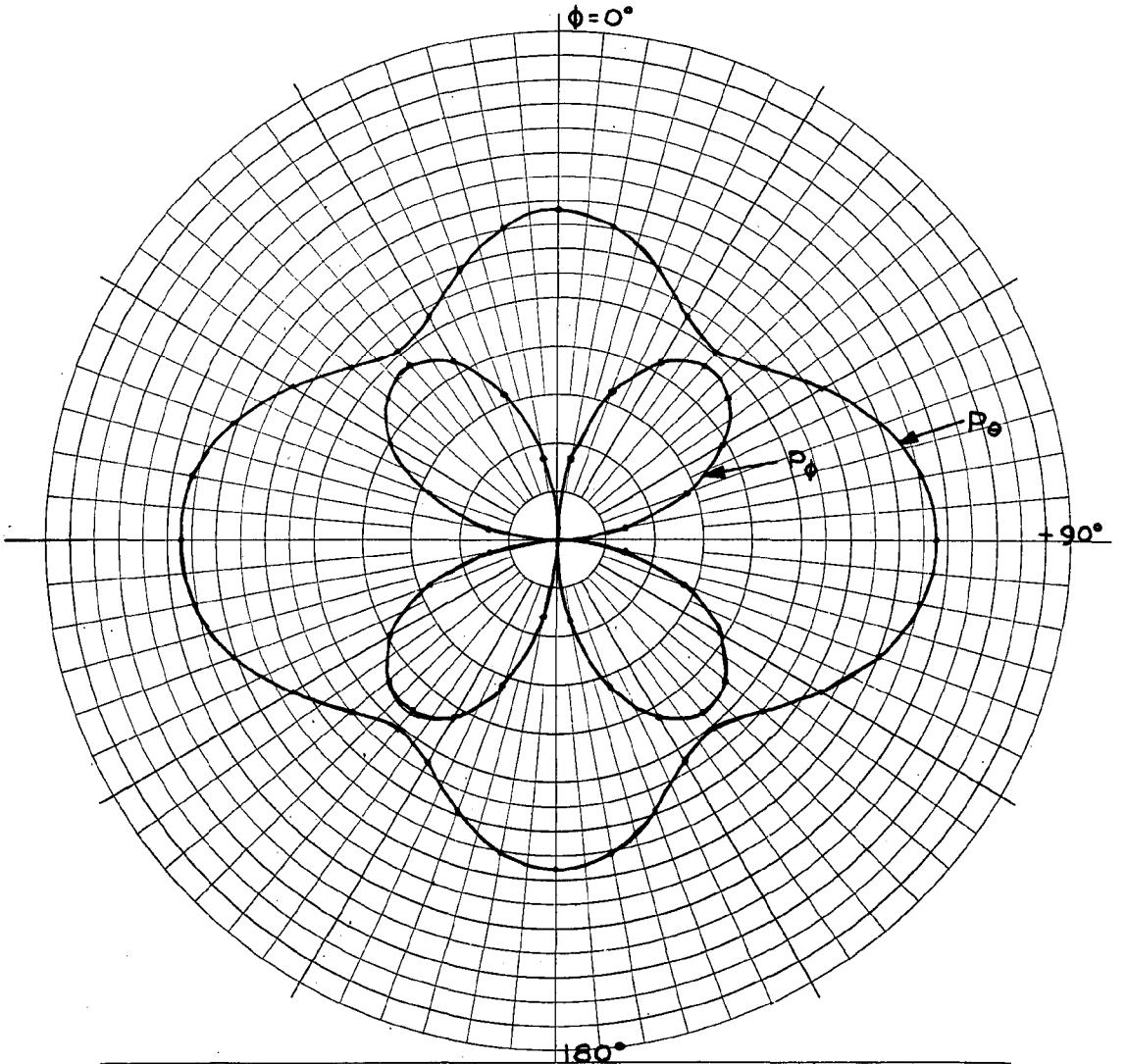

ANTENNA TYPE C. D.	LOCATION	USE	
TEST MODEL:		FREQUENCY: 445 MCS	
MODEL SCALE: 1:1		SCALE FREQUENCY: 1:1 MCS	
CONDITIONS:		POLARIZATION:	
CURVES PLOTTED IN:		E θ: X	
VOLTAGE: X		E φ: X	θ = 50°
POWER:		PATTERN AREA:	β = 0°
ENGINEER	OPERATOR	FILE NO.	DATE

Pattern scale: Each major radial increment = 0.02 units

FIGURE 32

PATTERN SUMMATION PLOTS FOR TWO DIAMETRICALLY OPPOSED SLOTS OPERATING SIMULTANEOUSLY FOR $\theta = 50^\circ$ AND $\beta = 0^\circ$

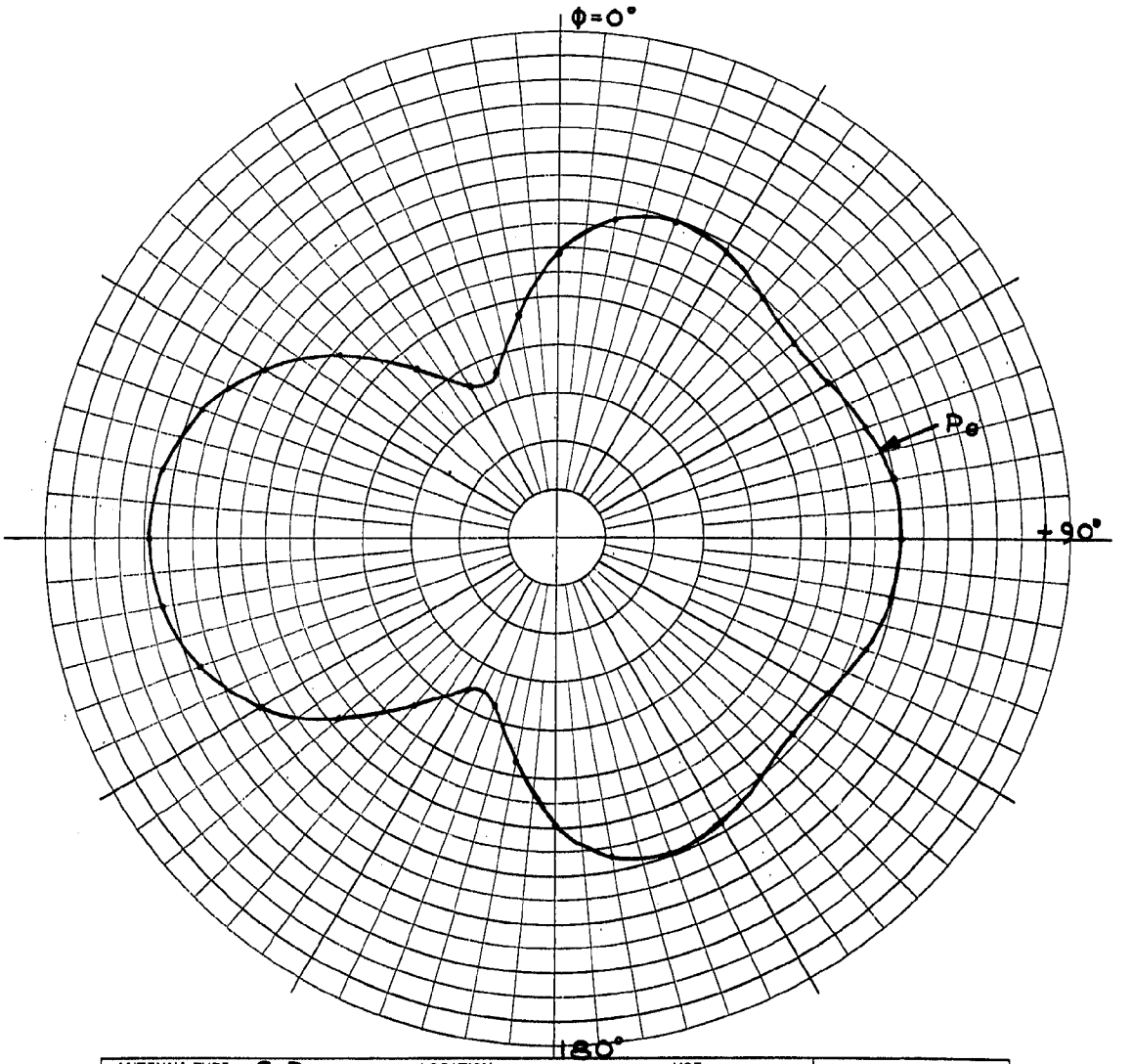

ANTENNA TYPE C.D	LOCATION	USE	
TEST MODEL:		FREQUENCY: 445 MCS	
MODEL SCALE: 1:1		SCALE FREQUENCY: 1:1 MCS	
CONDITIONS:		POLARIZATION:	
CURVES PLOTTED IN:		E_{θ}: X	
VOLTAGE: X		E_{ϕ}:	θ=50°
POWER:		PATTERN AREA:	β=60°
ENGINEER	OPERATOR	FILE NO.	DATE

Pattern scale: Each major radial increment = 0.02 units

FIGURE 33

PATTERN SUMMATION PLOT FOR TWO DIAMETRICALLY OPPOSED SLOTS OPERATING SIMULTANEOUSLY FOR $\theta = 50^{\circ}$ AND $\beta = 60^{\circ}$

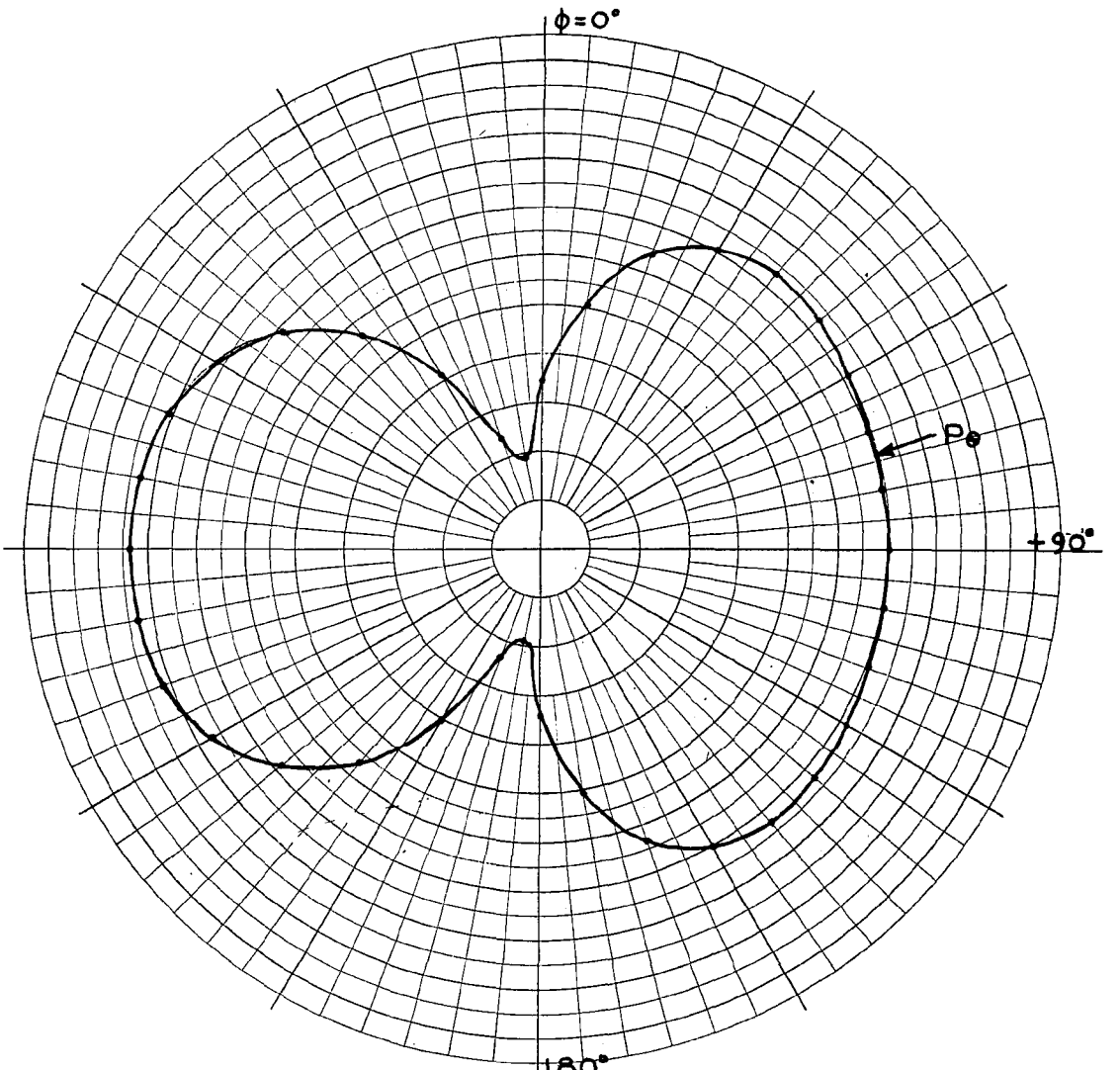

ANTENNA TYPE C.D.	LOCATION	USE	
TEST MODEL:		FREQUENCY: 445 MCS	
MODEL SCALE: 1:1		SCALE FREQUENCY: 1:1 MCS	
CONDITIONS:		POLARIZATION:	
CURVES PLOTTED IN:		Eθ: X	
VOLTAGE: X		Eϕ:	θ=50°
POWER:		PATTERN AREA:	β=120°
ENGINEER	OPERATOR	FILE NO.	DATE

Pattern scale: Each major radial increment = 0.02 units

FIGURE 34

PATTERN SUMMATION PLOT FOR TWO DIAMETRICALLY OPPOSED SLOTS OPERATING SIMULTANEOUSLY FOR $\theta = 50^{\circ}$ AND $\beta = 120^{\circ}$

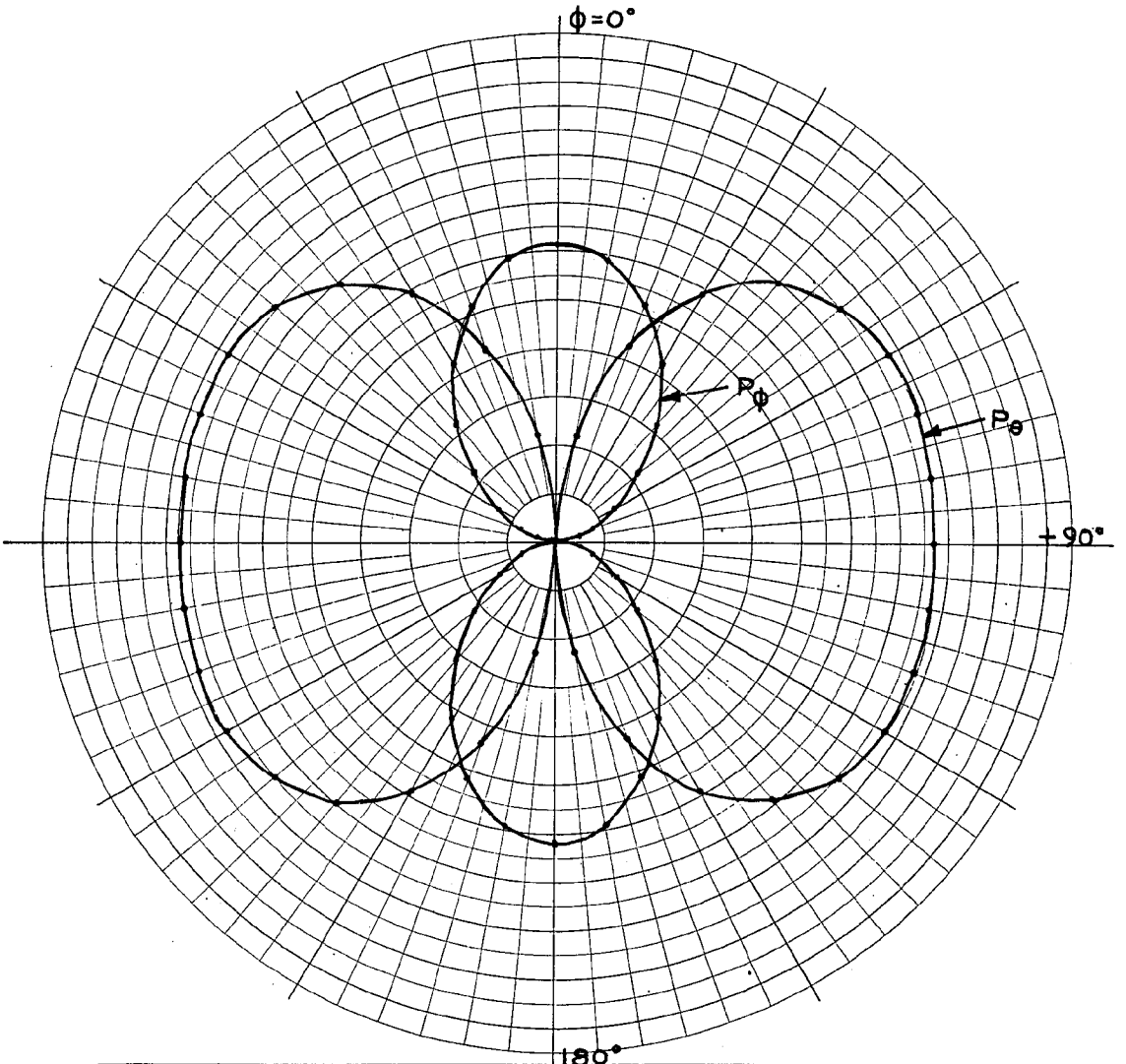

ANTENNA TYPE C.D.	LOCATION	USE
TEST MODEL:	FREQUENCY: 445 MCS	
MODEL SCALE: 1:1	SCALE FREQUENCY: 1:1 MCS	
CONDITIONS:	POLARIZATION:	
CURVES PLOTTED IN:	Eθ: X	
VOLTAGE: X	Eϕ: X	θ=50°
POWER:	PATTERN AREA:	β=180°
ENGINEER	OPERATOR	FILE NO. / DATE

Pattern scale: Each major radial increment = 0.02 units

FIGURE 35

PATTERN SUMMATION PLOTS FOR TWO DIAMETRICALLY OPPOSED SLOTS OPERATING SIMULTANEOUSLY FOR $\theta = 50^{\circ}$ AND $\beta = 180^{\circ}$

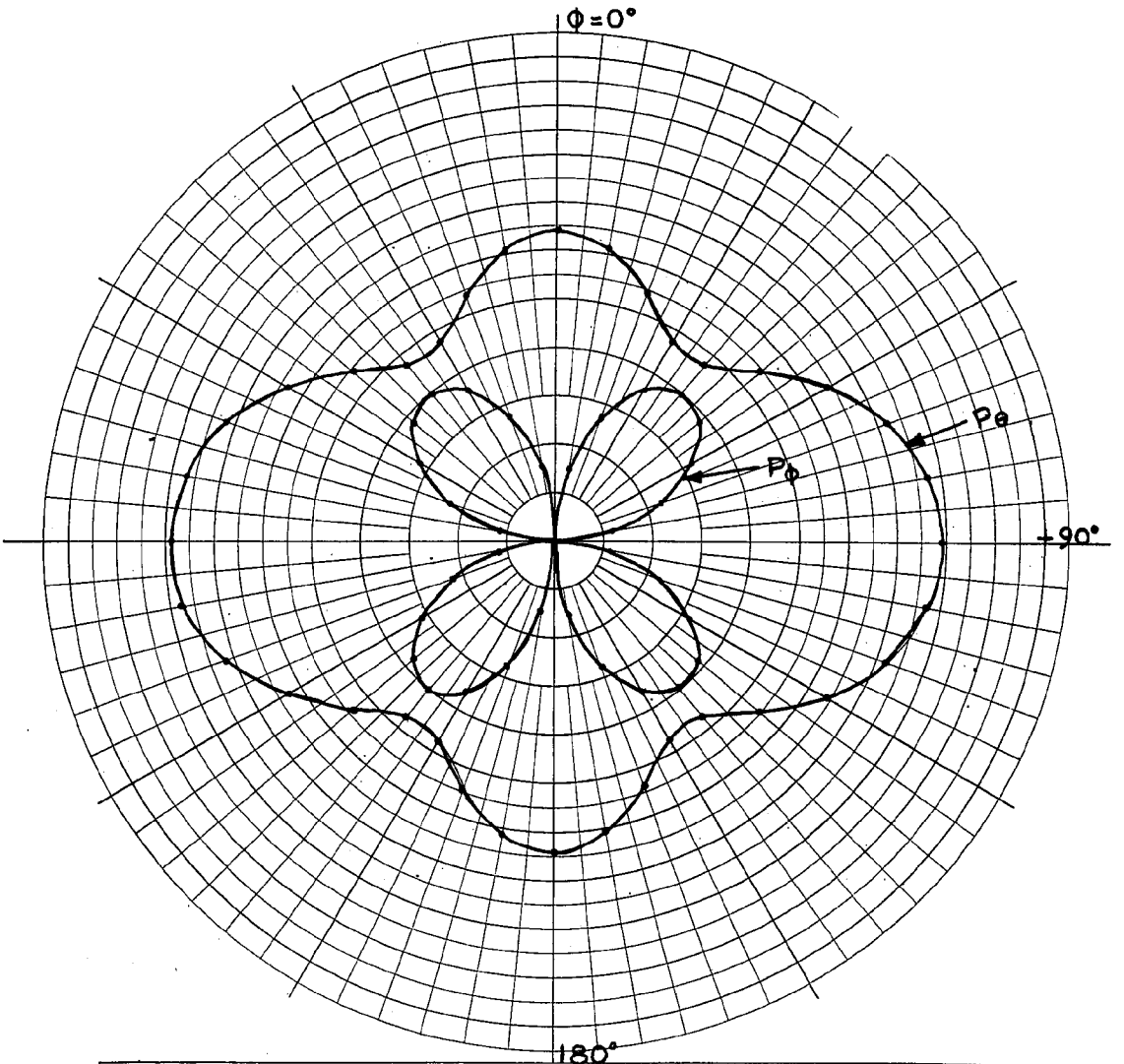

FIGURE 36

PATTERN SUMMATION PLOTS FOR TWO DIAMETRICALLY OPPOSED SLOTS OPERATING SIMULTANEOUSLY FOR $\theta = 60^{\circ}$ AND $\beta = 0^{\circ}$

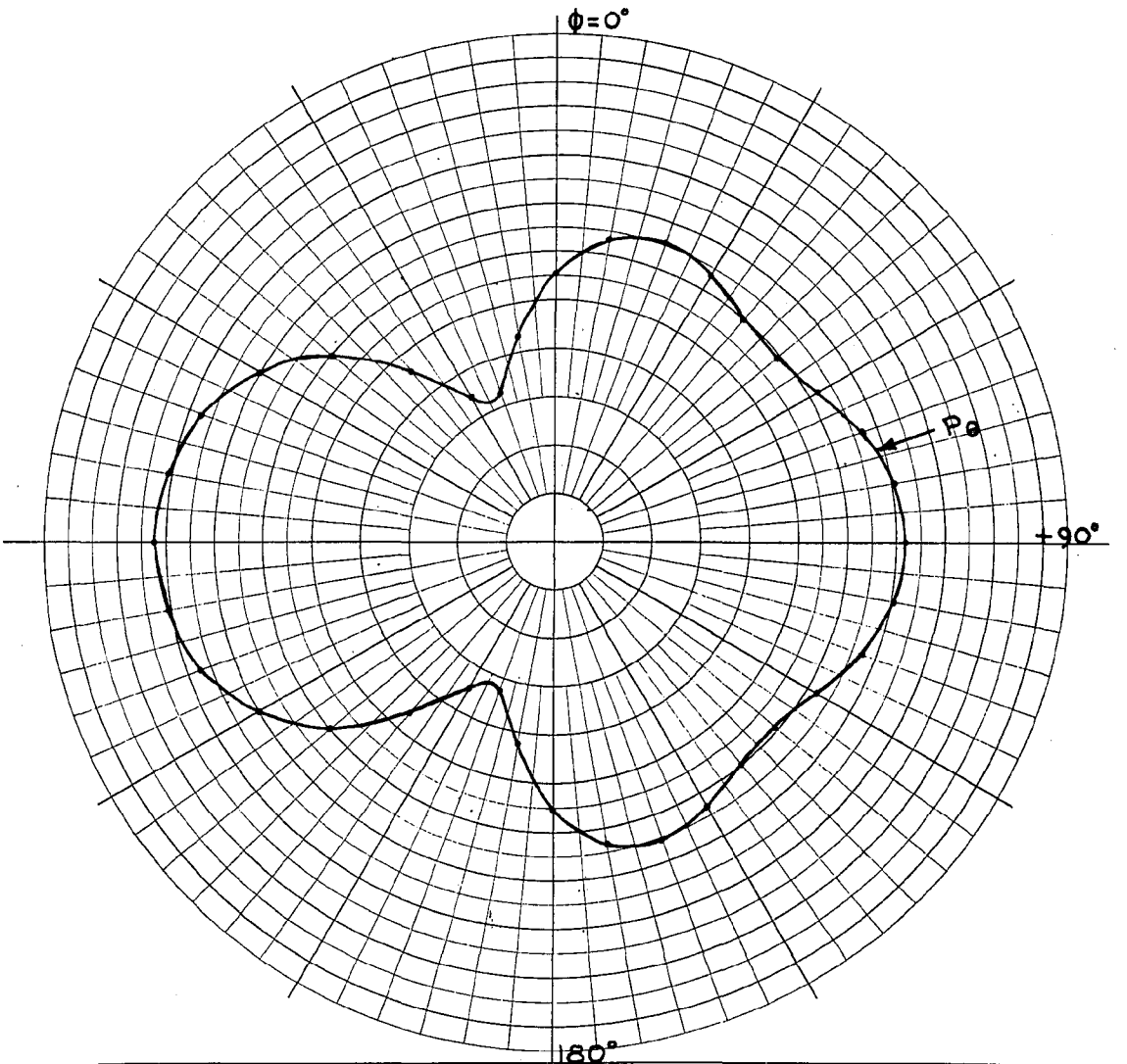

FIGURE 37

PATTERN SUMMATION PLOT FOR TWO DIAMETRICALLY OPPOSED SLOTS OPERATING SIMULTANEOUSLY FOR $\theta = 60^{\circ}$ AND $\beta = 60^{\circ}$

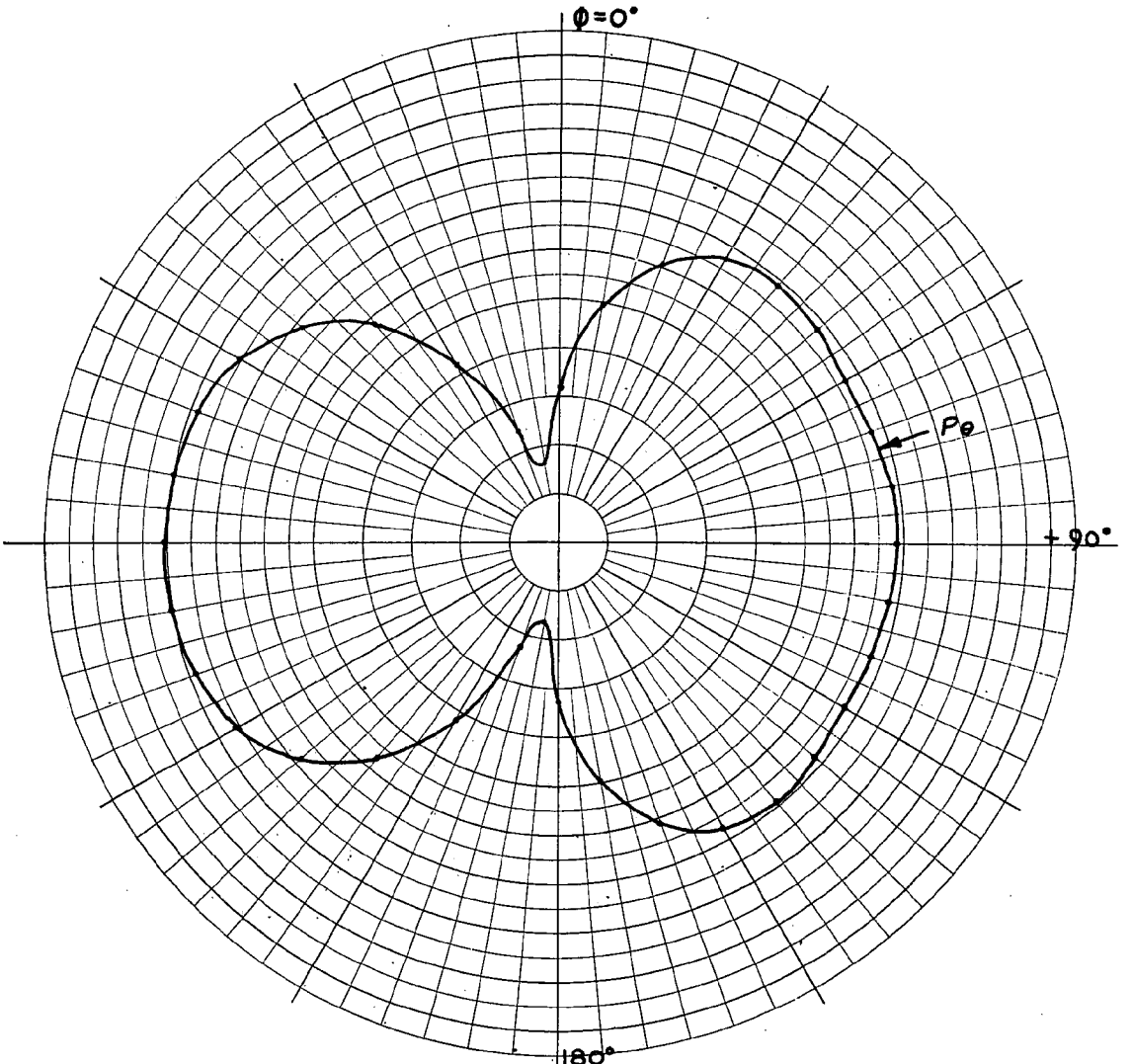

ANTENNA TYPE C. D.	LOCATION	USE	
TEST MODEL:		FREQUENCY: 445 MCS	
MODEL SCALE: 1:1		SCALE FREQUENCY: 1:1 MCS	
CONDITIONS:		POLARIZATION:	
CURVES PLOTTED IN:		Eθ: X	
VOLTAGE: X		Eφ:	θ=60°
POWER:		PATTERN AREA:	β=120°
ENGINEER	OPERATOR	FILE NO.	DATE

Pattern scale: Each major radial increment = 0.02 units

FIGURE 38

PATTERN SUMMATION PLOT FOR TWO DIAMETRICALLY OPPOSED SLOTS OPERATING SIMULTANEOUSLY FOR $\theta = 60^{\circ}$ AND $\beta = 120^{\circ}$

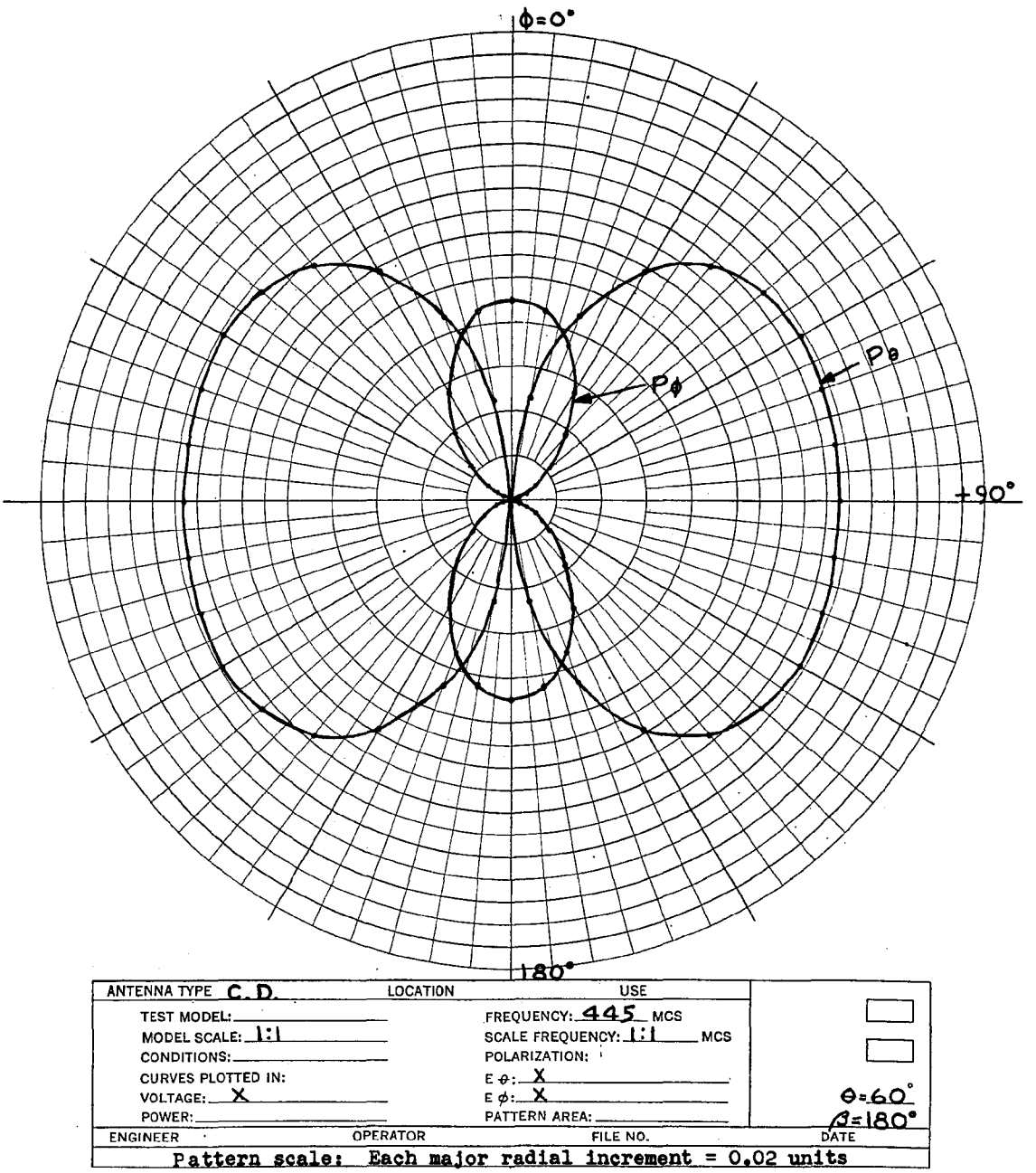

FIGURE 39

PATTERN SUMMATION PLOTS FOR TWO DIAMETRICALLY OPPOSED SLOTS OPERATING SIMULTANEOUSLY FOR $\theta = 60^{\circ}$ AND $\beta = 180^{\circ}$

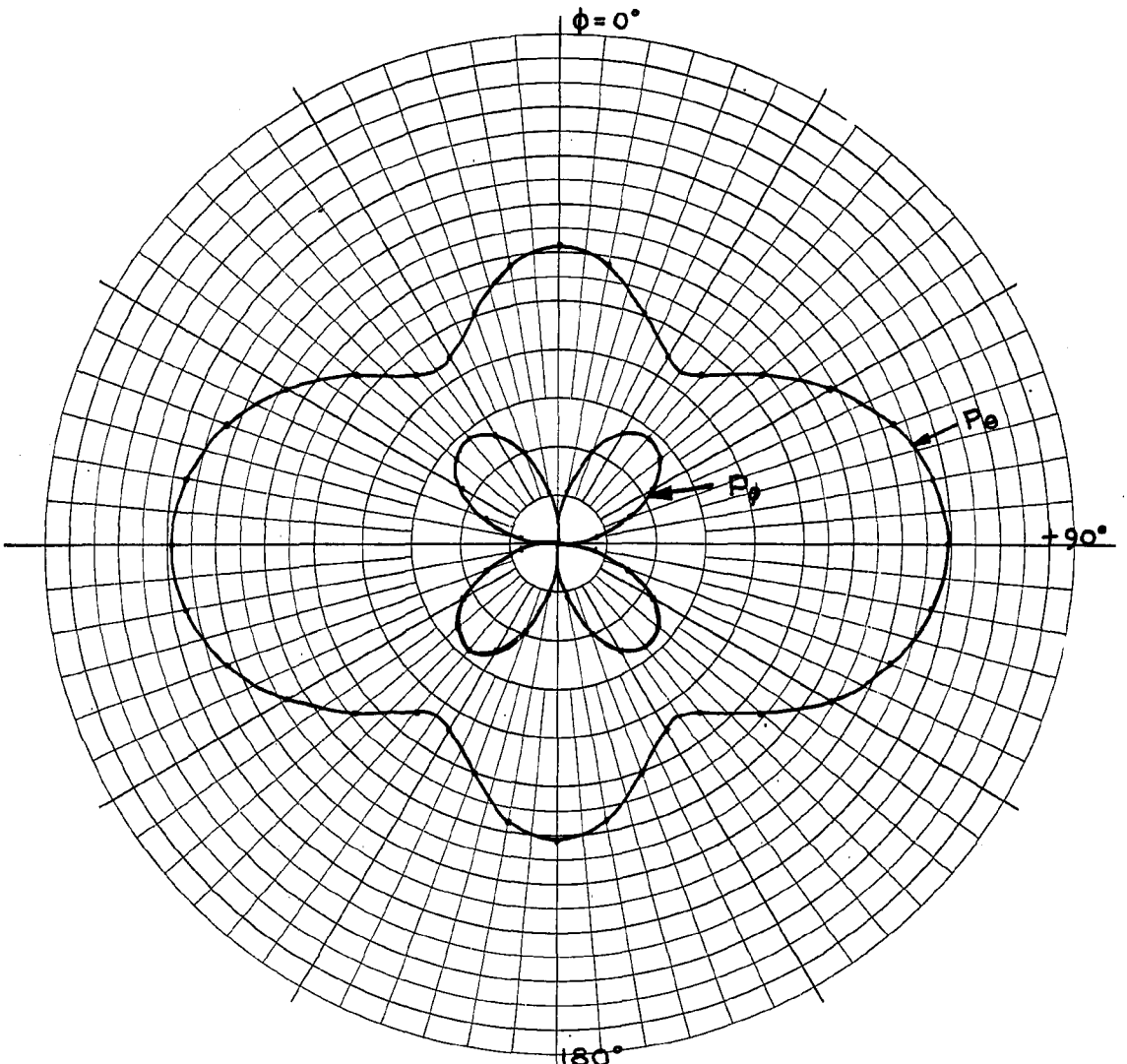

ANTENNA TYPE C. D.	LOCATION	USE
TEST MODEL:	FREQUENCY: 445 MCS	
MODEL SCALE: 1:1	SCALE FREQUENCY: 1:1 MCS	
CONDITIONS:	POLARIZATION:	
CURVES PLOTTED IN:	Eθ: X	
VOLTAGE: X	Eϕ: X	θ = 70°
POWER:	PATTERN AREA:	β = 0°
ENGINEER	OPERATOR	FILE NO. / DATE

Pattern scale: Each major radial increment = 0.02 units

FIGURE 40

PATTERN SUMMATION PLOTS FOR TWO DIAMETRICALLY OPPOSED SLOTS OPERATING SIMULTANEOUSLY FOR $\theta = 70^{\circ}$ AND $\beta = 0^{\circ}$

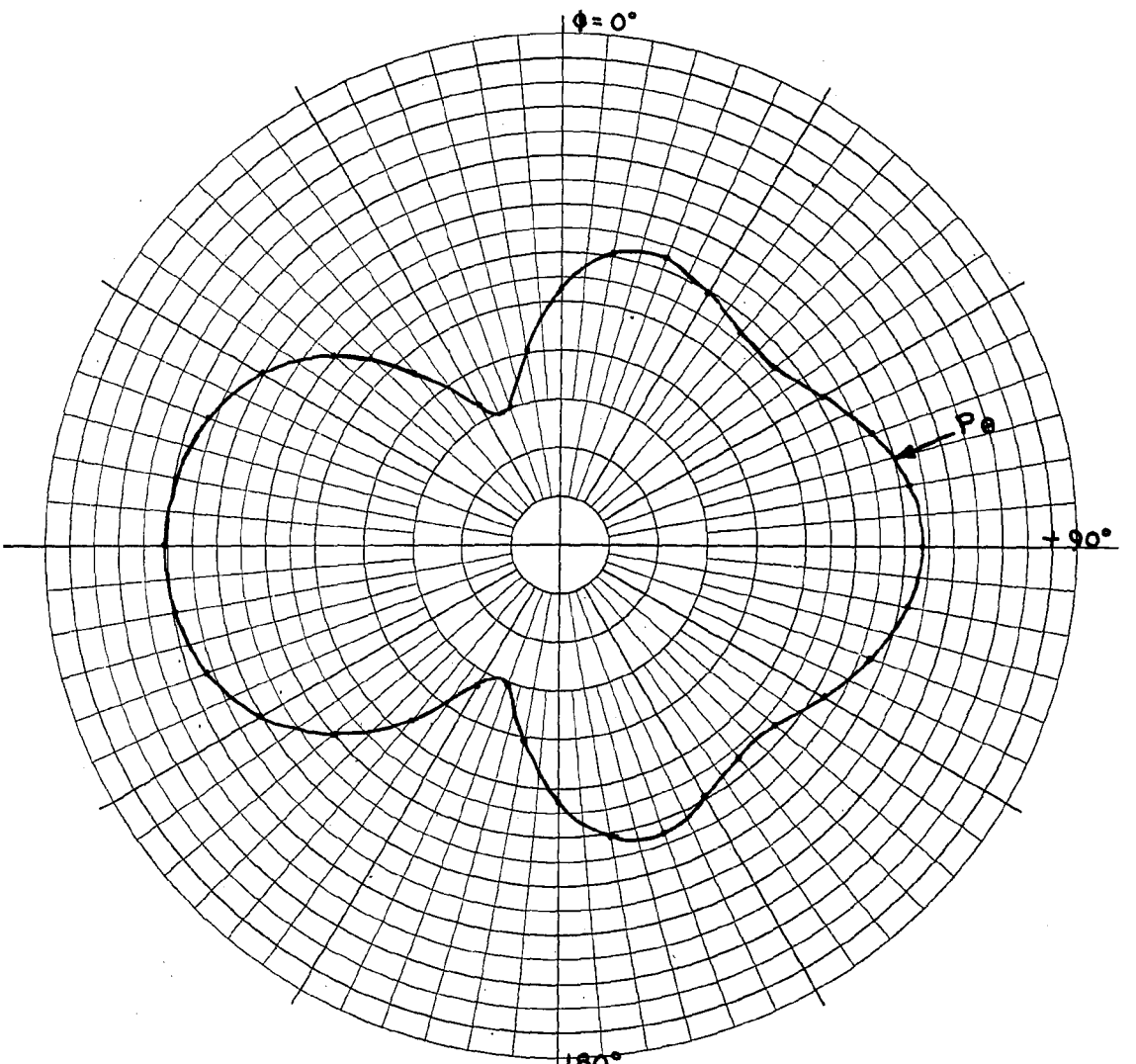

ANTENNA TYPE C. D.	LOCATION	USE
TEST MODEL:		FREQUENCY: 445 MCS
MODEL SCALE: 1:1		SCALE FREQUENCY: 1:1 MCS
CONDITIONS:		POLARIZATION:
CURVES PLOTTED IN:		E θ: X
VOLTAGE: X		E ϕ:
POWER:		PATTERN AREA:
ENGINEER	OPERATOR	FILE NO.

θ = 70°
β = 60°

DATE

Pattern scale: Each major radial increment = 0.02 units

FIGURE 41

PATTERN SUMMATION PLOT FOR TWO DIAMETRICALLY OPPOSED SLOTS OPERATING SIMULTANEOUSLY FOR $\theta = 70^{\circ}$ AND $\beta = 60^{\circ}$

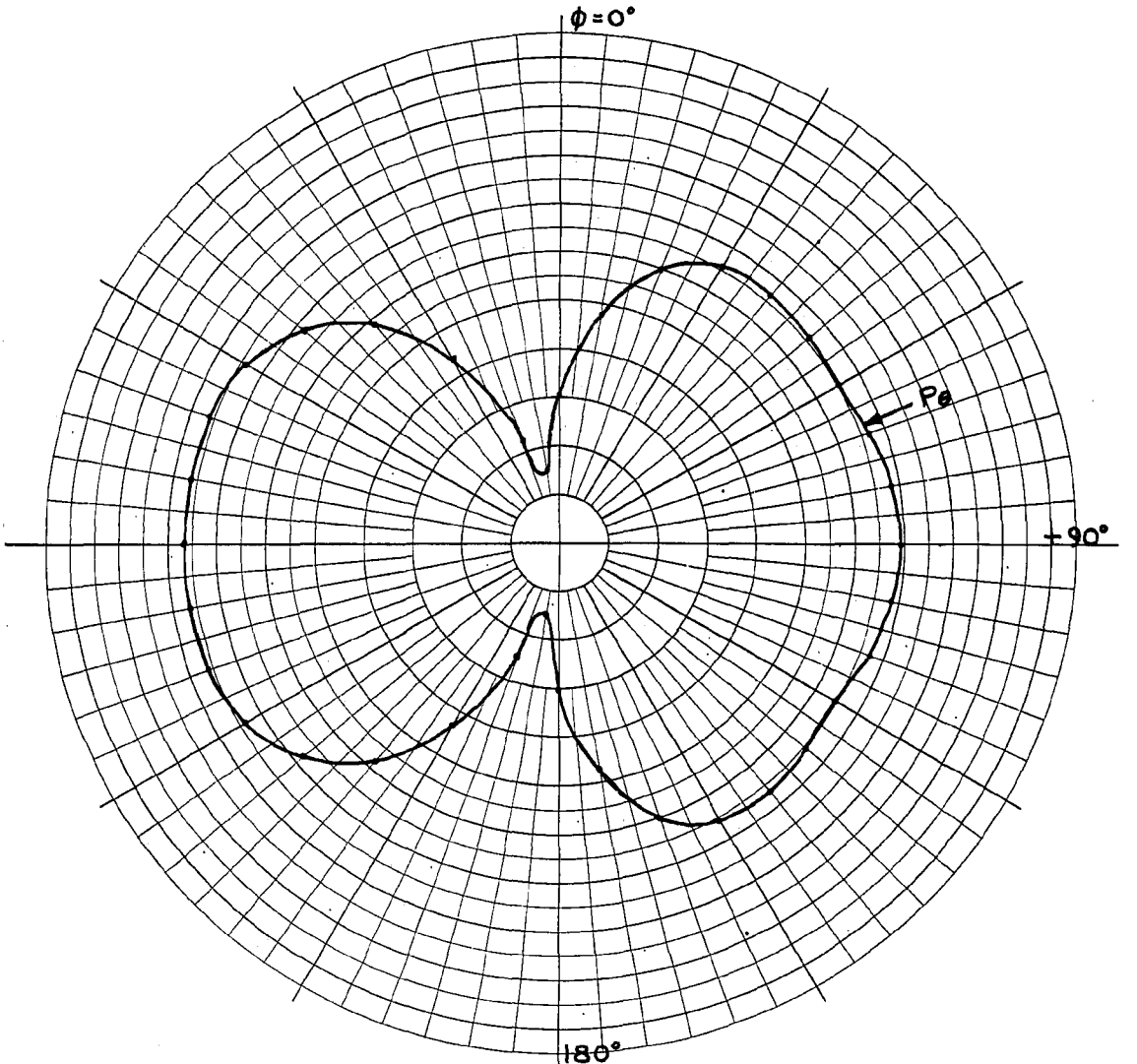

ANTENNA TYPE C.D.	LOCATION	USE
TEST MODEL:	FREQUENCY: 445 MCS	
MODEL SCALE: 1:1	SCALE FREQUENCY: 1:1 MCS	
CONDITIONS:	POLARIZATION:	
CURVES PLOTTED IN:	E θ: X	
VOLTAGE: X	E ϕ:	θ=70°
POWER:	PATTERN AREA:	β=120°
ENGINEER	OPERATOR	FILE NO. / DATE

Pattern scale: Each major radial increment = 0.02 units

FIGURE 42

PATTERN SUMMATION PLOT FOR TWO DIAMETRICALLY OPPOSED SLOTS OPERATING SIMULTANEOUSLY FOR $\theta = 70^{\circ}$ AND $\beta = 120^{\circ}$

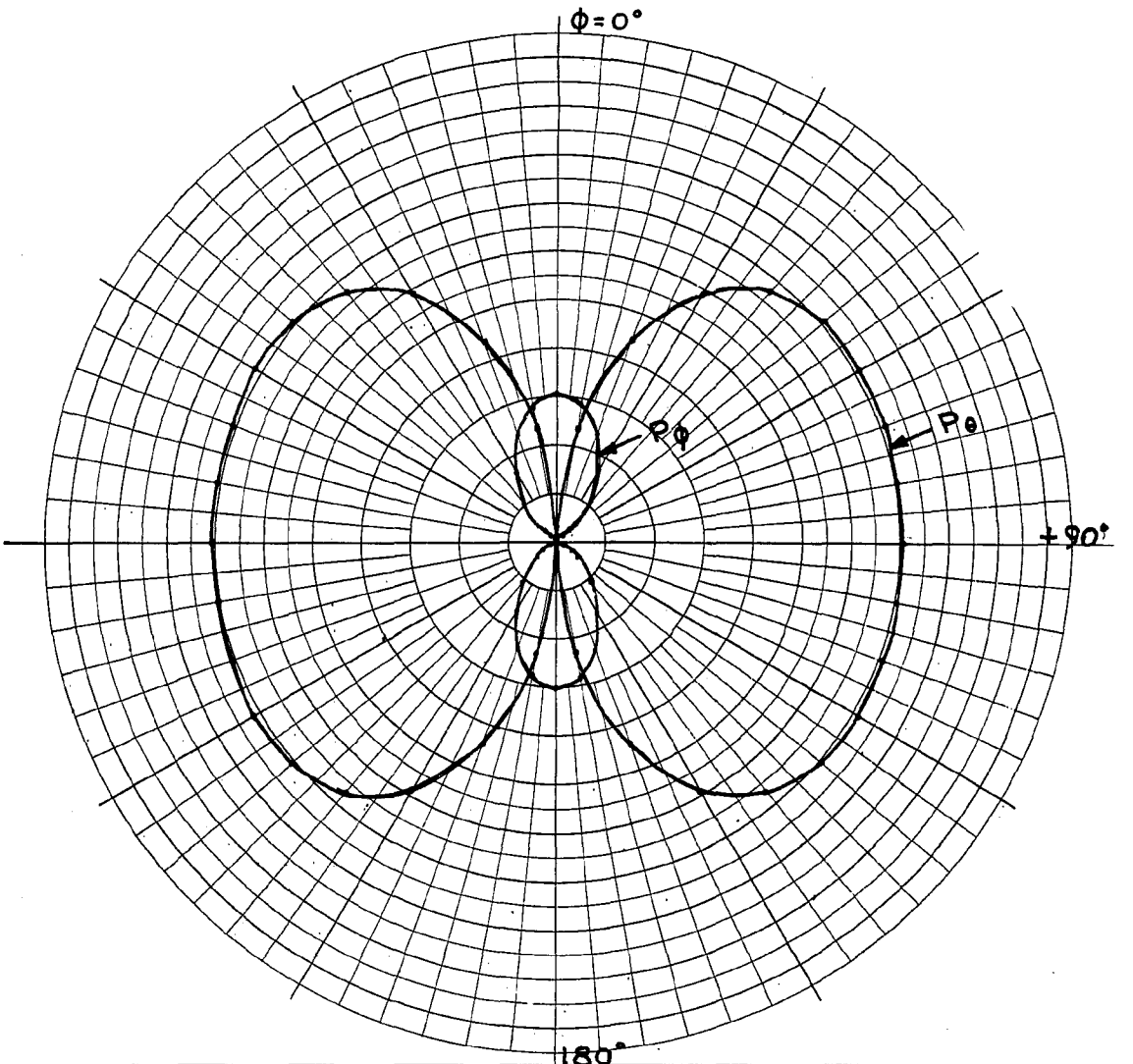

FIGURE 43

PATTERN SUMMATION PLOTS FOR TWO DIAMETRICALLY OPPOSED SLOTS OPERATING SIMULTANEOUSLY FOR $\theta = 70^{\circ}$ AND $\beta = 180^{\circ}$

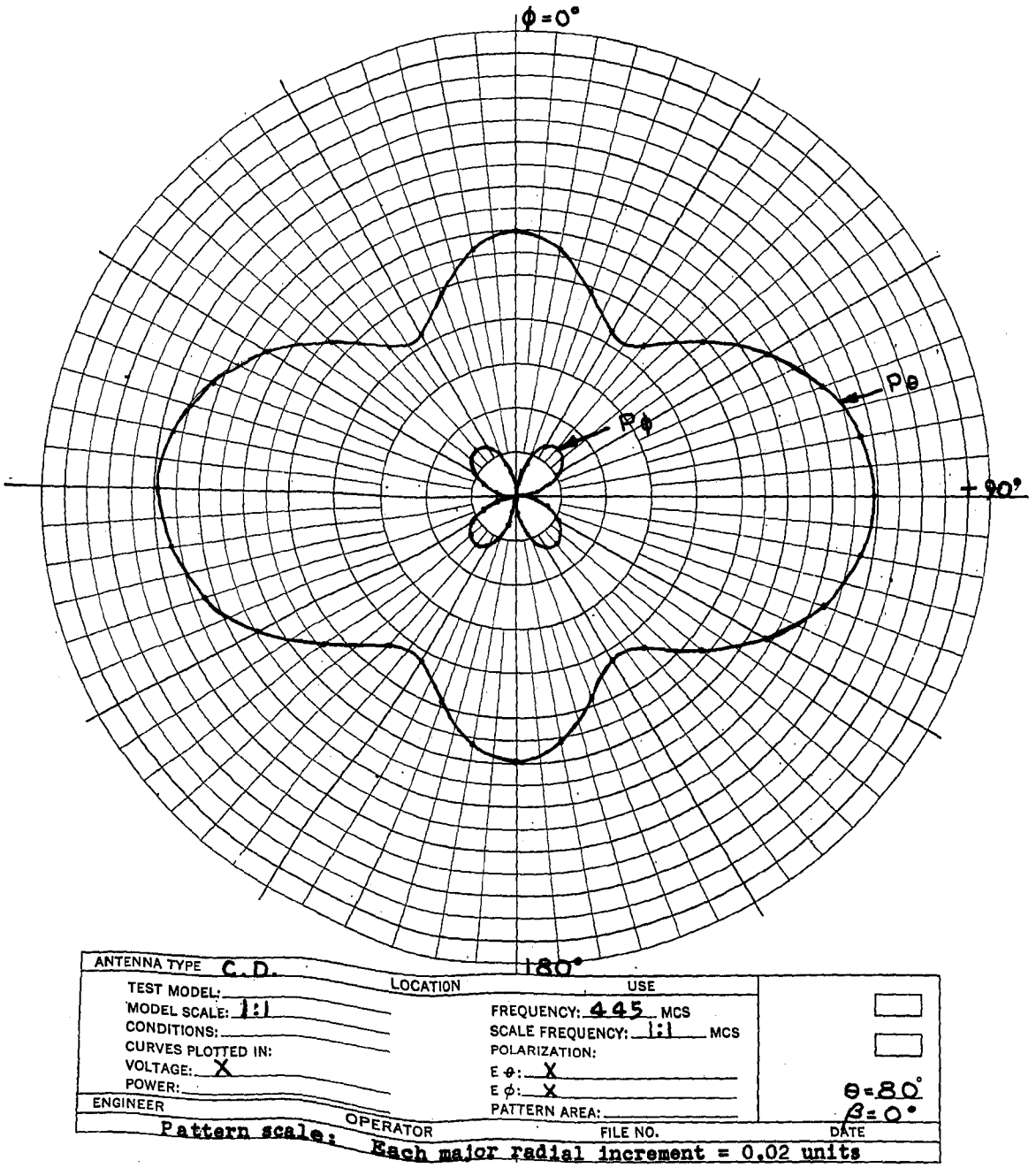

FIGURE 44

PATTERN SUMMATION PLOTS FOR TWO DIAMETRICALLY OPPOSED SLOTS OPERATING SIMULTANEOUSLY FOR $\theta = 80^{\circ}$ AND $\beta = 0^{\circ}$

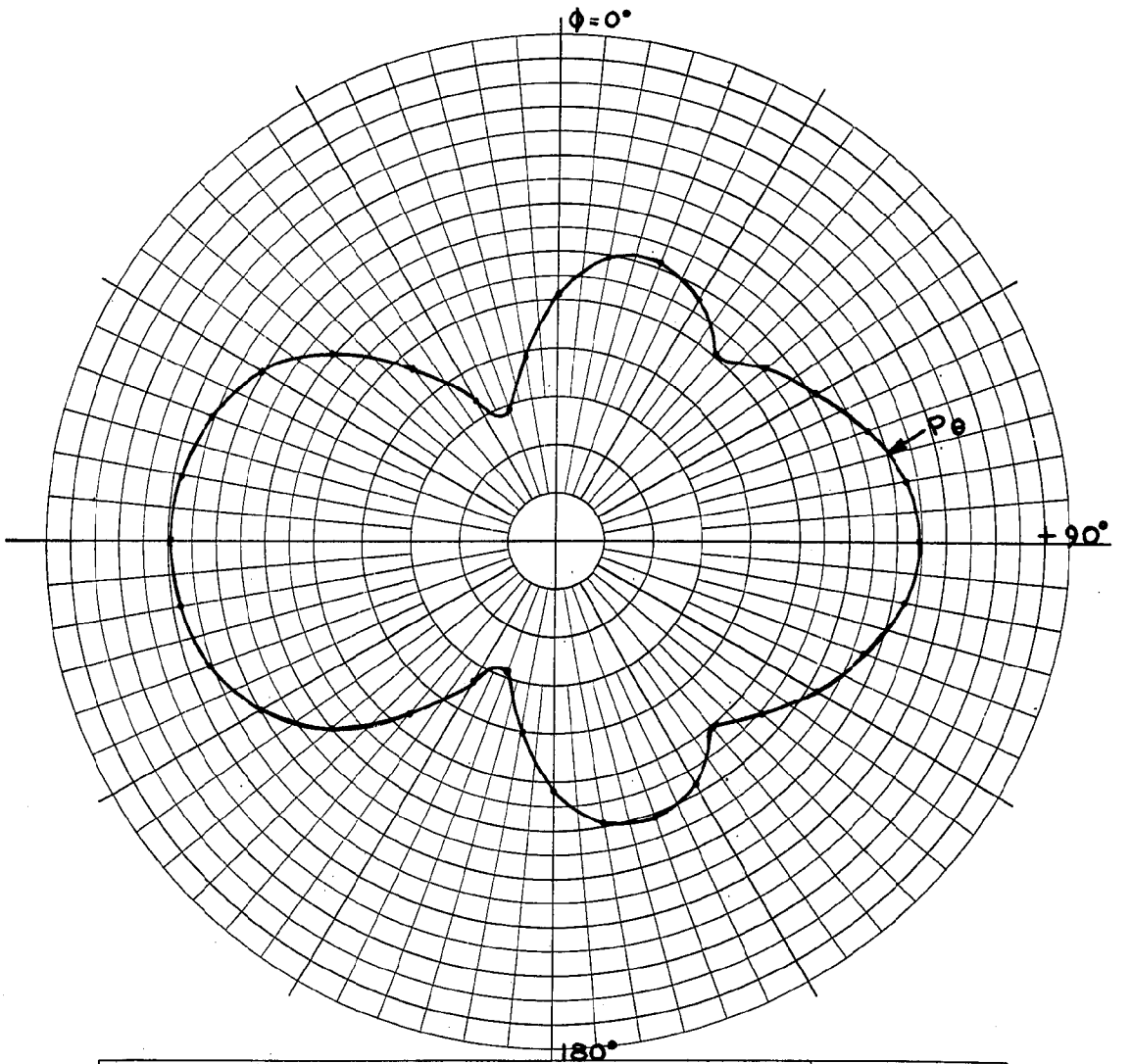

ANTENNA TYPE C.D.	LOCATION	USE	
TEST MODEL:		FREQUENCY: 445 MCS	
MODEL SCALE: 1:1		SCALE FREQUENCY: 1:1 MCS	
CONDITIONS:		POLARIZATION:	
CURVES PLOTTED IN:		E θ: X	
VOLTAGE: X		E φ:	θ=80°
POWER:		PATTERN AREA:	β=60°
ENGINEER	OPERATOR	FILE NO.	DATE

Pattern scale: Each major radial increment = 0.02 units

FIGURE 45

PATTERN SUMMATION PLOT FOR TWO DIAMETRICALLY OPPOSED SLOTS OPERATING SIMULTANEOUSLY FOR $\theta = 80^{\circ}$ AND $\beta = 60^{\circ}$

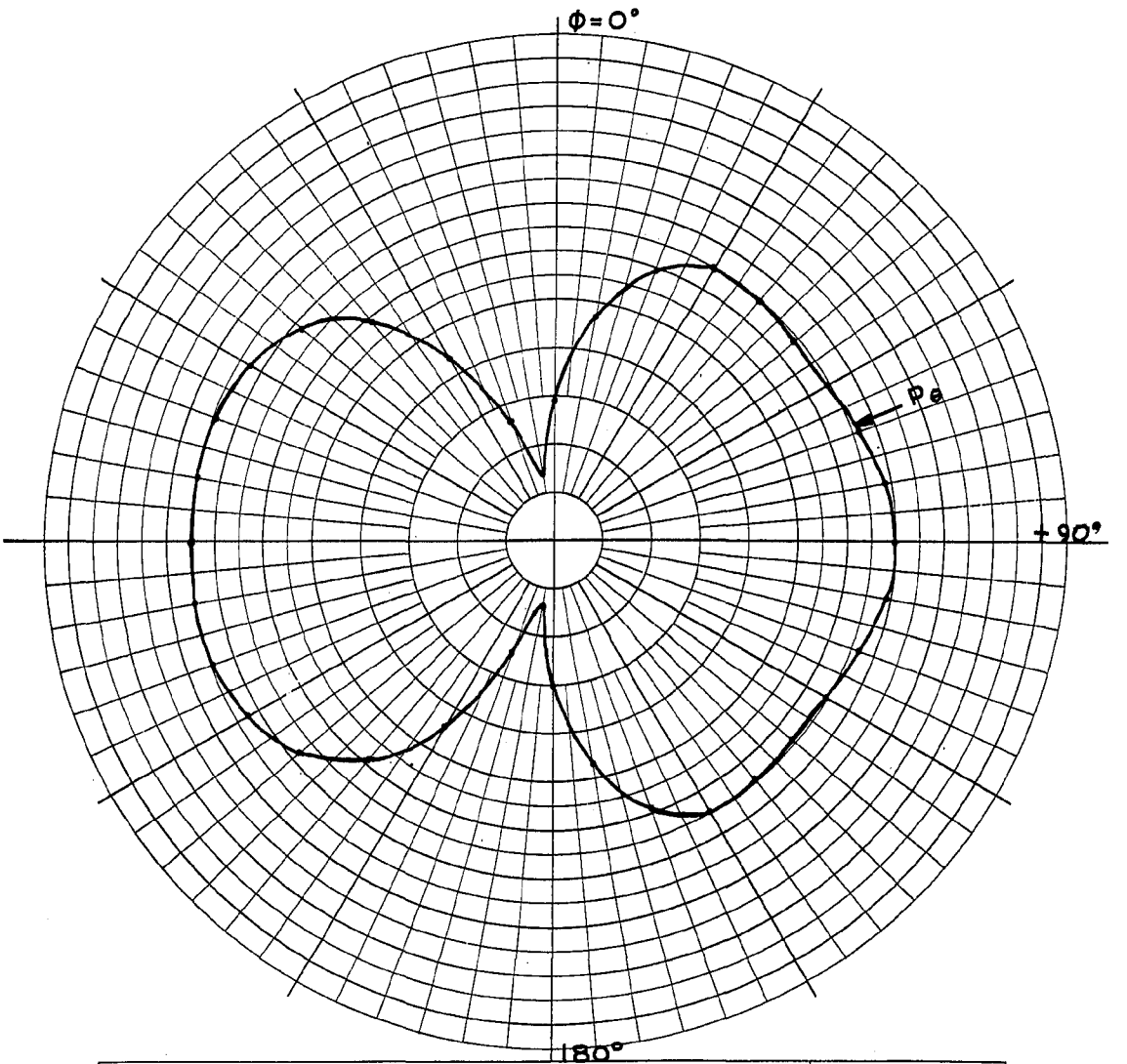

ANTENNA TYPE	LOCATION	USE	
TEST MODEL: C.D.		FREQUENCY: 445 MCS	
MODEL SCALE:		SCALE FREQUENCY: 1:1 MCS	
CONDITIONS: 1:1		POLARIZATION:	
CURVES PLOTTED IN:		E θ: X	
VOLTAGE: X		E φ:	θ=80°
POWER:		PATTERN AREA:	β=120°
ENGINEER	OPERATOR	FILE NO.	DATE

Pattern scale: Each major radial increment = 0.02 units

FIGURE 46

PATTERN SUMMATION PLOT FOR TWO DIAMETRICALLY OPPOSED SLOTS OPERATING SIMULTANEOUSLY FOR $\theta = 80^{\circ}$ AND $\beta = 120^{\circ}$

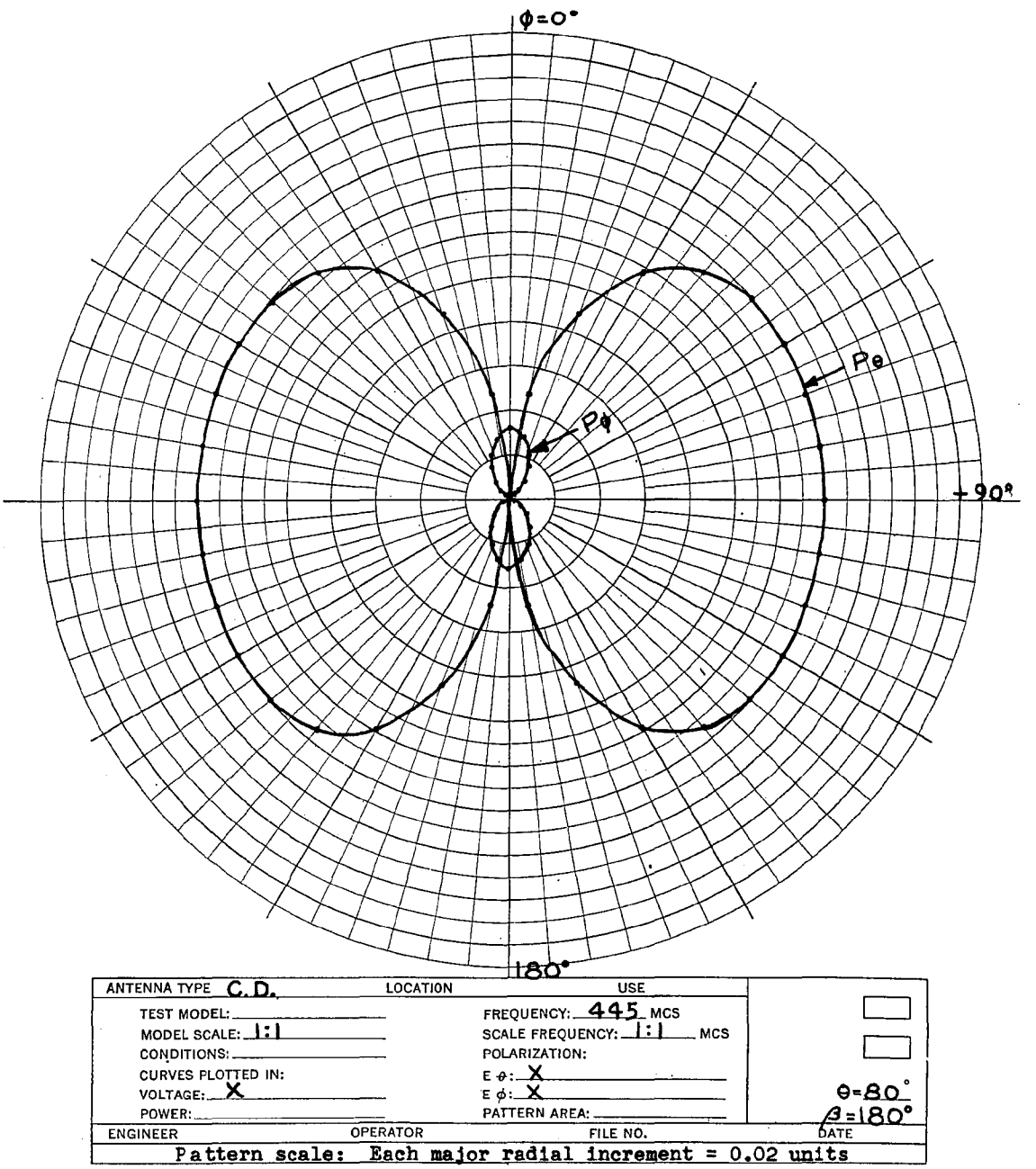

FIGURE 47

PATTERN SUMMATION PLOTS FOR TWO DIAMETRICALLY OPPOSED SLOTS OPERATING SIMULTANEOUSLY FOR $\theta = 80^{\circ}$ AND $\beta = 180^{\circ}$

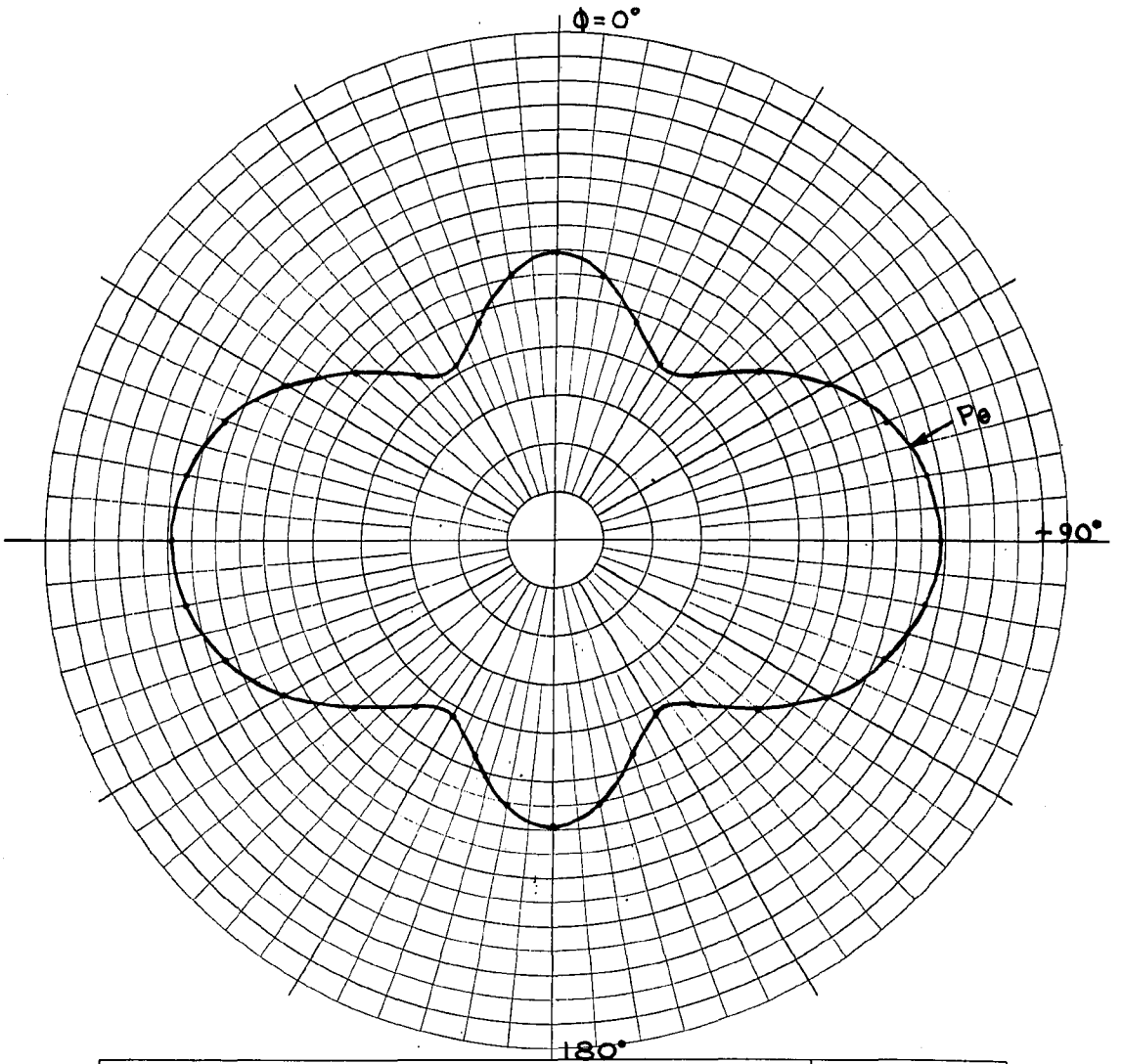

FIGURE 48

PATTERN SUMMATION PLOT FOR TWO DIAMETRICALLY OPPOSED SLOTS OPERATING SIMULTANEOUSLY FOR $\theta = 90^{\circ}$ AND $\beta = 0^{\circ}$

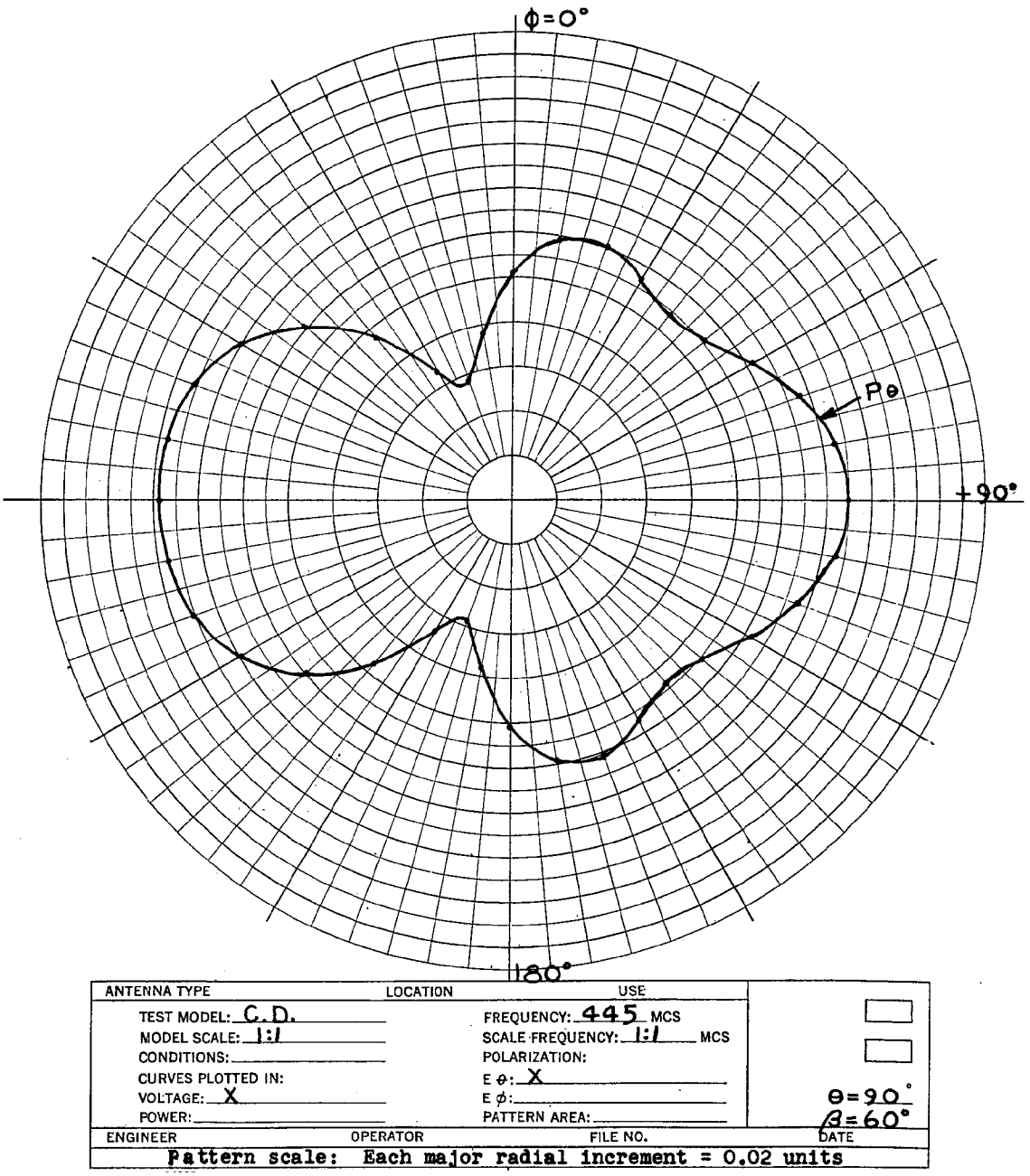

FIGURE 49

PATTERN SUMMATION PLOT FOR TWO DIAMETRICALLY OPPOSED SLOTS OPERATING SIMULTANEOUSLY FOR $\theta = 90^{\circ}$ AND $\beta = 60^{\circ}$

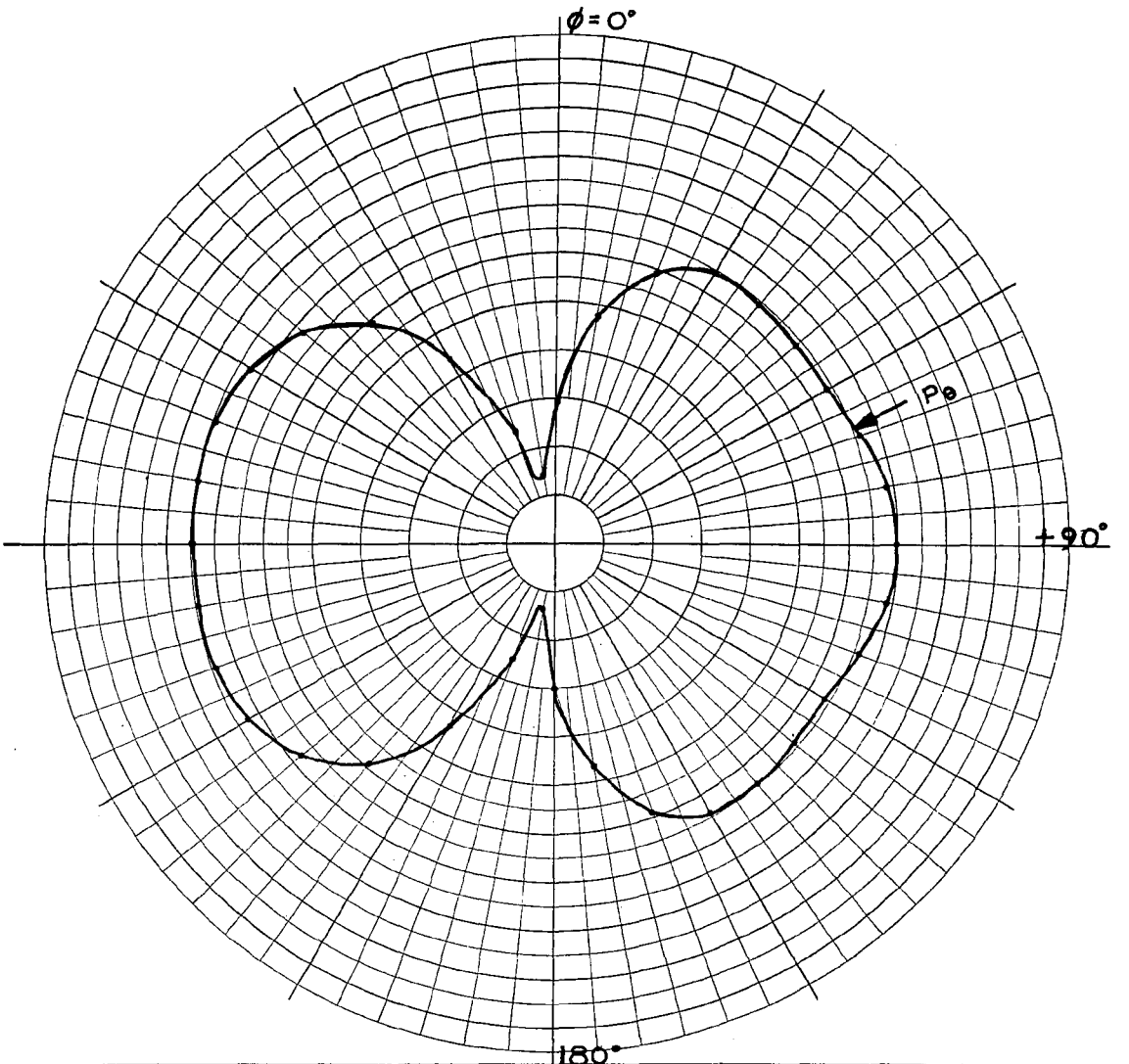

ANTENNA TYPE C. D.	LOCATION	USE	
TEST MODEL:		FREQUENCY: 445 MCS	
MODEL SCALE: 1:1		SCALE FREQUENCY: 1:1 MCS	
CONDITIONS:		POLARIZATION:	
CURVES PLOTTED IN:		E θ: X	
VOLTAGE: X		E ϕ:	θ=90°
POWER:		PATTERN AREA:	β=120°
ENGINEER	OPERATOR	FILE NO.	DATE

Pattern scale: Each major radial increment = 0.02 units

FIGURE 50

PATTERN SUMMATION PLOT FOR TWO DIAMETRICALLY OPPOSED SLOTS OPERATING SIMULTANEOUSLY FOR $\theta = 90^{\circ}$ AND $\beta = 120^{\circ}$

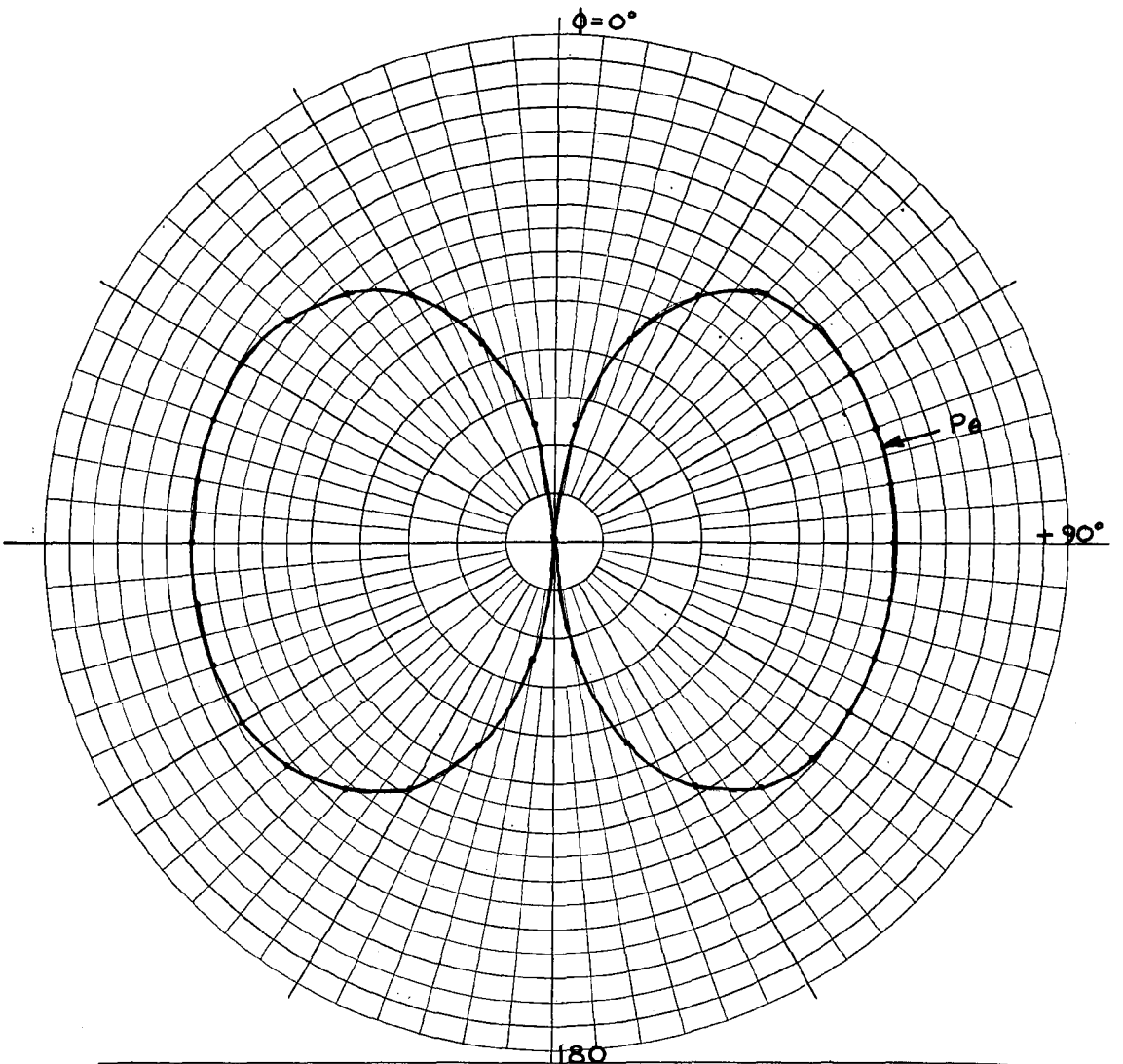

FIGURE 51

PATTERN SUMMATION PLOT FOR TWO DIAMETRICALLY OPPOSED SLOTS OPERATING SIMULTANEOUSLY FOR $\theta = 90^{\circ}$ AND $\beta = 180^{\circ}$

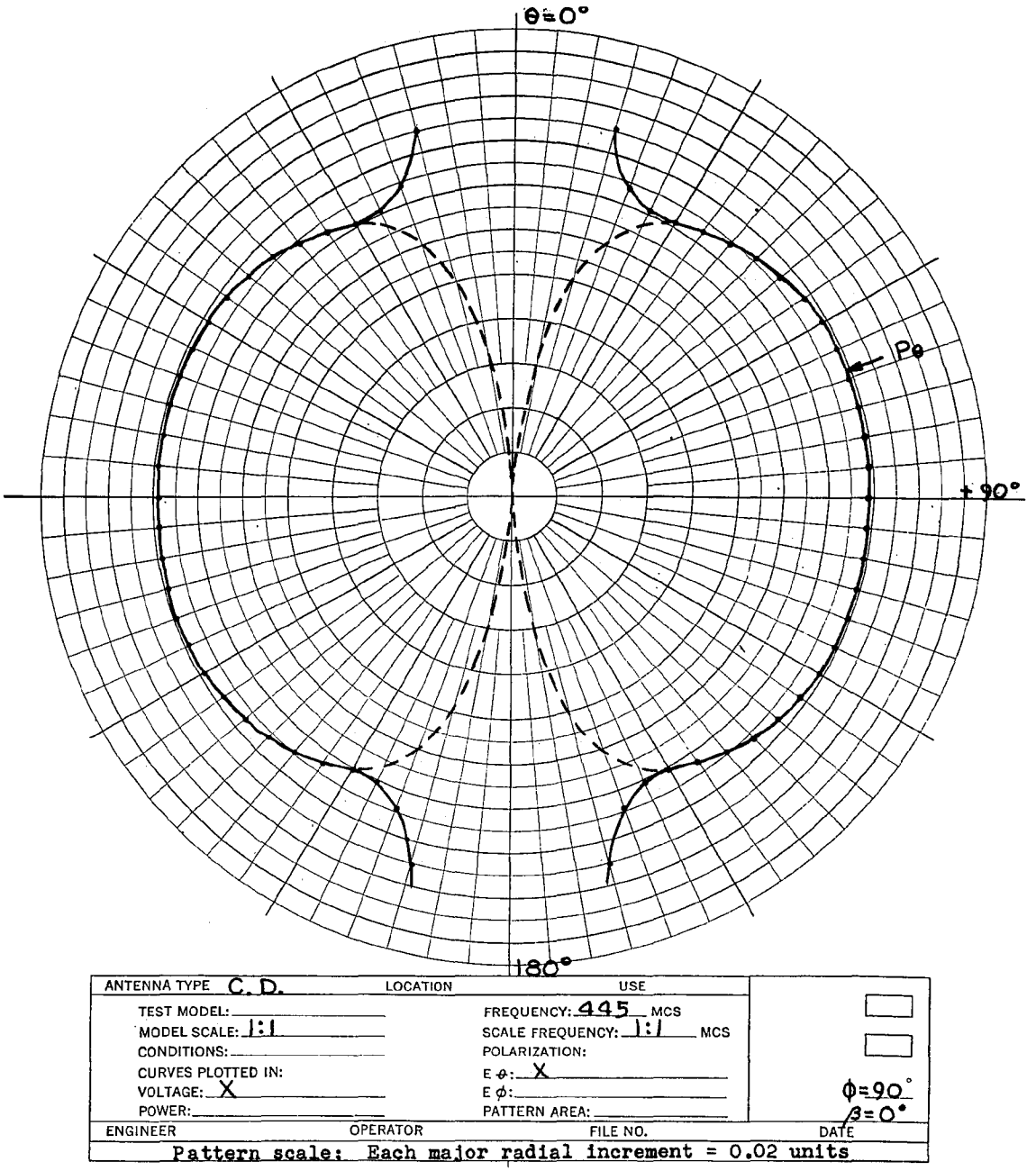

FIGURE 52

PATTERN SUMMATION PLOT FOR TWO DIAMETRICALLY OPPOSED SLOTS OPERATING SIMULTANEOUSLY FOR $\varphi = 90^{\circ}$ AND $\beta = 0^{\circ}$

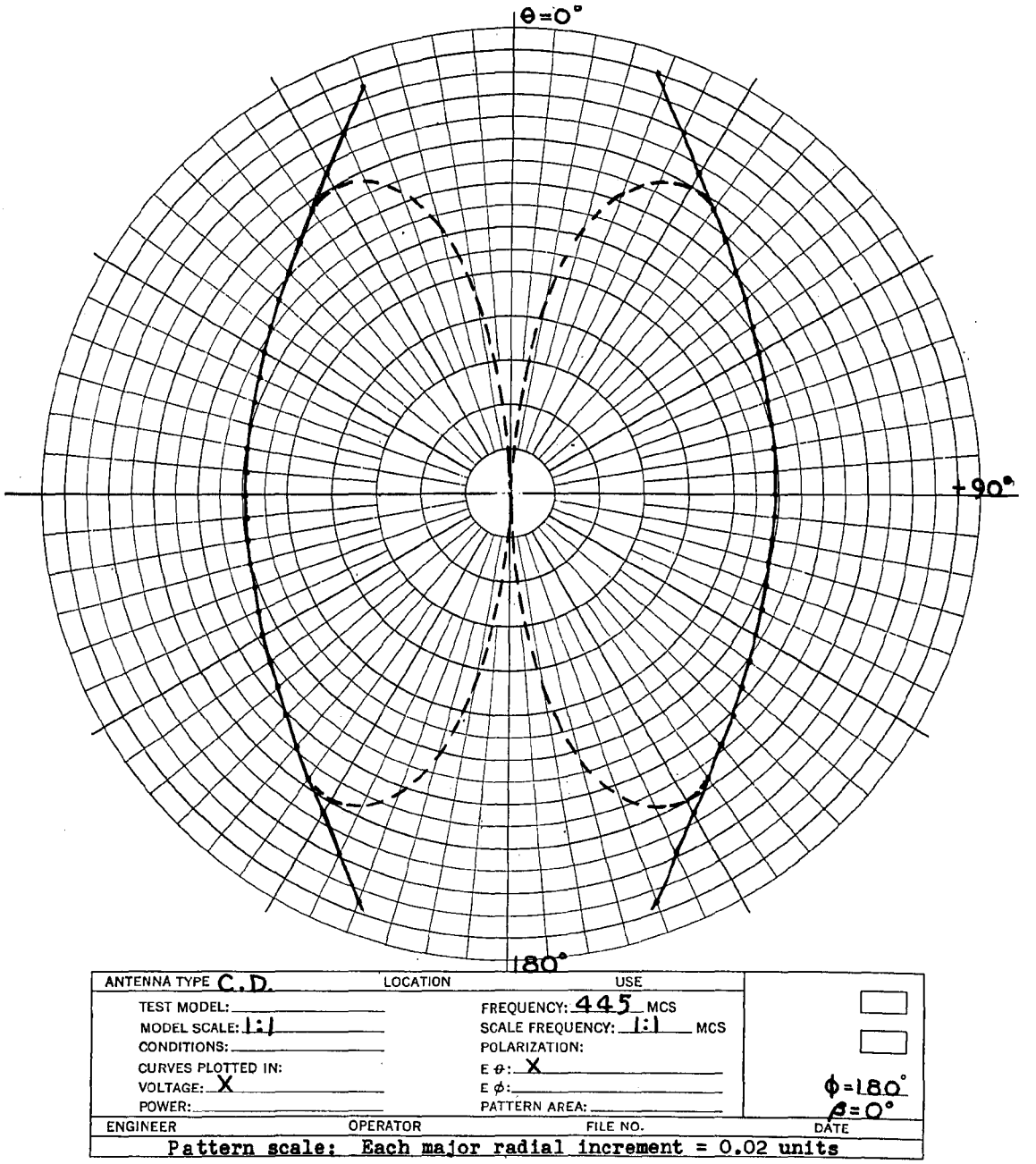

FIGURE 53

PATTERN SUMMATION PLOT FOR TWO DIAMETRICALLY OPPOSED SLOTS OPERATING SIMULTANEOUSLY FOR $\varphi = 180^{\circ}$ AND $\beta = 0^{\circ}$

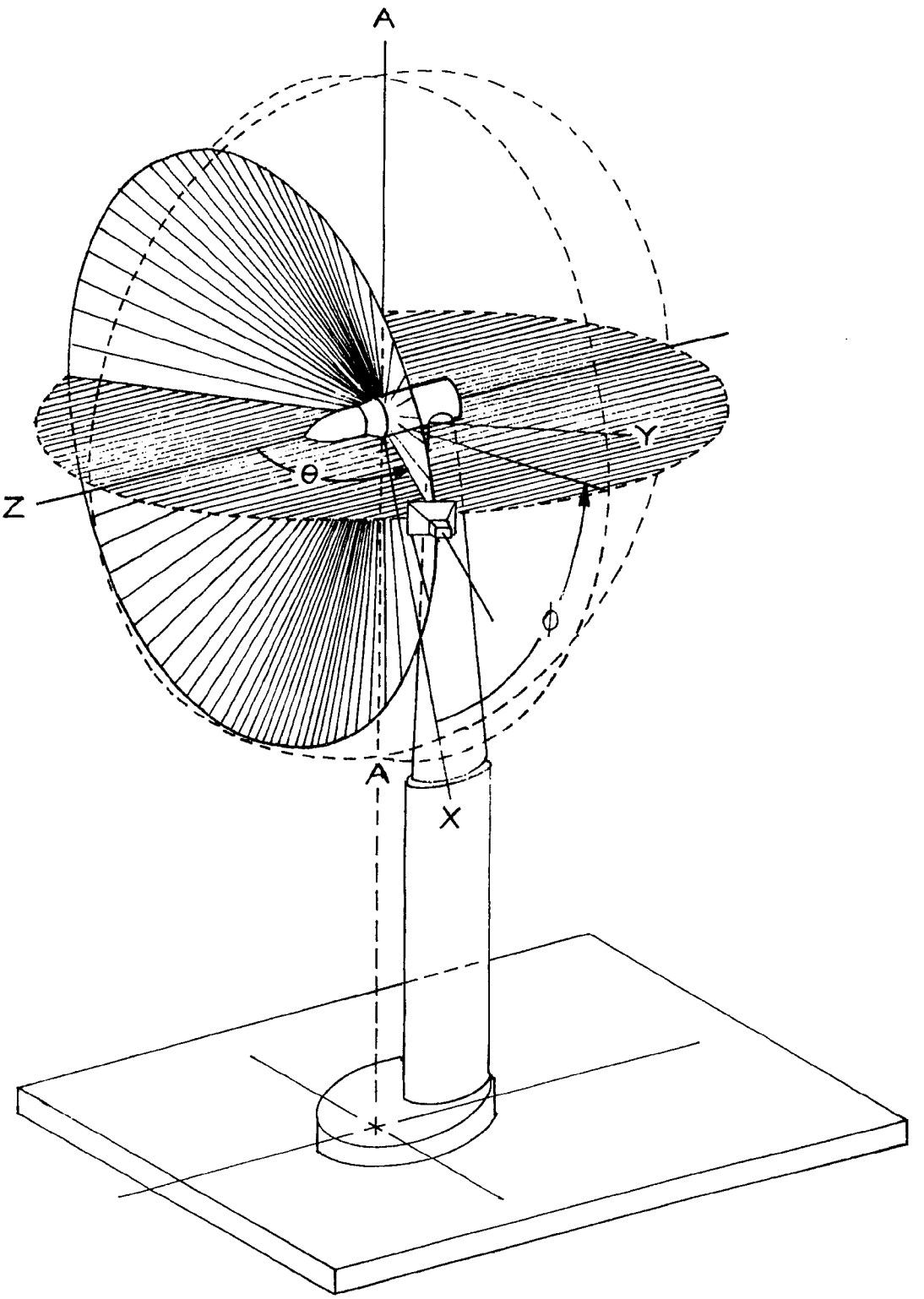

FIGURE 54

EXPERIMENTAL PATTERN MEASUREMENT TECHNIQUE

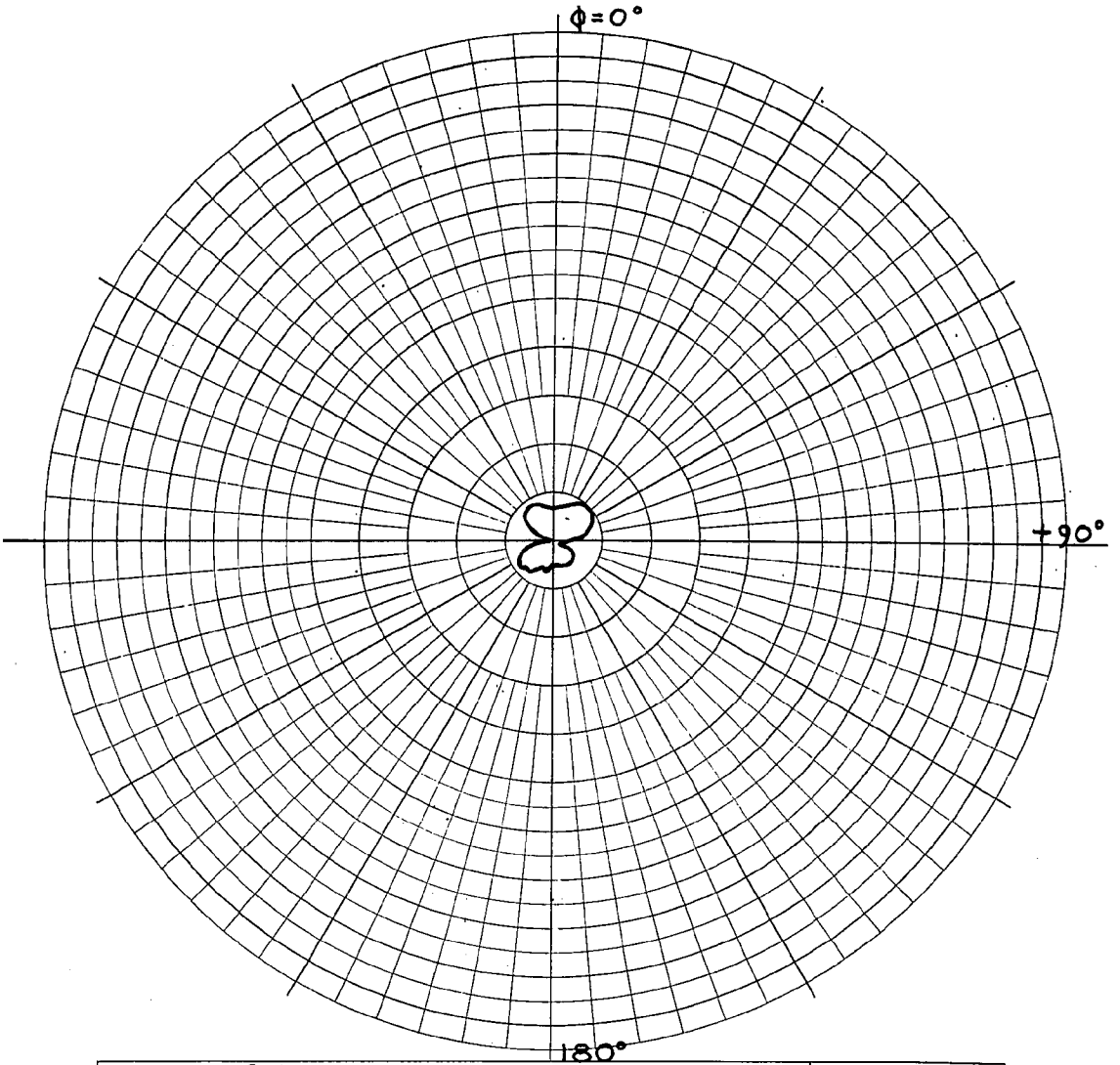

FIGURE 55

EXPERIMENTAL PATTERN FOR TWO DIAMETRICALLY OPPOSED SLOTS OPERATING SIMULTANEOUSLY INPHASE FOR $\theta = 0^{\circ}$

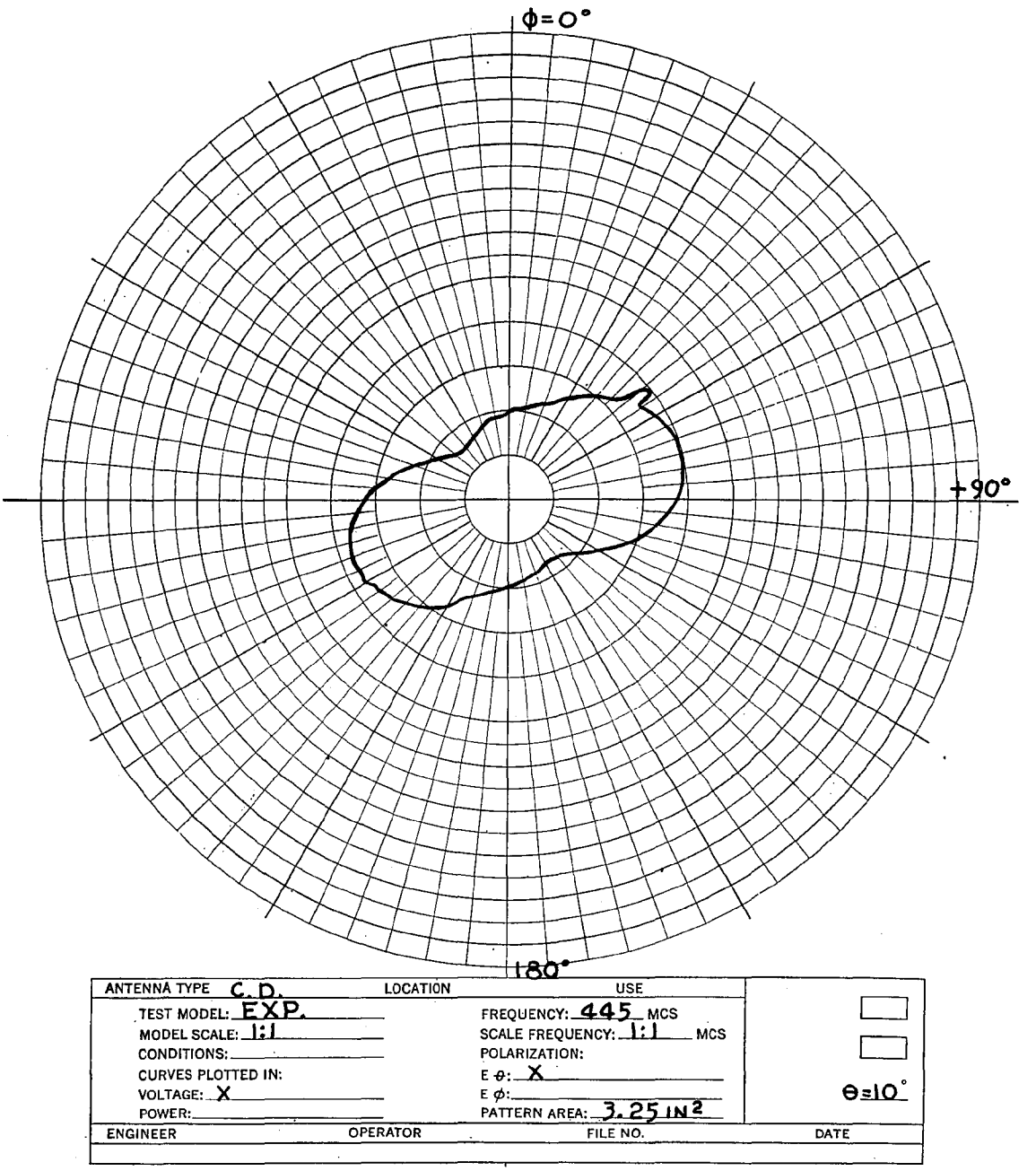

FIGURE 56

EXPERIMENTAL PATTERN FOR TWO DIAMETRICALLY OPPOSED SLOTS OPERATING SIMULTANEOUSLY INPHASE FOR $\theta = 10^{o}$

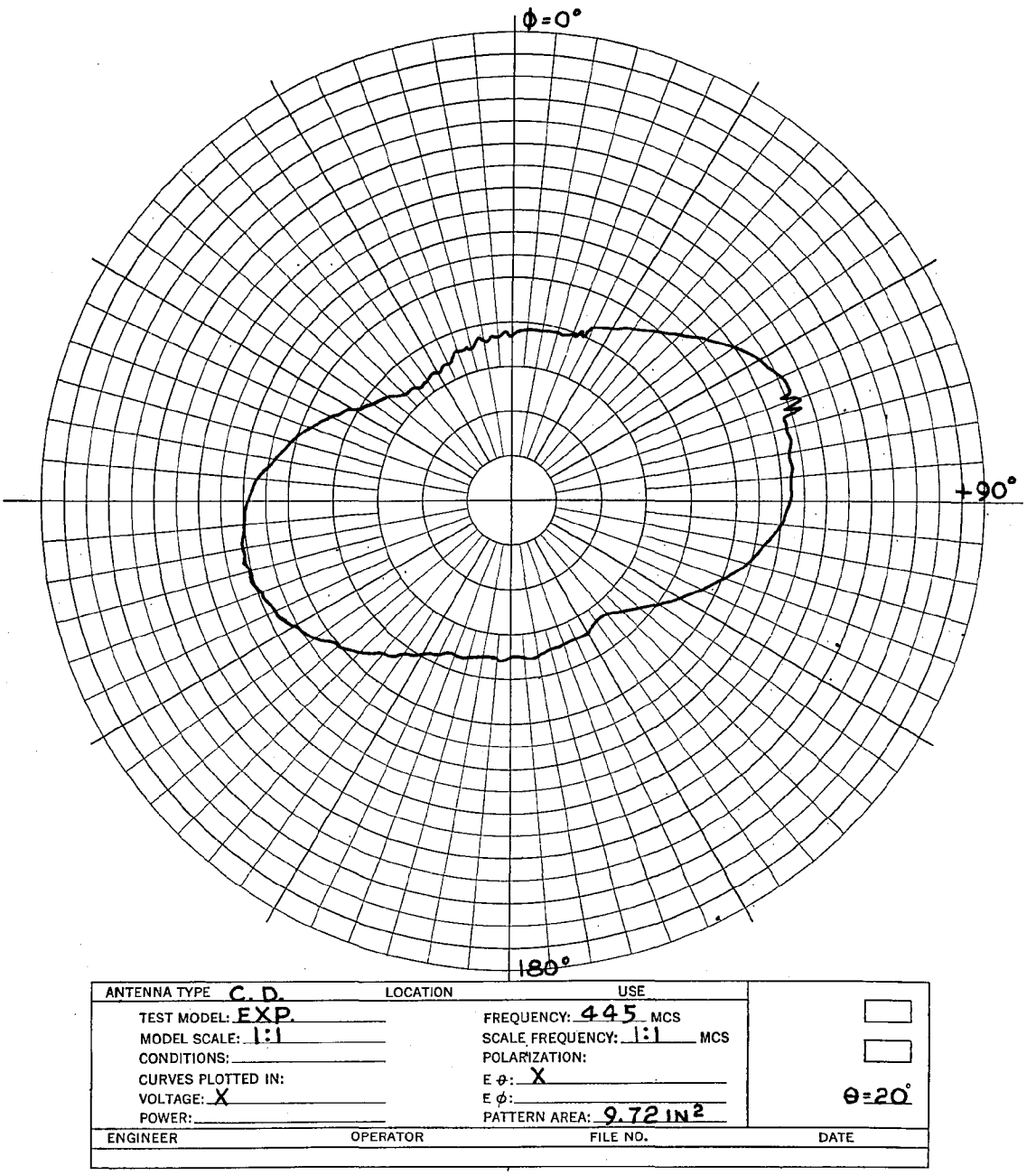

FIGURE 57

EXPERIMENTAL PATTERN FOR TWO DIAMETRICALLY OPPOSED SLOTS OPERATING SIMULTANEOUSLY INPHASE FOR $\theta = 20^{\circ}$

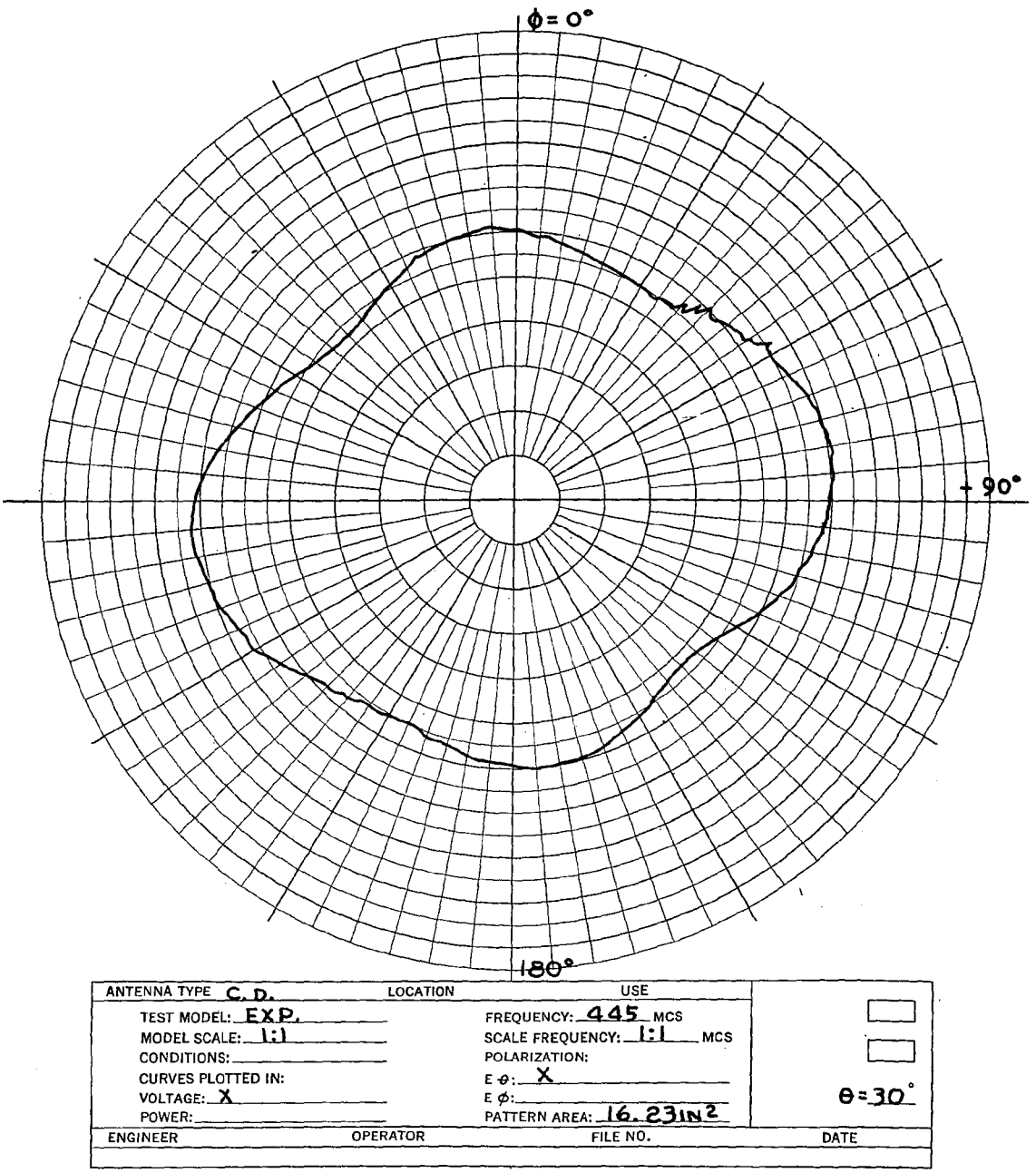

FIGURE 58

EXPERIMENTAL PATTERN FOR TWO DIAMETRICALLY OPPOSED SLOTS OPERATING SIMULTANEOUSLY INPHASE FOR $\theta = 30^{\circ}$

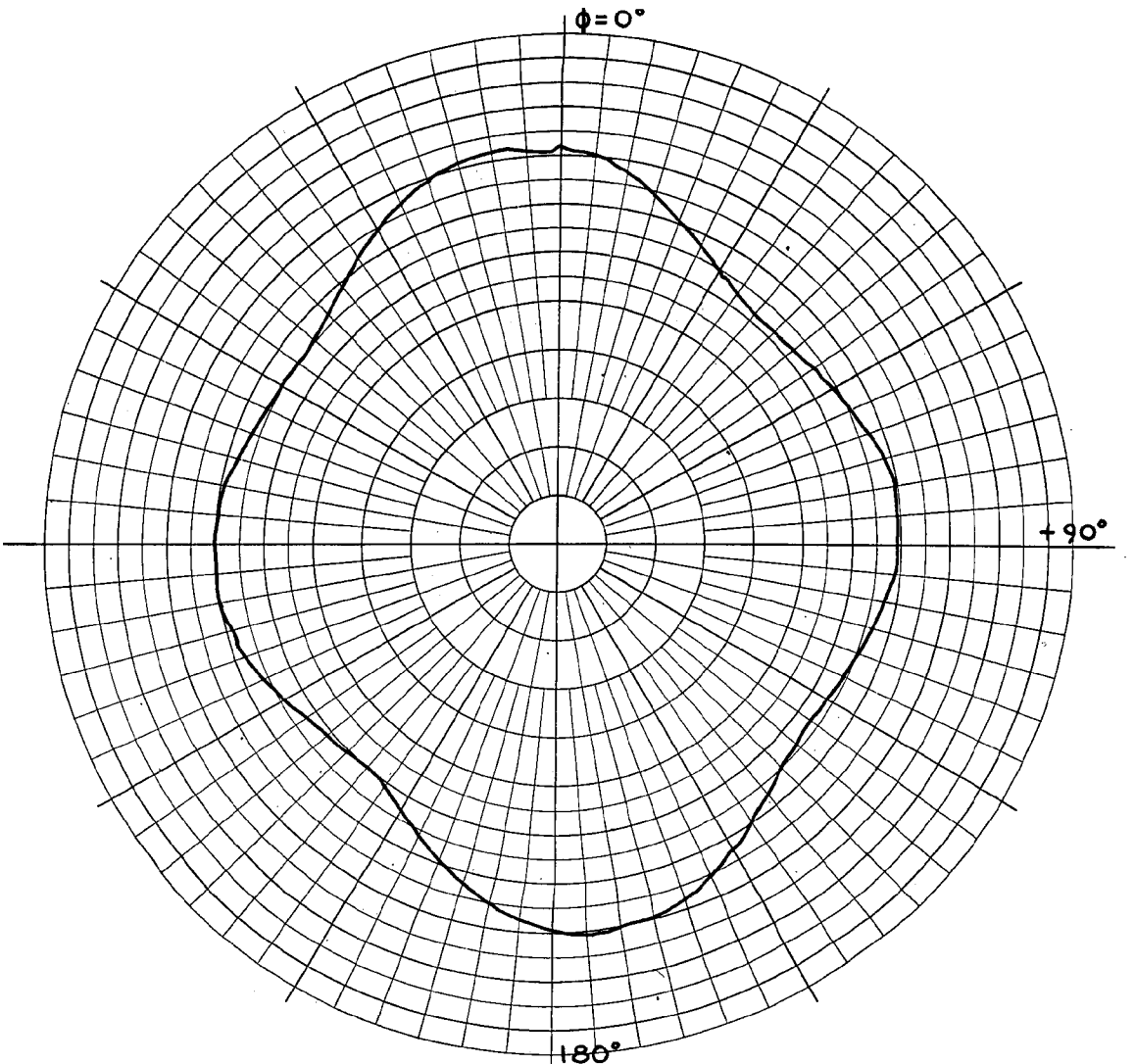

FIGURE 59

EXPERIMENTAL PATTERN FOR TWO DIAMETRICALLY OPPOSED SLOTS OPERATING SIMULTANEOUSLY INPHASE FOR $\theta = 40^{\circ}$

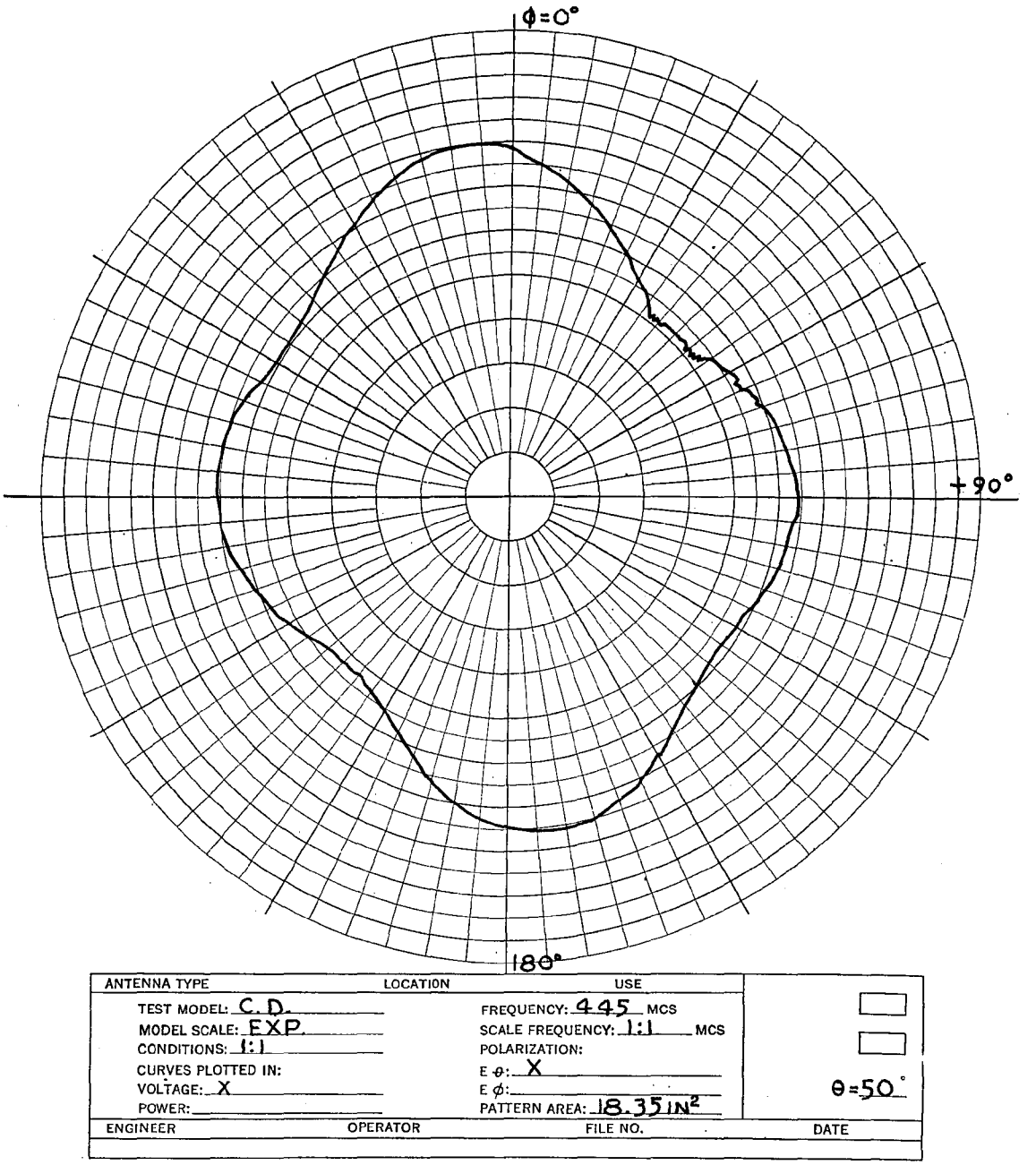

FIGURE 60

EXPERIMENTAL PATTERN FOR TWO DIAMETRICALLY OPPOSED SLOTS OPERATING SIMULTANEOUSLY INPHASE FOR $\theta = 50^{\circ}$

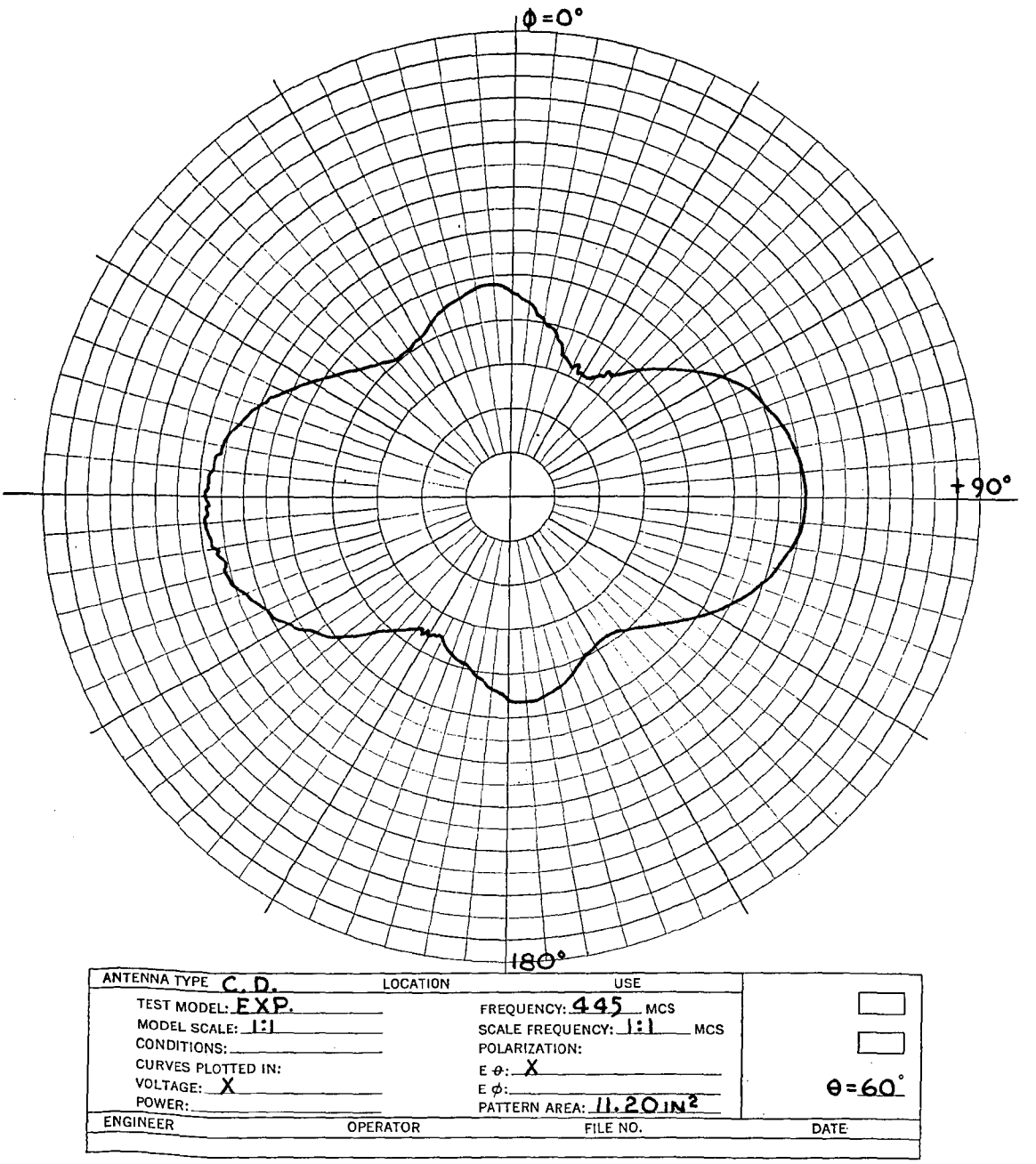

FIGURE 61

EXPERIMENTAL PATTERN FOR TWO DIAMETRICALLY OPPOSED SLOTS OPERATING SIMULTANEOUSLY INPHASE FOR $\theta = 60^{\circ}$

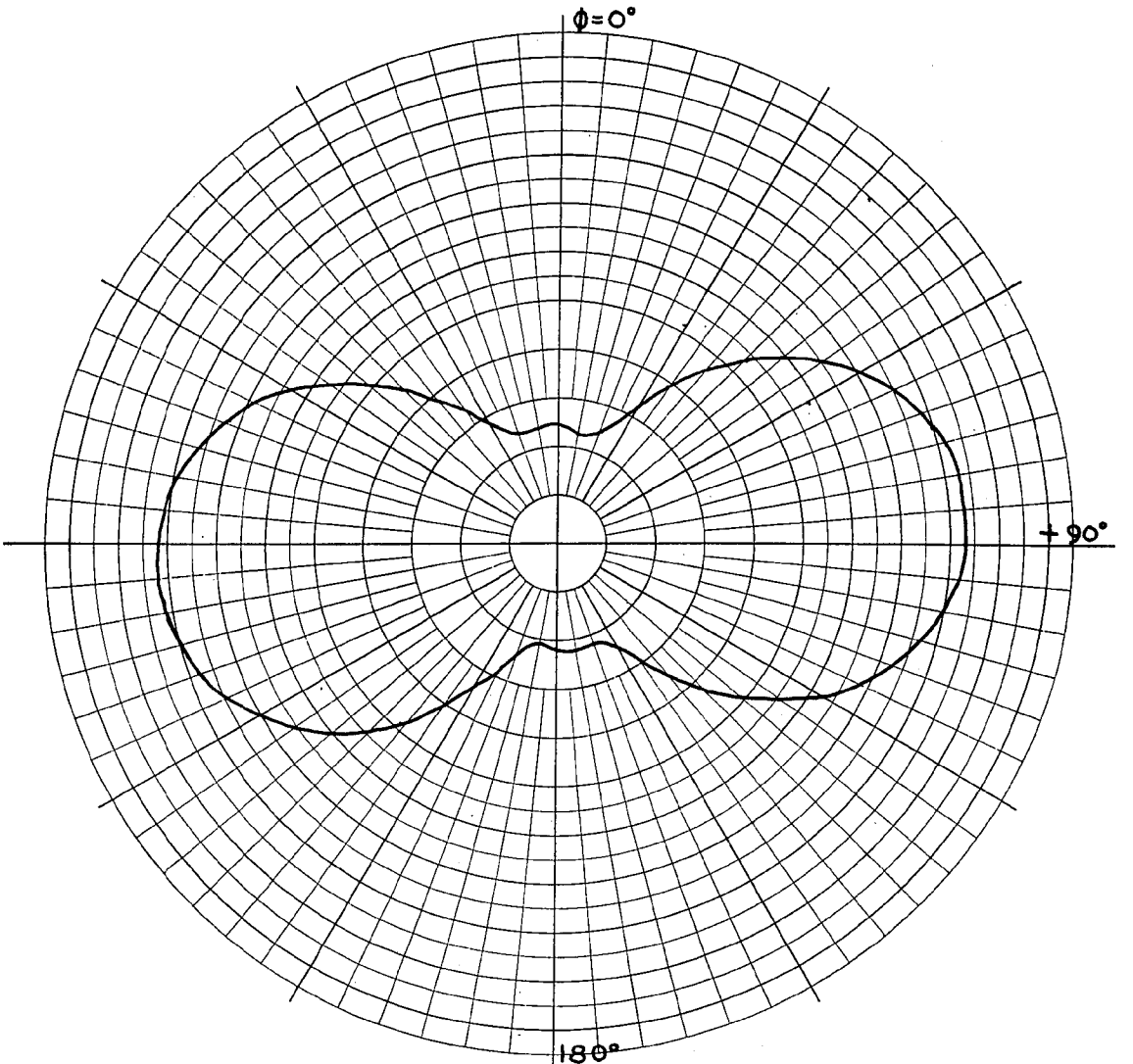

ANTENNA TYPE C.D	LOCATION	USE	
TEST MODEL: EXP.		FREQUENCY: 445 MCS	
MODEL SCALE: 1:1		SCALE FREQUENCY: 1:1 MCS	
CONDITIONS:		POLARIZATION:	
CURVES PLOTTED IN:		E θ: X	
VOLTAGE: X		E φ:	θ=70°
POWER:		PATTERN AREA: 13.37 IN²	
ENGINEER	OPERATOR	FILE NO.	DATE

FIGURE 62

EXPERIMENTAL PATTERN FOR TWO DIAMETRICALLY OPPOSED SLOTS OPERATING SIMULTANEOUSLY INPHASE FOR $\theta = 70^{\circ}$

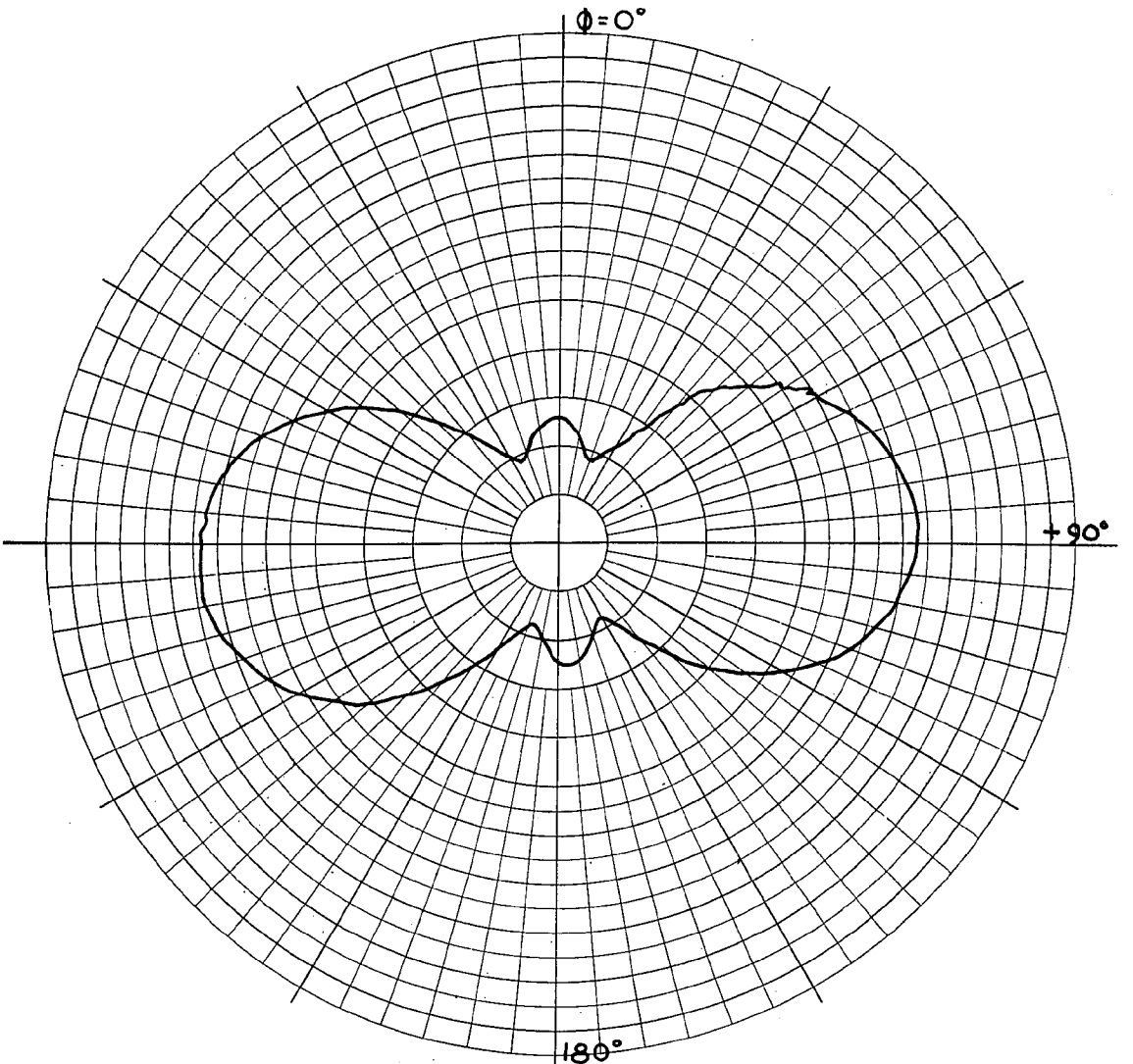

FIGURE 63

EXPERIMENTAL PATTERN FOR TWO DIAMETRICALLY OPPOSED SLOTS OPERATING SIMULTANEOUSLY INPHASE FOR $\theta = 80^{\circ}$

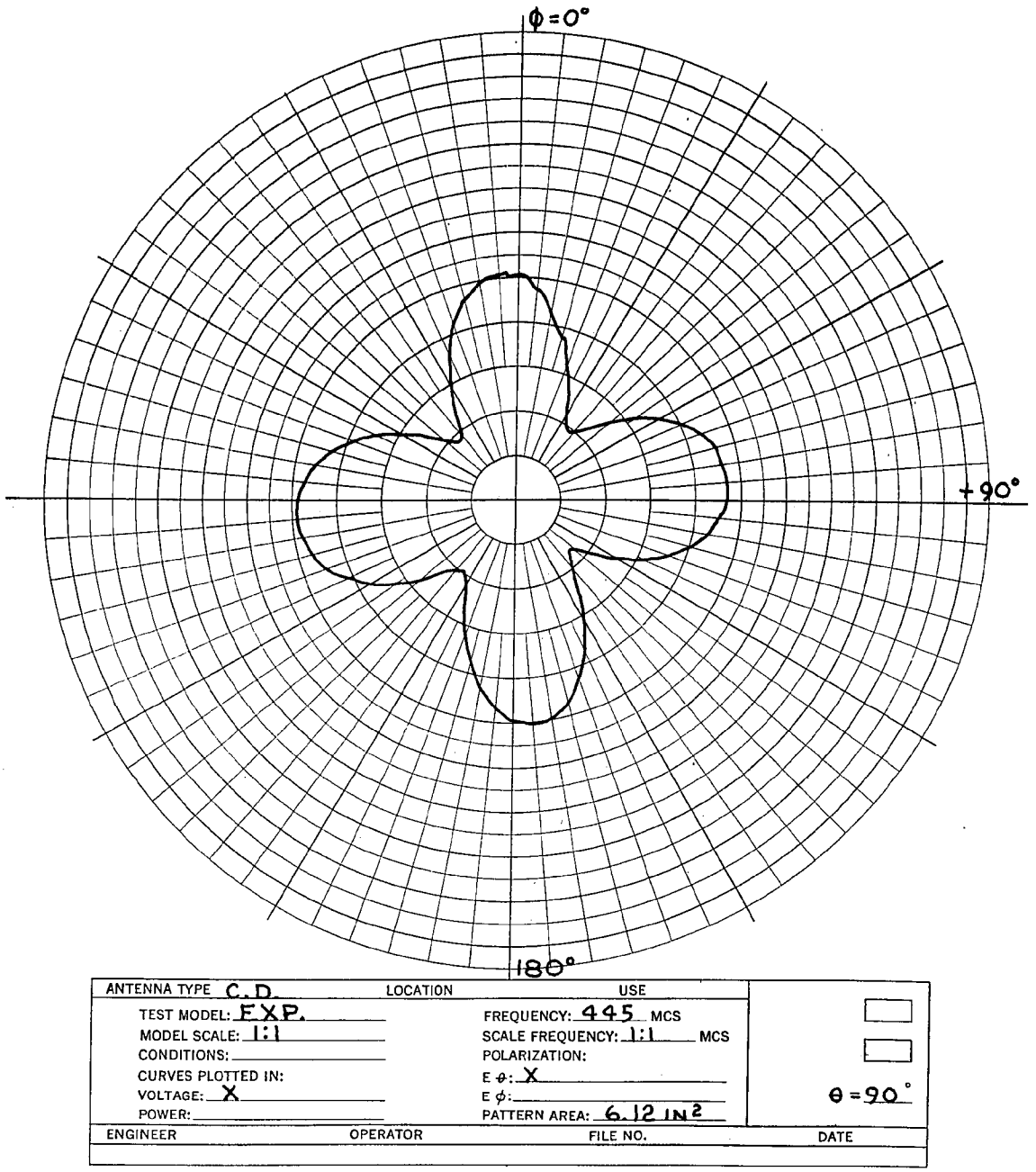

FIGURE 64

EXPERIMENTAL PATTERN FOR TWO DIAMETRICALLY OPPOSED SLOTS OPERATING SIMULTANEOUSLY INPHASE FOR $\theta = 90^{\circ}$

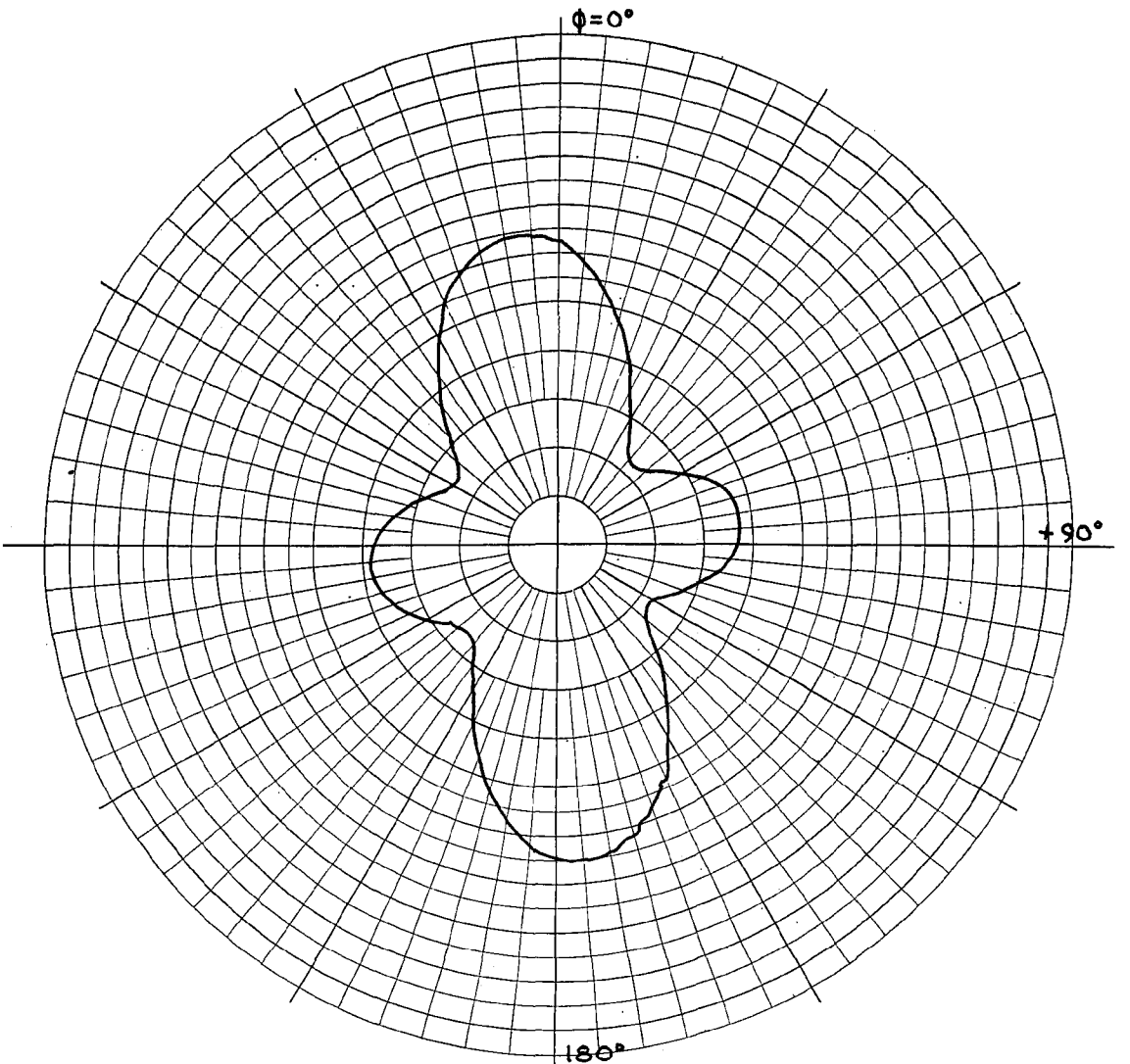

FIGURE 65

EXPERIMENTAL PATTERN FOR TWO DIAMETRICALLY OPPOSED SLOTS OPERATING SIMULTANEOUSLY INPHASE FOR $\theta = 100^{o}$

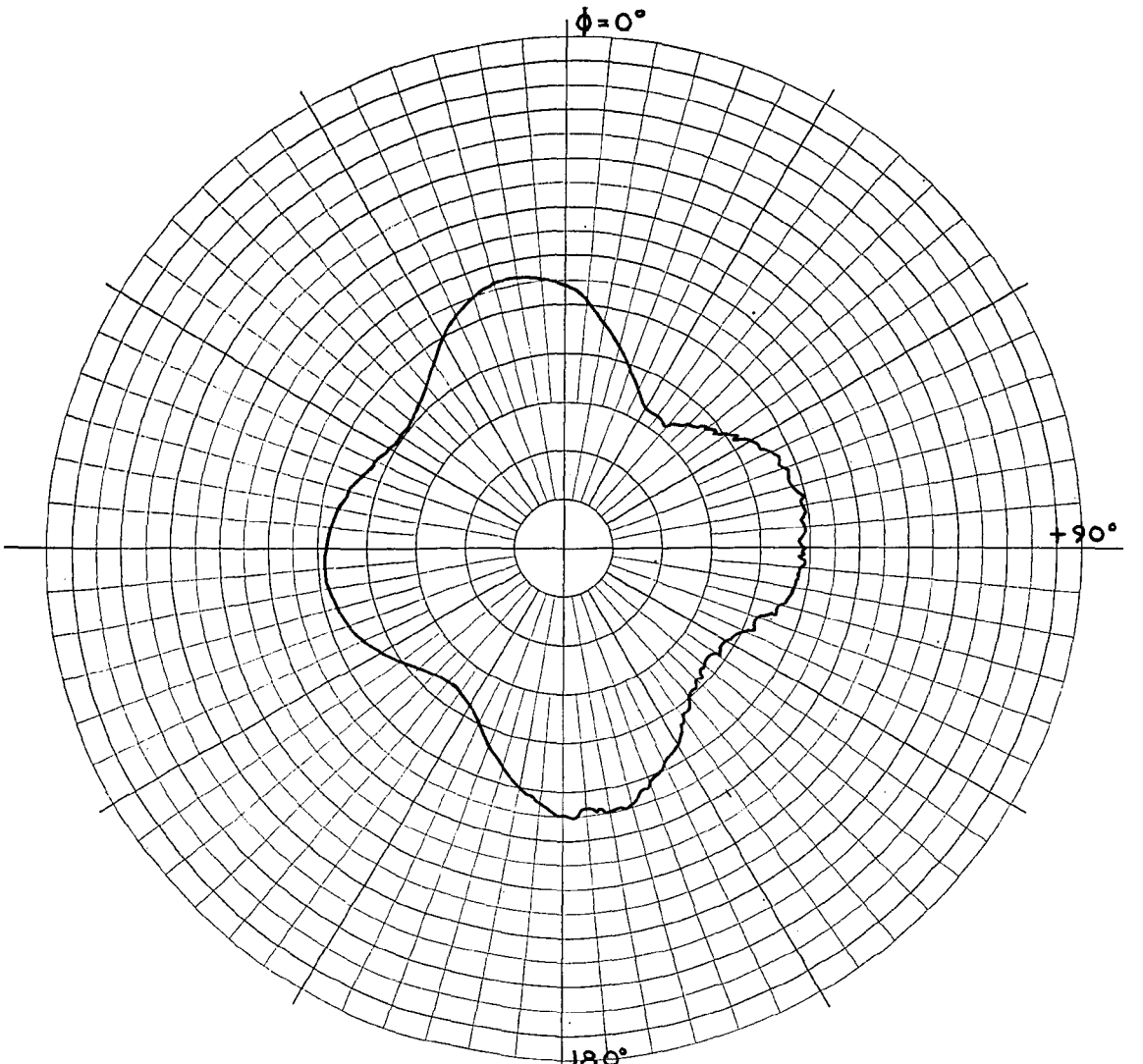

FIGURE 66

EXPERIMENTAL PATTERN FOR TWO DIAMETRICALLY OPPOSED SLOTS OPERATING SIMULTANEOUSLY INPHASE FOR $\theta = 110^{\circ}$

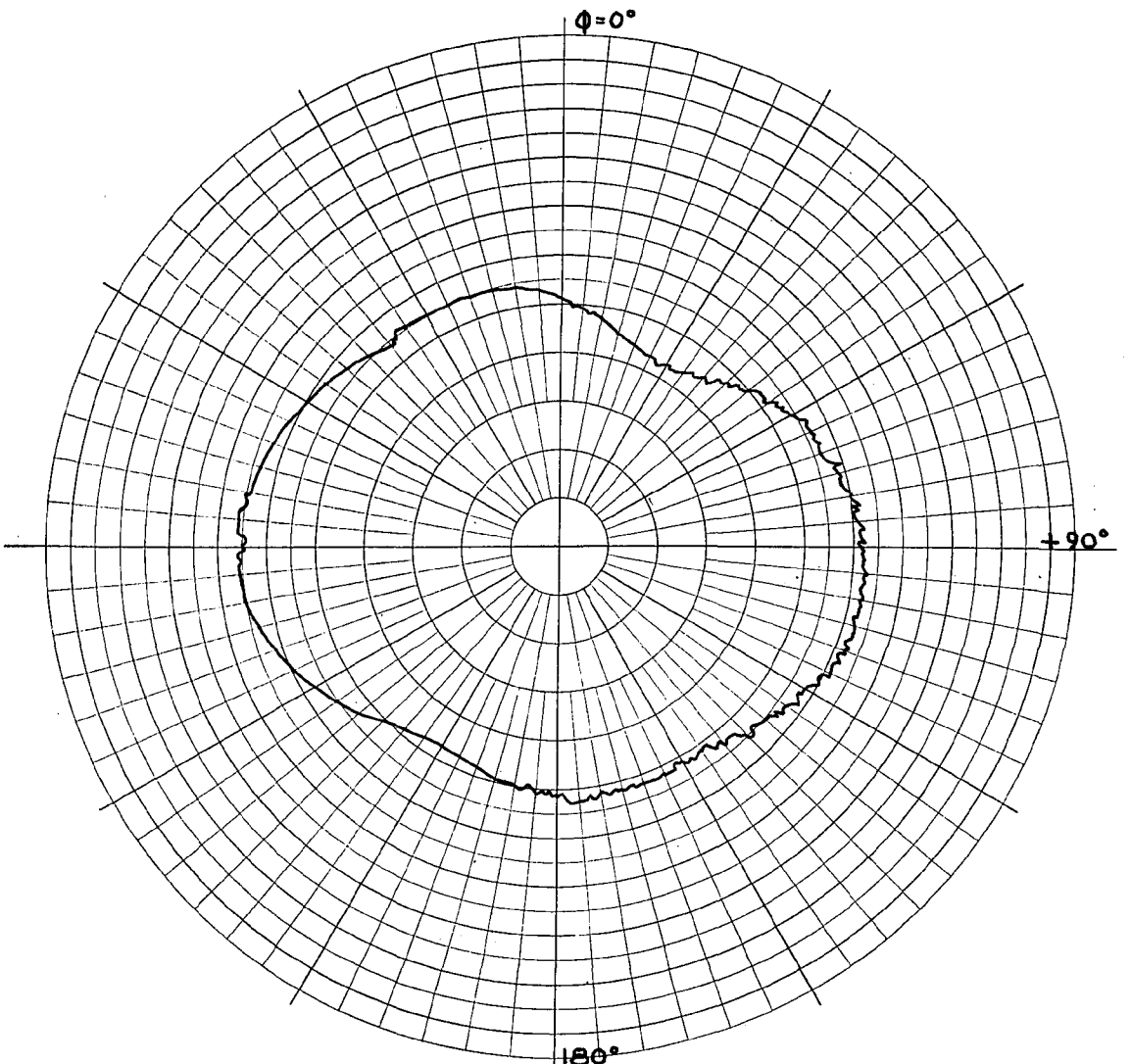

FIGURE 67

EXPERIMENTAL PATTERN FOR TWO DIAMETRICALLY OPPOSED SLOTS OPERATING SIMULTANEOUSLY INPHASE FOR $\theta = 120^{\circ}$

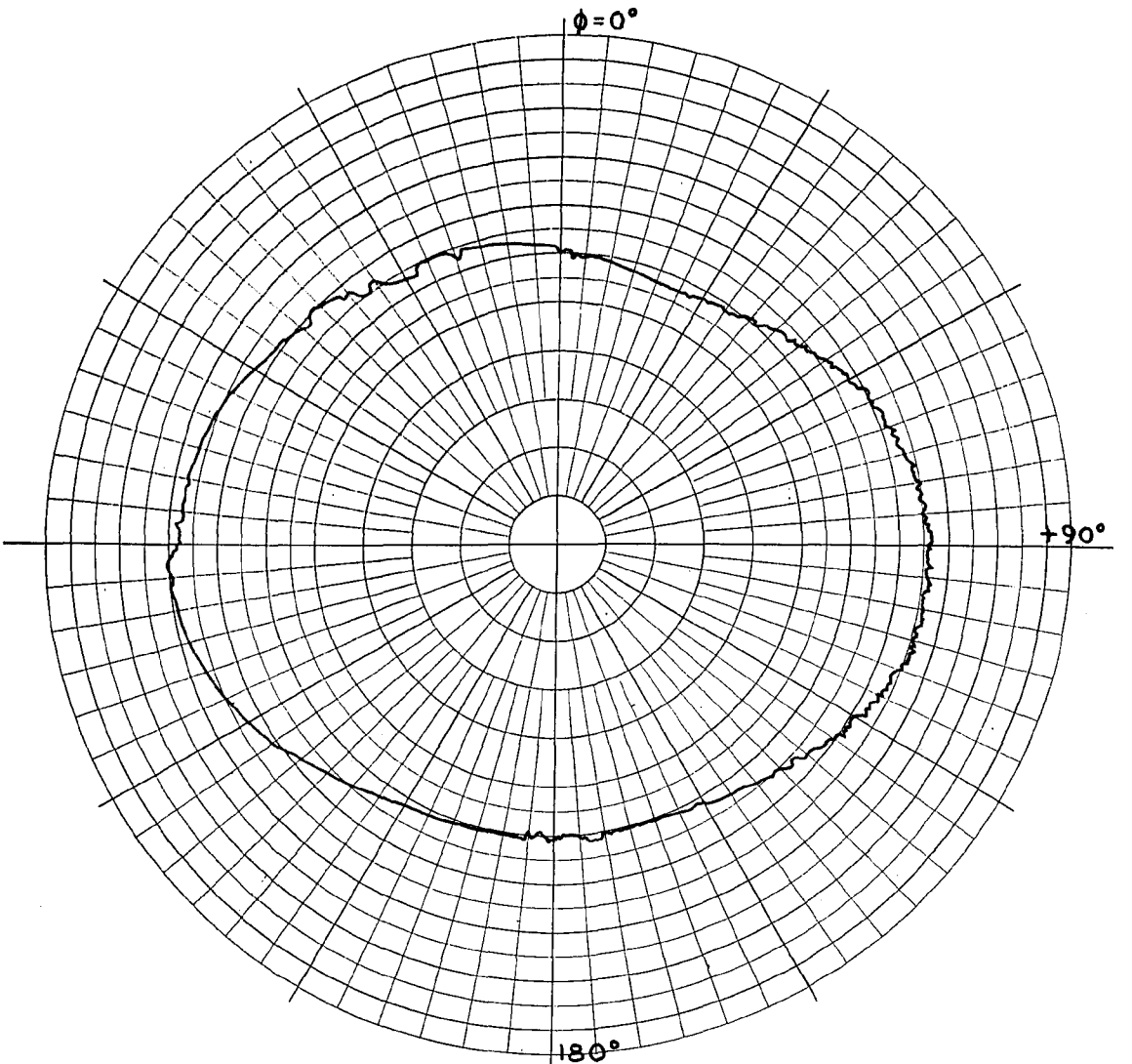

ANTENNA TYPE C.D.	LOCATION	USE	
TEST MODEL: EXP.		FREQUENCY: 445 MCS	
MODEL SCALE: 1:1		SCALE FREQUENCY: 1:1 MCS	
CONDITIONS:		POLARIZATION:	
CURVES PLOTTED IN:		Eϕ: X	
VOLTAGE: X		Eϕ:	θ=130°
POWER:		PATTERN AREA: 20.24 IN²	
ENGINEER	OPERATOR	FILE NO.	DATE

FIGURE 68

EXPERIMENTAL PATTERN FOR TWO DIAMETRICALLY OPPOSED SLOTS OPERATING SIMULTANEOUSLY INPHASE FOR $\theta = 130^{\circ}$

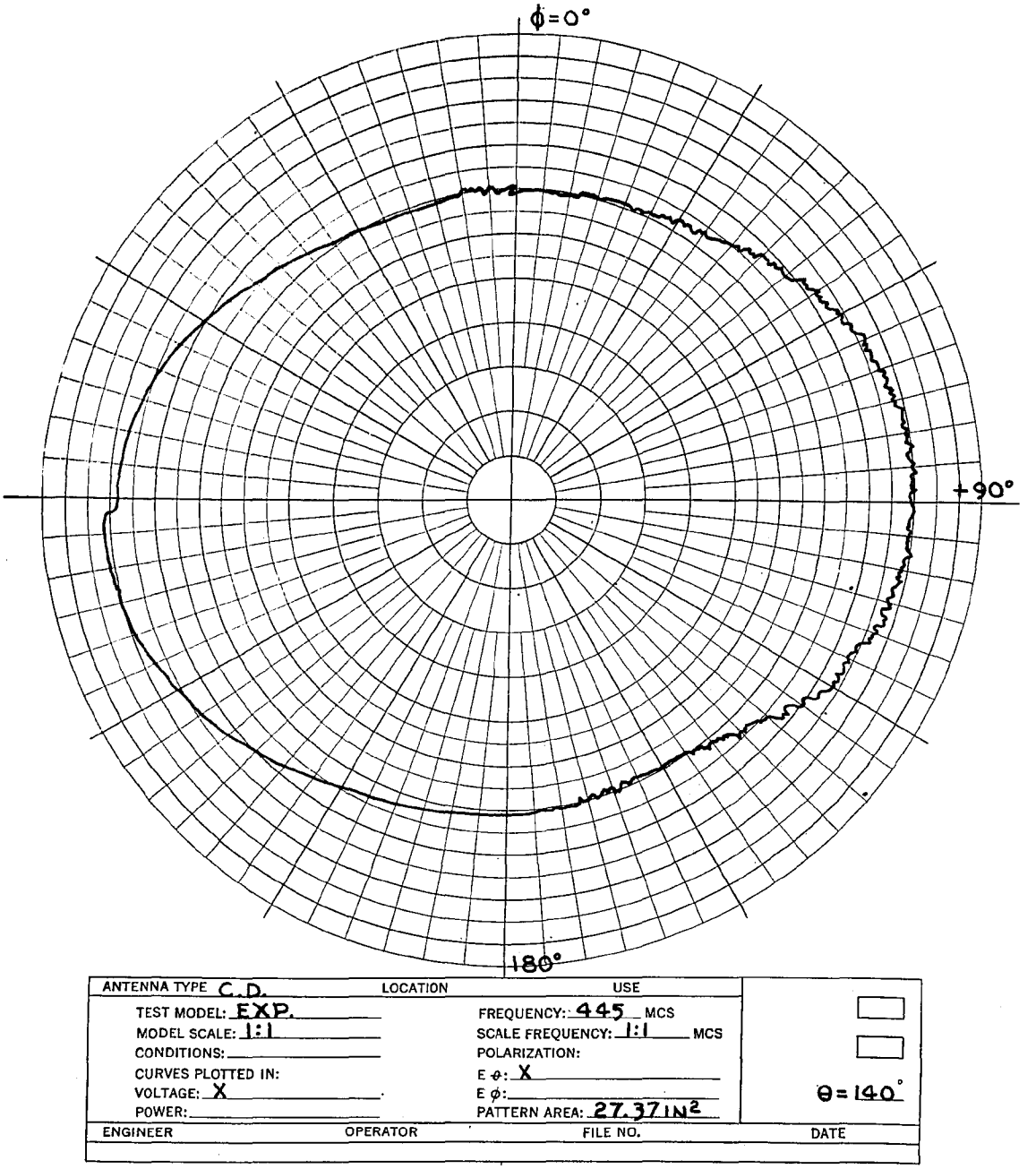

FIGURE 69

EXPERIMENTAL PATTERN FOR TWO DIAMETRICALLY OPPOSED SLOTS OPERATING SIMULTANEOUSLY INPHASE FOR $\theta = 140^{\circ}$

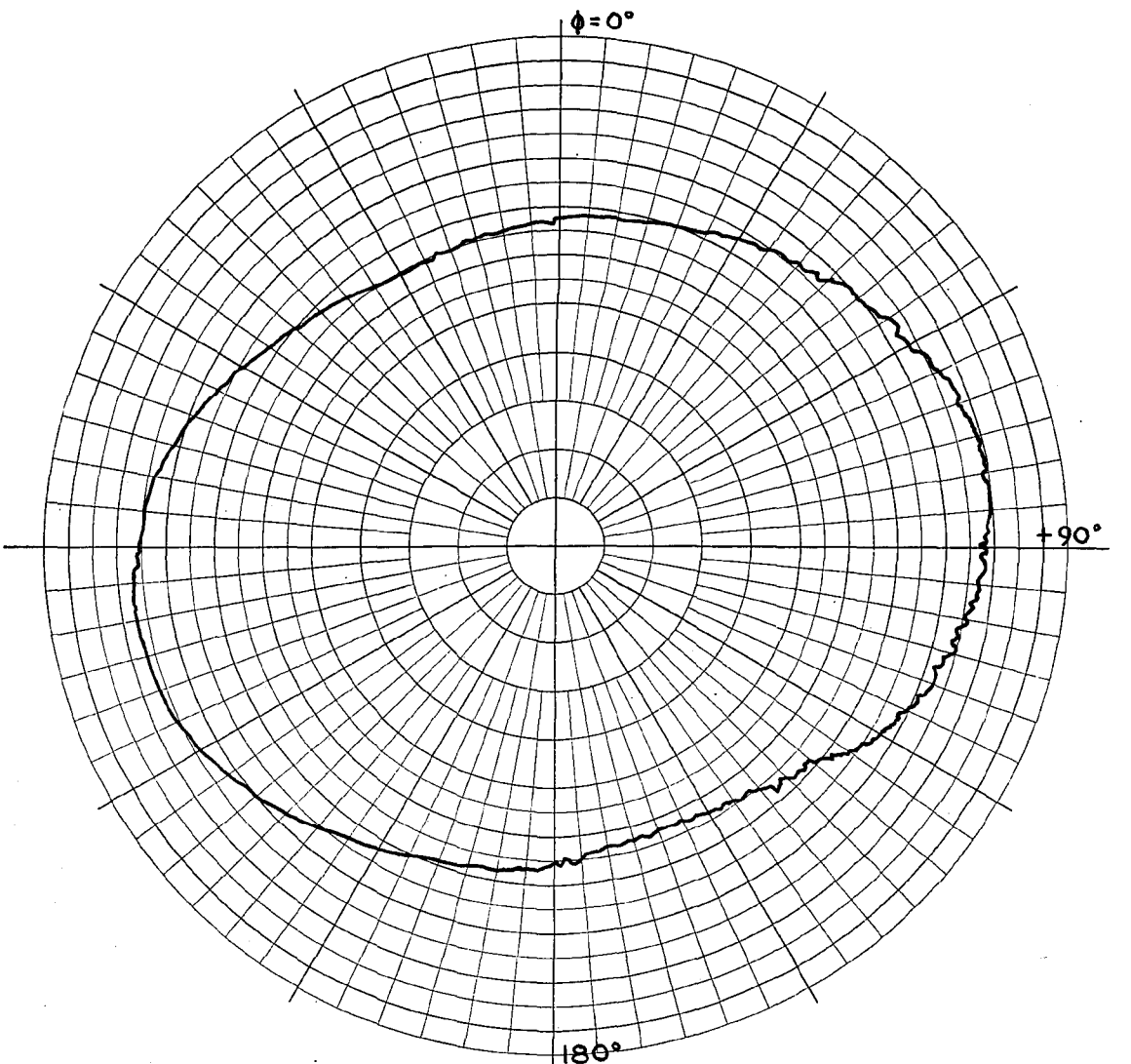

ANTENNA TYPE C.D.	LOCATION	USE	
TEST MODEL: EXP.		FREQUENCY: 445 MCS	
MODEL SCALE: 1:1		SCALE FREQUENCY: 1:1 MCS	
CONDITIONS:		POLARIZATION:	
CURVES PLOTTED IN:		Eϕ: X	
VOLTAGE: X		Eϕ:	θ = 150°
POWER:		PATTERN AREA: 25.17 IN²	
ENGINEER	OPERATOR	FILE NO.	DATE

FIGURE 70

EXPERIMENTAL PATTERN FOR TWO DIAMETRICALLY OPPOSED SLOTS OPERATING SIMULTANEOUSLY INPHASE FOR $\theta = 150^{\circ}$

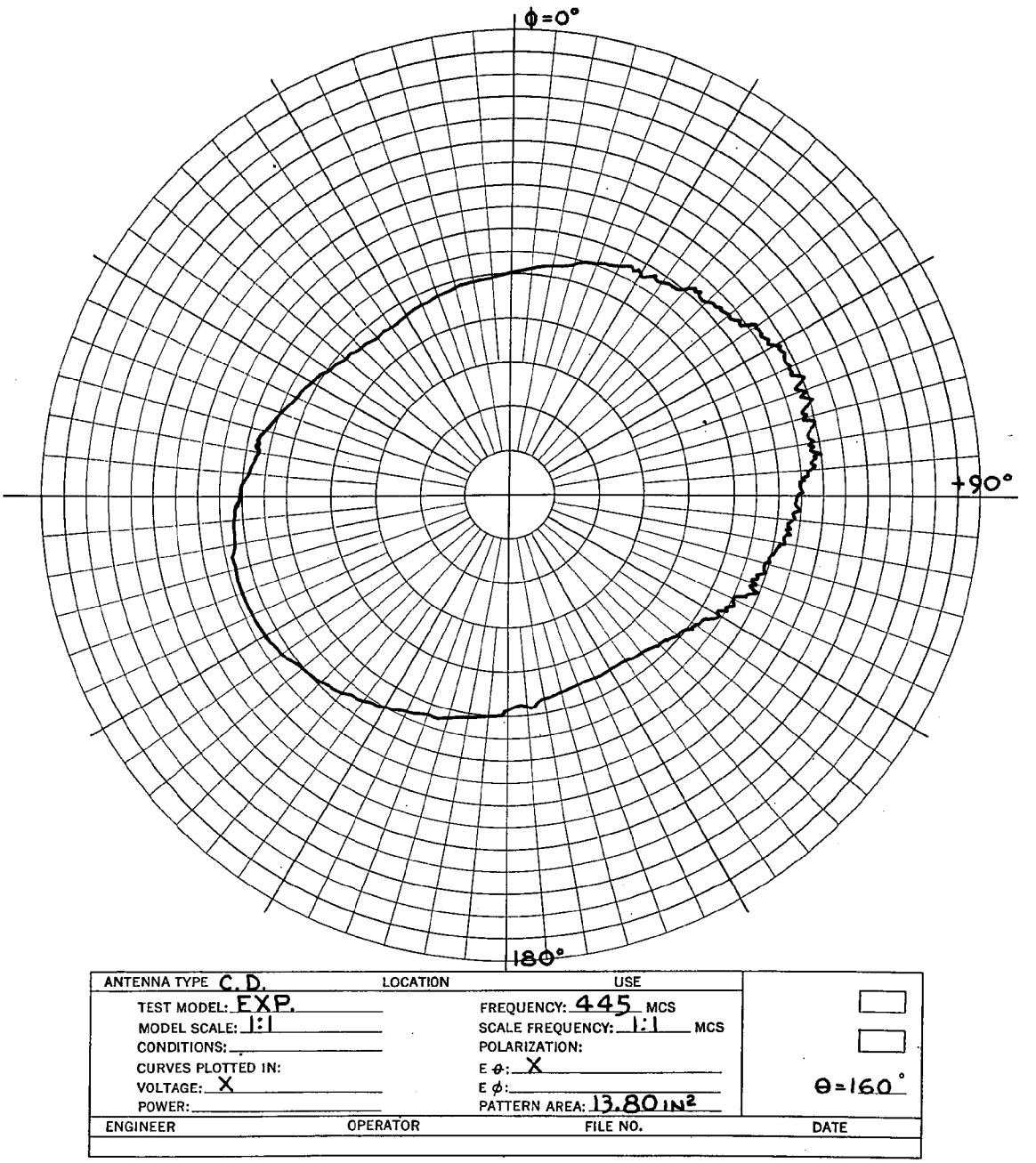

FIGURE 71

EXPERIMENTAL PATTERN FOR TWO DIAMETRICALLY OPPOSED SLOTS OPERATING SIMULTANEOUSLY INPHASE FOR $\theta = 160^{\circ}$

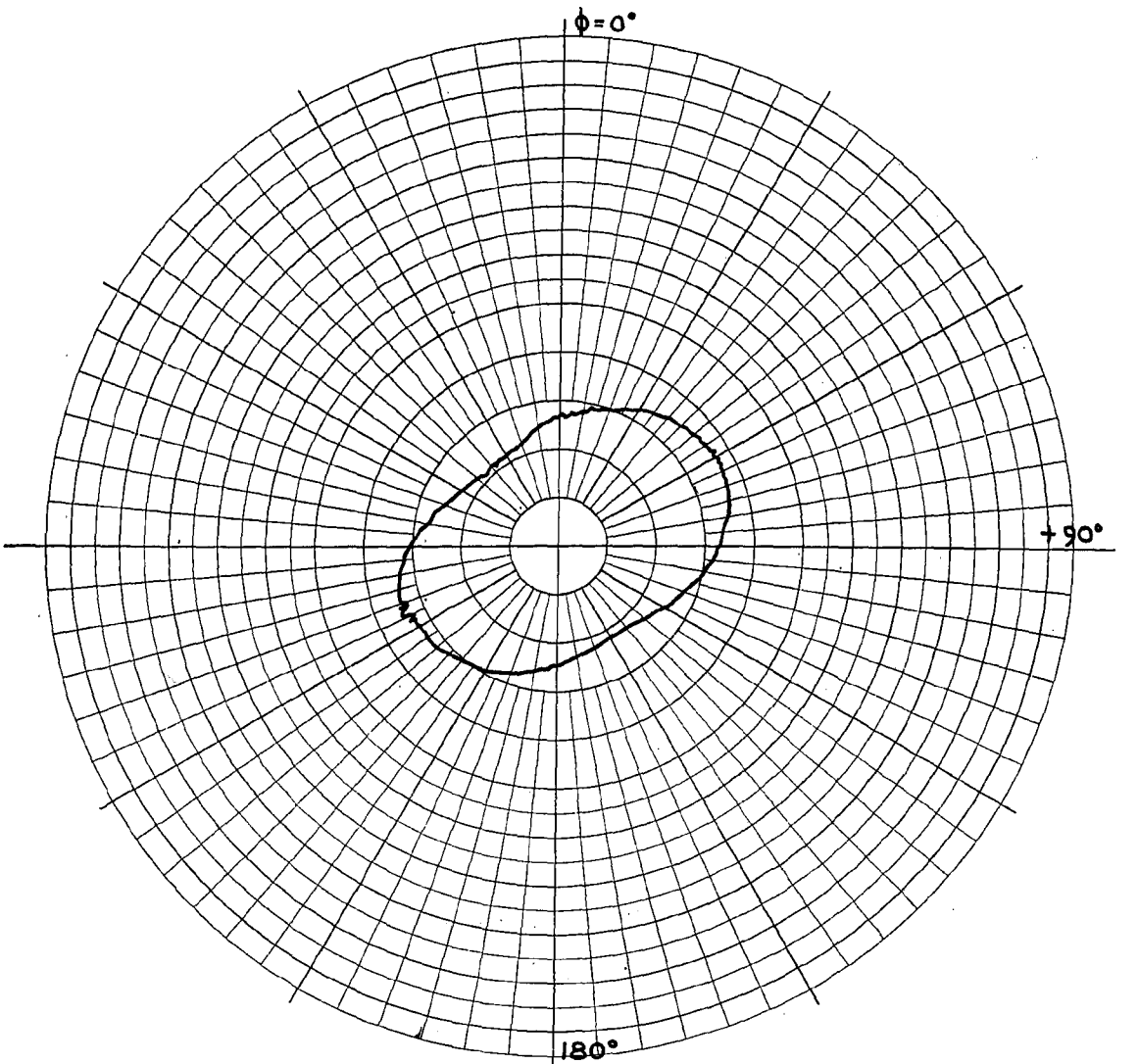

FIGURE 72

EXPERIMENTAL PATTERN FOR TWO DIAMETRICALLY OPPOSED SLOTS OPERATING SIMULTANEOUSLY INPHASE FOR $\theta = 170^{\circ}$

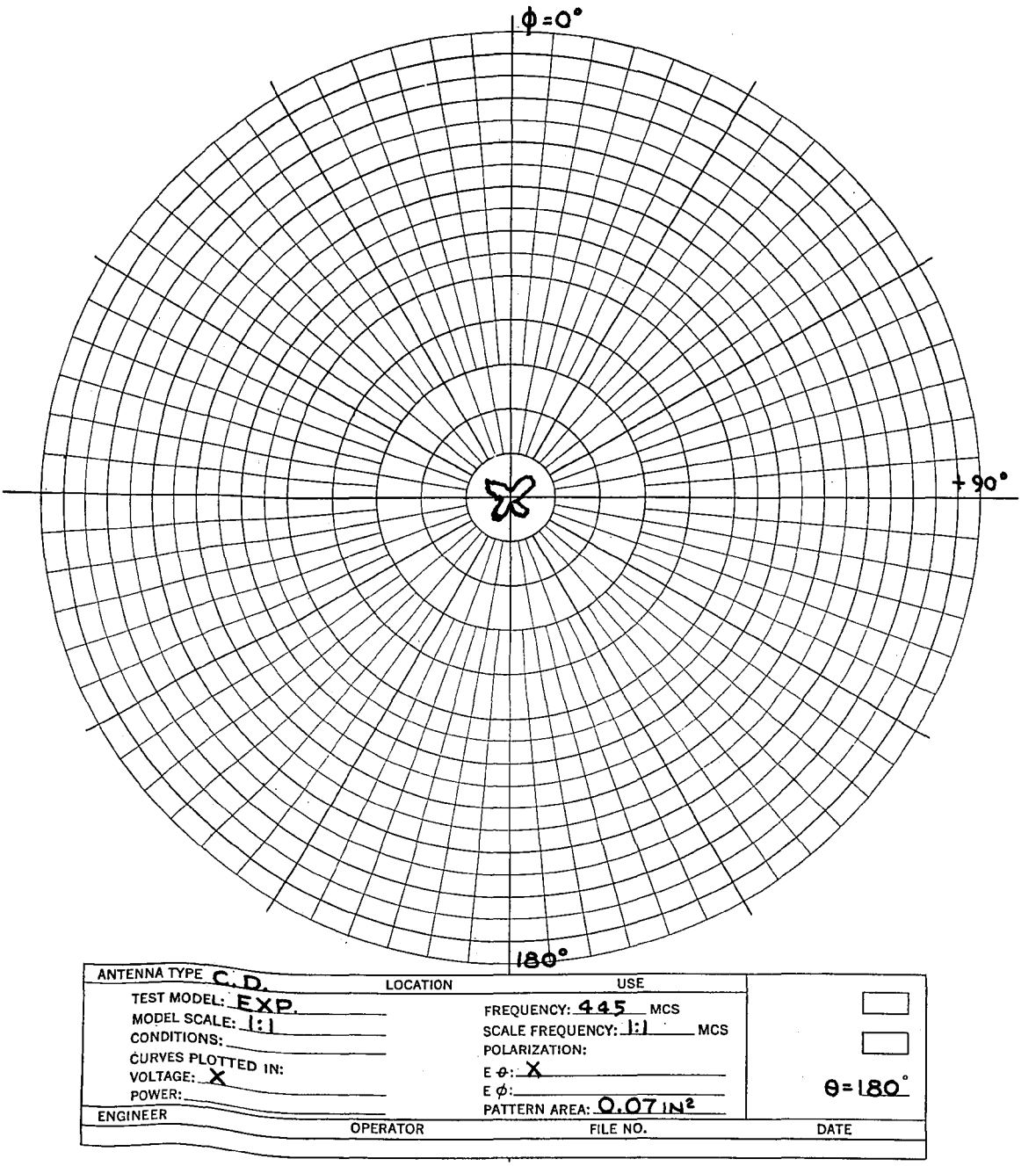

FIGURE 73

EXPERIMENTAL PATTERN FOR TWO DIAMETRICALLY OPPOSED SLOTS OPERATING SIMULTANEOUSLY INPHASE FOR $\theta = 180^{\circ}$

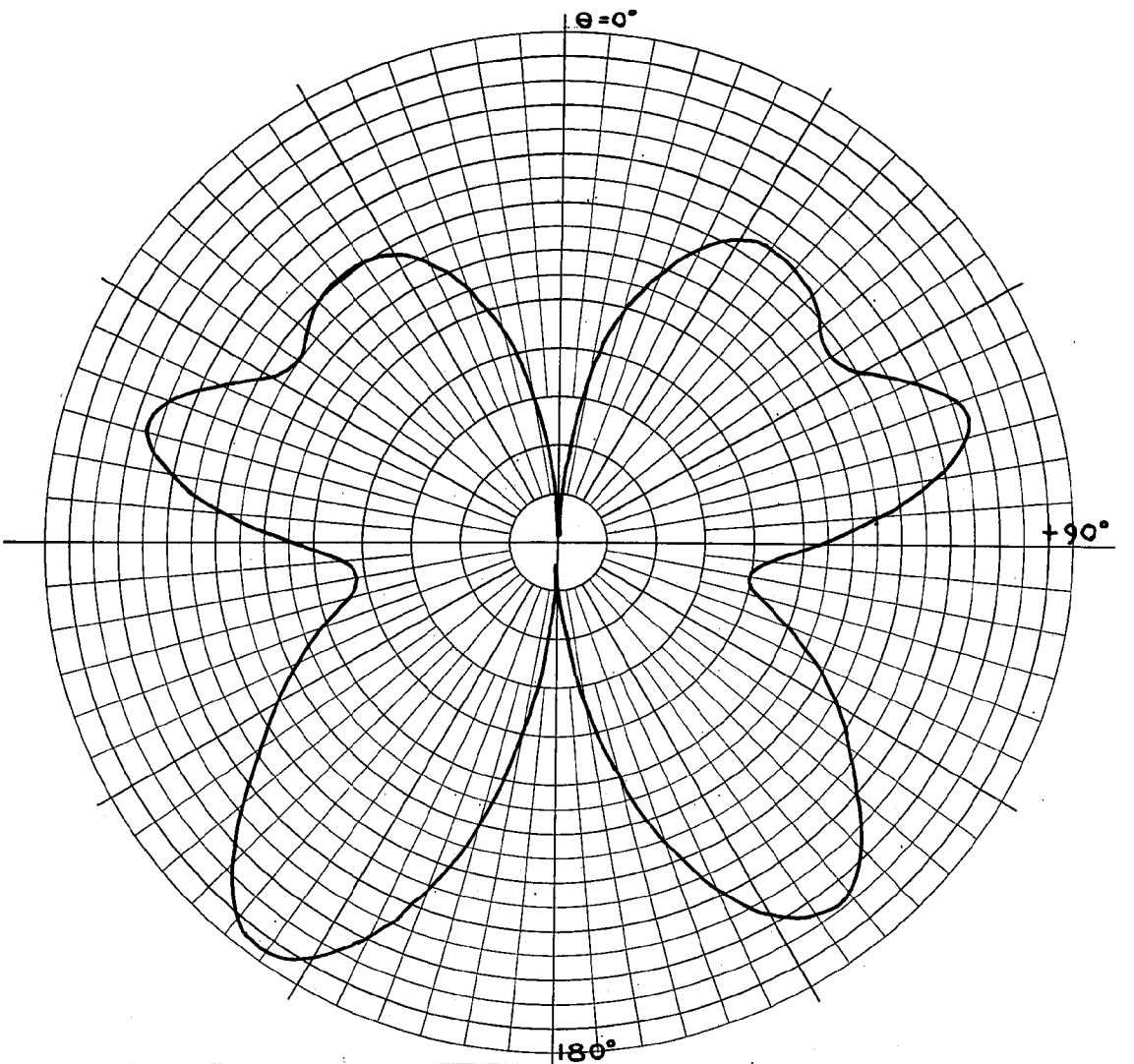

FIGURE 74

EXPERIMENTAL PATTERN FOR TWO DIAMETRICALLY OPPOSED SLOTS OPERATING SIMULTANEOUSLY INPHASE FOR $\varphi = 90^{\circ}$

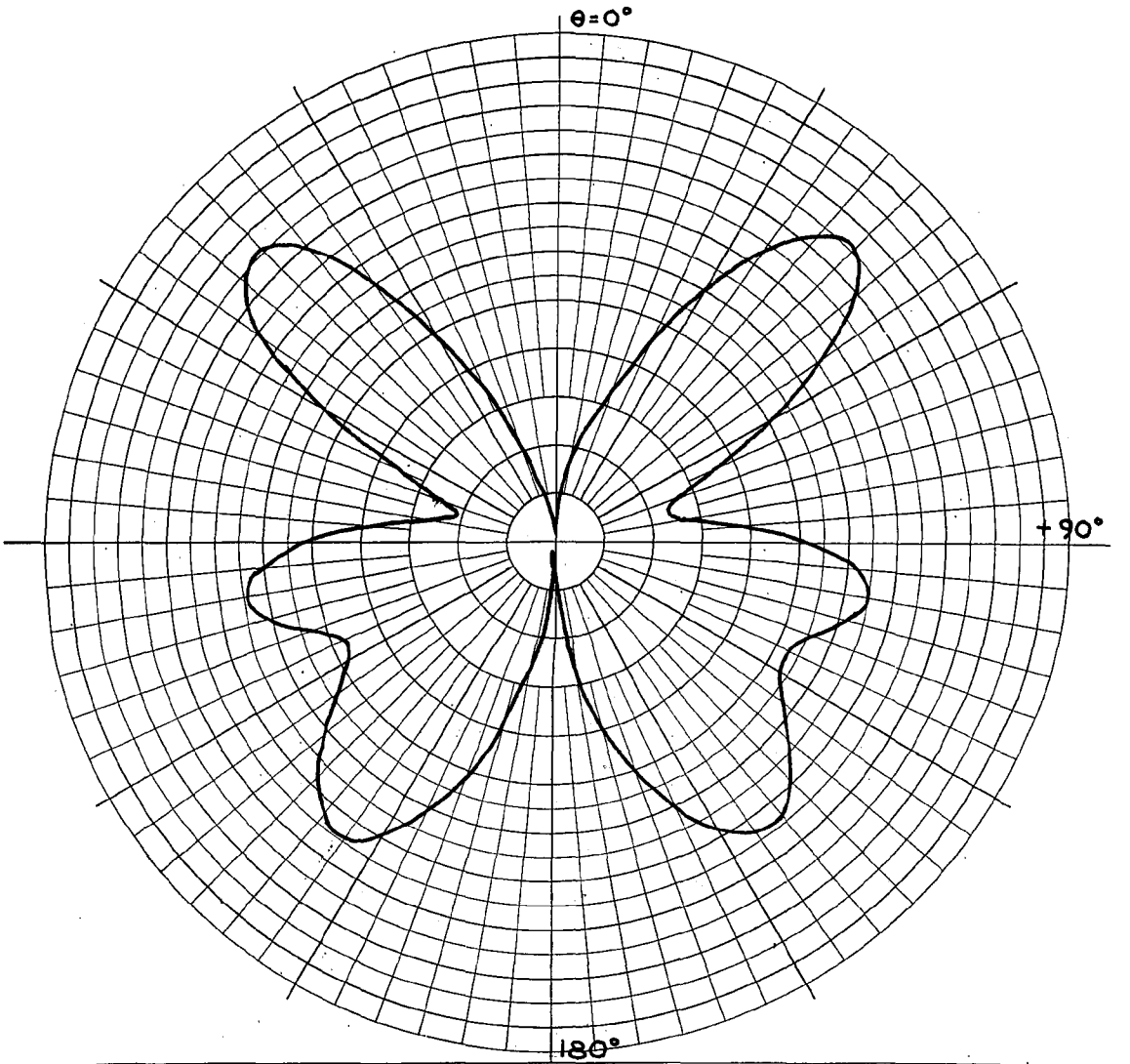

FIGURE 75

EXPERIMENTAL PATTERN FOR TWO DIAMETRICALLY OPPOSED SLOTS OPERATING SIMULTANEOUSLY INPHASE FOR $\varphi = 180^{\circ}$

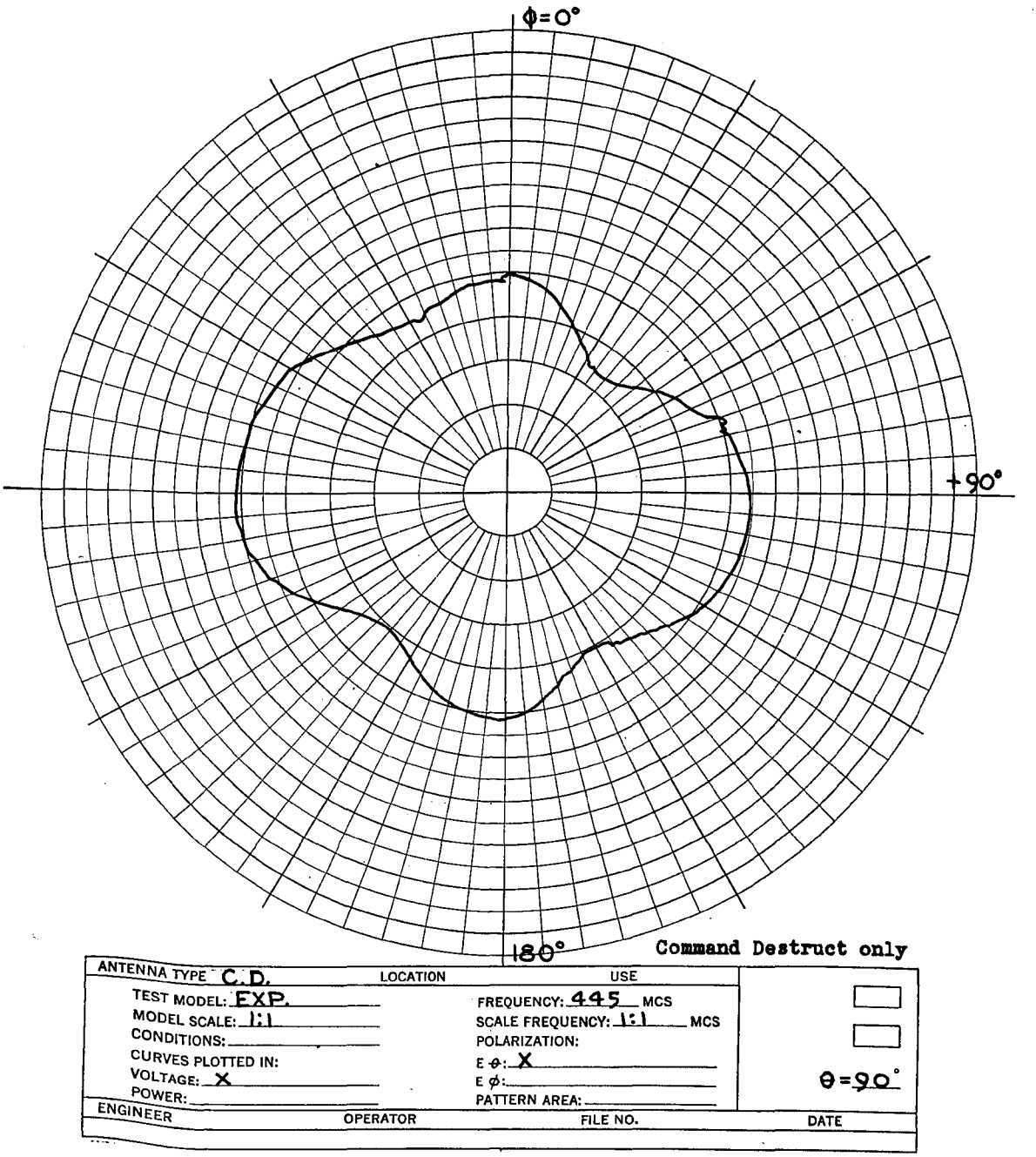

FIGURE 76

INTERFERENCE TEST PATTERN FOR TWO DIAMETRICALLY OPPOSED SLOTS OPERATING SIMULTANEOUSLY INPHASE FOR $\theta = 90^{\circ}$

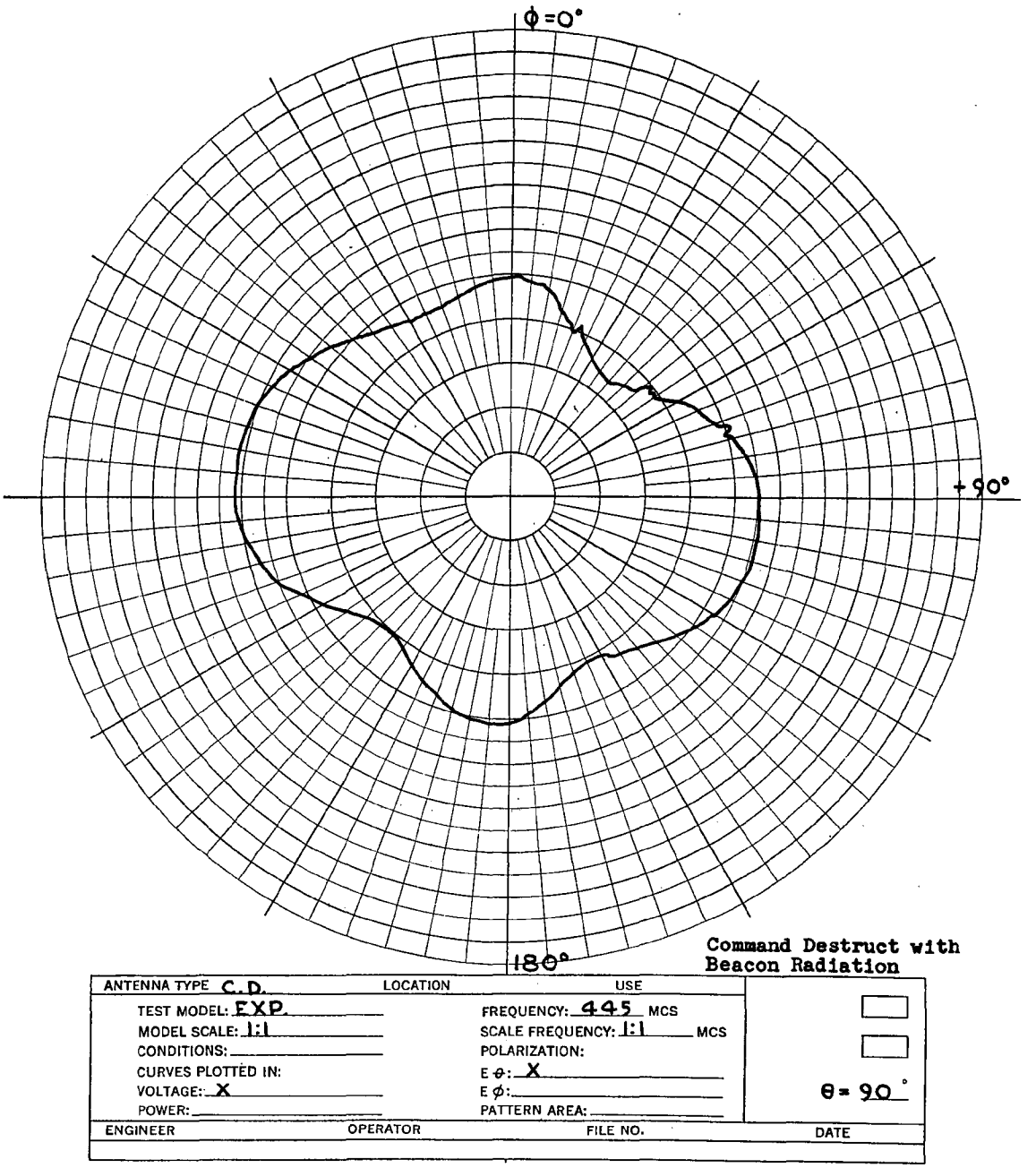

FIGURE 77

INTERFERENCE TEST PATTERN FOR TWO DIAMETRICALLY OPPOSED SLOTS OPERATING SIMULTANEOUSLY INPHASE FOR $\theta = 90^{\circ}$

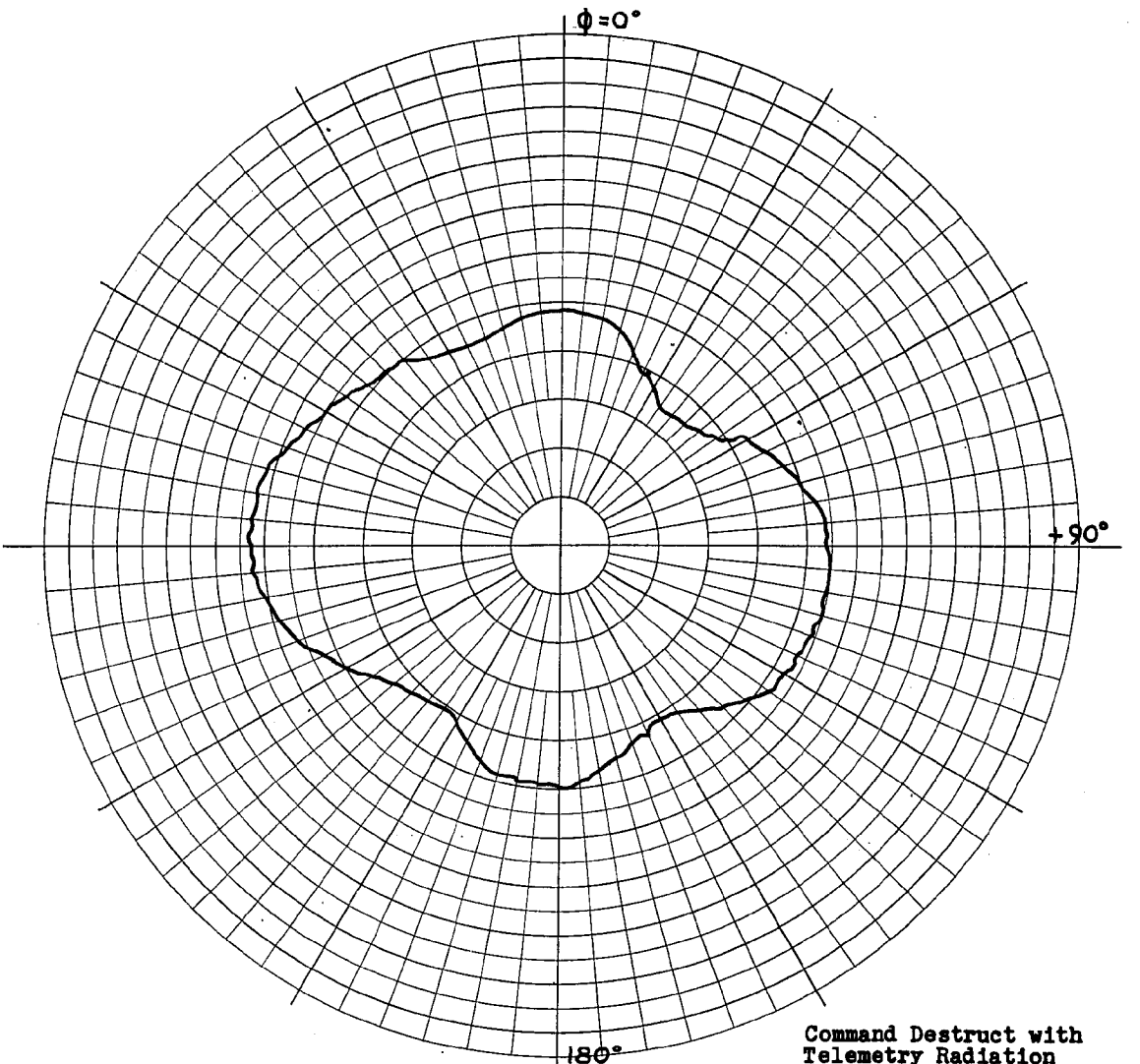

FIGURE 78

INTERFERENCE TEST PATTERN FOR TWO DIAMETRICALLY OPPOSED SLOTS OPERATING SIMULTANEOUSLY INPHASE FOR $\theta = 90^{\circ}$

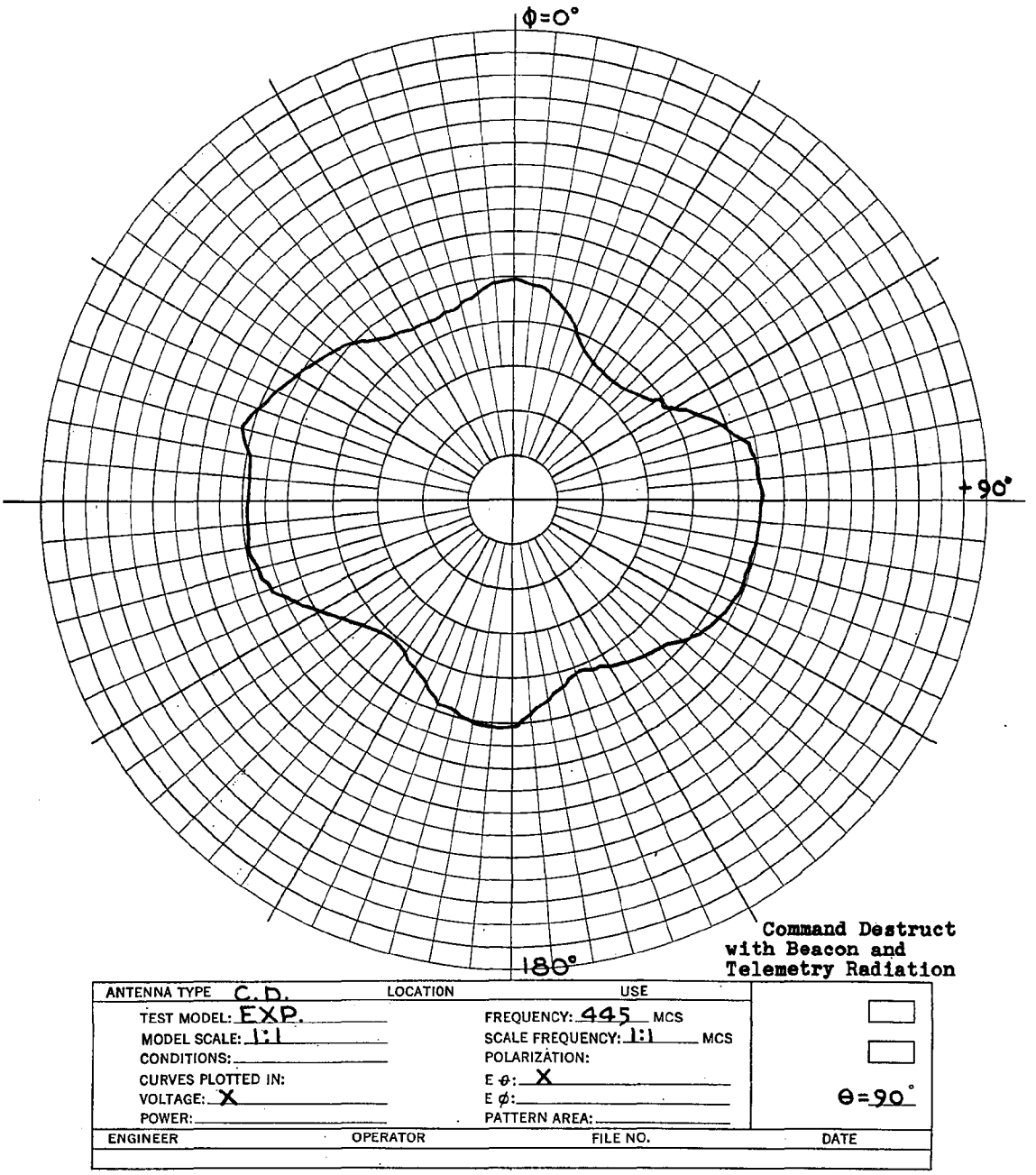

FIGURE 79

INTERFERENCE TEST PATTERN FOR TWO DIAMETRICALLY OPPOSED SLOTS OPERATING SIMULTANEOUSLY INPHASE FOR $\theta = 90^{\circ}$

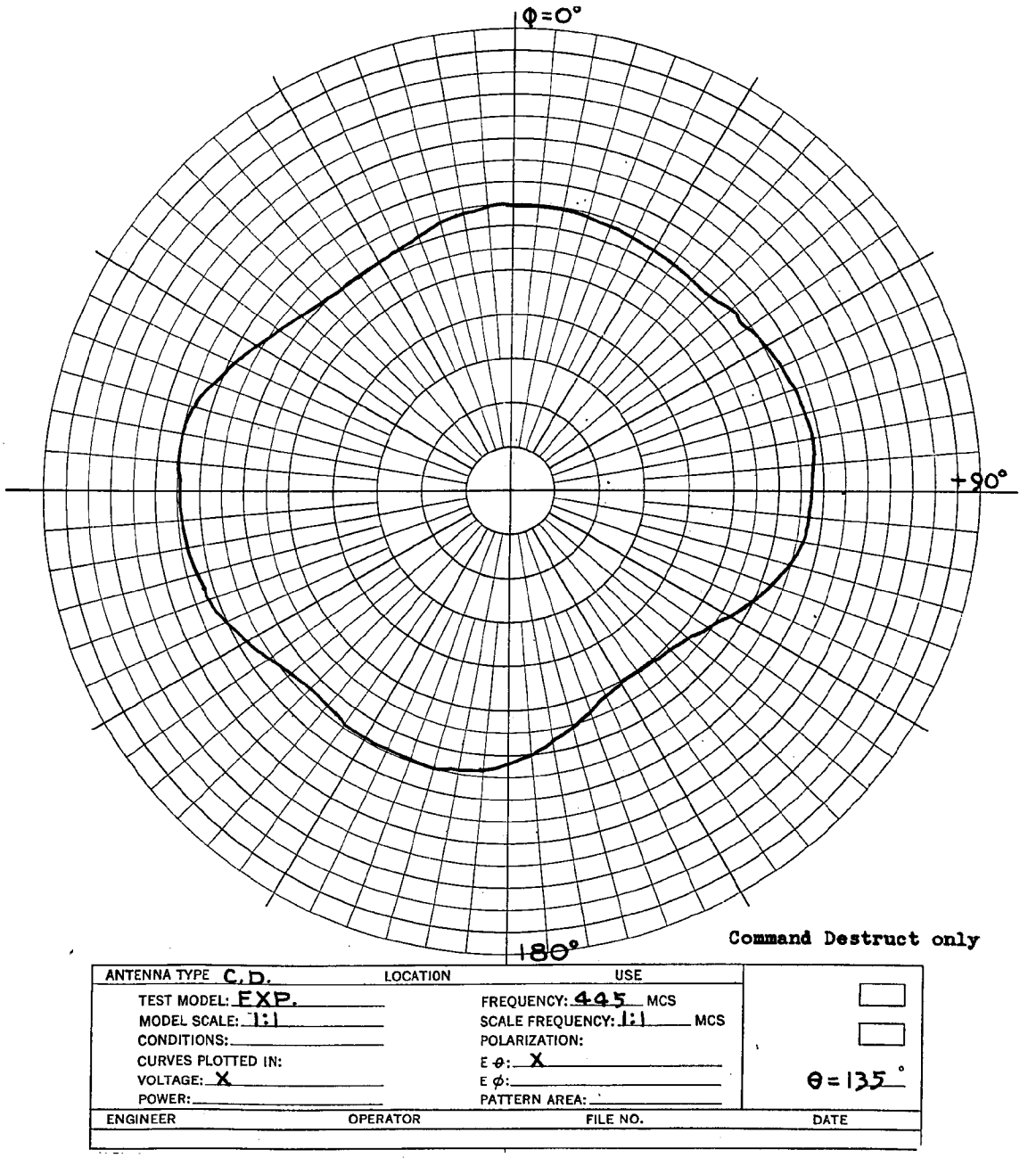

FIGURE 80

INTERFERENCE TEST PATTERN FOR TWO DIAMETRICALLY OPPOSED SLOTS OPERATING SIMULTANEOUSLY INPHASE FOR $\theta = 135^{\circ}$

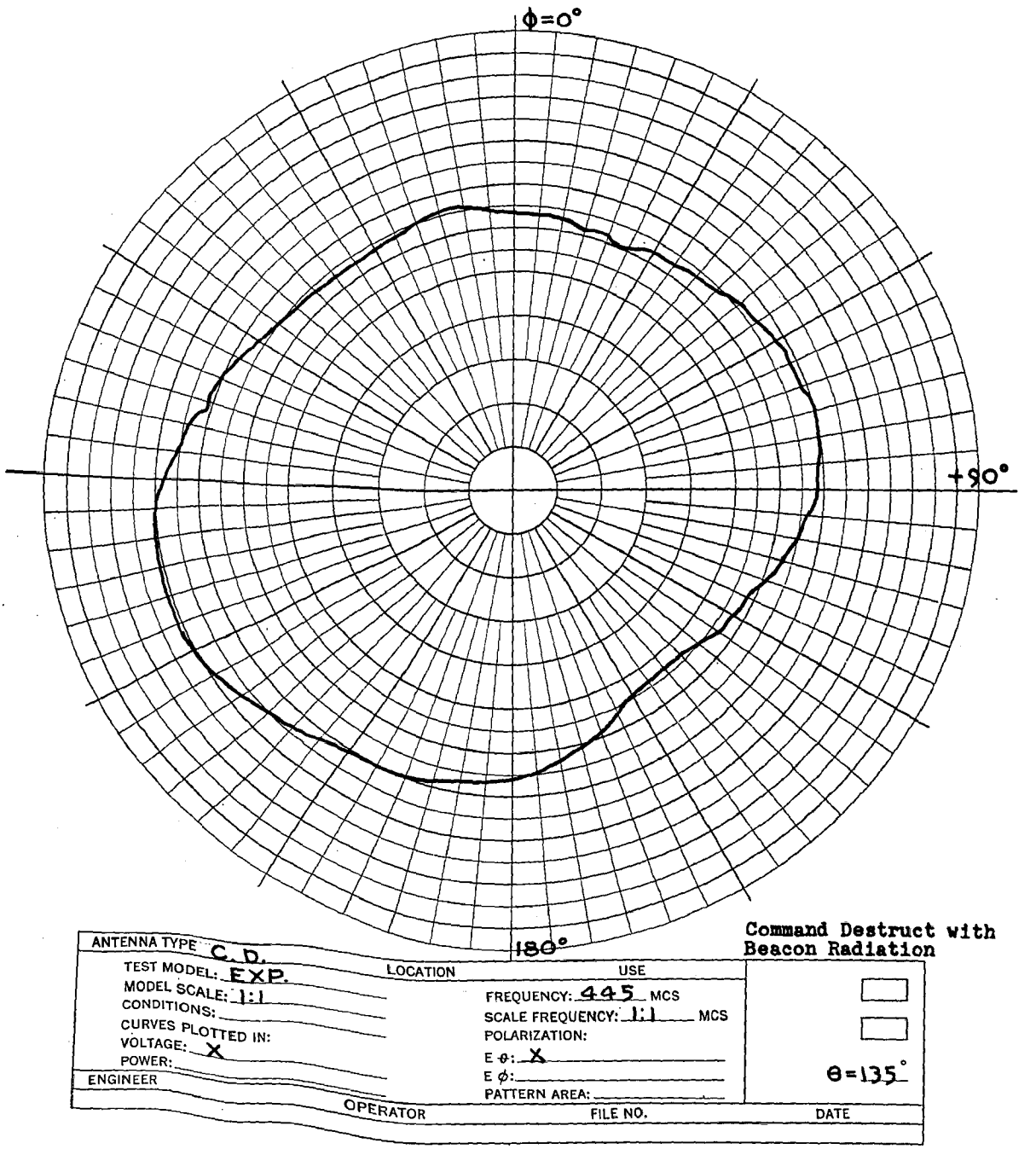

FIGURE 81

INTERFERENCE TEST PATTERN FOR TWO DIAMETRICALLY OPPOSED SLOTS OPERATING SIMULTANEOUSLY INPHASE FOR $\theta = 135^{\circ}$

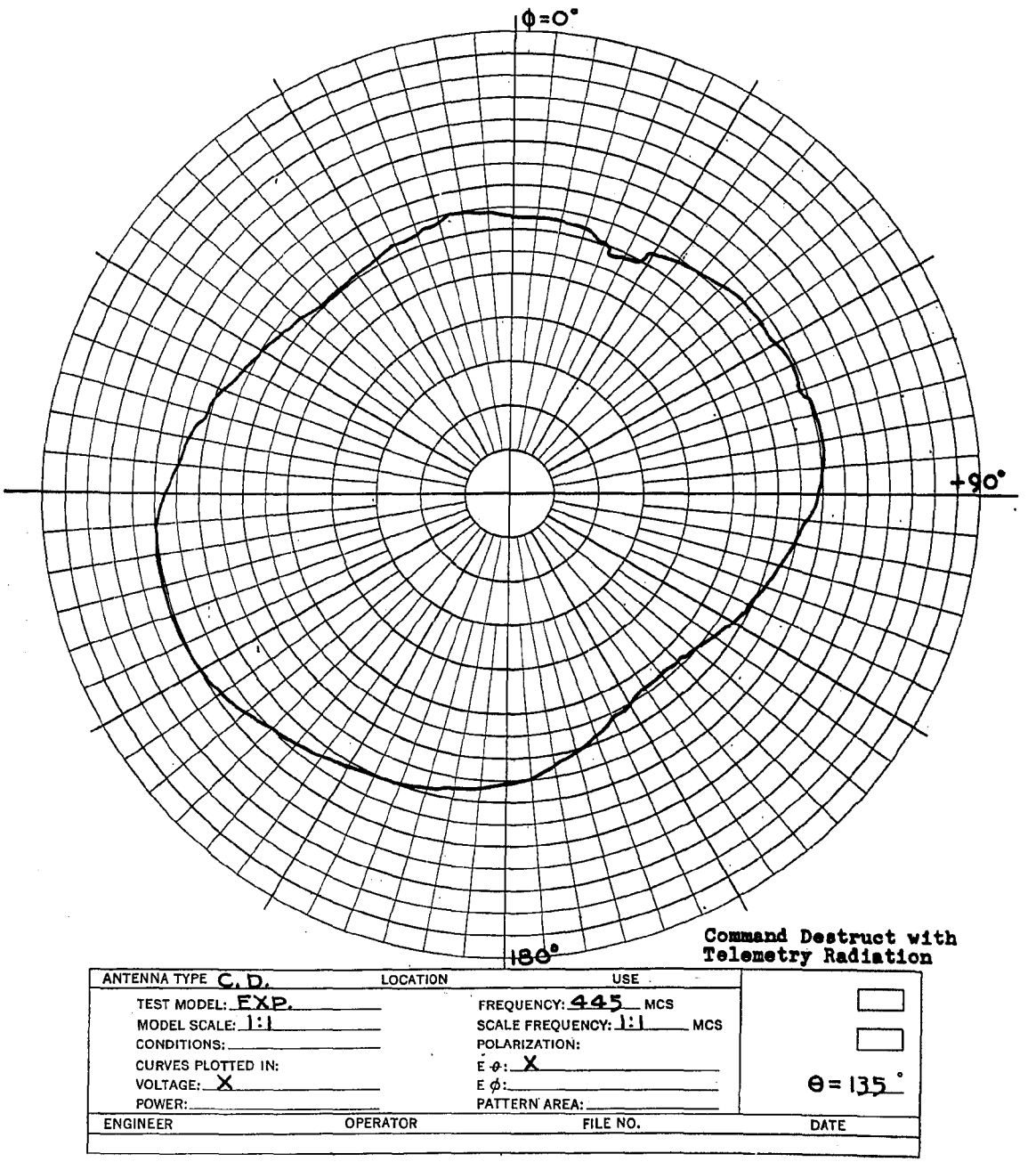

FIGURE 82

INTERFERENCE TEST PATTERN FOR TWO DIAMETRICALLY OPPOSED SLOTS OPERATING SIMULTANEOUSLY INPHASE FOR $\theta = 135^{\circ}$

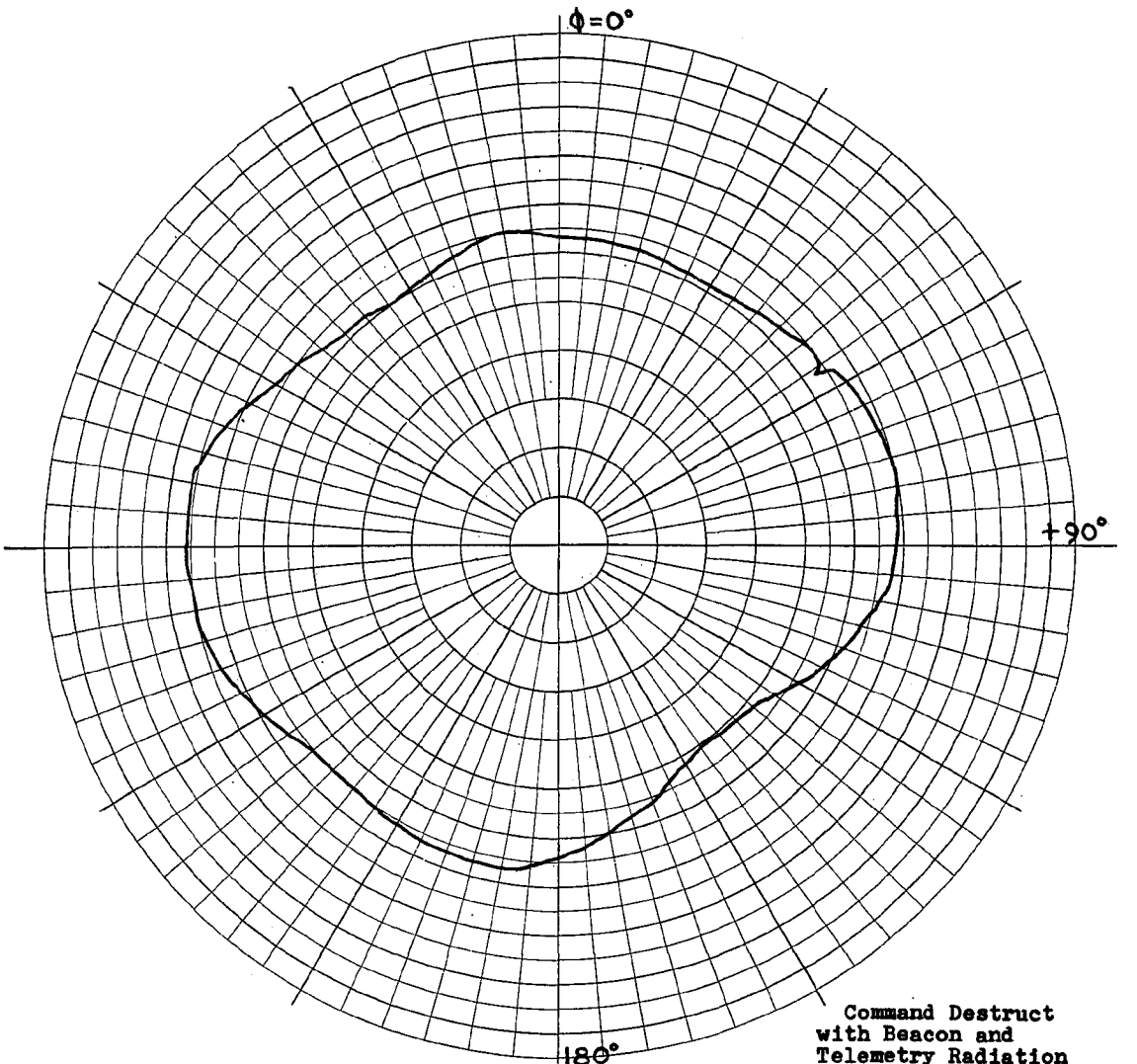

FIGURE 83

INTERFERENCE TEST PATTERN FOR TWO DIAMETRICALLY OPPOSED SLOTS OPERATING SIMULTANEOUSLY INPHASE FOR $\theta = 135^{\circ}$

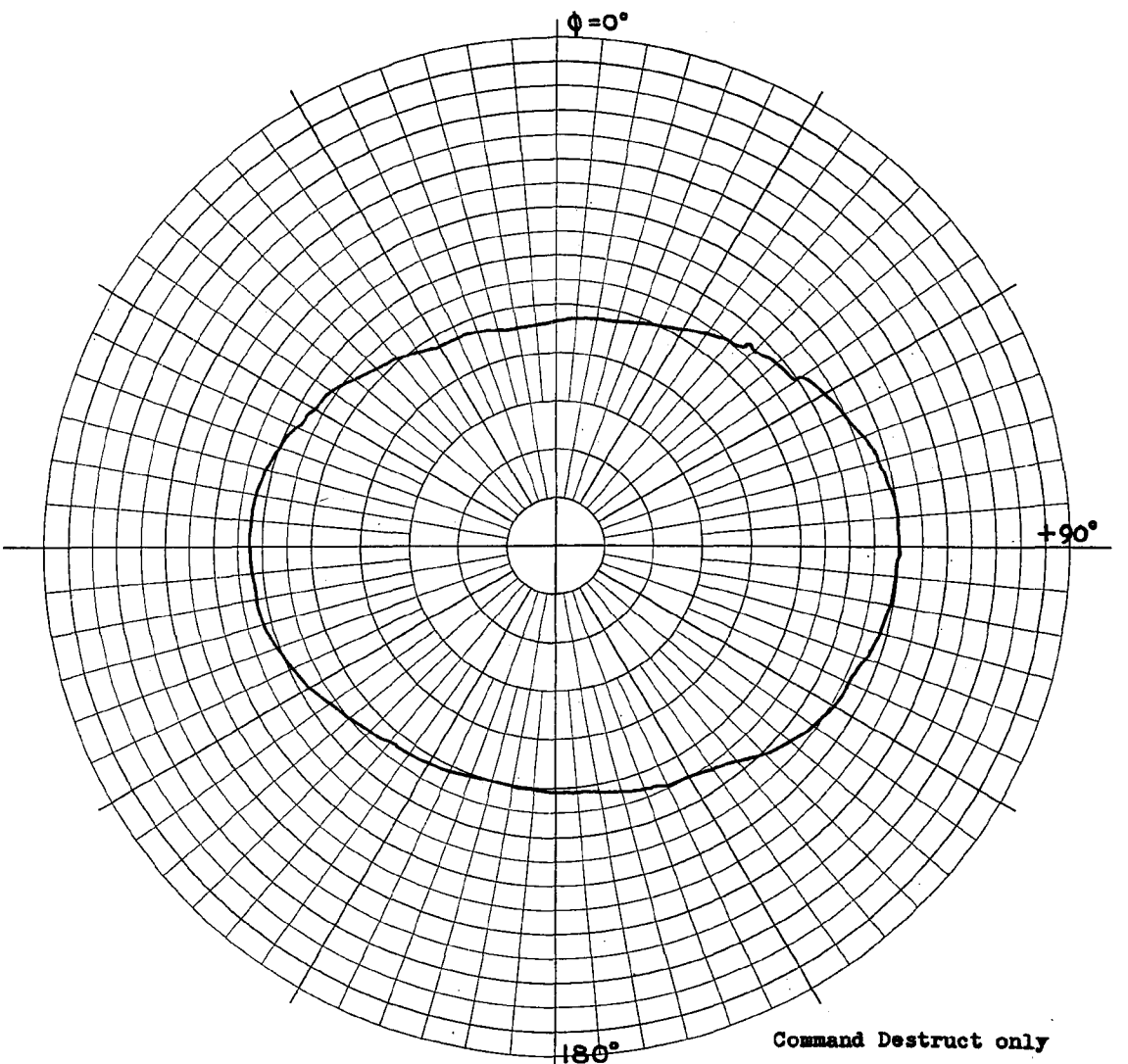

FIGURE 84

INTERFERENCE TEST PATTERN FOR TWO DIAMETRICALLY OPPOSED SLOTS OPERATING SIMULTANEOUSLY INPHASE FOR $\theta = 165^{\circ}$

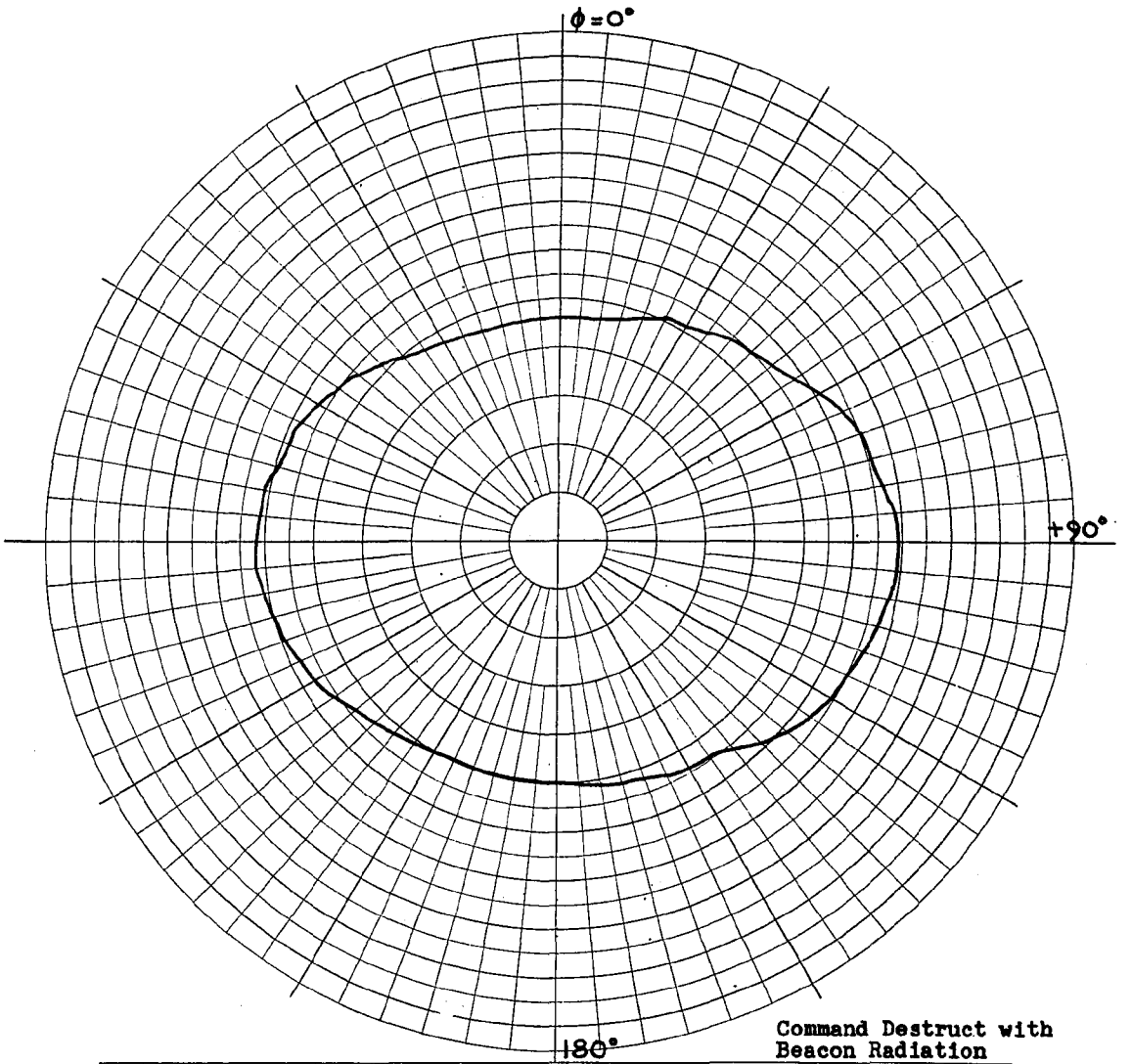

FIGURE 85

INTERFERENCE TEST PATTERN FOR TWO DIAMETRICALLY OPPOSED SLOTS OPERATING SIMULTANEOUSLY INPHASE FOR $\theta = 165^{\circ}$

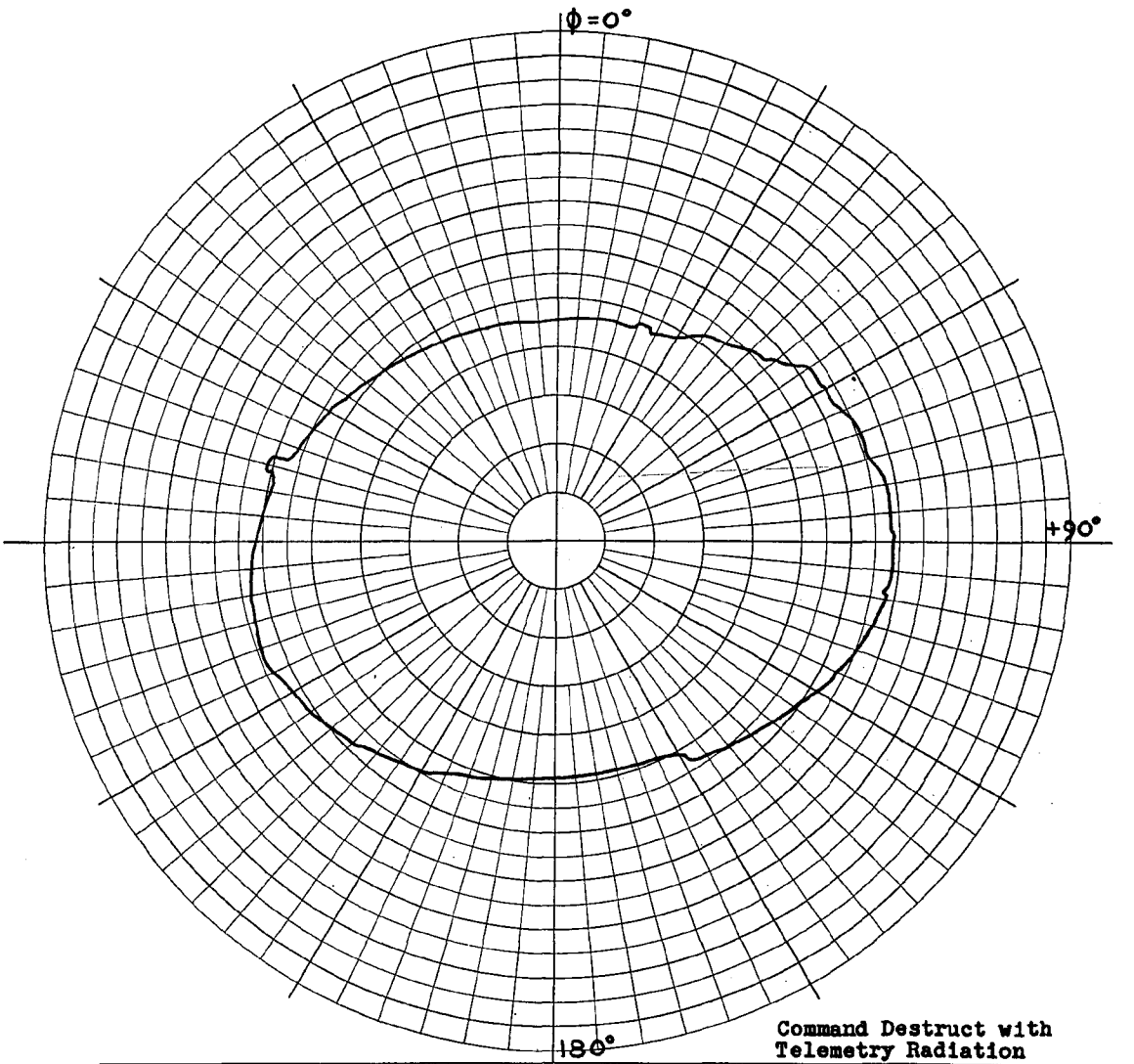

FIGURE 86

INTERFERENCE TEST PATTERN FOR TWO DIAMETRICALLY OPPOSED SLOTS OPERATING SIMULTANEOUSLY INPHASE FOR $\theta = 165^{\circ}$

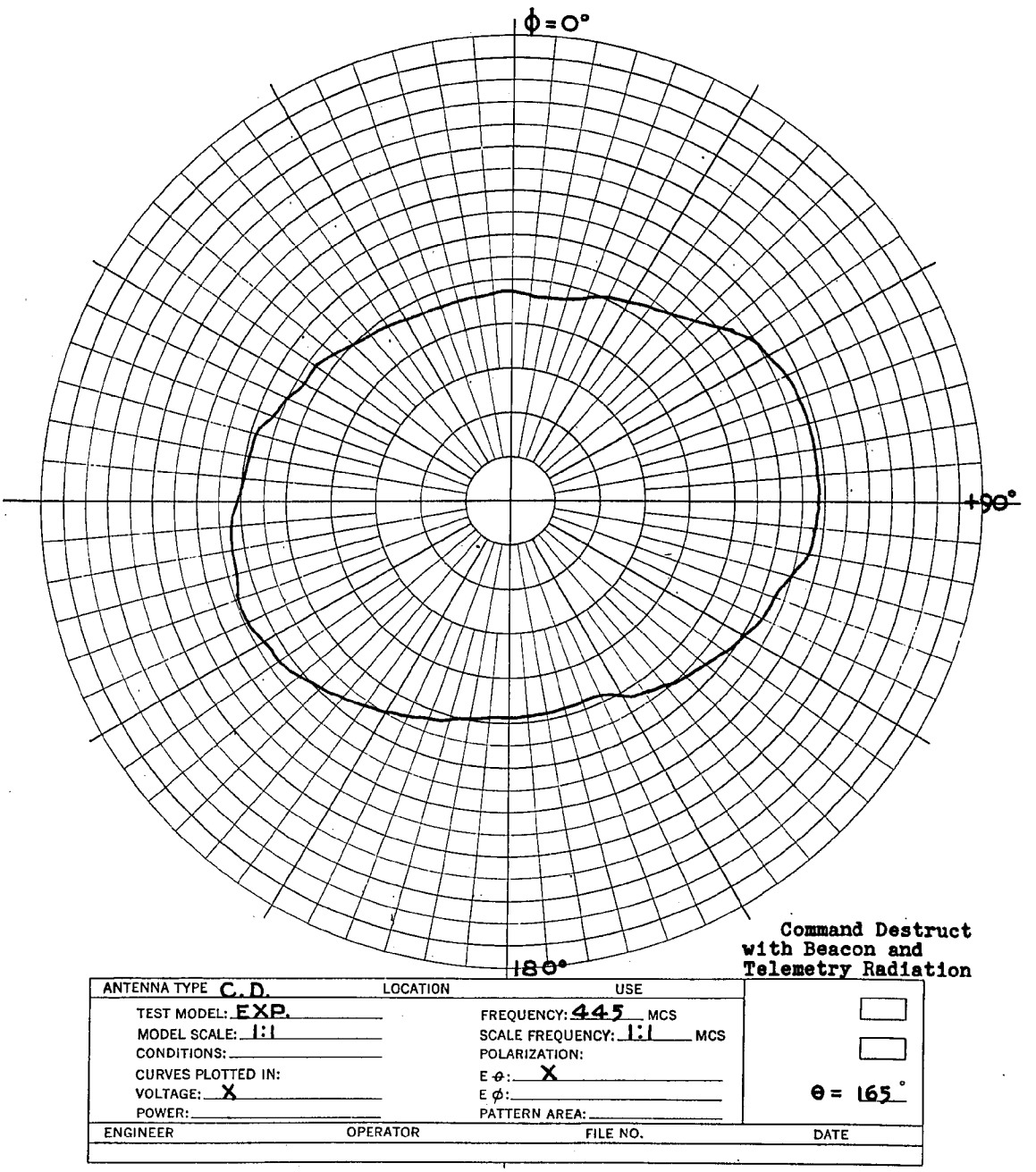

FIGURE 87

INTERFERENCE TEST PATTERN FOR TWO DIAMETRICALLY OPPOSED SLOTS OPERATING SIMULTANEOUSLY INPHASE FOR $\theta = 165^{\circ}$

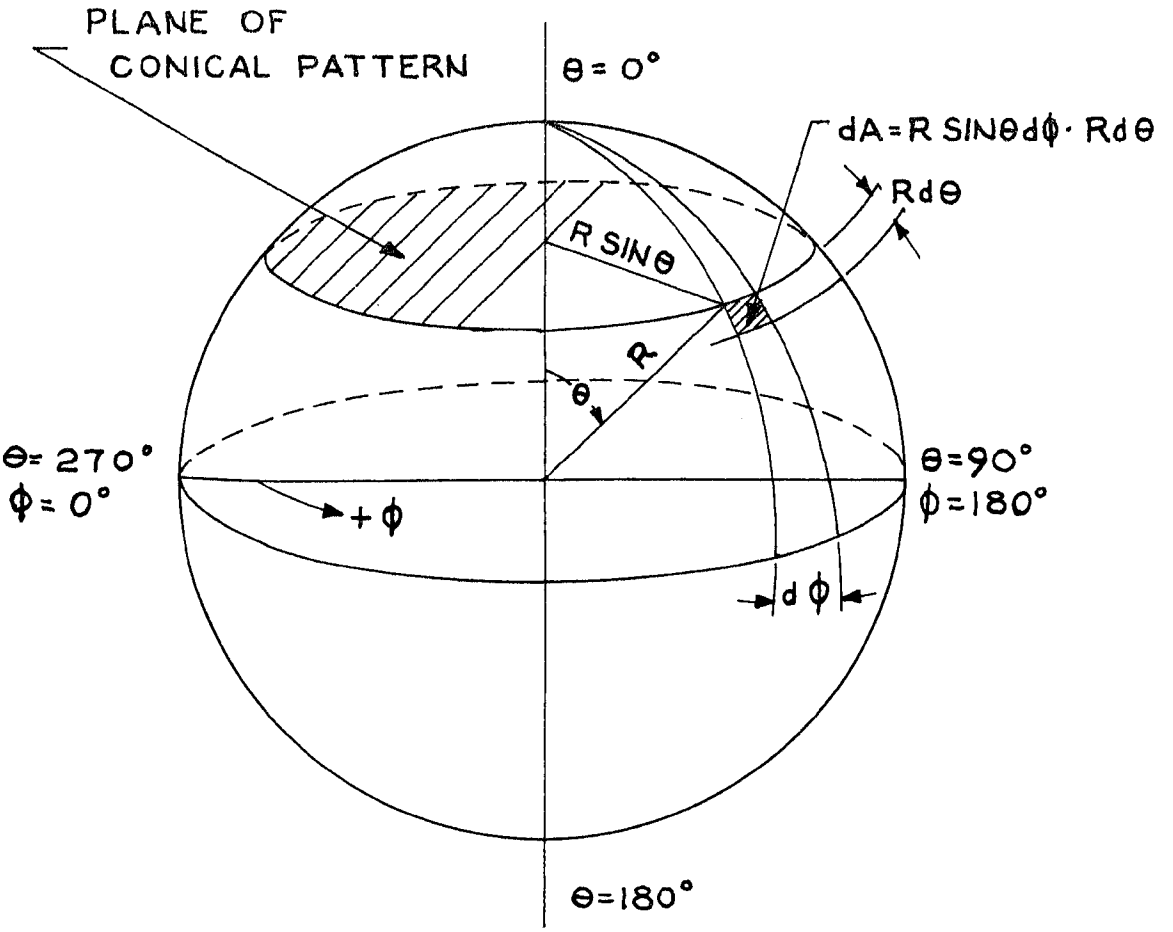

FIGURE 88

SPHERICAL GEOMETRY OF CONICAL PATTERN SYSTEM

USED IN ANALYSIS OF EXPERIMENTAL PATTERNS

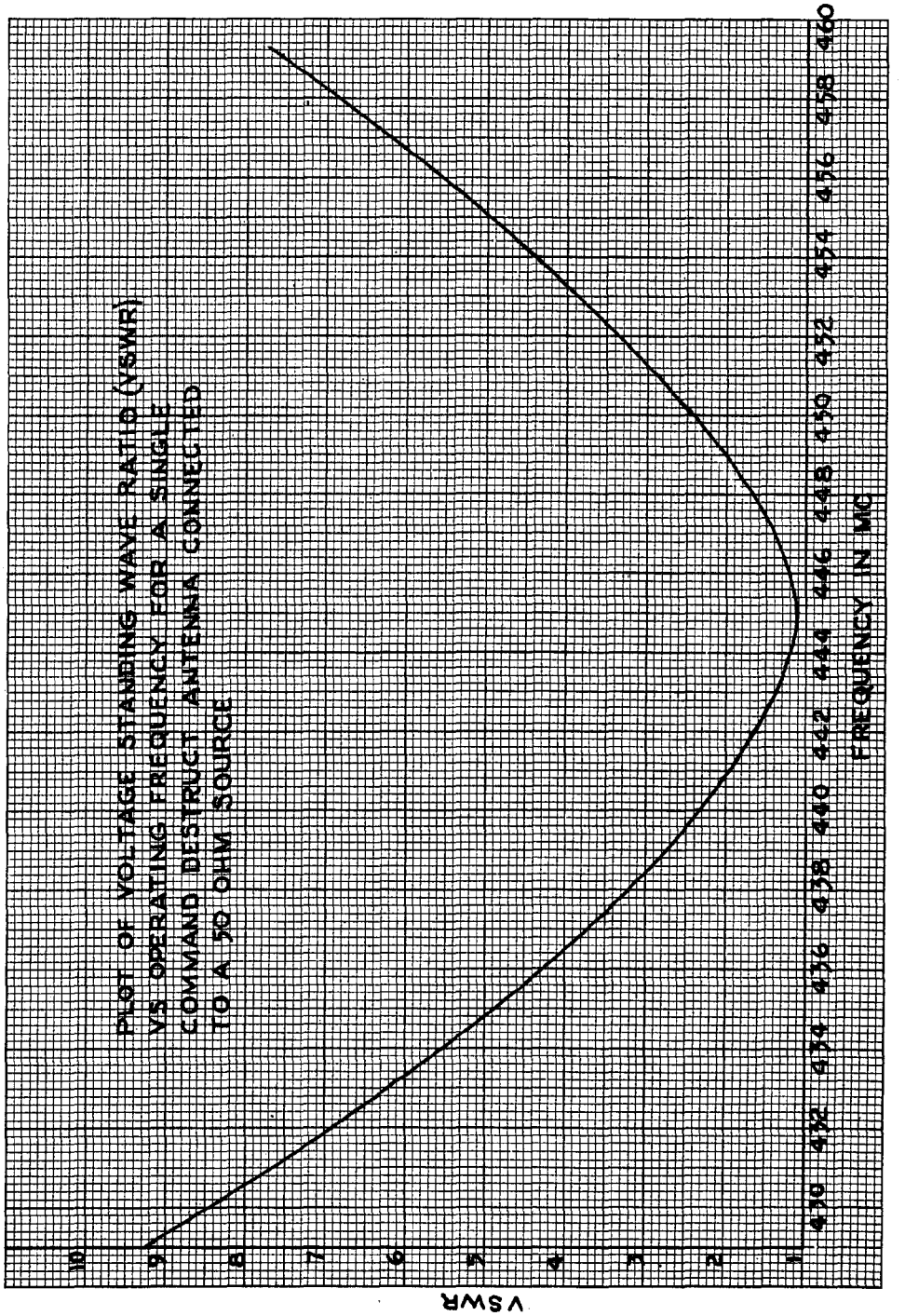

FIGURE 89

PLOT OF VOLTAGE STANDING-WAVE RATIO VS OPERATING FREQUENCY FOR A SINGLE SLOT CONNECTED TO A 50-OHM SOURCE

APPENDIX A

MAXWELL'S FIELD EQUATIONS AND SOME FUNDAMENTAL DERIVATIONS RELATIVE TO THE PROBLEM

Starting with Maxwell's field equations[23]

$$\nabla \times \vec{E} = -\frac{\partial \vec{B}}{\partial t} \tag{1a}$$

$$\nabla \times \vec{H} = \vec{J}_c + \frac{\partial \vec{D}}{\partial t} \tag{2a}$$

$$\nabla \cdot \vec{B} = 0 \tag{1b}$$

$$\nabla \cdot \vec{D} = \rho \tag{2b}$$

where

$\vec{E}$ = the electric field vector

$\vec{H}$ = the magnetic field vector

$\vec{B} = \mu\vec{H}$ = the magnetic flux density vector

$\vec{D} = \varepsilon\vec{E}$ = the electric flux density vector

$\vec{J}_c = \sigma\vec{E}$ = the conduction or convection current density vector

ρ = the volume charge density of the medium

μ = the permeability of the medium

ε = the permititivity of the medium

σ = the conductivity of the medium.

Then taking the curl of both sides of equation (1a) gives

$$\nabla \times \nabla \times \vec{E} = -\nabla \times \frac{\partial \vec{B}}{\partial t} = -\mu(\nabla \times \frac{\partial \vec{H}}{\partial t}) = -\mu\frac{\partial(\nabla \times \vec{H})}{\partial t} \; ; \tag{3}$$

---

[23] A. B. Bronwell and R. E. Beam, Theory and Application of Microwaves, McGraw-Hill Book Co., New York, N. Y., 1947, pp. 255-256.

and by making use of the vector analysis identity

$$\nabla \times \nabla \times \vec{A} = -\nabla^2\vec{A} + \nabla(\nabla \cdot \vec{A}) \ ,$$

equation (3) can be reduced to

$$\nabla^2\vec{E} - \nabla(\nabla \cdot \vec{E}) = \mu\frac{\partial(\nabla \times \vec{H})}{\partial t} \ . \tag{4}$$

Then from equation (2b), $\nabla \cdot \vec{E} = \frac{\rho}{\varepsilon} = 0$ since $\rho = 0$ for an unchanged medium, and from equation (2) and the relations between $\vec{J}_c$, $\vec{D}$ and $\vec{E}$, give

$$\nabla \times \vec{H} = \vec{J}_c + \frac{\partial\vec{D}}{\partial t} = \sigma\vec{E} + \varepsilon\frac{\partial\vec{E}}{\partial t} \ ,$$

so that equation (4) becomes

$$\nabla^2\vec{E} = \mu\frac{\partial(\sigma\vec{E} + \varepsilon\frac{\partial\vec{E}}{\partial t})}{\partial t}$$

$$\nabla^2\vec{E} = \mu\sigma\frac{\partial\vec{E}}{\partial t} + \mu\varepsilon\frac{\partial^2\vec{E}}{\partial t^2} \ . \tag{5}$$

Equation (5) is known as the wave equation for the electric field. By a similar procedure the wave equation for the magnetic field is

$$\nabla^2\vec{H} = \mu\sigma\frac{\partial\vec{H}}{\partial t} + \mu\varepsilon\frac{\partial^2\vec{H}}{\partial t^2} \ . \tag{6}$$

The problem under consideration assumes the customary steady-state harmonic time variation of the free space electromagnetic fields. Therefore, the electric field vector $\vec{E}(t)$ can be represented by a rotating phasor[24] $\overset{v}{\vec{E}}(t)$ where it is understood that the real part of $\overset{v}{\vec{E}}$ is used to obtain the actual instantaneous time function, i.e. $\vec{E}(t) = \mathrm{Re}[\overset{v}{\vec{E}}(t)]$

---

[24]B. J. Ley, S. G. Lutz and C. F. Rehberg, Linear Circuit Analysis, McGraw-Hill, New York, N. Y., 1959, pp. 134-137.

where $\vec{E}(t) = \vec{E}e^{j\omega t}$. The symbols $\vec{\ }$ designate a phasor vector independent of time and ω = the angular frequency of the harmonic time variation. By making use of the phasor principle, differentiation and integration are greatly simplified, thus from equation (5)

$$\nabla^2 \vec{E}e^{j\omega t} = \mu\sigma \frac{\partial \vec{E}e^{j\omega t}}{\partial t} + \mu\varepsilon \frac{\partial^2 \vec{E}e^{j\omega t}}{\partial t^2} ,$$

giving

$$\nabla^2 \vec{E}e^{j\omega t} = j\omega\mu\sigma \vec{E}e^{j\omega t} - \omega^2 \mu\varepsilon \vec{E}e^{j\omega t} .$$

Then canceling out the factor $e^{j\omega t}$ gives

$$\nabla^2 \vec{E} + [\omega^2\mu\varepsilon - j\omega\mu\sigma]\vec{E} = 0$$

$$\text{or} \quad \nabla^2 \vec{E} + k^2 \vec{E} = 0 \qquad (7)$$

where the parameter k is known as the intrinsic propagation constant.

Since the far field conditions assume a homogeneous free-space medium, free of charge and with the intrinsic impedance of free space, then $\sigma = 0$, $\mu = \mu_o$ and $\varepsilon = \varepsilon_o$; therefore $k^2 = \omega^2\mu_o\varepsilon_o$ or $k = \omega\sqrt{\mu_o\varepsilon_o} = \frac{2\pi}{\lambda}$ (8)

where λ = the free space wavelength which equals the free space phase velocity divided by the frequency or

$$\lambda = \frac{v}{f} = \frac{1}{f\sqrt{\mu_o\varepsilon_o}} = \frac{2\pi}{\omega\sqrt{\mu_o\varepsilon_o}} .$$

For the specified operating frequency

$$\lambda = \frac{300}{fmc} = \frac{300}{445}$$

$$= 0.674157 \text{ meters}$$

$$= 26.5416 \text{ inches}$$

The factor ka is a fundamental parameter in the final theoretical expressions for representing the far field radiation from a circumferential slot in a circular cylinder, where a = the cylinder radius. For the case under consideration ka has the value

$$ka = \frac{2\pi(6.5000)}{26.5416} \frac{\text{inches}}{\text{inches}}$$

or $ka = 1.53874.$ (9)

APPENDIX B

CALCULATION OF THE ANTENNA SLOT CIRCUMFERENTIAL ARC LENGTH

Since the missile radius at the command destruct antenna location is 6.500 inches and the slot opening cord length is 5.500 inches, the arc length is equal to the radius times the included angle, where the angle α is expressed in radians. Therefore

$$\alpha = 2 \text{ arc sin } \frac{5.500}{2(6.500)}$$

$$= 2 \text{ arc sin } 0.423077$$

$$= 2 \times \frac{25.029^{\circ}}{57.2958^{\circ}}$$

$$= 2(.436838)$$

$$= 0.873676 \text{ radians}$$

thus the arc length is $0.873676(6.500) = 5.67889$ inches which is equivalent to 0.21396λ, (rounded off to 0.2140λ) where λ is the free space wavelength.

APPENDIX C

SOLUTION OF THE WAVE EQUATION IN CYLINDRICAL COORDINATES FOR A STEADY-STATE HARMONIC TIME VARIATION IN FREE SPACE

Starting with equation (5) of Appendix A, which after applying the phasor principle to simplify the differentiation process, reduces the wave equation for the phasor vector electric field to

$$\nabla^2\vec{E} + k^2\vec{E} = 0 \qquad (1)$$

where

$$k^2 = \omega^2\mu_o\varepsilon_o \quad .$$

In rectangular coordinates the general solution of the wave equation is the same for either scalar or vector functions. However, in cylindrical coordinates it is considerably more difficult to derive the general solution for a vector function than for a scalar function. Consequently the solution for a scalar function will be obtained and then related to the vector function to be considered.

By using the principle of separation of variables, the partial differential wave equation can be separated into ordinary differential equations with the number of equations required equal to the number of independent variables. Then each ordinary second-order differential equation has two independent solutions, each containing an arbitrary constant. The general solution of the ordinary differential equations may be represented by the sum of the two independent solu-

tions. Then the general solution of the partial differential equation is the product of the general solutions of the ordinary differential equations. Therefore if equation (1) is expressed in terms of the scalar phasor function $\overset{v}{F}$, thus

$$\nabla^2 \overset{v}{F} + k^2 \overset{v}{F} = 0 \quad ; \tag{2}$$

or, in terms of cylindrical coordinates, equation (2) becomes

$$\frac{1}{\rho} \frac{\partial}{\partial \rho}\left(\rho \frac{\partial \overset{v}{F}}{\partial \rho}\right) + \frac{1}{\rho^2} \frac{\partial^2 \overset{v}{F}}{\partial \varphi^2} + \frac{\partial^2 \overset{v}{F}}{\partial z^2} + k^2 \overset{v}{F} = 0 \quad . \tag{3}$$

Using the method of separation of variables, let

$$\overset{v}{F} = \overset{v}{F}_1(\rho)\, \overset{v}{F}_2(\varphi)\, \overset{v}{F}_3(z) \quad . \tag{4}$$

Then by substitution and division by $\overset{v}{F}$,

$$\frac{1}{\overset{v}{F}_1 \rho} \frac{\partial}{\partial \rho}\left(\rho \frac{\partial \overset{v}{F}_1}{\partial \rho}\right) + \frac{1}{\overset{v}{F}_2 \rho^2} \frac{\partial \overset{v}{F}_2}{\partial \varphi^2} + \frac{1}{\overset{v}{F}_3} \frac{\partial^2 \overset{v}{F}_3}{\partial z^2} + k^2 = 0 \quad . \tag{5}$$

Since the third term is a function of z only, it may be set equal to a constant, thus $\dfrac{d^2 \overset{v}{F}_3}{dz^2} = a_z^2 \overset{v}{F}_3$ (6)

which has a general solution of the form

$$\overset{v}{F}_3 = C_1 e^{a_x z} + C_2 e^{-a_x z} \tag{7}$$

where C_1 and C_2 are arbitrary constants. Inserting a_z^2 for the third term in equation (5) and multiplying by ρ^2 gives

$$\frac{\rho}{\overset{v}{F}_1} \frac{\partial}{\partial \rho}\left(\rho \frac{\partial \overset{v}{F}_1}{\partial \rho}\right) + \frac{1}{\overset{v}{F}_2} \frac{\partial^2 \overset{v}{F}_2}{\partial \varphi^2} + (a_z^2 + k^2)\rho^2 = 0 \tag{8}$$

or

$$\frac{\rho^2}{\overset{v}{F}_1} \frac{d^2 \overset{v}{F}_1}{d\rho^2} + \frac{\rho}{\overset{v}{F}_1} \frac{d \overset{v}{F}_1}{d\rho} + \frac{1}{\overset{v}{F}_2} \frac{d^2 F_2}{d\varphi^2} + (a_z^2 + k^2)\rho^2 = 0 \quad . \tag{9}$$

Observing that the third term is a function of φ only it can likewise be set equal to a constant, thus

$$\frac{d^2F_2^{\nu}}{d\varphi^2} = -\nu^2 F_2^{\nu} \tag{10}$$

then equation (10) has a solution of the form

$$F_2^{\nu} = C_3 \cos \nu\varphi + C_4 \sin \nu\varphi \quad . \tag{11}$$

Inserting $-\nu^2$ in equation (9) and multiplying by F_1^{ν} gives

$$\rho^2 \frac{d^2F_1^{\nu}}{d\rho^2} + \rho \frac{dF_1^{\nu}}{d\rho} + (a_z^2 + k^2)\rho^2 - \nu^2 F_1^{\nu} = 0 \quad . \tag{12}$$

This is a form of Bessel's equation. It may be put in standard form by dividing through by ρ^2 plus letting $p^2 = a_z^2 + k^2$ and $x = P\rho$, thus, equation (12) becomes

$$\frac{d^2F_1^{\nu}}{d\rho^2} + \frac{1}{\rho}\frac{dF_1^{\nu}}{d\rho} + \left[p^2 - \frac{\nu^2}{\rho^2}\right] F_1^{\nu} = 0 \tag{13}$$

and after substituting for $x = P\rho$ equation (13) becomes

$$p^2 \frac{d^2F_1^{\nu}}{dx^2} + \frac{p^2}{x}\frac{dF_1^{\nu}}{dx} + \left[1 - \frac{\nu^2}{x^2}\right] p^2 F_1^{\nu} = 0 \tag{14}$$

or

$$\frac{d^2F_1^{\nu}}{dx^2} + \frac{1}{x}\frac{dF_1^{\nu}}{dx} + \left[1 - \frac{\nu^2}{x^2}\right] F_1^{\nu} = 0 \quad . \tag{15}$$

Equation (15) is the standard form of Bessel's differential equation[25]. Each value of the parameter ν is associated

---

[25] R. I. Sarbacher and W. A. Edson, Hyper and Ultrahigh Frequency Engineering, John Wiley & Sons, New York, N. Y., 1943, p. 236.

with a pair of fundamental solutions called Bessel functions of the order ν. One of these solutions is called a Bessel function of the first kind which is finite at $x = 0$. The other fundamental solution is called a Bessel function of the second kind which is infinite at $x = 0$. This type is also frequently called the Newman function. Linear combinations of these solutions are called Bessel functions of the third kind, or Hankel functions[26]. The two kinds of Hankel functions are

$$H_{\nu}^{(1)}(x) = J_{\nu}(x) + jY_{\nu}(x) \tag{16}$$

$$H_{\nu}^{(2)}(x) = J_{\nu}(x) - jY_{\nu}(x) \quad . \tag{17}$$

Equation (16) is called the Hankel function of the first kind of order ν, and represents a cylindrical wave traveling from infinity towards the origin, whereas, equation (17) is called the second kind of order ν, and represents a cylindrical wave traveling in the opposite direction. For a physical field which is a periodic multiple of 2π in its φ dependence, then $\nu = n$ is an integer and the Bessel functions have integral order. In synthesising the electric field surrounding a circular cylinder, Hankel functions are involved.

---

[26]Ibid.

APPENDIX D

EVALUATION OF THE SOURCE FIELD INTEGRAL FOR THE SLOT DISTRIBUTION IN THE φ DIRECTION FOR BOTH A ONE-HALF WAVELENGTH SLOT IN FREE SPACE AND FOR THE DIELECTRIC LOADED SLOT HAVING A CIRCUMFERENTIAL ARC LENGTH OF 0.2140λ

$$\text{Let} \quad I_n = \int_{-\varphi_o}^{\varphi_o} \overset{v}{F}(\beta) e^{jn\beta}\, d\beta. \tag{1}$$

Then for a $\frac{\lambda}{2}$ arc length slot in free space with the slot length defined by $\varphi = \frac{\pi}{2} - \varphi_o$ to $\varphi = \frac{\pi}{2} + \varphi_o$ with an assumed cosinusoidal field distribution in the φ direction of,

$$\overset{v}{F}(\beta) = \cos \frac{\pi}{2\varphi_o}\beta = \cos ka\beta = \begin{cases} 1 \text{ for } \beta = \pm\varphi_o \\ 0 \text{ for } \beta = 0 \end{cases}$$

where

$$\varphi_o = \frac{\lambda}{4a} = \frac{\pi}{2ka} \quad \text{and} \quad ka = \frac{2\pi a}{\lambda} \quad \text{or} \quad k = \frac{2\pi}{\lambda}$$

then

$$I_n = \int_{-\varphi_o}^{\varphi_o} \cos ka\beta\, e^{jn\beta} d\beta = \frac{e^{jn\beta}(jn \cos ka\beta + ka \sin ka\beta)}{(ka)^2 + (jn)^2}\Bigg]_{-\varphi_o}^{\varphi_o}$$

or

$$I_n = \frac{(\cos n\beta + j \sin n\beta)(jn \cos ka\beta + ka \sin ka\beta)}{(ka)^2 - n^2}\Bigg]_{-\varphi_o}^{\varphi_o}$$

$$= \frac{(\cos n\frac{\pi}{2ka} + j \sin n\frac{\pi}{2ka})(jn \cos \frac{\pi}{2} + ka \sin \frac{\pi}{2})}{(ka)^2 - n^2}$$

$$- \frac{[\cos n(-\frac{\pi}{2ka}) + j \sin n(-\frac{\pi}{2ka})][jn \cos(-\frac{\pi}{2}) + ka \sin(-\frac{\pi}{2})]}{(ka)^2 - n^2}$$

$$= \frac{[\cos n\frac{\pi}{2ka} + j \sin n\frac{\pi}{2ka}]ka - [\cos n\frac{\pi}{2ka} - j \sin n\frac{\pi}{2ka}][-ka]}{(ka)^2 - n^2}$$

$$= \frac{2ka \cos n\frac{\pi}{2ka}}{(ka)^2 - n^2} \qquad (2)$$

Whereas, for the dielectric loaded slot having a physical arc length of 0.2140λ, and the same assumed cosinusoidal field distribution in the φ direction, and with the slot length defined by $\varphi = \frac{\pi}{2} - \varphi'_o$ to $\varphi = \frac{\pi}{2} + \varphi'_o$ then

$$\varphi'_o = \frac{0.2140\lambda}{2a} = \frac{0.2140\pi}{ka}$$

therefore

$$\overset{v}{F}(\beta) = \cos\frac{\pi}{2\varphi'_o}\beta = \begin{cases} 1 \text{ for } \beta = \pm\varphi'_o \\ 0 \text{ for } \beta = 0 \end{cases}$$

and

$$I_n = \int_{-\varphi'_o}^{\varphi'_o} \cos\frac{\pi}{2\varphi'_o}\beta e^{jn\beta} d\beta = \frac{e^{jn\beta}(jn\cos m\beta + m\sin m\beta)}{m^2 + (jn)^2}\Bigg]_{-\varphi'_o}^{\varphi'_o}$$

where

$$m = \frac{\pi}{2\varphi'_o}$$

therefore,

$$I_n = \frac{(\cos n\beta + j\sin n\beta)(jn\cos m\beta + m\sin m\beta)}{m^2 - n^2}\Bigg]_{-\varphi'_o}^{\varphi'_o}$$

$$= \frac{(\cos n\varphi'_o + j\sin n\varphi'_o)(jn\cos m\varphi'_o + m\sin m\varphi'_o)}{m^2 - n^2}$$

$$- \frac{[\cos n(-\varphi'_o) + j\sin n(\varphi'_o)][jn\cos m(-\varphi'_o) + m\sin m(-\varphi'_o)]}{m^2 - n^2}$$

$$= \frac{(\cos n\varphi'_o + j\sin n\varphi'_o)(jn\cos m\varphi'_o + m\sin m\varphi'_o)}{m^2 - n^2}$$

$$- \frac{(\cos n\varphi'_o - j\sin n\varphi'_o)(jn\cos m\varphi'_o - m\sin m\varphi'_o)}{m^2 - n^2}$$

$$= \frac{\begin{matrix} jn \cos m\varphi'_o \cos n\varphi'_o + m \sin m\varphi'_o \cos n\varphi'_o \\ -jn \cos m\varphi'_o \cos n\varphi'_o + m \sin m\varphi'_o \cos n\varphi'_o \end{matrix}}{m^2 - n^2}$$

$$+ \frac{\begin{matrix} -n \cos m\varphi'_o \sin n\varphi'_o + jn \sin m\varphi'_o \sin n\varphi'_o \\ -n \cos m\varphi'_o \sin n\varphi'_o - jn \sin m\varphi'_o \sin n\varphi'_o \end{matrix}}{m^2 - n^2}$$

$$= \frac{2[m \sin \frac{\pi}{2} \cos n\varphi'_o - n \cos \frac{\pi}{2} \sin n\varphi'_o]}{m^2 - n^2}$$

$$= \frac{\frac{\pi}{\varphi'_o} \cos n\varphi'_o}{(\frac{\pi}{2\varphi'_o})^2 - n^2} = \frac{\frac{\pi ka}{0.2140\pi} \cos n\frac{0.2140\pi}{ka}}{[\frac{\pi ka}{2(0.2140\pi)}]^2 - n^2}$$

$$= \frac{\frac{ka}{0.2140} \cos n\frac{0.2140\pi}{ka}}{(\frac{ka}{0.4280})^2 - n^2} \quad . \qquad (3)$$

SELECTED BIBLIOGRAPHY

BOOKS

Bremmer, H., Terrestrial Radio Waves, Elsevier Publishing Co., Inc., New York, N. Y., 1949.

Bronwell, A. B. and R. E. Beam, Theory and Application of Microwaves, McGraw-Hill Book Co., Inc., New York, N. Y., 1947.

International Telephone and Telegraph Corporation, Reference Data for Radio Engineers (4th edition), American Book-Stratford Press, Inc., New York, N. Y., 1956.

Kraus, J. D., Antennas, McGraw-Hill Book Co., Inc., New York, N. Y., 1950.

Laport, E. A., Radio Antenna Engineering, McGraw-Hill Book Co., Inc., New York, N. Y., 1952.

Ley, B. J., S. G. Lutz, and C. F. Rehberg, Linear Circuit Analysis, McGraw-Hill Book Co., Inc., New York, N. Y. 1959.

Reed, H. R. and C. M. Russell, Ultra High Frequency Propagation, John Wiley and Sons, Inc., New York, N. Y., 1953.

Sarbacher, R. I. and W. A. Edson, Hyper and Ultrahigh Frequency Engineering, John Wiley and Sons, Inc., New York, N. Y., 1943.

Schelkunoff, S. A., Advanced Antenna Theory, John Wiley and Sons, Inc., New York, N. Y., 1952.

Schelkunoff, S. A. and H. T. Friis, Antennas Theory and Practice, John Wiley and Sons, Inc., New York, N. Y., 1952.

Silver, S., Microwave Antenna Theory and Design, McGraw-Hill Book Co., Inc., New York, N. Y., 1949.

Smythe, W. R., Static and Dynamic Electricity, McGraw-Hill Book Co., Inc., New York, N. Y., 1950.

Stratton, J. A., Electromagnetic Theory, McGraw-Hill Book Co., Inc., New York, N. Y., 1941.

Terman, F. E., Radio Engineer's Handbook, McGraw-Hill Book Co., Inc., New York, N. Y., 1943.

Wait, J. R., Electromagnetic Radiation from Cylindrical Structures, Pergamon Press, New York, N. Y., 1959.

Watson, G. N., A Treastise on the Theory of Bessel Functions, The MacMillan Co., New York, N. Y., 1944.

Williams, P. H., Antenna Theory and Design, Vol. II, Sir Isaac Pitman and Sons, London, England, 1950.

PUBLICATIONS OF THE GOVERNMENT

Rowland, H. J., A. W. Jayne, and R. T. Hall, "A System of UHF Omni-Directional Slot Antennas for the Blossom IV-A Warhead," Cambridge Field Station Air Material Command Report No. E5047, June 1949.

Wait, J. R., "A Survey of the Recent Literature on Slot Radiators," Nat. Bur. of Stds., Report No. 5051, 11 March 1957.

PERIODICALS

Bailin, L. L., "The Radiation Field Produced by a Slot in a Large Circular Cylinder," Proc. of Inst. Radio Engrs. PGAP, pp. 128—137, July 1955.

Haycock, O. C. and F. L. Wiley, "Radiation Patterns and Conductances of Slotted-Cylinder Antennas," Proc. of Inst. Radio Engrs., vol. 40, pp. 349—352, March 1952.

Jordon, E. C. and W. E. Miller, "Slotted Cylinder Antenna," Electronics, vol. 20, pp. 90—93, February 1947.

Lindenblad, N. E., "Slotted Antennas," Proc. of Inst. Radio Engrs., vol. 35, pp. 1472—1479, December 1947.

Papas, C. H., "Radiation from a Transverse Slot in an Infinite Cylinder," J. Math. Phys., vol. 28, pp. 227—236, January 1950.

Pistolkors, A. A., "Radiation from a Transverse Slit on the Surface of a Circular Cylinder," J. Tech. Phys., U.S.S.R., vol. 17, pp. 377—388, 1947 (In Russian).

Sensiper, S., "Cylindrical Radio Waves," Trans. Inst. Radio Engrs., vol. AP-5, pp. 56—70, January 1957.

Silver, S. and W. K. Saunders, "The Radiation from a Transverse Rectangular Slot in a Circular Cylinder," J. Appl. Phys., vol. 21, pp. 745—749, August 1950.

Silvers, S. and W. K. Saunders, "The External Field Produced by a Slot in an Infinite Circular Cylinder," J. Appl. Phys., vol. 21, pp. 153—158, February 1950.

Sinclair, G., "The Patterns of Slotted Cylinder Antennas," Proc. of Inst. Radio Engrs., vol. 36, pp. 1487—1492, December 1948.

Sinclair, G., E. C. Jordon, and E. W. Vaughn, "Measurements of Aircraft Antenna Patterns Using Models," Proc. of Inst. Radio Engrs., vol. 35, pp. 1451—1471, December 1947.

Wait, J. R. and S. Kahana, "Calculated Patterns of Circumferential Slots on a Circular Conducting Cylinder," Can. J. Tech., vol. 33, pp. 77—97, January 1955.

Wait, J. R. and J. Kates, "Radiation Patterns of Circumferential Slots on Moderately Large Conducting Cylinders," Monograph No. 167R, Inst. Elect. Engrs. (London), February 1956, republished in Proc. Inst. Elect. Engrs., vol. 103, Pt.C., pp. 289—296, September 1956.

Watson, G. N., "The Diffraction of Radio Waves by the Earth," Proc. Roy. Soc. London, vol. A95, pp. 83—99, 1918; vol. A95, pp. 546—563, 1919.